

Development of a numerical model for Cutter Suction Dredgers

A time domain analysis of a CSD in operation

A. Kagie
2/21/2018

Development of a numerical model for Cutter Suction Dredgers

A time domain analysis of a CSD in operation.

Anton Kagie

Date: 21st of February 2018

Master Thesis Offshore & Dredging Engineering – Bottom Founded Structures

Graduation Committee:

Prof. dr. A. Metrikine

Ir. C. Keijdener

Dr. ir. K. N. van Dalen

Ir. R. J. van der Wal



Abstract

A Cutter Suction Dredger (CSD) is a vessel that is used to cut hard soils with precision. It is moored stiffly through a spud pile while the soil is being cut. This, in combination with wave loads, causes the whole system to be dynamically challenging and nonlinear. Previous attempts to model a CSD in operation have been limited to the frequency domain. However, in order to be able to include these nonlinear effects occurring during the operation of a CSD, a time domain analysis is necessary. The hydrodynamic forces in the time domain analysis will be calculated using Ansys AQWA. The external forces which occur during operation will be calculated by a custom script written in Python. The script consists out of 3 modules; a spud module, a winch module and a soil module. The spud module is responsible for calculating the mooring forces on the spud pile in order to maintain its position. The spud has been modeled as a beam with 3 pinned supports. This linear model has been expanded to include the option to take the presence of a flexible spud carriage into account. This means that if the buffer of the flexible carriage is activated, the stiffness of the system changes accordingly in order to reduce the loading on the spud with increasing displacements. The winch module is responsible for determining the force required to achieve the swing around the spud at the desired velocity. Within the module, the application of a PID controller ensures that the tension in the side wires is adjusted dynamically in order to maintain a stable swing velocity throughout the whole process. Tuning the controller correctly is critical to avoid unnecessary tension peaks while at the same having a sufficiently quick response to sudden changes. The soil module is responsible for calculating the reaction forces on the CSD as a consequence of the cutting of the soil. The soil is characterized by the specific energy characteristic, which enables the module to be applied to all types of soil, from soft clay to hard rock. The 3D force vector on the cutterhead is then calculated using the volume cut and the rotational torque of the cutterhead. Furthermore, the module keeps track of where the soil has been cut, adjusting the new height as the cutterhead passes. This enables to realistically create a time series where the volume cut during each timestep will vary due to the oscillations of the cutter. The final result is a model in 7 degrees of freedom which can dynamically respond to the nonlinear reactions caused by cutting soil, wave loads, mooring through a flexible carriage and varying side wire forces. This model is now ready to be used to investigate the effects of different combinations of soil types and wave conditions.

Preface

This thesis is the last hurdle to be taken in order to obtain the Master of Science degree in Offshore and Dredging Engineering at the TU Delft. It describes the process which was made in a timespan of nearly 12 months to create a numerical model for the simulation of cutter suction dredgers. It was a long road with a variety of challenges. The complexity of the big picture required a stepwise approach, starting with the very basics and adding each component one step at a time. One of the first steps to be taken was to become an expert in Python, a language I learned to appreciate throughout this process.

The idea of this numerical model was conceived by Boskalis, coinciding with the acquisition of their most powerful CSD to date: the Helios. This self-propelled megacutter was used to determine the dimensions and operational parameters for the numerical model. However, I feel confident that with virtually no adjustments, other than a different 3D model of the hull, the created numerical model can be used to simulate any CSD. This is in part due to the stepwise approach taken throughout the process.

I would like to thank Remmelt and Gertjan for providing guidance, patience, and insight which has helped me a lot in to complete my goals and deliver the final result. I would also like to thank my family, especially Valentina, for motivating me to always keep moving forward.

Anton Kagie

Amsterdam, 21st of February 2018

Contents

Abstract	1
Preface	2
List of Figures	6
List of Tables	8
Nomenclature	9
1 Introduction	10
1.1 Cutter Suction Dredgers	10
1.2 Cutting Process	11
1.3 Problem definition	14
1.4 Research Objective	14
1.5 Approach	15
2 Helios	16
2.1 Overview	16
2.2 Cutting at -20 meters	16
2.2.1 Determining the new center of gravity	18
2.2.2 Two body approach	20
2.3 Drag Force	21
2.3.1 Linearized drag	23
3 General Modeling	24
3.1 Input in AQWA	24
3.2 Python	25
3.3 Geometric models	27
4 Frequency domain	29
4.1 Free Floating	29
4.2 Modeling the spud pile with a single spring	31
4.3 Modeling the cutting process and spud pile with two springs	32
4.4 Conclusion	33
5 Spuds	34
5.1 Physical properties of the spud system	34
5.1.1 Theory	36
5.2 Spud Module	37
5.2.1 Cantilever Spud	37
5.2.2 Pinned Spud	39
5.3 Results	40
5.3.1 Expected results	40
5.3.2 Actual results	41
5.4 Adding clearance and buffers	42

5.5	Step Force.....	42
5.6	Possible improvements.....	44
6	Winches.....	45
6.1	Function of the winches.....	45
6.2	Winch Module.....	46
6.3	Fixed Wire Force.....	47
6.4	Fixed Wire Length.....	50
6.5	PID Controller.....	53
6.6	Conclusion.....	57
6.7	Possible improvements.....	58
7	Cutting Soil.....	59
7.1	Cutterhead.....	59
7.2	Reality.....	59
7.3	Soil module.....	61
7.3.1	Static test of soil model.....	63
7.3.2	1 DOF test of ladder.....	65
7.3.3	Single swing.....	68
7.3.4	Full process.....	70
7.4	Different soil types.....	72
7.5	Conclusion.....	72
7.6	Possible Improvements.....	72
8	Waves.....	74
8.1	Flexible spud carriage.....	74
8.2	Combination of waves and cutting.....	75
8.3	1 Body vs 2 Body.....	76
8.4	Conclusion.....	78
8.5	Recommendations.....	78
9	Results.....	79
10	Recommendations.....	81
	Bibliography.....	82
	Appendix A. General Arrangement and data Helios.....	83
	Appendix B. Initial time domain verifications.....	84
	Comparison of the different geometric models used.....	84
	First time domain run of the free-floating body.....	87
	Appendix C. PID Tuning.....	89
	PID Explanation.....	89
	Ziegler-Nichols method.....	89
	Appendix D. Results of the comparison between AQWA and Seaway.....	90

Freefloating.....	90
1 Spring	94
2 Springs.....	100
Appendix E. Free floating in time domain results	105
Free-floating single rigid body	105
Free floating with ladder as separate body	106
Appendix F. Results of Spud tests	107
Cantilever Spud	107
Pinned Spud	109
Flexible spud carriage	111
Appendix G. Results of Winch tests.....	113
Fixed Force.....	113
Fixed Length	116
PID Controller, P-dominated.....	119
PID Controller, I-dominated	122
Appendix H. Soil tests.....	125
Static soil test	125
1 DOF test	126
Single swing	128
Full simulation for 3 soil types	133
Full simulation for 3 soil types including waves.....	137
Comparison of single rigid body and 2 body approach	141
Appendix I. Python script.....	Error! Bookmark not defined.

List of Figures

Figure 1 Key elements of a CSD source: TU Delft	10
Figure 2 Cutterhead	11
Figure 3 Small CSD barge source: damen.com	11
Figure 4 The Helios	16
Figure 5 Side view of Helios cutting at -20 m.....	17
Figure 6 Top view of cutting at -20 m.....	17
Figure 7 Buoyant compartments of ladder, for an angle of 15 degrees	18
Figure 8 Graph to determine additional buoyancy through ladder angles	19
Figure 9 A-frame with hoisting wires visible and ladder hoisted	21
Figure 10 Schematic of distributed drag force	22
Figure 11 Drag force comparison for a linearized velocity of $v_{\text{swing}} = 0.4 \text{ m/s}$	23
Figure 12 Overview of interaction	25
Figure 13 Flow chart of the custom Python script.....	26
Figure 14 Overview of the hull in Octopus Seaway, note the slightly changing breadth in the top view	27
Figure 15 Overview of the Hull with mesh in AQWA for use in the Seaway comparison	28
Figure 16 Single rigid body model used for time domain.....	28
Figure 17 Ladder and hull as 2 separate rigid bodies, connected to each other with hinge and hoist wire.....	28
Figure 18 Wave directions	29
Figure 19 Difference in damping and displacement of AQWA and Seaway	30
Figure 20 Comparison of free-floating responses between AQWA and Seaway	30
Figure 21 Surge response due to beam waves, due to the eccentrically placed spud	31
Figure 22 Comparison of AQWA - Seaway using one spring to model the spud reaction	32
Figure 23 Comparison AQWA - Seaway with 2 springs for soil and spud reactions	33
Figure 24 Comparison AQWA - Seaway with 2 springs for soil and spud reactions	33
Figure 25 Spud pile	34
Figure 26 Detailed view of the spud carriage.....	35
Figure 27 Schematics of spud in carriage and difference in penetration depth for hard and soft soils.	36
Figure 28 Visualization of modeling process	37
Figure 29 Schematic of the clamped connection with stiffness correction	38
Figure 30 Schematic of the pinned model of the spud	39
Figure 31 Schematic of testing scenario.....	41
Figure 32 Force in spud tip compared to the test force	41
Figure 33 Resulting forces in the spud guides for the pinned model.....	41
Figure 34 Deflection during spud test	42
Figure 35 Stiffness of the Spud including buffer	42
Figure 36 Overview of cutting with a step of 1.5 m per swing	43
Figure 37 Effect of taking steps on spud pile.	43
Figure 38 Winches on top of the ladder provide tension in the side wires	45
Figure 39 Sophisticated automated systems largely control the swing motion of the cutter	46
Figure 40 Overview of side wires and side anchors	47
Figure 41 Winch forces over time with fixed force in pulling direction	49
Figure 42 Resultant forces on spud due to fixed force in wires	50
Figure 43 Schematic for fixed wire length.....	51
Figure 44 Forces over time due to wire strain.....	52

Figure 45 Resultant spud force from wire strain 53

Figure 46 Vector diagram PID controller, $F_{\text{haul}} = F_{\text{PID}} - F_{\text{brake}}$ 54

Figure 47 Forces over time when using a P-dominated controller 55

Figure 48 Forces over time with I-controller..... 56

Figure 49 Resultant spud force for P-dominated controller 57

Figure 50 Resultant spud forces for I-dominated controller..... 57

Figure 51 Cutterhead 59

Figure 52 Schematic of vector representing the rotation axis..... 59

Figure 53 Difference between overcutting and undercutting 60

Figure 54 Collection of the grid points within radius r of cutterhead center 61

Figure 55 Schematic of forces on cutterhead per grid point for overcutting (left) and undercutting (right)..... 62

Figure 56 Volume cut in static test..... 63

Figure 57 Resulting forces in static test 64

Figure 58 Contour plot of the static trajectory 64

Figure 59 1 DOF model..... 65

Figure 60 Single degree of freedom model motions, excluding cutting forces 66

Figure 61 Single Degree of Freedom model motions, including cutting forces 66

Figure 62 Cut and normal forces due to the 1DOF motion 67

Figure 63 Cutting forces for a single swing..... 69

Figure 64 Volume cut and corresponding cutterhead torque..... 70

Figure 65 Resultant winch force when cutting soil..... 71

Figure 66 Spud force at full operation..... 71

Figure 67 Resultant force at spud tip for 3 different soil types..... 72

Figure 68 Overview of stiffness and wave direction 74

Figure 69 Surge motion with linear and flexible carriage..... 74

Figure 70 Spud forces due to waves with linear and flexible carriage..... 75

Figure 71 Overview of combination of waves and cutting soil 75

Figure 72 Resultant spud forces due to waves and cutting soil..... 76

Figure 73 Cutterhead motions due to the cutting of soil in waves 77

Figure 74 Difference between 1-body and 2-body approach..... 77

Figure 75 Pitch motions of 1-body and 2-body approach 78

Figure 76 Comparison of the 3 geometric models in the frequency domain 87

Figure 77 Initial balance for the free-floating vessel 88

List of Tables

Table 1 Dimensions of Helios with ladder horizontal	16
Table 2 Mass distribution overview	18
Table 3 Dimensions of the Helios with ladder at -20 m	20
Table 4 Radii of gyration of the individual bodies in 2 body approach	20
Table 5 Parameters for drag force	23
Table 6 Overview of the AQWA suite	24
Table 7 Spring stiffness, 1 spring.....	31
Table 8 Spring stiffness, 2 springs.....	32
Table 9 Spud parameters.....	40
Table 10 Fixed Force Parameters	48
Table 11 Parameters for fixed wire length controller	51
Table 12 Gain values used	54
Table 13 Typical energy values per soil type.....	59
Table 14 Variables for soil module.....	63
Table 15 Directions of the force components	64
Table 16 Parameters used in the 1 DOF test	65
Table 17 Values used for comparison of soil types	72
Table 18 Parameters used in comparison	74
Table 19 Parameters used for cutting of 3 soil types in waves.....	76
Table 20 New values for initial stability	88

Nomenclature

A_{pp}	Aft Perpendicular; the rear of the hull and origin of the local axes system
C/N	Ratio between cutting force and normal force on a blade
CoG	Center of Gravity
CSD	Cutter Suction Dredger
G'M	Metacentric Height, adjusted for free surface effect.
E_{sp}	Specific energy of soil
e	Error, for use in a PID controller
ϵ	Strain in wire
H_s	Significant wave height
K_d	Derivative gain, for use in a PID controller
K_i	Integral gain, for use in a PID controller
K_p	Proportional gain, for use in a PID controller
l_0	Unstretched length of wires
l_1	Actual length of wires
L_1	Distance between spud guides
L_2	Distance between lower guide and spud tip
LCG	Longitudinal Coordinate of CoG, from A_{pp}
L_{pp}	Length Perpendicular; Length of Hull
ω	Rotational velocity
ϕ	Pitch angle
PID	Proportional, Integral and Derivative controller
r	Radius cutterhead
R	Swing radius
ρ	Density of seawater
TCG	Transverse Coordinate of CoG, from centerline
T_p	Peak period
θ	Yaw angle
VCG	Vertical Coordinate of CoG, above keel
v_s	Swing velocity
w_{low}	Displacement of lower guide
w_{tip}	Displacement of spud tip
w_{up}	Displacement of upper guide

1 Introduction

1.1 Cutter Suction Dredgers

A Cutter Suction Dredger (CSD) is a vessel which is used to cut soil for dredging purposes. Pumps on board the vessel are responsible for sucking up the cut material and transporting it to the surface and discharging it either in a barge or to shore. There are two main types of cutter suction dredgers. They can be built as a barge or as a self-propelled vessel. The latter are generally much larger, more powerful and can operate further offshore than barges. Although compared to other dredging equipment their use is in relatively shallow water, with the largest self-propelled CSD's now being able to operate at a depth of 35 meters.

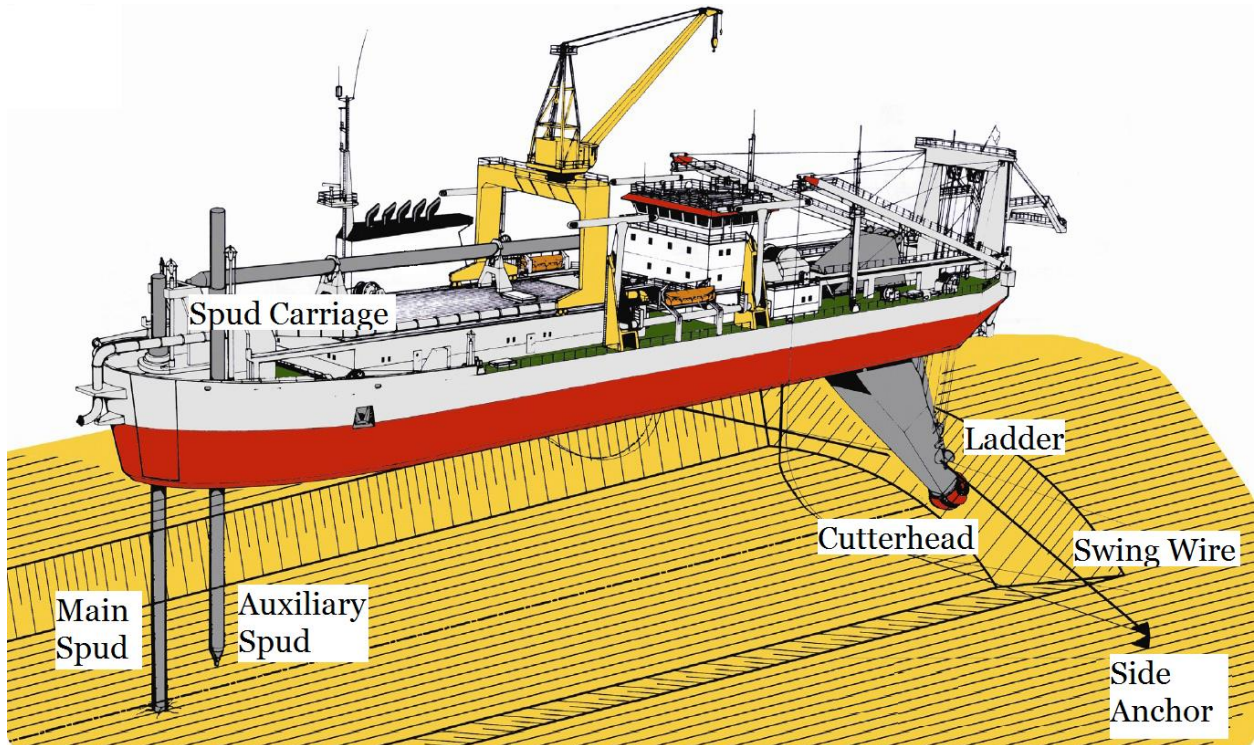


Figure 1 Key elements of a CSD source: TU Delft

The main advantage of a CSD is that it is able to cut very hard soils with high precision. This precision is attained through its stiff mooring system which makes use of a spud pile. The spud is dropped into the soil and the vessel transfers its loads to the spud pile via the spud carriage. The spud carriage can move in longitudinal direction to allow the CSD to move forward while cutting without loss of accuracy. When the CSD moves forward it is called a step, or it steps forward. If the maximum amount of steps of the carriage have been taken, the auxiliary spud is lowered to maintain position while the main spud is relocated by moving the carriage back to its starting position.

Cutter suction dredgers make cuts in a swinging motion around the spud. The swings are done by tensioning swing wires which are connected to the side anchors. These anchors can be placed by anchor booms installed on the ship or by anchor handling tugs if they need to be placed further away.

The tool which actually cuts the soil is the cutterhead, visible in Figure 2. A cutterhead functions similar to a drill bit. It rotates in order for the teeth to cut the soil. The part of the soil which is being cut is called the breach. It is important that the cutterhead is equipped with the correct teeth for the given soil. As both shape and hardness of the teeth greatly influence the rate in which they are worn out. Therefore, the right choice of teeth for a certain soil will have a large effect on the total costs of a project. Worn teeth are less efficient which results in lower productivity, furthermore replacing the

teeth is a time-consuming matter. In very hard soils even the best teeth only last in the order of 30 minutes to an hour, while in soft, sandy soils the teeth can be used for many days of operation.

The cutterhead is connected to the hull of the CSD through the ladder. The ladder of a CSD houses the suction pipe and the cutterhead powertrain. The presence of the powertrain makes the ladder quite heavy, the weight is required to keep the cutterhead in the breach. If the ladder is not heavy enough the cutterhead can jump out of the breach when cutting hard soils, resulting in less accurate cutting and undesirable forces. The ladder is held in place by a hinge connected to the hull. Hoisting wires control the ladder angle and cutting depth. During transport and inactivity, the ladder is hoisted, giving the vessel a more hydrodynamic efficient shape. The ladder also needs to be hoisted to replace teeth on the cutterhead.



Figure 2 Cutterhead



Figure 3 Small CSD barge source: damen.com

When the soil is cut, the suction pipe mounted in the ladder will suck up the mixture of sediment and water. The centrifugal pumps on board the CSD have to be powerful enough to transport the slurry from the seabed to the surface, and if connected to a floating pipeline, until the end of that line. The amount of cut soil that isn't sucked up by the pumps is called spillage. It is important that spillage is always reduced to a minimum. Therefore, for each soil there is an optimum in rotation speed and swing speed which will lead to maximum productivity with minimum spillage. Spillage, apart from being a productive loss, also needs to be avoided from an environmental point of view. As loose sediment is able to travel larger distances through the sea currents.

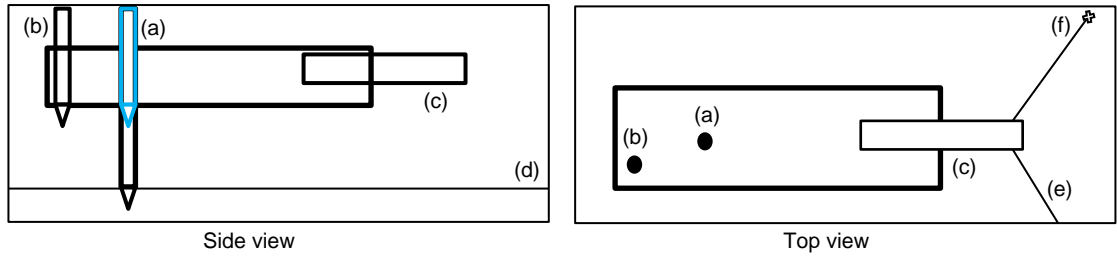
The big advantage of a CSD is the ability to cut many different soil types from loose sand to hard rock while maintaining fairly high accuracy due to its rigid mooring system. This same mooring system causes the whole process to be dynamically challenging, both the reactions of the spud and the cutterhead will be nonlinear. Large forces can be experienced during operation and passive moored position. The rigid mooring system has as disadvantage that the vessel has relatively low limits on workability in certain wave conditions such as low-frequency waves. If swell is a big problem a more flexible mooring solution can be used, which is called a Christmas tree, created using a bundled combination of mooring lines. The use of Christmas trees, however, is beyond the scope of this research.

1.2 Cutting Process

The whole cutting process can best be explained in a series of steps.

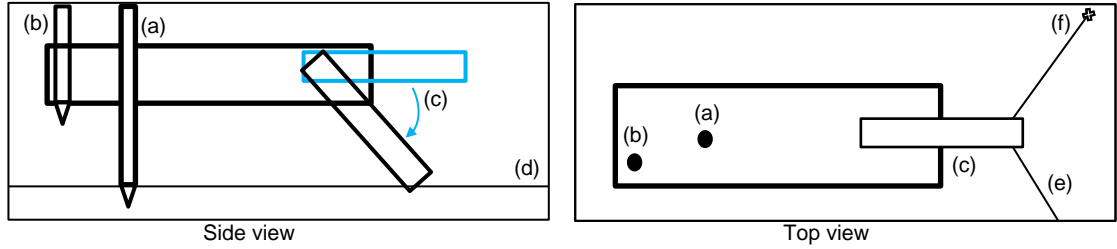
1. Lowering main spud (a) into the soil (d)

The spud is dropped in free fall, which upon impact penetrates the soil providing a point of anchorage and mooring. The side anchors (f) also should be placed at sufficient distance before starting operation.



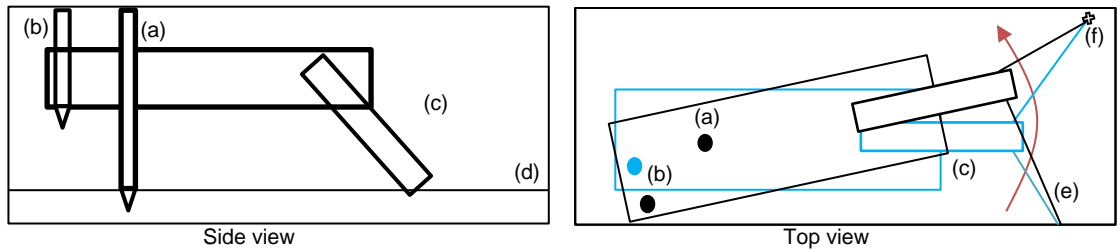
2. Lowering ladder (c) into the breach (d)

With the cutterhead rotating the ladder is lowered to the cutting depth and make the initial cut in the breach. Usually this is done with the cutterhead on the centerline, or a swing angle of 0 degrees.



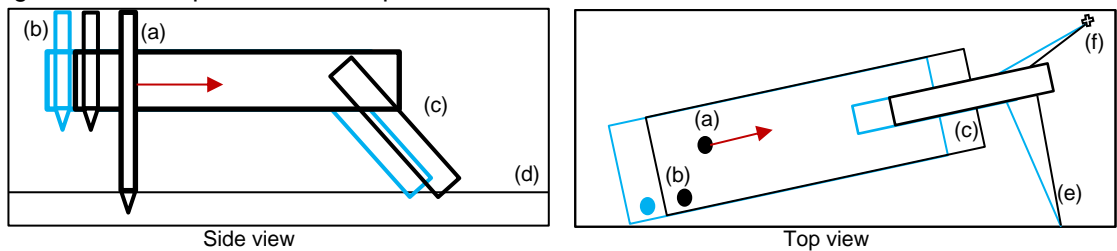
3. Start swing to port or starboard

With the cutterhead in the breach, the swing wires (e) have to pull the ladder sideways, creating cutting arcs with the spud as pivot point. A swing generally consists of a single arc, avoiding to cut the same part of soil twice as much as possible.



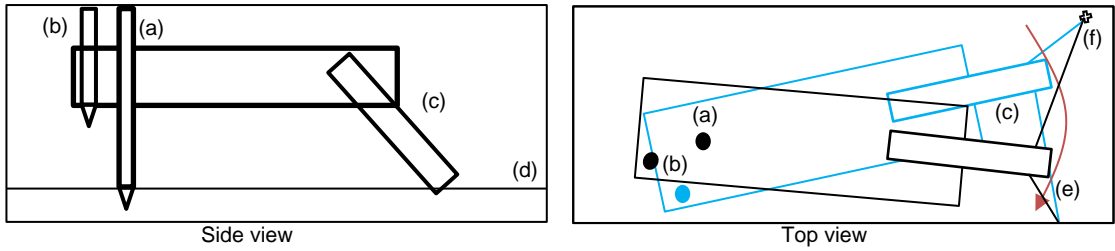
4. Step forward

At the end of the swing, when the maximum swing angle has been reached, the CSD steps forward. In soft soils this happens while still swinging, creating a continuous motion. In hard soils this is not always possible and the CSD has to pause swinging at the maximum swing angle until the step has been completed.

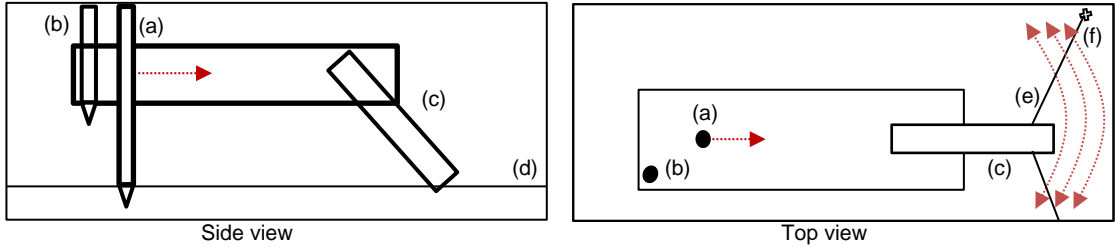


5. Swing in opposite direction

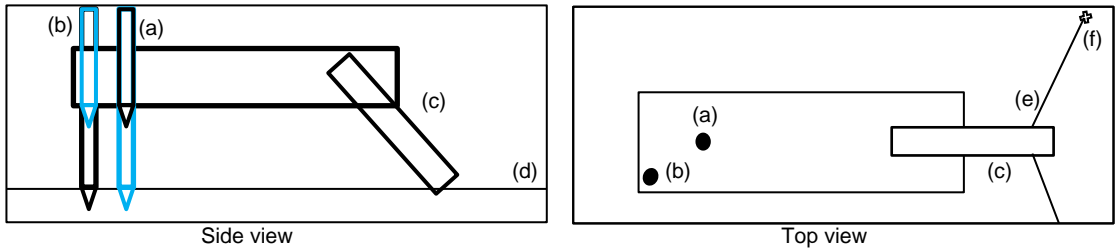
The swing wire on the other side of the ladder will now start pulling the vessel to swing in the other direction. Note that the rotation of the cutterhead is fixed and therefore does not change with the swing direction.



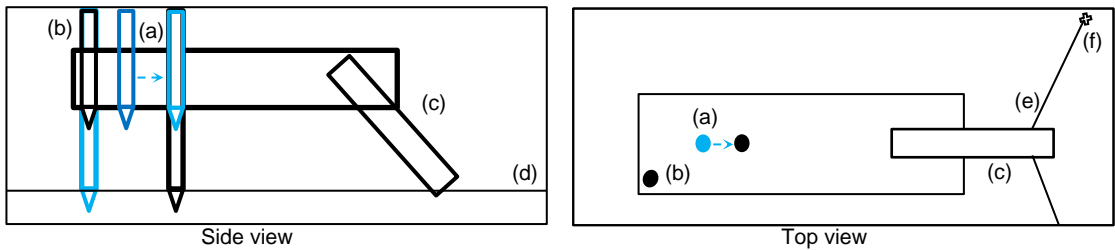
6. Repeat steps 4. and 5. until carriage reaches maximum step.
 At the end of each swing, the CSD steps forward ensuring that throughout every swing new soil is cut. When the carriage has reached its limit for steps, the swing should stop at the centerline.



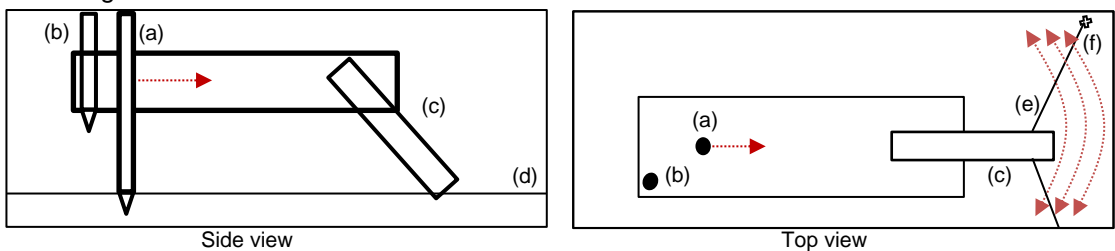
7. Drop auxiliary spud (b) and raise main spud (a)
 The auxiliary spud ensures that the position of the CSD is maintained while the main spud is moved forward with the carriage returning to its starting position.



8. Drop main spud (a) and raise auxiliary spud (b)
 With the carriage back in its starting position, the main spud can be dropped into the soil again. The auxiliary spud should be raised in order to be able to swing and the cutterhead has maintained its position at the centerline.

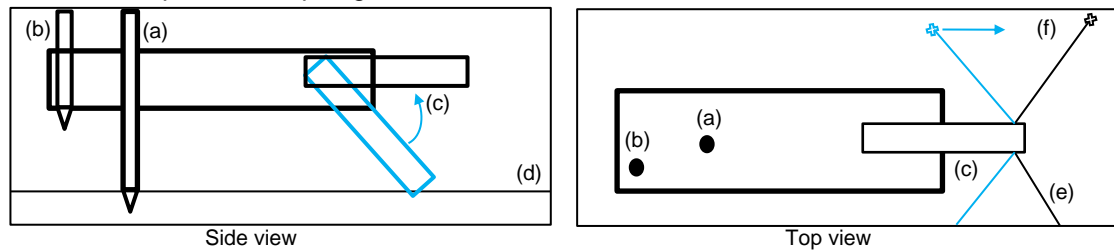


9. Start again from step 3.
 Proceeding in the direction when the CSD stopped to relocate the spud, the process of swinging and stepping as outlined in steps 3. to 5. continues until the maximum step is reached again.



10. Repeat steps 3. to 9.

When the cutterhead teeth need to be replaced or when the side anchors (f) need to be relocated the operation stops again until these issues have been resolved.



This thesis will focus on the activities taken in step 3. to step 6., the starting situation is, therefore, a vessel with both the spud and ladder already lowered. The simulation ends before the maximum carriage step has been made.

1.3 Problem definition

On the first of July 2017, a Boskalis press release announced that their newest, largest and most powerful Cutter Suction Dredger named the Helios, had been taken into service. With an equally large and powerful sister ship planned to be delivered in 2020, Boskalis thought it was time to develop an accurate time domain model to further investigate the exact behavior of these vessels.

Since the 1980s various studies to describe the behavior of CSD's have been made. These models were usually limited to study the responses in the frequency domain. The limitations of the frequency domain impose a linear approach to the whole system. The combination of a stiff mooring system, hydrodynamic interaction and continuously changing soil reactions causes the system to be dynamically challenging and nonlinear. In order to be able to include these nonlinear effects occurring during the operation of a CSD, a time domain analysis is necessary.

Several advanced programs already exist to calculate the hydrodynamic interaction between a ship and waves in the time domain. Using this existing software can reduce the complexity of the problem, leaving only the development to correctly model the mooring system and soil cutting interaction to be researched.

1.4 Research Objective

The objective is to develop a numerical model which enables the ability to obtain insight into the dynamic behavior of a cutter suction dredger. The model will be applied in a time domain analysis of its operation, including the hydrodynamic interaction, mooring forces and cutting reaction forces.

Therefore the main research question is "How to accurately model the forces working on a Cutter Suction Dredger in operation?"

To achieve this the following related questions have to be answered.

- Which model is most suitable for an accurate description of the spud pile and carriage?
- How can the cutting process be modeled by including the cutting history?
- How to obtain accurate swing forces and velocities?
- Should the vessel and ladder be modeled as a single rigid body or should the ladder be modeled as a separate body in the hydrodynamic analysis?

1.5 Approach

The software to model the hydrodynamic interaction in a time domain analysis which will be used in this research is the Ansys AQWA suite. This provides the possibility to include an external script in Python which will be responsible for calculating the mooring forces and cutting forces. Using these forces as additional input the interaction, between waves, soil and structure can then be fully executed.

Since the problem is quite complex, with each specific component showing a particular type of behavior, the creation and testing of the model will be done gradually and with increasing complexity. Each component will be examined on its own and tested accordingly before the interaction with other components will be investigated. This thesis is set up in roughly the same order as the work was executed, therefore the following approach is also a good indication of the general thesis outline.

The order in which the complexity increases is:

1. Frequency domain analysis of the Helios
 - a. Free floating
 - b. Moored with the spud pile
 - c. Cutting soil while moored with the spud pile
 - d. Comparison with the program Octopus Seaway
2. Free floating in time domain analysis
 - a. Single rigid body
 - b. Two rigid bodies
3. Moored using spud
 - a. Rigid carriage
 - b. Flexible carriage
4. Swinging without soil, modeling of winch forces
 - a. Static force
 - b. Dynamic force
5. Addition of Soil forces
 - a. Static soil forces
 - b. 1 Degree of Freedom ladder motions
 - c. Full interaction
 - d. One Body vs. Two Body
 - e. Addition of waves
 - f. Effects of a flexible spud carriage

2 Helios

2.1 Overview



Figure 4 The Helios

The Helios is Boskalis' newest Cutter Suction Dredger. The vessel, including ladder, is 152 meters long and has a draught of 5.35 meters, with a maximum of 6 meters. These dimensions make this ship belong to the category of self-propelled mega cutter suction dredgers. An interesting feature is that the breadth of the ship, with a maximum of 28 meters, is not constant over the length of the vessel. To prevent excessive peaks due to roll motions on the spud pile at the bow while maintaining stability at the aft. Therefore, the vessel has the full breadth around the ladder recess and decreases towards the front where the spud is located. With a total installed power of 23,886 kW, of which 7,000 kW in cutting power, it is one of the most powerful CSD's in operation today. The ladder with cutterhead has a mass of 2,020 tonnes, which allows it to cut very hard soils and rock. The ladder measures 55 meters in length which gives a maximum cutting depth of 35 meters at a 60 degrees angle. Furthermore, it is equipped with a flexible spud carriage which reduces the loads on the spud due to long waves, thereby increasing its workability at sea.

Table 1 Dimensions of Helios with ladder horizontal

Variable	Value	Unit	Remarks
Length	152	m	Full length including cutterhead crane
Breadth	28	m	Maximum breadth
Draught	6.0	m	Fully loaded
G'M	5.0	m	Metacentric height
LCG	63.1	m	Longitudinal Coordinate of the CoG
VCG	9.3	m	Vertical Coordinate of the CoG
k_{xx}	8.7	m	Transverse radius of gyration
k_{yy}	38.5	m	Longitudinal radius of gyration
k_{zz}	39.1	m	Vertical radius of gyration
Displacement	16747	tonnes	Fully loaded
Ladder angle	0	Degrees	Fully hoisted

2.2 Cutting at -20 meters

For this assignment a cutting depth of 20 meters will be investigated. The distance from the ladder pivot to the end of the cutterhead mount is approximately 46 meters, from this it can be calculated that the cutting angle is about 30 degrees. The stability values for the ladder in horizontal position have already been calculated during the design of the vessel¹. From these calculations, the load case with the spuds upright and maximum deadweight has been chosen as reference. Using the values from

¹ Stability book by IHC for the Helios

this case, the required stability parameters will be calculated for the case where the ladder is submerged at -20 m.

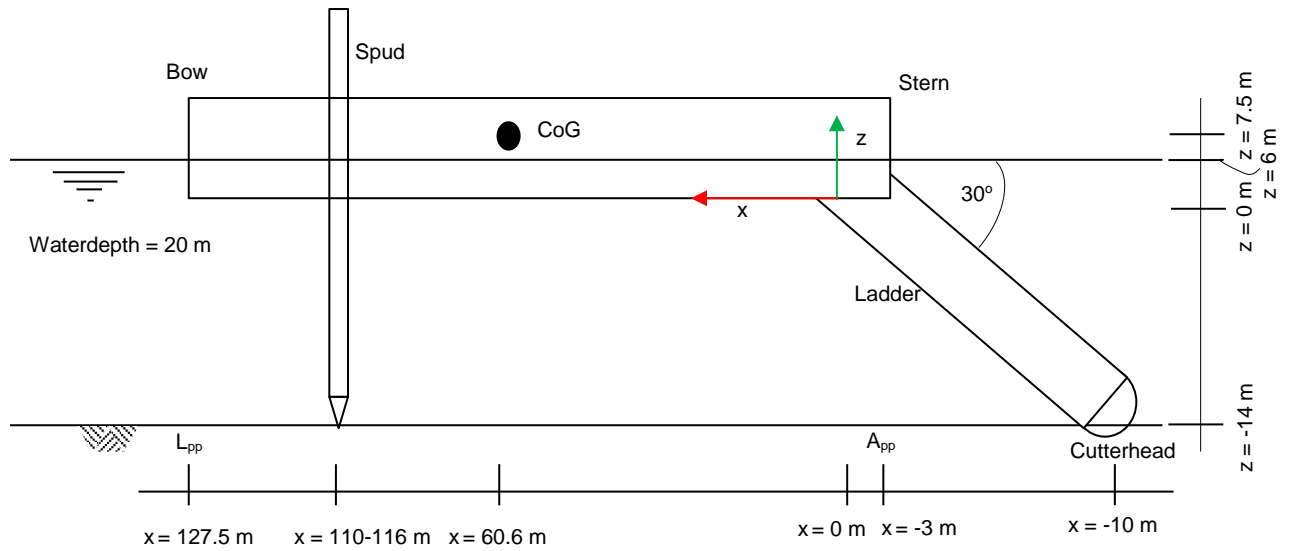


Figure 5 Side view of Helios cutting at -20 m

It should be noted that general ship convention for the axes places the ladder at the rear of the ship. This might be a bit confusing as the local axes of the cutterhead are in opposite direction, the front of the cutterhead is actually the point furthest in the back of the ship. This also means that starboard and port side are reversed when looking at the local axes system. To avoid confusion the ship's axes convention is used unless stated otherwise. In all cases the vertical z-axis is positive from the seabed up towards the water surface.

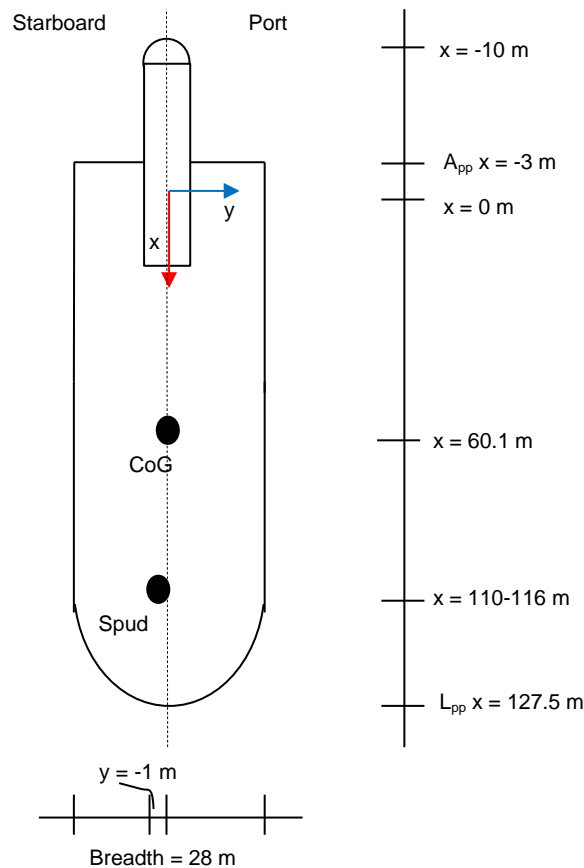


Figure 6 Top view of cutting at -20 m

2.2.1 Determining the new center of gravity

In hoisted/horizontal position the Center of Gravity (CoG) for the ladder and ship are located at LCG = 63.1 m from A_{pp}, VCG = 9.3 m above the keel and TCG = 0.079 m from the centerline, with a total displacement of 16727 tonnes. The main spud pile can be subtracted from this as during operation it will rest on the seabed and not contribute to the mass distribution. This means a mass of 250 t with LCG = 114 m, VCG = 24 m and TCG = -1 m has to be removed from the mass distribution. The next step is then to rotate the ladder to 30 degrees and calculate the new mass distribution. It should be noted that the center of gravity of the Helios is slightly out of the centerline due to the spud recess being asymmetrically placed in the hull. The CoG is only 0.05 meters out of the centerline but this will generate a transverse spud force nonetheless.

Table 2 Mass distribution overview

Component	Displacement (tonnes)	LCG from A _{pp} (m)	VCG above keel (m)
Total	16727	63.1	9.3
Spud (raised)	250	114.0	24.0
Ladder horizontal	1972	16.0	9.3
Ship without ladder and spud	14505	68.7	9.0
Ladder at -20m	1972	13.1	0.7
Ship with ladder at -20m	16477	60.6	7.5

With the ladder at -20m the buoyancy of the vessel will change as well. The total waterplane area can initially be estimated as $16727 \cdot 10^3 / 6 = 2787 \cdot 10^3 \text{ m}^2$. Using the figure below with specifications of the contribution to the buoyancy of the ladder per compartment the buoyancy of the ladder was determined to be about 480 t, making the submerged mass of the ladder 1.540 t. This means the new draft of the vessel is now $16227 / 2787 = 5.8 \text{ m}$.

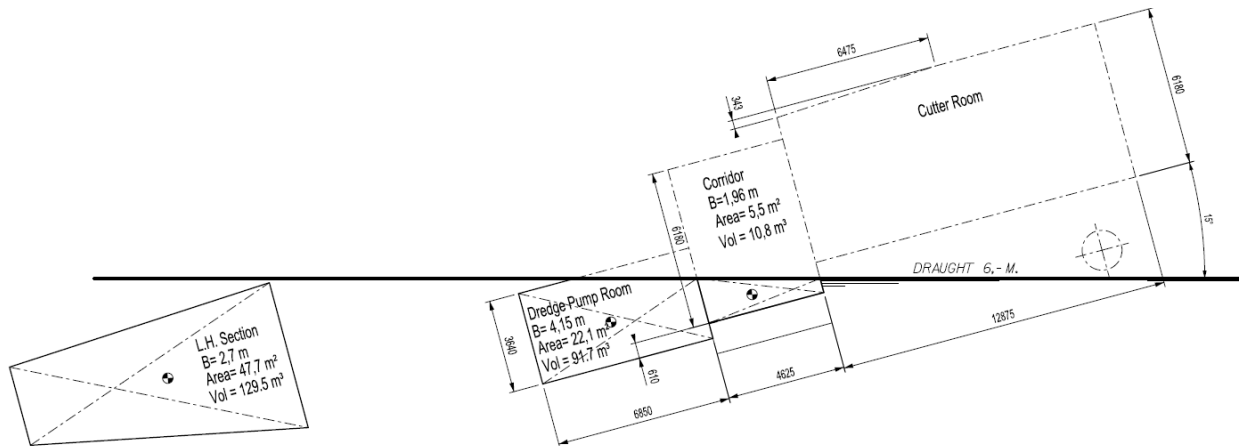


Figure 7 Buoyant compartments of ladder, for an angle of 15 degrees

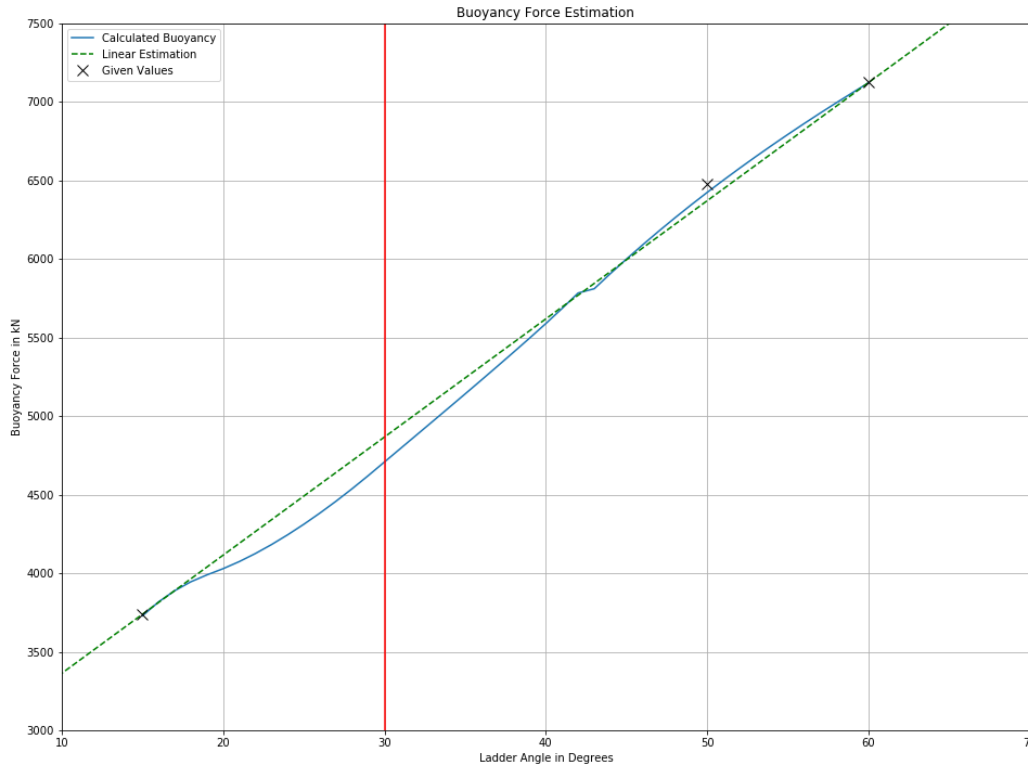


Figure 8 Graph to determine additional buoyancy through ladder angles

Now that the new draft is known, the stability parameter G'M needs to be updated. The value of G'M is known as the metacentric height, a parameter which is a good indication of the initial stability of a vessel and its natural roll period. The metacentric height GM has to be adjusted with the value of GG' if storage of liquids on the vessel can reduce the stability because of the free surface effect, the adjusted metacentric height is written as G'M.

For the situation where the draught is 6m, the distance from keel to metacenter KM is given as 14.471m and the free surface correction is GG' = 0.181m. Using G'M = KM – KG – GG' = 14.471 – 7.51 – 0.181 = 6.8 m. The final stability parameters that need to be determined are the radii of gyration. Simplifying the vessel as a collection of regular beams can give a good estimate on the radii of gyration.

$$k_i = \sqrt{\frac{\sum \frac{m_n}{12} * (B_n^2 + H_n^2) + m_n * ((y_n - y_{CoG})^2 * (z_n - z_{CoG})^2)}{\sum m_n}}$$

In this formula per radius of gyration *i* and beam element *n* the following variables are used:

- k_i = radius of gyration for i = xx, i = yy, i = zz
- m_n = mass of beam *n*
- B_n = Width/Length, beam *n*
- H_n = Height/Width of beam *n*
- y_n = Transverse/Longitudinal centroid of beam *n*
- y_{CoG} = Transverse/Longitudinal coordinate of CoG
- z_n = Vertical/Transverse centroid of beam *n*
- z_{CoG} = Vertical/Transverse coordinate of CoG

The resulting radii of gyration are k_{xx} = 9.5 m, k_{yy} = 35.7 m, k_{zz} = 36.1 m.

Table 3 Dimensions of the Helios with ladder at -20 m

Variable	Value	Unit	Remarks
Length	137.5	m	Full length including cutterhead crane
Breadth	28	m	Maximum breadth
Draught	5.8	m	Fully loaded
G'M	6.8	m	Metacentric height
LCG	60.6	m	Longitudinal Coordinate of the CoG
VCG	7.5	m	Vertical Coordinate of the CoG
k_{xx}	9.5	m	Transverse radius of gyration
k_{yy}	35.7	m	Longitudinal radius of gyration
k_{zz}	36.1	m	Vertical radius of gyration
Displacement	16227	t	Fully loaded
Ladder angle	30	Degrees	Cutterhead at -20 m

2.2.2 Two body approach

Under the assumption that the relative motion between ladder and hull is sufficiently small to neglect the whole system can be modeled as a single rigid body. However, to find the forces acting on the hinge between ladder and hull and the tension in the hoisting wires, see Figure 9, a multi-body approach is required. In this case, the CSD would be modeled as two separate rigid bodies, connected through a hinge and a spring, which can only give a force as a result of tension.

Separating the ladder from the rest of the CSD leads to the new radii of gyration for the vessel $k_{xx} = 9.2$ m, $k_{yy} = 33.3$ m, $k_{zz} = 34.1$ m and for the ladder, $k_{xx} = 9.0$ m, $k_{yy} = 16.0$ m, $k_{zz} = 13.5$ m relative to the local Center of Gravity.

Table 4 Radii of gyration of the individual bodies in 2 body approach

Radii of gyration	Value	Unit		Value	Unit
Hull			Ladder		
k_{xx}	9.2	m	k_{xx}	9.0	m
k_{yy}	33.3	m	k_{yy}	16.0	m
k_{zz}	34.1	m	k_{zz}	13.5	m

In Figure 9 the hoisting wire is visible, which runs through 3 sheaves on each side of the ladder, leading to a total of 6 times that the wire is passed through a sheave. The sheaves increase the unstretched length l_0 of the wire before it is loaded; for 6 sheaves the wire becomes 12 times the distance between ladder and A-frame. For a water depth of 20 m the distance between the A-frame and the top of the ladder is approximately 26.5 meters, leading to a total wire length of $L = 12 \cdot 26.5 = 318$ meters. Since the input for a wire in AQWA requires the unstretched length to be given and the sheaves cannot be taken into account directly, a reduction of the stiffness of the wire has to be made. In reality the stiffness of the wire is $EA = 2 \cdot 10^{11} \cdot (\pi/4) \cdot 0.076^2 = 9 \cdot 10^8$ N/m with an unstretched length $l_0 = 316.2$ m. This length is much longer than the distance AQWA will see and therefore this needs to be reduced. When lowered to -20 m, the strain in the wire is $\epsilon = (318 - 316.2)/318 = 0.0057$. To achieve a similar stiffness in AQWA the value of $EA = 1 \cdot 10^7$ N/m is used, which leads to a corresponding unstretched length of 26.2 m.



Figure 9 A-frame with hoisting wires visible and ladder hoisted

2.3 Drag Force

When a ship has a relative velocity compared to the surrounding water, it experiences viscous drag. A cutter suction dredger rotating around the spud pile will also cause drag as it will have a rotational velocity in the water due to the yaw motion. The lateral velocity of the hull resulting from the rotation causes friction with the water. The velocity profile increases as the distance from the spud increases. This results in the highest lateral velocity, and therefore also the highest contribution to the total drag force on the vessel, to occur at the aft of the ship, where the cutterhead is located.

AQWA by itself does not take viscous effects into account. This means that both viscous damping and viscous drag are unaccounted for. There are several options to add damping and drag coefficients, one of these options is adding a linear 6x6 damping matrix in AQWA-LINE.

Drag is actually a nonlinear phenomenon; the drag force is related to the velocity squared. Therefore it also worth considering taking the drag into account in the external Python script. In the model of the CSD, the drag is primarily expected to be a result of the angular velocity ω due to the yaw motion around the spud pile.

The general equation to calculate the drag force is given by

$$F_{drag} = \frac{1}{2} * \rho * v_x * |v_x| * C_D * A_x$$

Integrating over the submerged part of the hull of the vessel and using that the speed at an arbitrary point x at distance R_x from the spud during a swing is $v_x = \omega * R_x$ and that the area with draft H is $A_x = H * R_x$, the equation then becomes

$$q_x = \frac{1}{2} * \rho * C_d * (\omega * R_x) * |\omega * R_x| * H * R_x$$

Integrating this load over the length of the vessel will lead to finding the sideways force and moment due to drag.

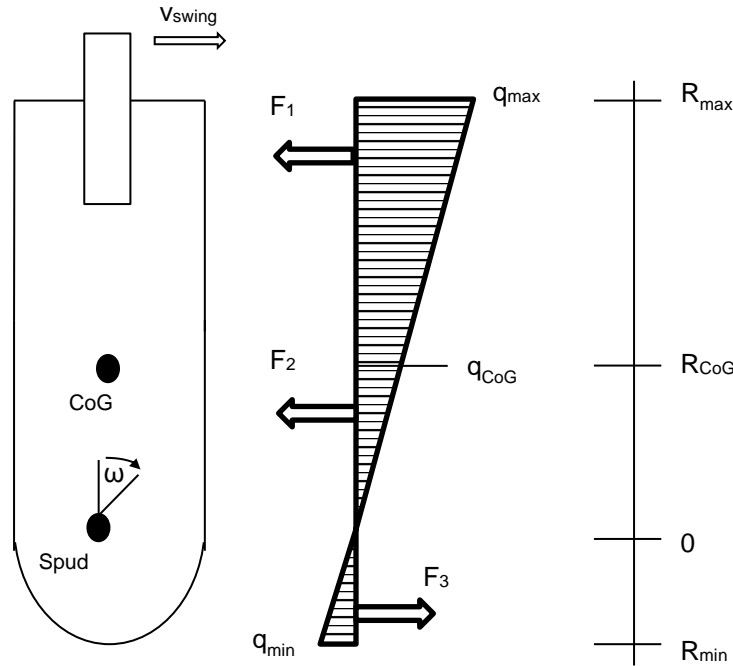


Figure 10 Schematic of distributed drag force

Since AQWA calculates the motions and forces at the CoG, the drag force needs to be calculated as a moment around the CoG instead of a moment around the spud. This can be done by dividing the distributed load into 3 parts, each consisting of a lateral Force and yaw Moment. At the CoG the distributed load can thus be summed as

$$F_1 = \frac{1}{2} * (q_{max} + q_{CoG}) * (R_{max} - R_{CoG}) = \frac{1}{4} * \rho * C_D * H * \omega * |\omega| * (R_{max}^3 + R_{CoG}^3) * (R_{max} - R_{CoG})$$

$$M_1 = F_1 * \frac{2}{3} * (R_{max} - R_{CoG}) = \frac{1}{6} * \rho * C_D * H * \omega * |\omega| * (R_{max}^3 + R_{CoG}^3) * (R_{max} - R_{CoG})^2$$

$$F_2 = \frac{1}{2} * q_{CoG} * R_{CoG} = \frac{1}{4} * \rho * C_D * H * \omega * |\omega| * R_{CoG}^4$$

$$M_2 = F_2 * \frac{1}{3} * -R_{CoG} = -\frac{1}{12} * \rho * C_D * H * \omega * |\omega| * R_{CoG}^5$$

$$F_3 = \frac{1}{2} * q_{min} * R_{min} = -\frac{1}{4} * \rho * C_D * H * \omega * |\omega| * R_{min}^4$$

$$M_3 = F_3 * -\left(\frac{2}{3} * R_{min} + R_{CoG}\right) = \frac{1}{4} * \rho * C_D * H * \omega * |\omega| * R_{min}^4 * \left(\frac{2}{3} * R_{min} + R_{CoG}\right)$$

Leading to $F_{drag} = F_1 + F_2 + F_3$ and $M_{drag} = M_1 + M_2 + M_3$ at the CoG.

The value of C_D is not precisely known. The ship is mostly flat underneath, which makes a representation by a cylinder incorrect, however, the walls of the hull are slightly rounded, making it not rectangular shaped either. The value in this research is taken as $C_D = 1$, for reference a study by Journée (1993) takes the value of $C_D = 1.5$ for a rectangular barge. The relation between total drag force and C_D is linear which means that a C_D which is 2 times as big will give a total drag force of also twice the force of the original C_D . Also note, that the distance R changes as the spud takes steps forward.

Table 5 Parameters for drag force

Variable	Value	Unit	Remark
ρ	1025	kg/m ³	Density of seawater
H	6	m	Draft of vessel
C_D	1 – 1.5	-	Drag coefficient
Rmax	110	m	Distance from spud to aft of hull
RCoG	43.3	m	Distance from spud to CoG
Rmin	20	m	Distance from spud to bow
ω	0.0018 – 0.0055	rad/s	Angular yaw velocity

2.3.1 Linearized drag

Throughout the various test runs of the Python script, it became apparent that the calculation of the drag force in the Python script would require a reduction in timestep to maintain stability. Therefore, it would be very convenient to be able to use the linear damping matrix input in AQWA. To verify whether this is possible for the swings around the spud pile, a comparison is made between the linearized forces and the actual quadratic forces. The use of a linearized drag force is very plausible due to the limited velocity range at which the CSD can rotate. A tangential velocity for the cutterhead of 1 m/s is extremely high, which comes down to an angular velocity around the spud pile of 0.009 rad/s. During operation a tangential velocity of about 0.2 to 0.6 m/s is normal, depending on the soil type being cut. This comes down to angular velocities ranging from 0.0018 rad/s to 0.0055 rad/s. This range is sufficiently limited to linearize the drag force without compromising much on accuracy, see Figure 11. Furthermore, taking into account that many exact values, such as the exact value for C_D , are unknown, it can be reasoned that a linearized drag force will be sufficiently accurate for the purpose of this research. Using a tangential velocity of 0.4 m/s or angular velocity of 0.0036 rad/s, and filling in all the other variables, the linearized drag force is $F_{drag} = d_{26} = 5 \cdot 10^8$ Ns/rad and moment around the CoG is $M_{drag} = d_{66} = 1.6 \cdot 10^{10}$ Nms/rad.

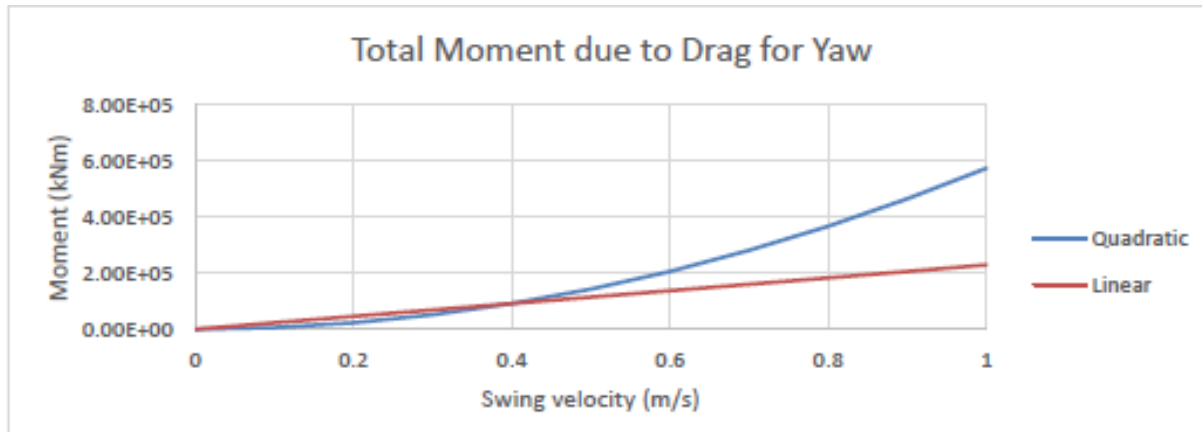


Figure 11 Drag force comparison for a linearized velocity of $v_{swing} = 0.4$ m/s

3 General Modeling

3.1 Input in AQWA

The AQWA-suite consists of 5 programs which each have their own specific function. In this research only the programs FER, LINE and DRIFT are used, of which DRIFT has the option to add a custom script for external forces. FER and LINE are programs limited to the frequency domain and therefore can't incorporate external forces.

Table 6 Overview of the AQWA suite

Program	Description
AQWA-LINE	Radiation diffraction potential solver in the frequency domain. It solves the hydrostatics and creates the RAO's for free-floating structures
AQWA-FER	Linear solver in the frequency domain which can recalculate the RAO's with the presence of mooring systems and irregular wave spectra
AQWA-LIBRIUM	Calculates the position of the structures when in equilibrium with the hydrodynamic forces.
AQWA-DRIFT	Time domain analysis using the RAO's calculated by AQWA-LINE.
AQWA-NAUT	Time domain analysis specifically for the situation where the waterplane area can change significantly due to varying hull shape or submersion of the deck.
Ansys Workbench	A Graphical User Interface for Ansys products, including the AQWA-suite

Before running any other program in the suite, AQWA-LINE always has to be run first to solve for the hydrostatics and RAO's. The hull geometry with its most important properties and a regular wave range are the mandatory input. In AQWA-LINE it is not possible to take mooring systems or other external influences into account.

To be able to take linear effects of mooring into account in the frequency domain AQWA-FER can be used. It takes the RAO's generated by AQWA-LINE and recalculates them using the additional parameters for mooring provided. AQWA-FER can also work with an irregular wave spectrum. Since the program is still limited to the frequency domain, any mooring system has to be simplified as a linear spring.

The file containing the output of either AQWA-LINE or AQWA-FER can then be used as input for AQWA-DRIFT. In AQWA-DRIFT the time domain analysis will be performed. In this research AQWA-DRIFT will use the output of AQWA-LINE, as the mooring system will be incorporated through the external Python script, and therefore the RAO's of the free-floating vessel should be taken.

AQWA-DRIFT uses a two-stage predictor-corrector method to calculate the solution to the equation of motion every timestep. In practice it is therefore observed that every timestep is calculated twice, which is important to know when communicating with an external force module. To distinguish between timesteps and the step of the predictor and corrector stage, the difference between the latter will be referred to as a stagestep. This means that two stagesteps are made during each timestep. The equation of motion is solved using the Cummins equations for all 6 degrees of freedom for each structure. According to Cummins (1962) the equations of motion for a floating rigid body can be written as:

$$\sum_{j=1}^6 \left\{ (M_{i,j} + A_{i,j}) * \ddot{x}_j(t) + \int_0^{\infty} B_{i,j}(\tau) * \dot{x}_j(t - \tau) * d\tau + C_{i,j} * x_j(t) = F_i(t) \right\}$$

For $i = 1, 2, \dots, 6$

It is important to know that the connection with an external force module, such as Python, only influences what happens on the right-hand side of the equation, as the left-hand side is all handled by AQWA internally. The process can be schematized as follows:

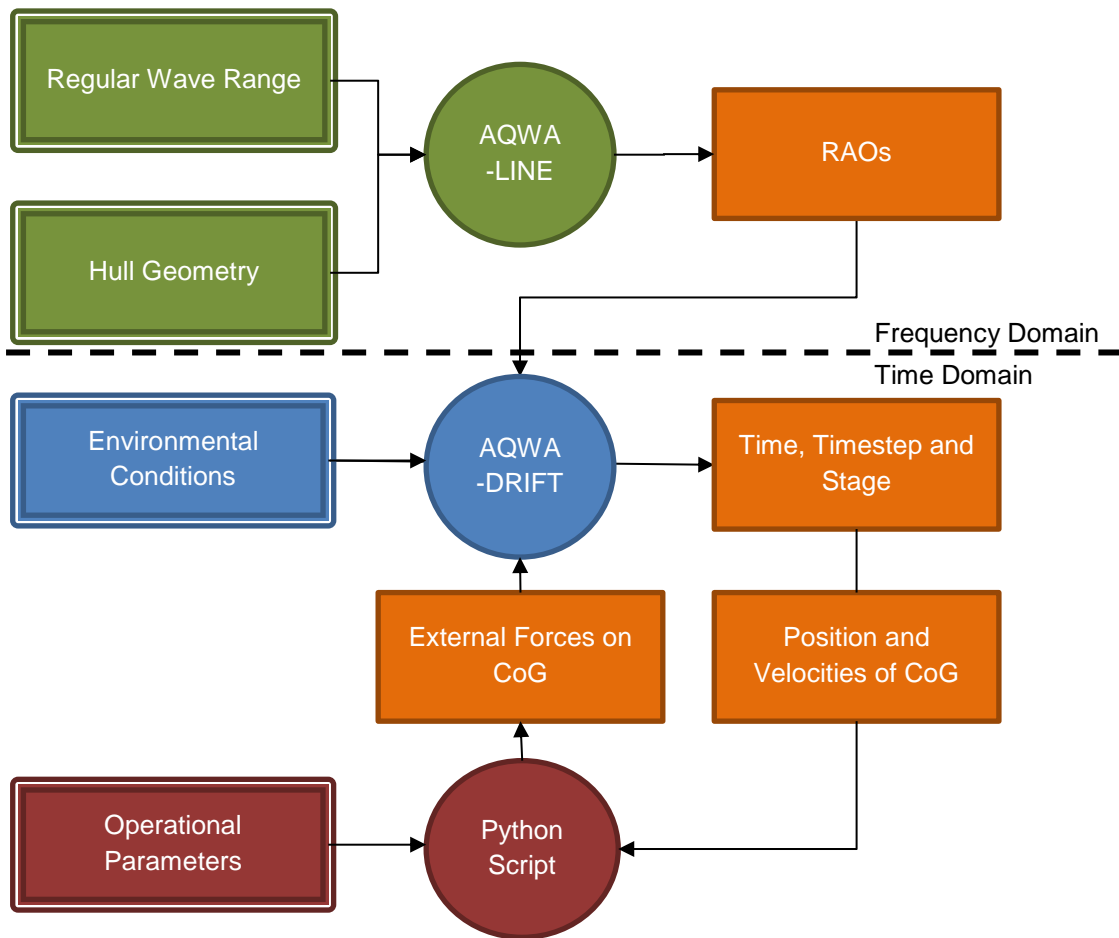


Figure 12 Overview of interaction

3.2 Python

Since the release of version 17 of AQWA, there is the possibility to communicate with the program through an external Python script. The communication between the script and the AQWA executable is done through a virtual server which sends and receives the data.

Besides running the server, the script also provides tools to translate the motion and forces of arbitrary points to, and from, the center of gravity of the structure. This is important because, as stated in the determination of the drag force, AQWA only performs calculations at the CoG. The communication between AQWA and the custom script is done by sending the position as 6x1 vector and velocities as a 6x1 vector of the CoG per structure to the Python script.

Specific points such as the location of the cutterhead can be defined at the beginning with their initial coordinates. The tools provided in the script then translate these points to their current position. Note that these points have to be defined in the Python script, and not in AQWA, where it is also possible to find and track points, but they are not accessible outside the program.

With the actual location of each point known and with the velocities of the CoG known, it is now possible to calculate the resulting force due to the motion of the vessel. The force is then translated back to the center of gravity, including the moment which is created if the force is not in line with the CoG. This results in a 6x1 force vector per structure which is sent back to AQWA. A small note that it doesn't matter how many different components in the Python script generate a force, at the end of the stagestep it is all summed together at the CoG and only a single 6x1 force vector is sent back to

AQWA per structure. A consequence is, that if there are a force pushing and an opposite force pulling at equal distance of the CoG, with the same magnitude, that the force vector which is sent back to AQWA is 0.

It is important to know that direction of all the vectors are related to the Fixed Reference Axes (FRA), also known as the Global Axes. In practice this means that if a vessel rotates with a force fixed to a local point, the direction of the force also should be rotated prior to translation to the CoG. An example is a force located at the bow of the vessel, which in the initial condition will be pointed in x-direction causing a surge motion. If the vessel is rotated 90 degrees, and the same force is applied at the bow, it will now cause a yaw and sway motion because the vessel rotated but the force did not.

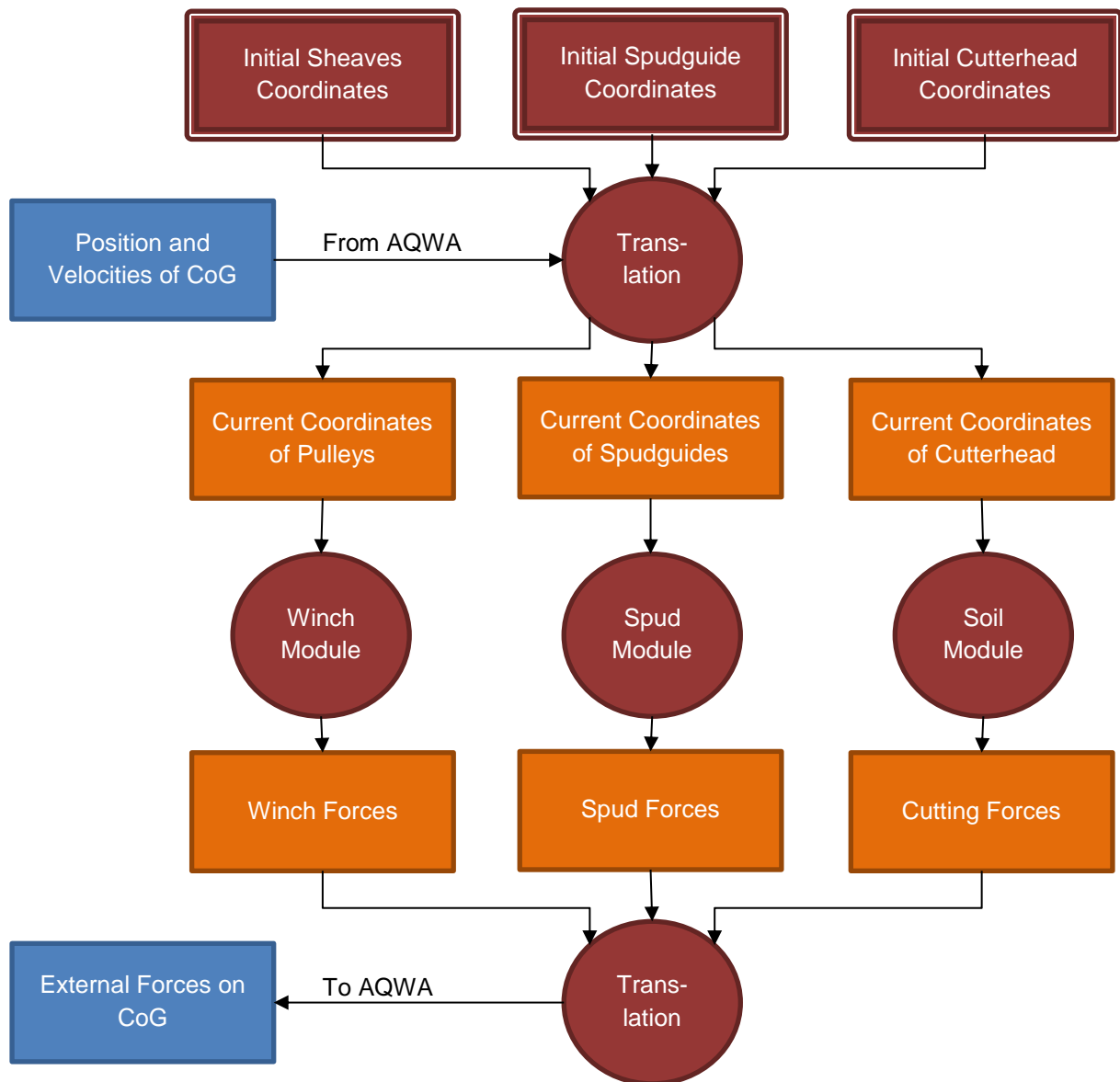


Figure 13 Flow chart of the custom Python script

3.3 Geometric models

Using the line plan of the Helios a 3D model was created in Rhinoceros 5. This model can be used to create the points and panels in the calculation software. For AQWA the easiest way to do this is to import the model into Workbench and then create the mesh file. For Octopus Seaway it means to find all necessary points on the hull required to fill in the hull text file. It should be noted that the model in Seaway, and therefore also the model used in the frequency domain comparison in AQWA, has the spud and ladder recesses closed. The model which has been used for the time domain analysis in AQWA has both areas open, although in the two body model a part where the ladder is 'inside' the hull is modeled as closed due to the very narrow lateral gap between hull and ladder which leads to errors in the potentials and could also lead to numerical resonance, creating standing waves at very high frequencies while in reality none occur. In order to prevent this and at the same time be able to have a diffracting model of the ladder, a sufficiently large gap between hull and ladder has to exist. The choice has been made to cut a part of the middle section open and model only the area near the cutterhead with diffracting panels.

Geometrically interesting numbers are:

- The cutterhead is located approximately 10 meters behind A_{pp} ($x = -10\text{m}$)
- the ladder becomes indistinguishable from the hull in the model, as it is found completely above the keel, at 20 meters forward of A_{pp} ($x = 20\text{m}$). The

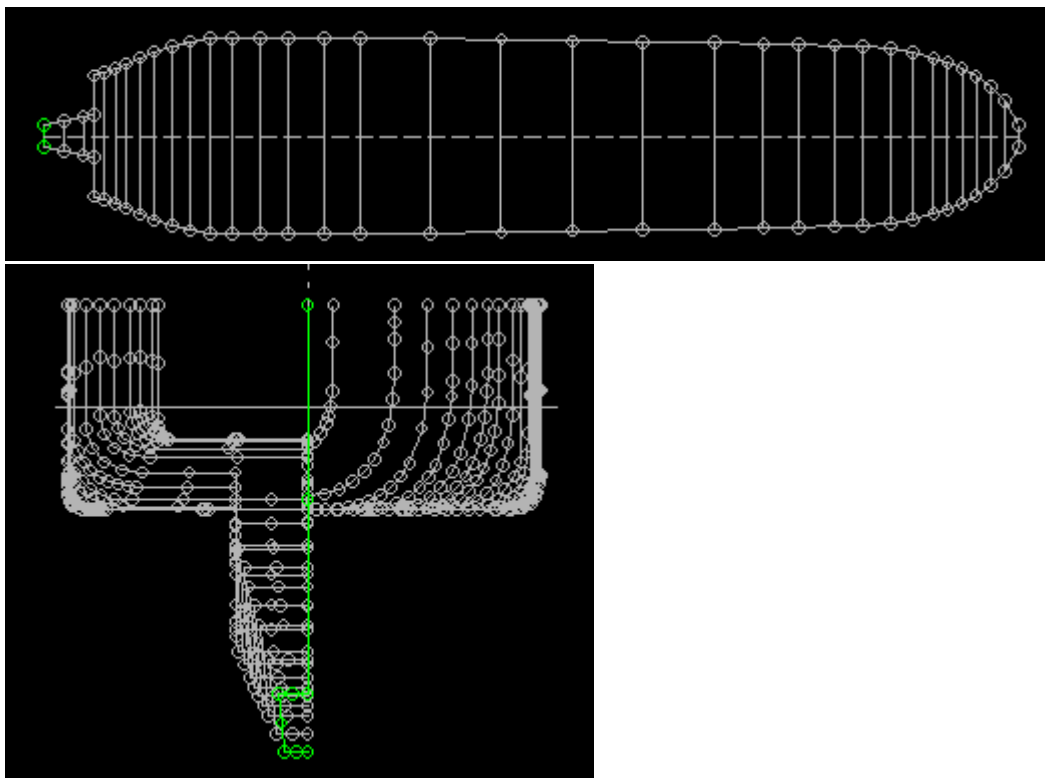


Figure 14 Overview of the hull in Octopus Seaway, note the slightly changing breadth in the top view

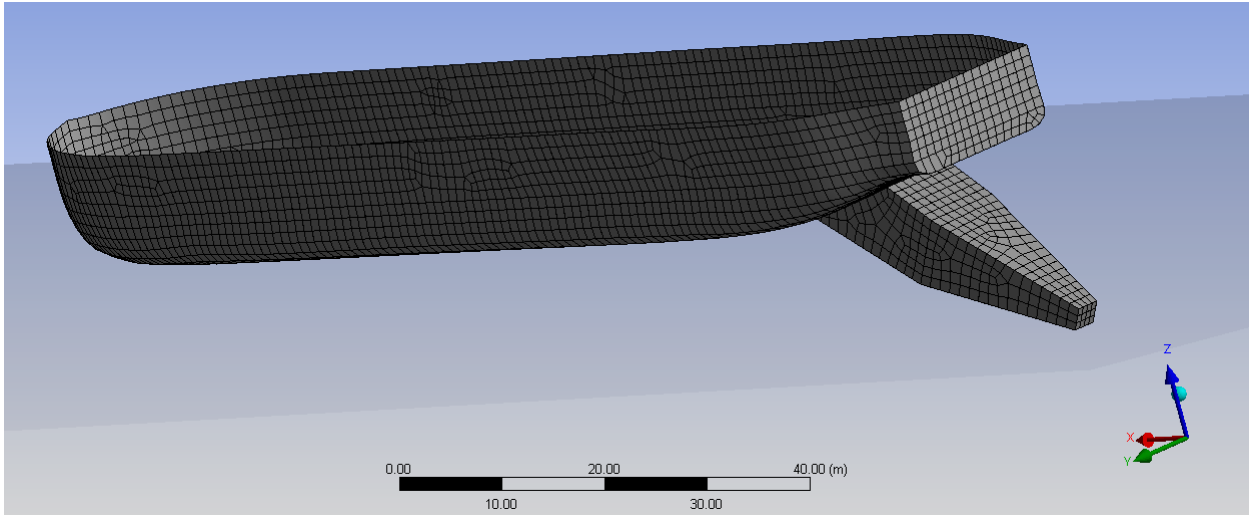


Figure 15 Overview of the Hull with mesh in AQWA for use in the Seaway comparison

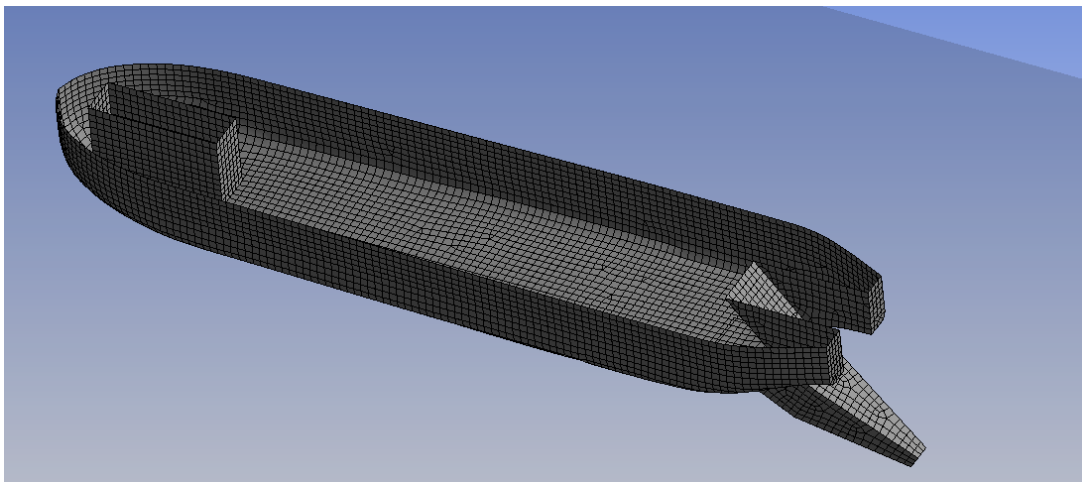


Figure 16 Single rigid body model used for time domain

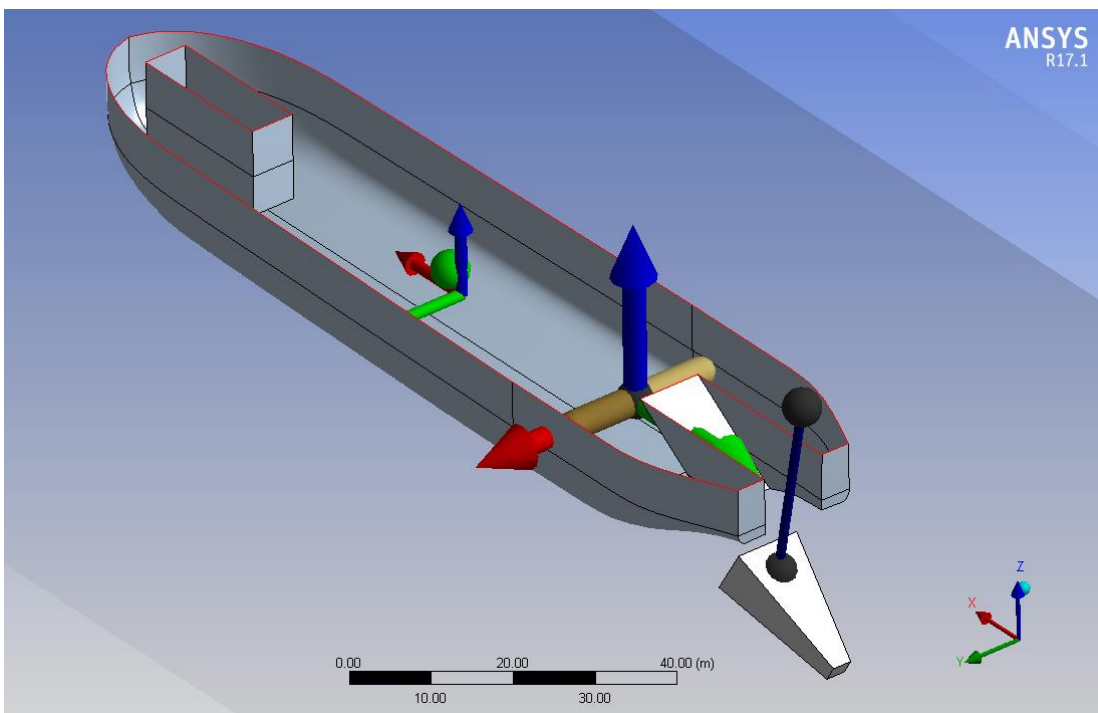


Figure 17 Ladder and hull as 2 separate rigid bodies, connected to each other with hinge and hoist wire.

4 Frequency domain

4.1 Free Floating

AQWA uses the results of AQWA-LINE, hydrostatics and RAO's, for the time domain analysis in AQWA-DRIFT. Therefore it is important to verify whether the results of AQWA-LINE are realistic. The program Octopus Seaway uses diffraction in combination with strip theory. It has been used in-house Boskalis for many years and its advantages and drawbacks are well known. Therefore a comparison between the results of both programs is made in order to check whether AQWA can be used for the time domain analysis. First, both models will be compared free floating as a single rigid body, then springs will be added to model the spud and soil reactions. The comparison including springs will be done with AQWA-FER instead of AQWA-LINE.

Once the panel mesh in Workbench had been created the input was completed with regular waves ranging from 0.05 rad/s to 2.0 rad/s and wave height $H_s = 1$ m. The wave directions were taken every 22.5 degrees, ranging from 0 degrees to 360 degrees, leading to a total of 17 directions in AQWA and 9 in Seaway because it mirrors the directions after the 180 degrees mark.

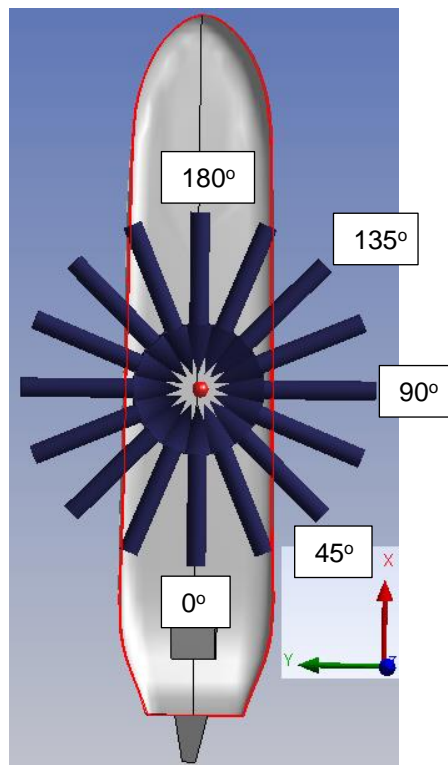


Figure 18 Wave directions

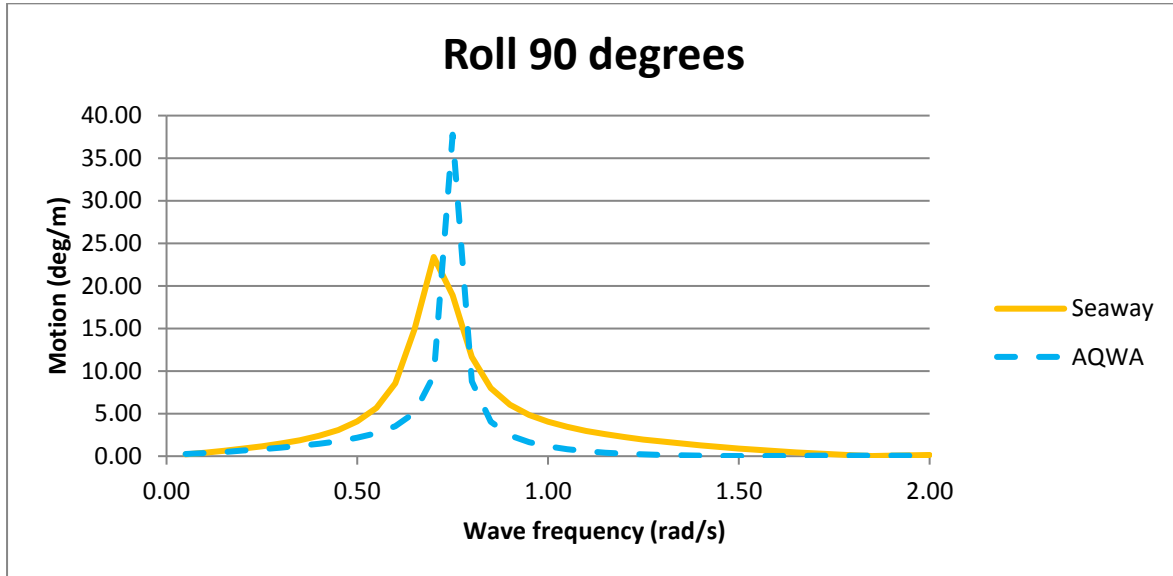


Figure 19 Difference in damping and displacement of AQWA and Seaway

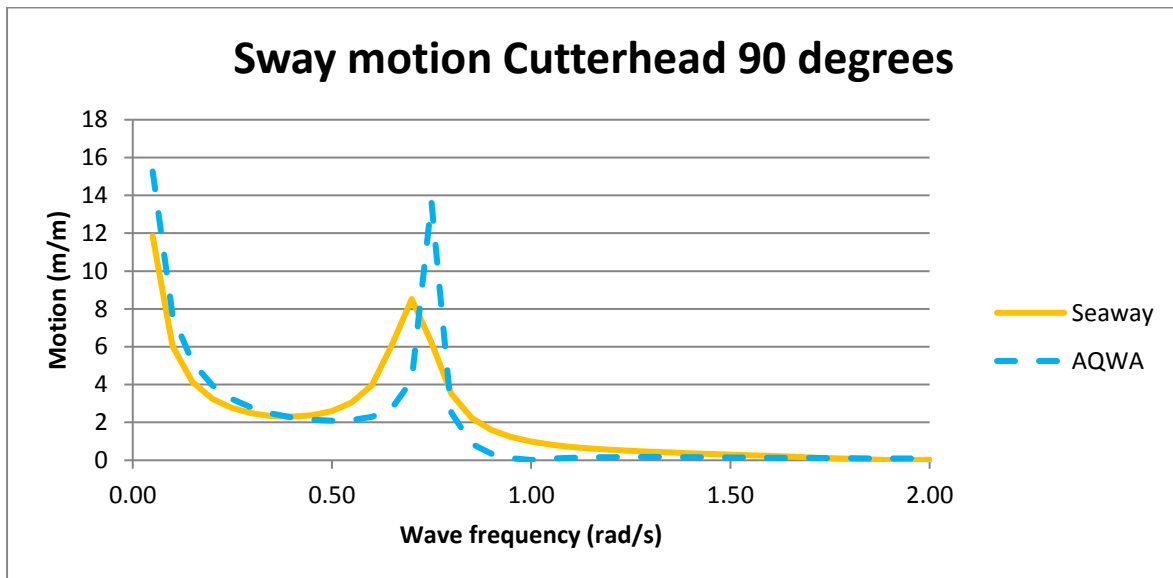


Figure 20 Comparison of free-floating responses between AQWA and Seaway

The graphs, which can be found in Appendix A, show good similarities, with the largest difference occurring in the roll motion for waves coming from an angle of 90 degrees. As has been noted before, AQWA does not take damping, other than potential damping, into account while in Seaway the option is used to add an empirical roll damping formula. A small shift in the peak in roll motion is visible, this is most likely caused due to the fact that the mesh in AQWA is stated to have a volume larger than the displacement of the ship. This makes sense given the fact that the spud recess and ladder recess, as well as open parts of the ladder itself, have been closed in the mesh, leading to a larger displacement than found in reality. A difference in the mass used in both programs explains the shift in the peaks, the difference in height is attributed to the addition of empirical damping in Seaway.

4.2 Modeling the spud pile with a single spring

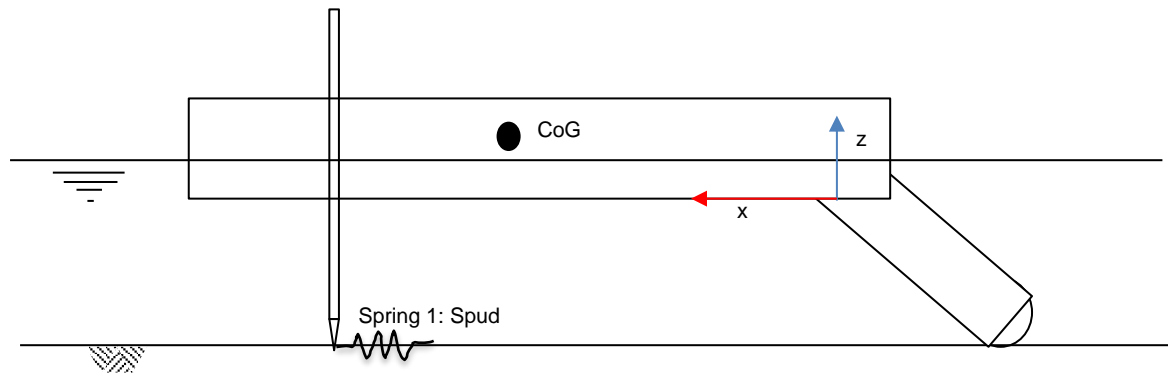


Table 7 Spring stiffness, 1 spring

Spring modeling Spud	Kx (kN/m)	Ky (kN/m)	Kz (kN/m)
Standard value	5000	7500	10
Variation range	2500-10000	2500-10000	0-10

As stated before this comparison will be done using AQWA-FER and Seaway. The results of the free-floating run in AQWA-LINE are used in combination with the input parameters of the spring in AQWA-FER. In Seaway the same input file can be used with the addition of the springs.

The next step is to run the calculations for a vessel with the spud lowered. This can be modeled using one linear spring connected at the location of the spud tip. Since the Helios is equipped with a flexible spud carriage, the spring stiffness in x- and y-direction will be different. The spring stiffness has been estimated to be 5000 kN/m in x-direction, and 7500 kN/m in y-direction. To simulate friction between the spud and the spud guides a 10 kN/m spring in z-direction is applied. A small note about the application of more than one spring, both programs create a single stiffness matrix in which the direction and magnitude of all the springs are summed. Therefore it makes no difference if 3 separate springs are used to create the combination described above or if a single spring with the correct magnitude and direction is placed.

Due to the fact that the spud is located 1 meter outside the centerline, there is a coupling between x- and y-motions, therefore a beam wave can cause an excitation in x-direction, this can be seen in Figure 21. In z-direction there is virtually no effect which can also be expected, due to the low stiffness value. Compared to the free-floating graphs a shift in the peak frequency can be seen in some motions, due to creating a stiffer system which results in a shift in the natural frequency.

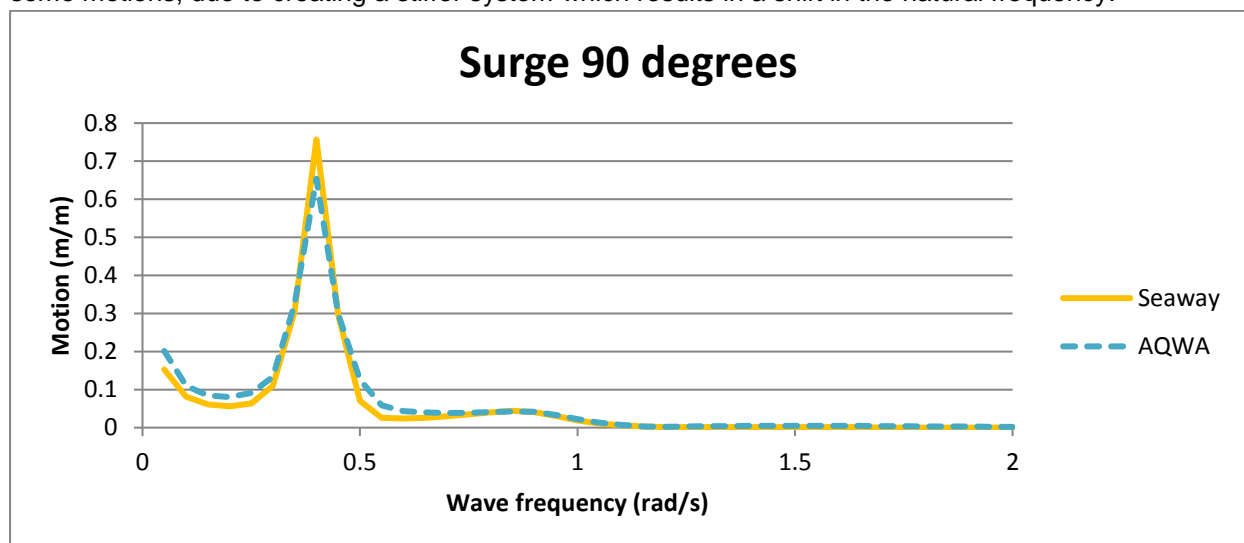


Figure 21 Surge response due to beam waves, due to the eccentrically placed spud

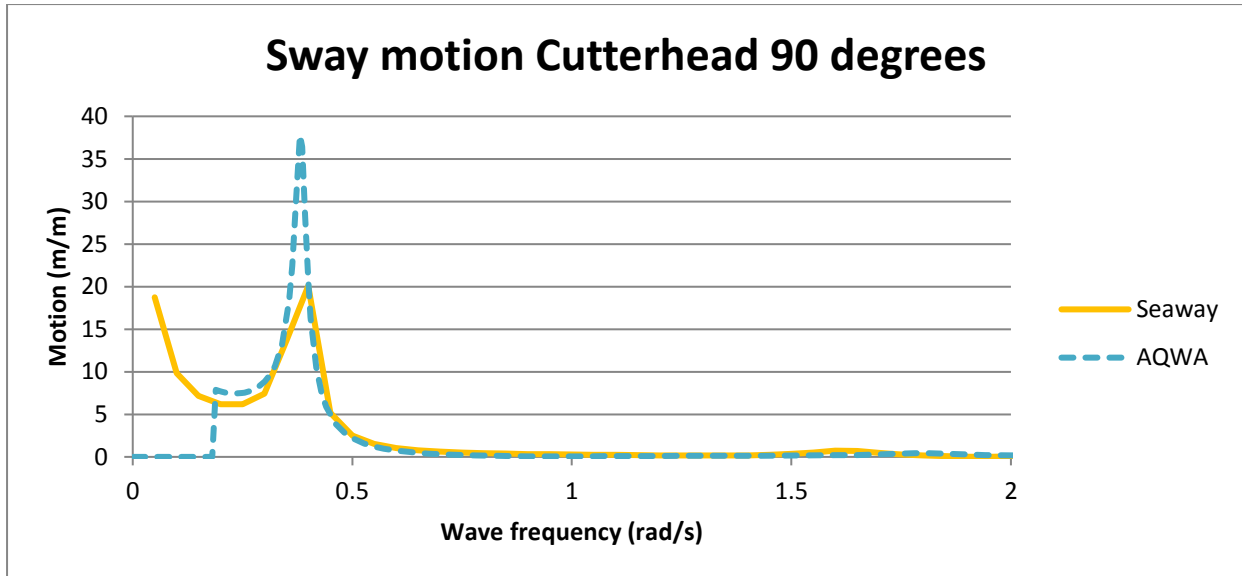


Figure 22 Comparison of AQWA - Seaway using one spring to model the spud reaction

The first graph shows a beam wave which results in a surge response. The eccentric location of the spud causes this, as a test run with the spud on the centerline showed the response to be practically zero. The difference between the two programs is a lot smaller and the adaptation of the attached mooring system seems to work well. The general trend is that AQWA estimates the responses slightly higher than Seaway. This can be seen in Figure 22 where the total response of the cutterhead is almost twice as large in AQWA-FER as the response in Seaway. The RAO's of both programs are more similar than their calculation for the cutterhead node, as can be seen in Appendix D.

4.3 Modeling the cutting process and spud pile with two springs

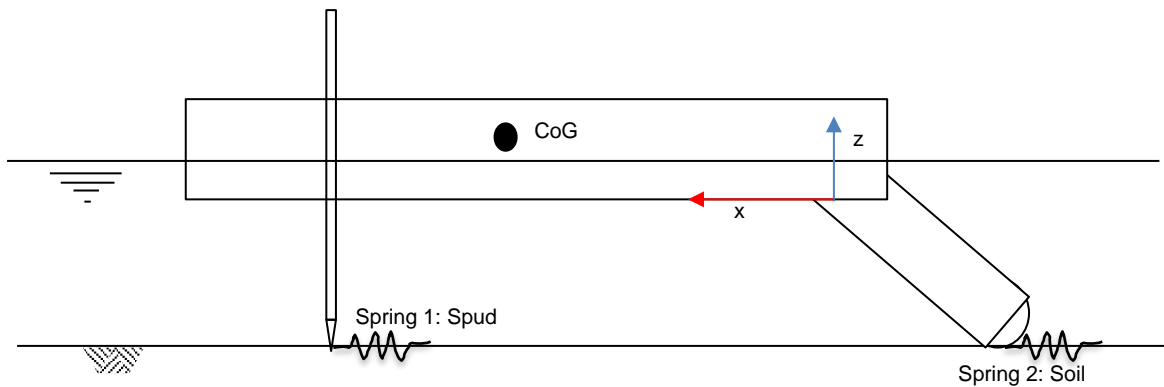


Table 8 Spring stiffness, 2 springs

Springs attached	Kx (kN/m)	Ky (kN/m)	Kz (kN/m)
Standard value spud spring	5000	7500	10
Standard value soil spring	100.000	100.000	100.000
Variation range soil spring	1000-100.000	1000-100.000	1000-100.000

Adding an additional linear spring will change the stiffness matrix used by both programs. The spring which is added represents the soil reaction from cutting. These forces can be quite large for hard soils and therefore the stiffness of the spring can become quite extreme as well. The value used for the soil spring is that of a very hard rock which can be approximated to be about 100,000 kN/m in x-, y-, and z-direction. This high stiffness should be visible in the motion RAO's. Since the calculation is done in the frequency domain, the consequences of the swing trajectory on the soil are not taken into account.

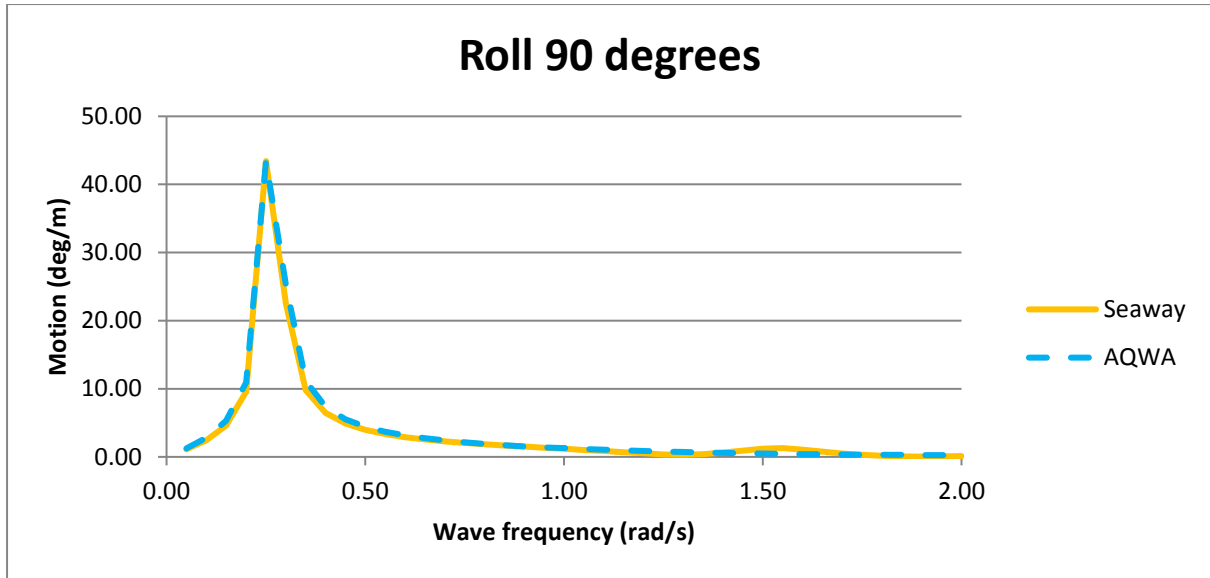


Figure 23 Comparison AQWA - Seaway with 2 springs for soil and spud reactions

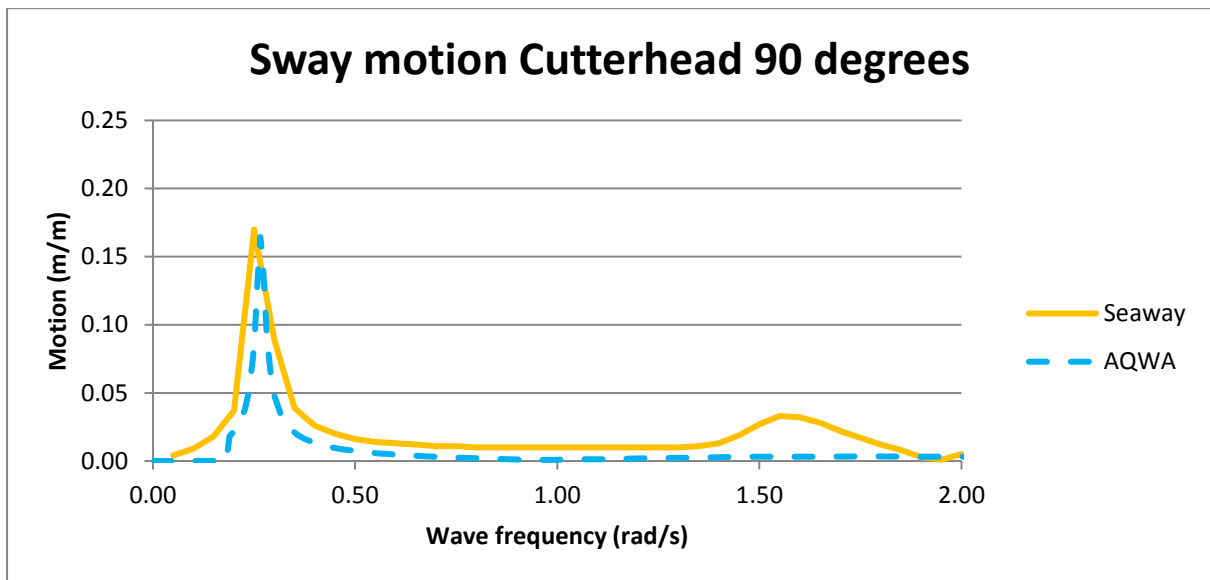


Figure 24 Comparison AQWA - Seaway with 2 springs for soil and spud reactions

The motion of the cutterhead is now very similar in both programs, most RAO's have also reduced greatly with the exception of the sway and roll in beam waves. This is most likely because the stiff spring in the program at the cutterhead and spud tip are both located at the seabed, this means that the only restoring force at the water surface is the water itself. The stiffness of the soil is much higher than that of the water which means that the vessel is more or less free to rotate in lateral direction, leading to large roll responses.

4.4 Conclusion

Comparing the situations of free-floating, a single spring for the spud and the complete situation of a spring for the spud and a spring for the soil, it can be seen that most responses are smaller when the cutterhead is in operation and largest if the spud is lowered but the cutterhead is not in operation. An exception is the sway and roll motions for 90-degree waves, where the situation of the cutterhead in operation leads to a larger response. Although some differences between AQWA and Seaway are visible, and some are to be expected as well, the results are generally sufficiently similar to be satisfactory. In general, for calculations in the frequency domain Octopus Seaway has a few advantages and performs the calculations much faster than AQWA, making it the better choice.

5 Spuds

5.1 Physical properties of the spud system

The spud pile is responsible for holding the cutter suction dredger in its place. It is a very stiff mooring system which is in part responsible for large reactions on the vessel. The spud is a heavy steel pile which is lowered onto the seabed in a freefall to penetrate the soil and provide a good point of anchorage. This means that the pile can have a slightly different behavior in soft soils than harder soils, as the penetration depth will vary.

The spud is held in its place at the vessel by the spud carriage. The spud carriage is responsible for transferring the forces of the vessel onto the spud pile. The contact points of the carriage with the spud are called spud guides. Usually, there is some margin for movement, thus the vessel can have a surge or sway motion of a few centimeters before the guides and spud make actual contact. Once this margin is passed the guides will also provide a friction force. This force may affect the heave motions of the CSD. The interaction with these guides can be modeled in a variety of ways. Independent of the modeling choice, the bending stress will be largest at the lower guide, as well as the shear stress. If these stresses exceed the yield stress plastic deformation will occur and the spud will have to be replaced. Of course in certain situations, the soil could fail prior to spud failure.



Figure 25 Spud pile

To reduce the moment acting on the spud, a flexible spud carriage is often installed on modern mega cutters. This carriage is attached to the hull through wires and cylinders filled with gas which allow additional controlled movement of the carriage creating a less rigid connection with the hull. Strain in the wires together with the stroke of the cylinders are responsible for additional motion. In general, it can be said that a flexible carriage can rotate about 2 degrees before its limit is reached and the connection with the hull can be taken as rigid. Of course deflection of the ship's hull, the guides, the connections and the carriage itself already reduce the overall stiffness of the system as well.

The cylinder activates once a threshold stress has been reached and continues to work until its maximum stroke has been extended. The presence of a flexible spud carriage causes nonlinear behavior and is mainly to reduce the loads due to motions in the pitch direction. A simple calculation can show that long head waves can cause a large moment on the spud.

As stated before the spud of the Helios is not located on its centerline but 1 meter portside of it.

A large cylinder is located between the guide which exerts a force on the spud to move the carriage forward. Because the spud is fixed in the soil, the vessel will then move in the opposite direction, allowing a new swing to be made to cut more soil. This process is called stepping forward.



Figure 26 Detailed view of the spud carriage

5.1.1 Theory

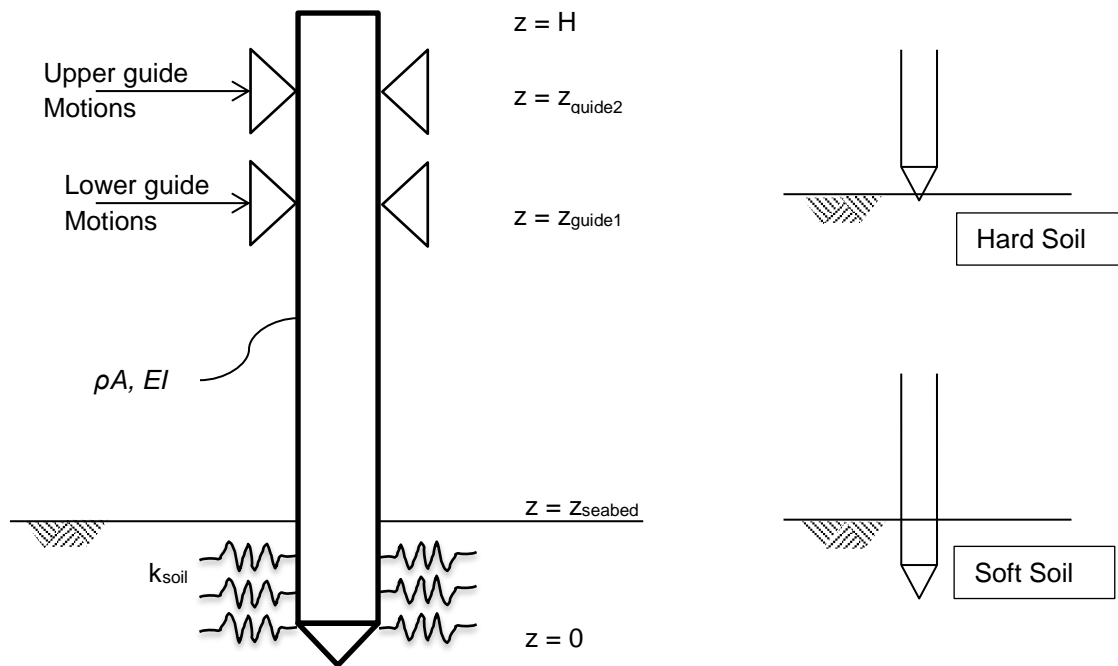


Figure 27 Schematics of spud in carriage and difference in penetration depth for hard and soft soils.

The spud has basically 3 points of external connection: the 2 spud guides and the soil, although in reality the step cylinder could be a 4th connection point, it is only active during stepping. The guides are unable to take up a moment and can thus be represented by pinned supports. In the case of extremely hard soil, the spud tip will not be able to penetrate the soil when dropped and this means that this also acts as a ball and socket joint which can be represented by a pinned support. In the case of softer soils, the spud tip will penetrate further, which means the soil will act more as a clamped connection which can take up a moment unlike the pinned joint for hard soils. The difference in penetration depth for two different soil types is visible in Figure 27.

Since this moment will bend in the opposite direction as the bending caused by the motion of the guides, there will be a point between the seabed and the spud tip where the moment changes of sign and thus is zero. Moving the pinned support from the seabed for hard soils to this point where the moment is zero for soft soils allows the use of a single model for all soil types. In Figure 28 is schematized how the length between lower spud guide and seabed, L_2 , has to be adjusted according to the penetration depth. It should be noted that the spud tip can move in the soil when high loads are involved since the soil is not infinitely stiff. Therefore when using a pinned support to model the soil should always be verified with this occurrence.

Note that if the soil is modeled as a collection of springs, that the total lateral force found will be more or less the same for hard and soft soils due to the stiffness k_{soil} varying with the soil hardness and the penetration depth compensating. For very hard soils k_{soil} will be very large, but since the spud will hardly penetrate, the contact area over which k_{soil} can act is much smaller. In comparison with softer soils, k_{soil} will be a much lower value but because the spud tip will go much deeper, the total contact area over which k_{soil} acts is quite large. The combination of the contact area with the stiffness should give fairly similar results for the lateral force found in both hard and soft soils.

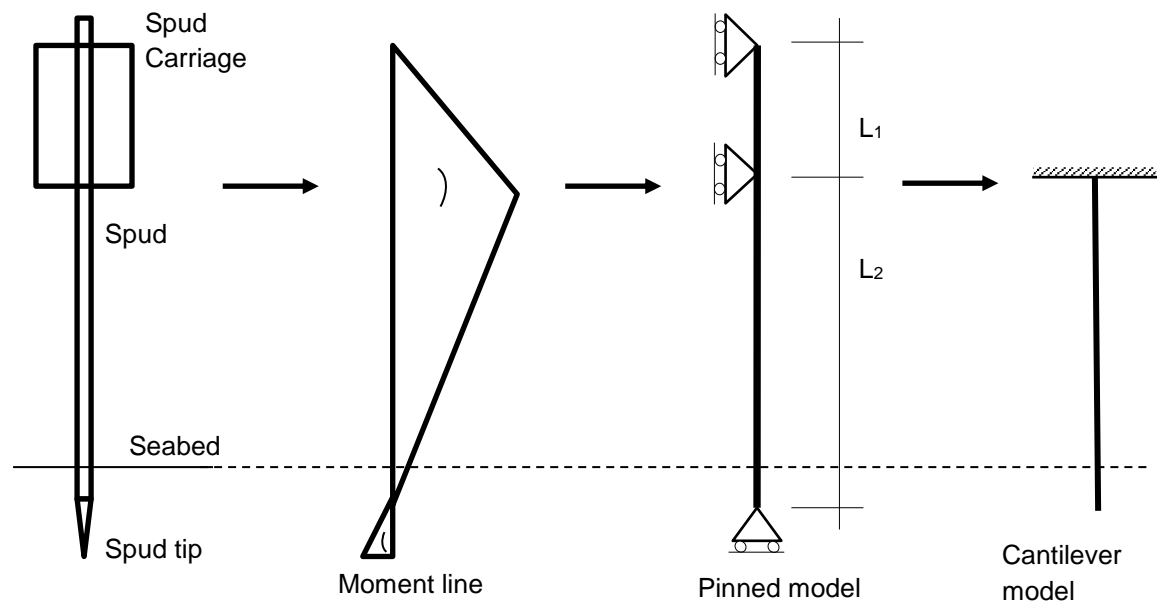


Figure 28 Visualization of modeling process

5.2 Spud Module

5.2.1 Cantilever Spud

The preferred way to model the spud in previous research attempts such as Wichers (1980) and De Reus (2015) is to model the connection between spud and vessel as clamped. The main advantage is that there is only one variable needed to express the deflection, which is the deflection at the tip.

The upper spud guide is located at a height of L_1 above the lower spud guide. This allows for a moment to exist at the lower spud guide. Therefore the connection with the lower spud guide can also be modeled as a clamp. When using this approach all motions are taken into account by the total deflection of the spud tip. The stiffness of the pile, EI , can be adjusted to include effects of components which can affect the total stiffness of the system. The adjusted stiffness of the pile is called the effective stiffness EI_{eff} . An example of one of these components is the fact that the clamped connection is in reality not an infinitely stiff connection, see Figure 29

Without clearances and buffers, the system can be assumed to act linear. The effective stiffness then simply becomes:

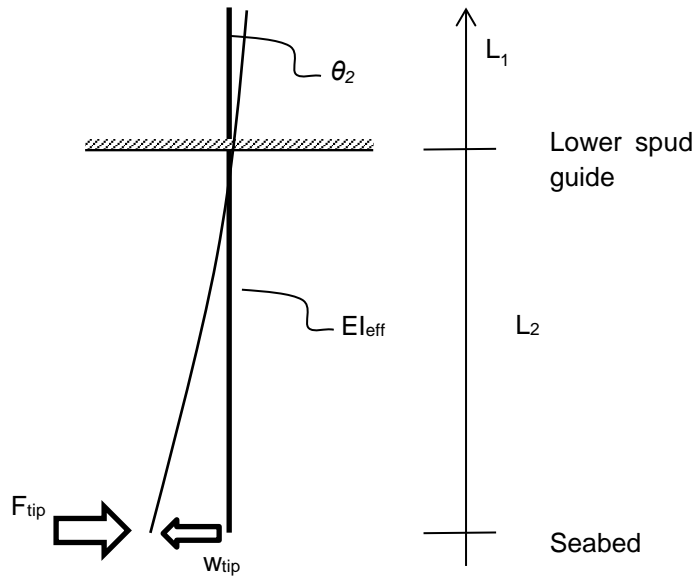


Figure 29 Schematic of the clamped connection with stiffness correction

The formula for the deflection of a cantilever beam is:

$$w_{tip} = \frac{F_{tip} * L_2^3}{3EI}$$

In this formula, w_{tip} is the deflection of the spud tip, or the point at which the moment below the seabed can be taken to be 0 and L_2 is the distance between that point and the lower spud guide.

However due to the fact that in reality the connection at the lower guide is not a full clamp but actually has a stiffness, a reduction to the total stiffness of the system has to be done by calculating how the angle caused by the motion of the upper guide, θ_2 , causes an initial rotation at the clamp instead of staying rigidly straight. The angle in this approach is a result of the moment due to the force F_{tip} exerted by the soil on the spud tip. The moment then is taken up by the section between the two spud guides. The moment is taken up according to:

$$T = F_{tip} * L_2 = \theta_2 * \frac{3EI}{L_1} \rightarrow \theta_2 = F_{tip} * \frac{L_2 L_1}{3EI}$$

$$w_{tip} = F_{tip} * \frac{L_2^3}{3EI} + \theta_2 * L_2 = F_{tip} * \left(\frac{L_2^3}{3EI} + \frac{L_2^2 L_1}{3EI} \right) = F_{tip} * \frac{L_2^3}{3EI_{eff}}$$

Which leads to

$$EI_{eff} = \frac{L_2}{L_2 + L_1} * EI$$

$$F_{tip} = w_{tip} * \frac{3EI_{eff}}{L_2^3}$$

The reaction force the spud exerts on the vessel due to its motions can always be adjusted by adding additional clearances or motions into the value of w_{tip} . If for example the spud is located in very loose soil where a lot of movement of the spud takes place, the value calculated by AQWA can be added to the already estimated value of the soil movements. The same can be done for additional freedom of a flexible spud carriage. These movements can also be included in the calculation of the effective stiffness EI_{eff} rather than the spud tip deflection.

If the individual spud guide forces still have to be known they can be calculated according to

$$F_{low} = -F_{tip} * (L_1 + L_2) / L_1 \text{ and } F_{up} = -F_{low} - F_{tip} = F_{tip} * ((L_1 + L_2) / L_1 - 1)$$

5.2.2 Pinned Spud

A visually more appealing approach is the spud modeled as a beam with 3 pin supports, one at the seabed and one at each spud guide. This first degree statically indeterminate system can easily be solved to find the reaction forces due to the motion of the spud guides. The main advantage is that the applied forces are located at the spud guides, which is the only contact between spud and vessel in reality as well. This provides a straightforward interpretation of the motions which cause deflection. Any nonlinear effects such as flexibility of the carriage can be taken into account by adjusting the effect on the spud at its contact locations.

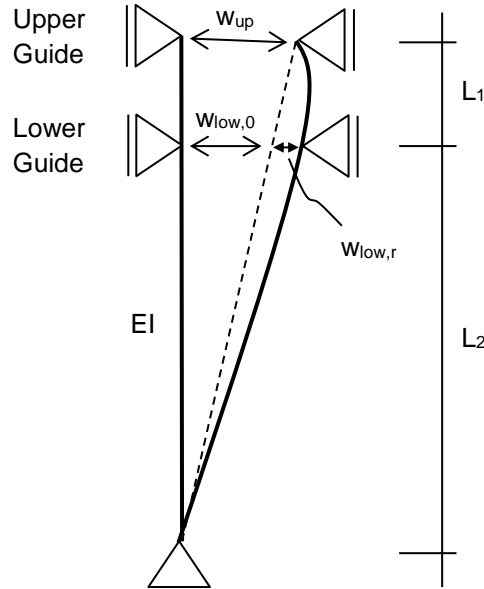


Figure 30 Schematic of the pinned model of the spud

Assuming free rotation around the spud tip, which is accurate for hard soils, the spud will not undergo any bending if the upper and lower guides displace with the same relative angle to the spud tip. The chord of zero deflection is a straight line from the bottom support through the upper and lower guide supports with a displacement of $w_{up,0}$ and $w_{low,0}$ respectively. Relative to this line any deviation will cause bending in the spud. The total displacement of the guides can then be separated into a component due to rotation of the spud, w_0 and a component due to bending of the spud, w_r . In Figure 30 the motion of the upper guide only causes the rotation around the spud tip and the relative motion of the lower guide causes bending. A pure surge motion will give equal displacements of w_{up} and w_{low} . This will cause bending in the spud since the relative angle to the spud tip will be different. The spud forces can be determined as follows:

$$w_{low,r} = w_{low} - w_{low,0} \rightarrow w_{low,0} = w_{up} * \frac{L_2}{L_1 + L_2}$$

$$F_{low} = w_{low,r} * \frac{3EI * (L_1 + L_2)}{L_1^2 L_2}$$

$$F_{up} = F_{low} * \frac{L_2}{L_1 + L_2} = w_{low,r} * \frac{3EI}{L_1^2 L_2} \text{ and } F_{tip} = F_{low} * \frac{L_1}{L_1 + L_2} = w_{low,r} * \frac{3EI}{L_1 L_2}$$

5.3 Results

Table 9 Spud parameters

Parameter	Value	Unit	Remarks
E	$2 \cdot 10^{11}$	N/m ²	Young's modulus for steel
d _{out}	2.0	m	Outer Diameter
d _{in}	1.92	m	Inner diameter
L ₁	12	m	Length between guides
L ₂	14	m	Length from lower guide to point near spud tip where moment is zero
I	0.118	m ⁴	$64/\pi \cdot (d_{out}^4 - d_{in}^4)$
EI	$2.3 \cdot 10^{10}$	Nm ²	E*I

5.3.1 Expected results

To test the spud module and the implemented formulas a virtual bollard pull will be done. This means that the ship will try to move forward with a certain force which will lead to a deflection and reaction force of the spud. In order to prevent numerical instabilities, the force will be gradually increased and then kept constant at its maximum of $5 \cdot 10^4$ kN. It is worth mentioning that the test force applied on the spud is of order magnitude which would never occur in reality. The large deflection and forces involved do give a better insight on how the module acts.

For either approach discussed in 5.2 the results should be the same. The reaction force F_{tip} should be equal to the test force since it is the only force capable of creating equilibrium. This means that the expected results are $F_{tip} = -5 \cdot 10^7$ N and

$$w_{tip} = 5 \cdot 10^7 \cdot \frac{14^3}{3 \cdot 2.3 \cdot 10^{10} \cdot \frac{14}{14+12}} = 3.59 \text{ m}$$

Using the force at the spud tip and taking the balance of moments at the upper guide the force in the lower guide can be determined as

$$M_{up} = -F_{test} \cdot (L_1 + L_2) + F_{low} \cdot L_1 = 0 \rightarrow F_{low} = F_{test} \cdot (L_1 + L_2) / L_1 = 5 \cdot 10^4 \cdot (14 + 12) / 12 = 1.08 \cdot 10^5 \text{ kN}$$

The upper guide force is then $F_{up} = F_{test} - F_{low} = 5 \cdot 10^4 - 1.08 \cdot 10^5 = -5.8 \cdot 10^4$ kN.

Using the equations of 5.2.2, the forces on the spud guides correspond to a deflection of $w_{low,r} = 1.08 \cdot 10^8 \cdot 12^2 \cdot 14^2 / (3 \cdot 2.3 \cdot 10^{10} \cdot 26) = 1.74$ m, using $w_{up} + w_{low} = 3.59$ m, since the result should be equal to the tip deflection, the values for the motions of the spud guides are expected to be $w_{low} = 4.0$ m and $w_{up} = 4.375$ m.

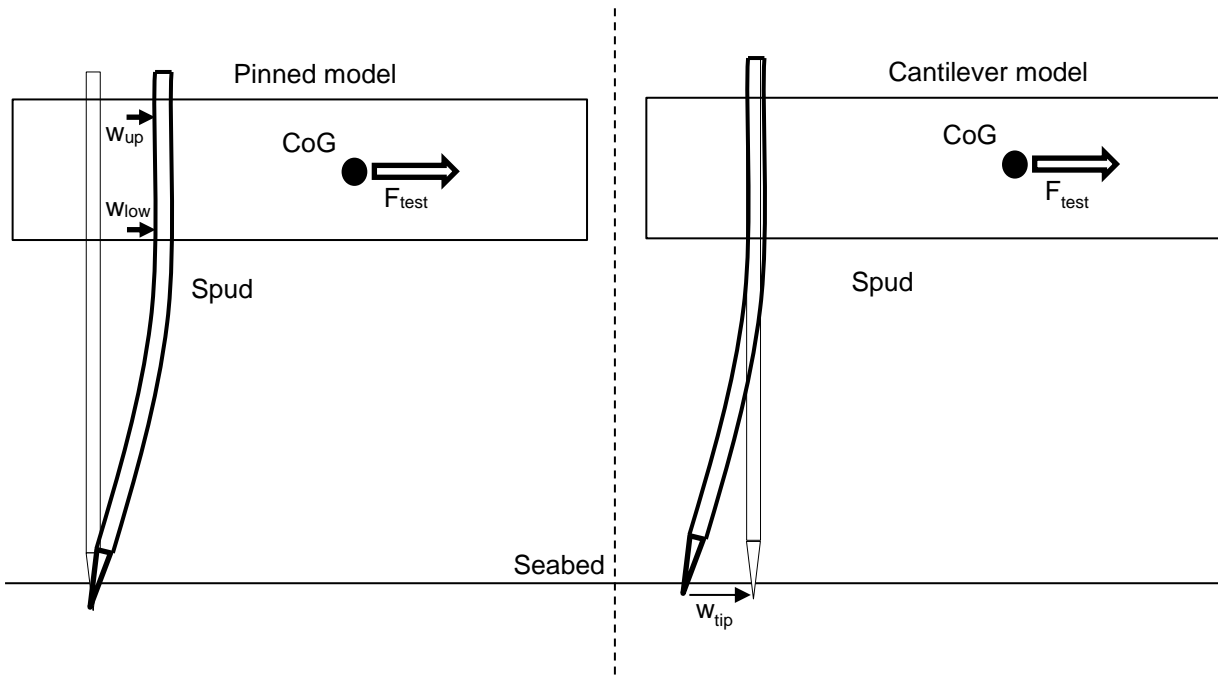


Figure 31 Schematic of testing scenario

5.3.2 Actual results

Executing the test as described in 5.3.1, the results for each model are presented below.

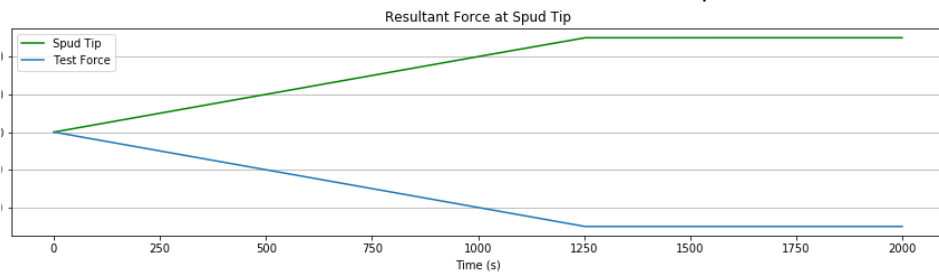


Figure 32 Force in spud tip compared to the test force

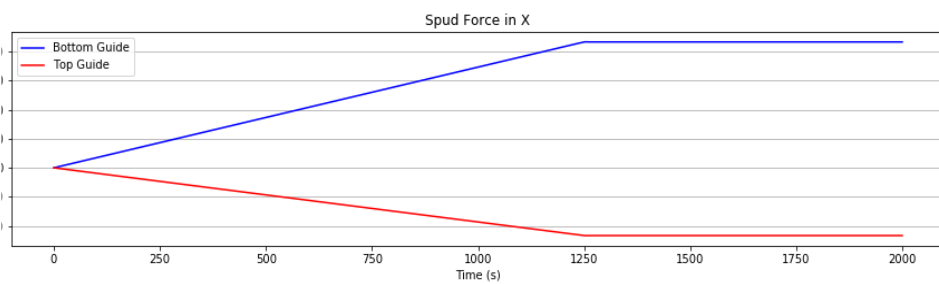


Figure 33 Resulting forces in the spud guides for the pinned model

The forces in the individual guides are similar to what was expected. The resulting force in the spud tip matches the test force and therefore there is equilibrium of forces. It is worth to note that the different methods indeed do give identical results. A negligible difference can be seen in the lateral direction, where the pinned approach shows less sway and roll motions, see Appendix C for a complete overview of all the results of the test.

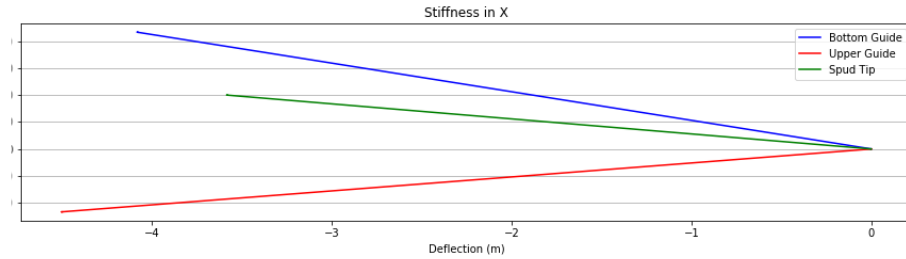


Figure 34 Deflection during spud test

The deflection due to the test force is exactly as predicted. The spud tip has a deflection of about 3.6 m for a force of $5 \cdot 10^4$ kN. The top and bottom guides have larger deflections, resulting in the 4.0 and 4.4 m which were calculated before.

5.4 Adding clearance and buffers

In reality the spud does not perform exactly as a linear spring. If a flexible spud carriage is installed, it will create a buffer zone when a certain stress is exceeded. In addition, small clearances and deformations of different components can also reduce the stiffness of the system when the stress is high enough. These processes all cause nonlinear behavior. The easiest way to take this into account is to adjust the deflection caused by the motion of the spud guides or spud tip using a set of conditional statements. The focus here is on a small gap between spud and guide to allow some free motion prior to contact and the activation of a buffer zone if a certain force occurs in the spud guides. The result of this approach is presented below in the form of a stiffness diagram, using the same test setup as described above.

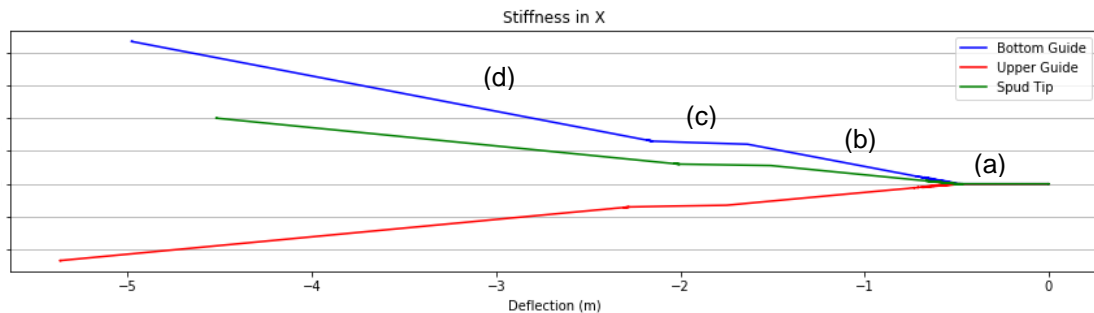


Figure 35 Stiffness of the Spud including buffer

A short explanation of the graph above is as follows:

- Represents a void area between spud pile and spud guide, the free motion that can occur between the two before physical contact is made.
- Is the linear increase due to direct deflection of the spud. The motions of the vessel are directly visible in the deflection of the spud.
- Marks the activation of the buffer zone by the flexible spud carriage system. The carriage starts to rotate to prevent the moment on the spud from increasing, this is visible by the constant spud force with increasing motion.
- Occurs when the maximum stroke of the flexible spud carriage is reached and further motions linearly increase the deflection of the spud pile and thereby also the reaction force of the spud.

Note that the diagram shows a negative displacement due to the orientation of the global axes system.

5.5 Step Force

At the end of each swing, the step cylinder is activated to move the cutterhead forward. For the model, this means that the distance between spud and CoG increases. The forward motion of the cutterhead during stepping is a slow process, approximately 0.1 to 0.3 meter per minute. This means

that a time-dependent function needs to be implemented into the model to slowly increase the force on the spud to push the cutter forward.

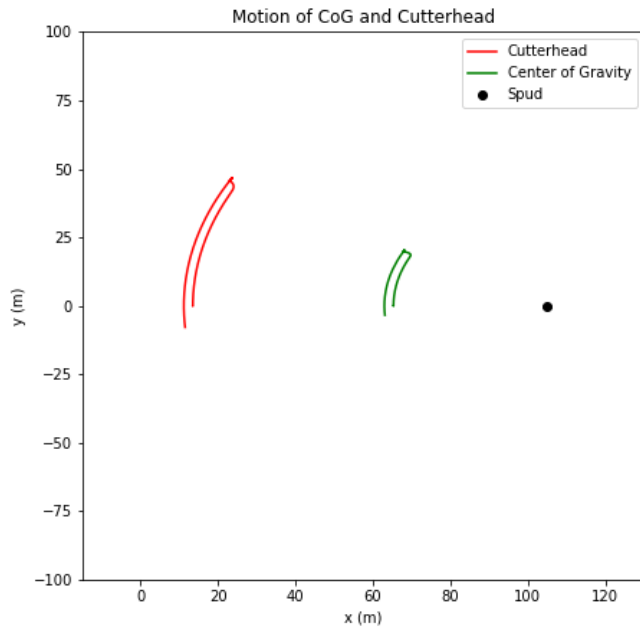


Figure 36 Overview of cutting with a step of 1.5 m per swing

The step is done by applying a deflection on the spud which then in return gives a corresponding force. This force pushes the vessel forward, and the new equilibrium is found when the complete deflection which was applied has been converted into forward motion. Of course, a CSD in operation will experience many forces which each can cause the spud to undergo a deflection. In theory, the step force can get lost between the occurrence of other simultaneous motions. In the approach used in the script, this is also the case.

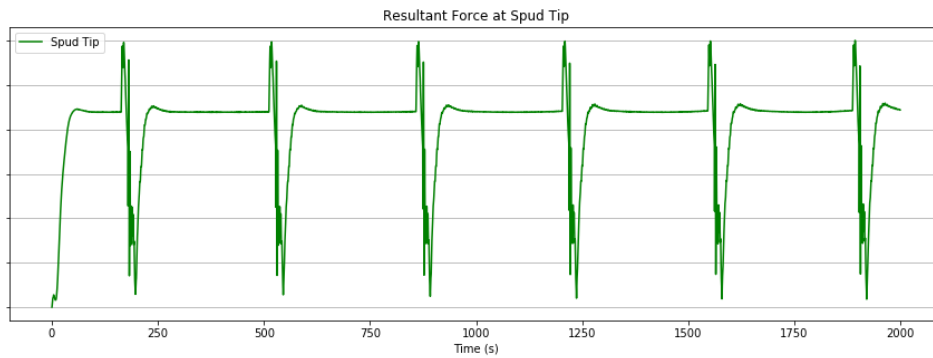


Figure 37 Effect of taking steps on spud pile.

In Figure 37 some oscillations are visible when the stepping force is applied. The reason is that in order to prevent the ship from returning to the initial condition of the spud, the step distance needs to be added to the distance from spud to CoG. However, due to the inertia of the whole system the vessel will never move as much forward in a single timestep as the intended step on the spud pile is applied. Therefore the step on the spud becomes larger over time since the step in the memory is larger than the actual distance stepped. After the script completes the step, the vessel will slowly come closer until this step is reached. This reduces the loads on the spud and, as a consequence, it will slow its vibration. Many other motions, such as the swing of the side wires and the motions due to the cutting forces, influence the position of the vessel. This makes it very difficult to isolate how much the ship actually moves in one timestep due to the applied step force, in order to avoid the vibrations.

5.6 Possible improvements

The main goal of the spud module is to maintain the CSD in the correct position. This goal has been achieved, it is able to maintain position and even move forward when desired. Also, a free rotation is possible as the swing to cut soil requires. The forces which are found due to spud-vessel interaction have been discussed thoroughly. These forces have not yet been validated with results from actual operation, as the Helios at the time of writing still has limited experience in the real world. Validating these forces is an important improvement for the future.

Further possible improvements focus mainly on specific details which have been left out of the scope of this research but do contribute to the functioning of the spud or spud carriage.

A few examples of relatively simple details which could be taken into account by including them in the Python script are:

- Forces in carriage wires or nitrogen tanks; by taking into account the strain of the wire in the flexible spud carriage, as well as the maximum stroke and stroke speed of the cylinder which allows a controlled flexibility, better insight in the relation between the operation of the CSD and the need for flexibility of the carriage can be obtained.
- Auxiliary spud change; the auxiliary spud is situated at a different position than the main spud. As the main spud is relocated the auxiliary spud will provide the mooring capabilities for the vessel. Because it is located at a different location it might have a slightly different reaction to the motions. The time that the auxiliary spud is used is quite limited compared to the main spud and no swing motion or soil cutting is done while the auxiliary spud is down. This has been the main reason it has been kept outside the scope of this model.
- Soil penetration and corresponding soil motions around spud tip; currently soil motions can be taken into account by adjusting the spud guide motions in the same way as done for the flexible spud carriage. It is also possible to develop a module which can relate the specific energy parameter of the soil to the penetration depth and soil stiffness that the spud tip encounters. The effects of this can then be incorporated to adjust the effective stiffness EI_{eff} or the angle of the zero deflection chord of the spud automatically.
- Friction; friction between spud and spud guides has been mentioned but not implemented. Vertical friction is only present if there is a horizontal force acting on the guides. Usually the friction coefficient μ is used to translate the horizontal force into a vertical one. However, this vertical force only occurs if there is relative motion between the contact points on the spud and the guides. Given that for steel surfaces μ is generally very small, it was chosen to leave it out of this thesis.

6 Winches

6.1 Function of the winches



Figure 38 Winches on top of the ladder provide tension in the side wires

The winches create the driving force behind the rotational swing of the cutter suction dredger. They primarily control the yaw motion around the spud pile. In addition, they also provide some mooring capabilities.

The swing motion is accomplished by two winches, one on each side of the ladder. Each winch controls a swing wire which runs through a sheave on the ladder towards the side anchors in the soil. The winch drum winds in or out to control the tension in the wire. When swinging to starboard the starboard drum increases the tension pulling the ladder towards the side anchors. The portside drum in return ensures that the wire on portside doesn't fall slack, resulting in a slight braking force. At the end of the swing, when the ladder needs to swing in the other direction, the portside drum will increase the tension while the starboard drum will reduce the tension to the value where the wire does not fall slack. As a result, the ladder will stop swinging in one direction and start swinging in the other. Once the swing velocity is reached the tension in the wires is kept constant in order to maintain that velocity while avoiding either wire from falling slack.

In small CSD's, such as barges, this process is sometimes still found to be manual. Where the crew aboard needs to set the RPM for a certain wind in or pay out speed of the drum in order to obtain the desired tension in the wire. In advanced CSD's, such as the Helios, this process is fully automated. A sophisticated PID controller ensures that the input values such as desired swing velocity and maximum swing angle are reached and maintained.

In some cases, when the soil is very hard, the winch drums operate at full capacity and are unable to reach the desired swing velocity. In this case, the process becomes force controlled, which means that the PID controller seeks to optimize the forces in the wires, rather than the velocity, and avoid exceeding the maximum tension the wires, anchors or the winches themselves can handle.

As the vessel advances its rotation towards the maximum swing angle the directional vector of the force on the ladder will change accordingly. It always runs from the sheave on the ladder towards the side anchor, and the angle will vary as the swing angle varies. The consequence is that the lateral component of the tension in the wire, which is responsible for enforcing the rotation, will change as the angle the wire makes with the ladder changes. This can result in very high tensions in the wires

when the angle between ladder and anchor becomes impractical. If this is the case, the side anchors need to be relocated such that many more swings can be made until this angle is reached again.

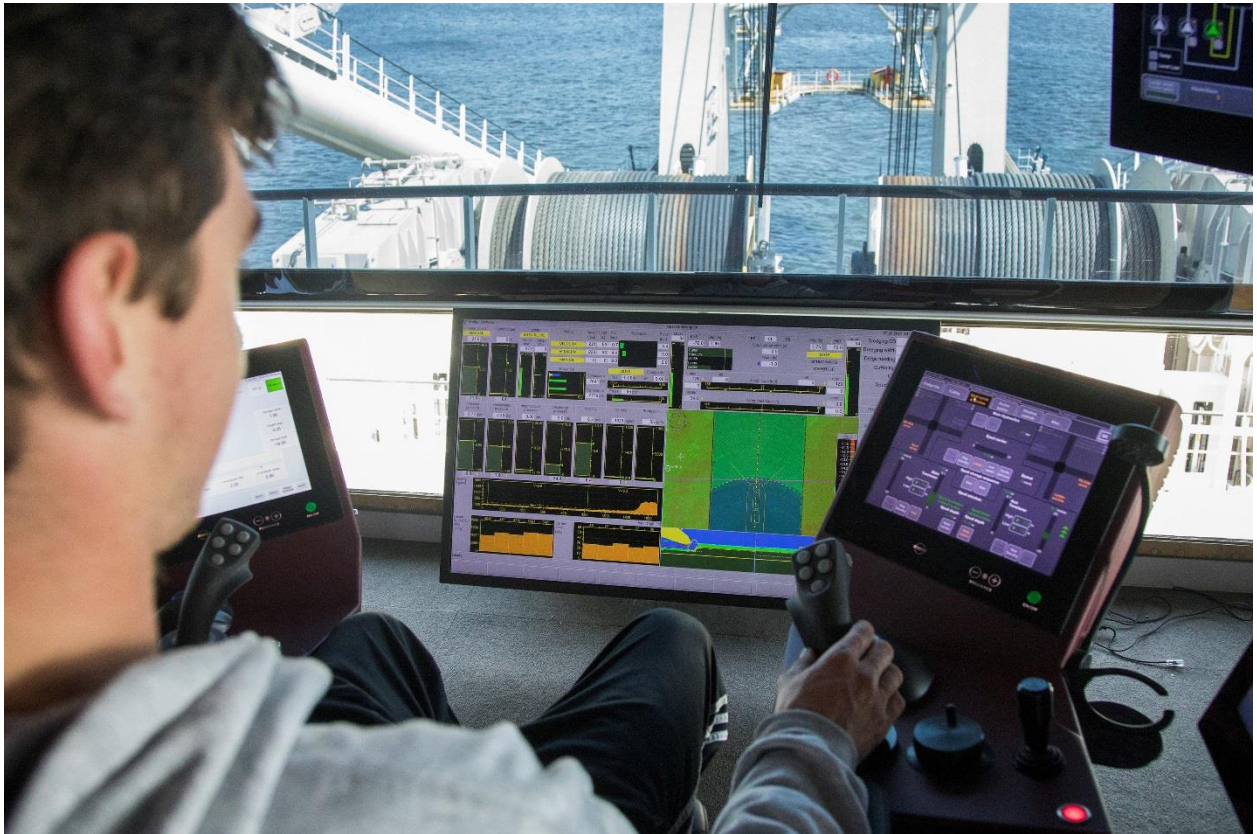


Figure 39 Sophisticated automated systems largely control the swing motion of the cutter

6.2 Winch Module

To model the winch system in AQWA there are a few different options available. For the most accurate description, the winch module would have to take as many factors into account as the controller on the actual ship, which would result in quite a complex piece of code. To avoid this, several assumptions can be made. The different possible approaches and their assumptions are listed below in order of increasing complexity.

- Fixed wire force, assuming that the cutting force can be considered more or less constant
- Fixed wire length, assuming that the wire can be described by a linear strain relation
- PID controller, assuming the physical limits of the system are respected

It should be noted that with all approaches the actual limitations of the physical system are absent, although they can be incorporated empirically. The retardation of the drum rotation and its effect on the wire is a great example of a missing process in the numerical approach, where everything happens instantaneously.

As a benchmark, the tension in the side wires are in reality found to be between a minimum of 10 tonnes to avoid slack and reaching the maximum pulling force. For a swing without soil reactions or waves, the tension found in the hauling wire at constant speed should be somewhere between 40 and 60 tonnes, this would allow to have sufficient additional pulling capacity if hard soils would require it.

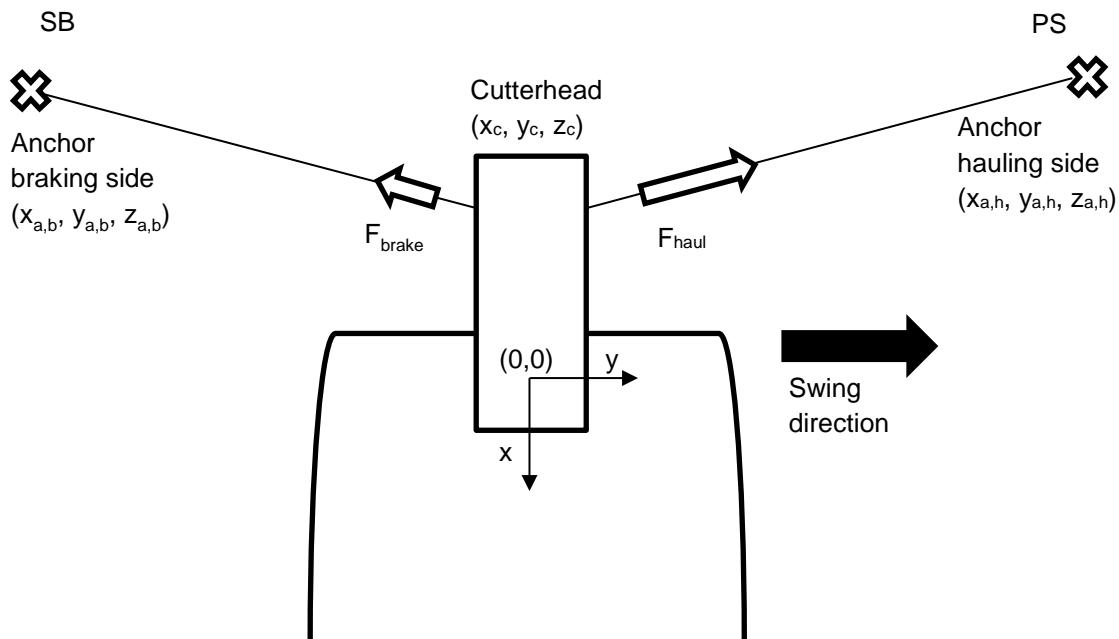


Figure 40 Overview of side wires and side anchors

6.3 Fixed Wire Force

The easiest approach to model the winch tension in the wires attached to the ladder is to define a fixed tension in each wire. The x- and y-components will then vary as the angle of the wire changes, but the total resultant force per wire will stay constant throughout the swing. A quick calculation per soil type can give an estimate of the required tension in the hauling wire to reach a certain velocity. The main advantage is that this model is numerically very stable since there is very little fluctuation in the forces. However, the principal disadvantage is that as conditions might change during the swing, the velocity can fluctuate considerably.

This option can work well with very hard soils where the desired swing speeds cannot be reached, as well as in a situation without soil where it can be expected that the tension in the wires will not vary greatly throughout the swing. However, in between these two extremes, the intermittent nature of cutting soil might be a problem for this approach as a required increase or decrease in tension is not possible.

This module calculates the resultant forces acting on the ladder by setting a fixed value for the hauling wire, $F_{wire,h}$ and braking wire $F_{wire,b}$. Depending on the swing direction the port side or starboard wire is assigned the value for hauling or braking. The resultant force acting on the ladder is then simply

$$\vec{F}_{winch} = F_{wire,h} * \begin{pmatrix} \frac{x_{a,h} - x_c}{L_h} \\ \frac{y_{a,h} - y_c}{L_h} \\ \frac{z_{a,h} - z_c}{L_h} \end{pmatrix} + F_{wire,b} * \begin{pmatrix} \frac{x_{a,b} - x_c}{L_b} \\ \frac{y_{a,b} - y_c}{L_b} \\ \frac{z_{a,b} - z_c}{L_b} \end{pmatrix}$$

Note that since the starboard side anchor has a negative y-coordinate, its force vector is also in the opposite direction even though the tension is always positive. At the end of each swing, the tensions in the wires reverse to obtain the swing in the new direction.

Table 10 Fixed Force Parameters

Variable	Value	Unit	Remark
F_{haul}	600	kN	Hauling wire
F_{brake}	100	kN	Braking wire
θ_{max}	30	Degrees	Maximum swing angle
v_{swing}	0.4	m/s	Desired swing velocity
$(X_{a,p}, Y_{a,p}, Z_{a,p})$	(-50, 100, -20)	m	Coordinates of portside anchor in global axes
$(X_{a,s}, Y_{a,s}, Z_{a,s})$	(-50, -100, -20)	m	Coordinates of starboard anchor in global axes
L_h, L_b	time-dependent	m	Length of hauling and braking wire
(X_c, Y_c, Z_c)	time-dependent	m	Cutterhead coordinates in global axes system

To test this approach for the winch module, several swings will be done without soil reactions and in still water. The desired swing velocity is 0.4 m/s or 24 m/min, solely for comparison purposes since in this approach there is no way to actually adjust the forces to the velocity. For the hauling wire, a constant tension of 600 kN or 60 t is set while the braking wire tension is set at 100 kN or 10 t. At the beginning of the run the starboard wire is set as hauling wire and the starting position is at the centerline of the vessel. This means that both side wires are equal in length and relative angle to the ladder since the anchors are positioned symmetrically.

As the vessel swings to starboard, it will reach the maximum swing angle, θ_{max} , at this point the tension in the wires will be reversed. Now the portside wire is set at the hauling tension, and the starboard wire is set at 10 t. At the maximum angle of $-\theta_{\text{max}}$, the starboard wire will be designated as hauling wire again. The results of this test can be found in the figures below.

| Winches

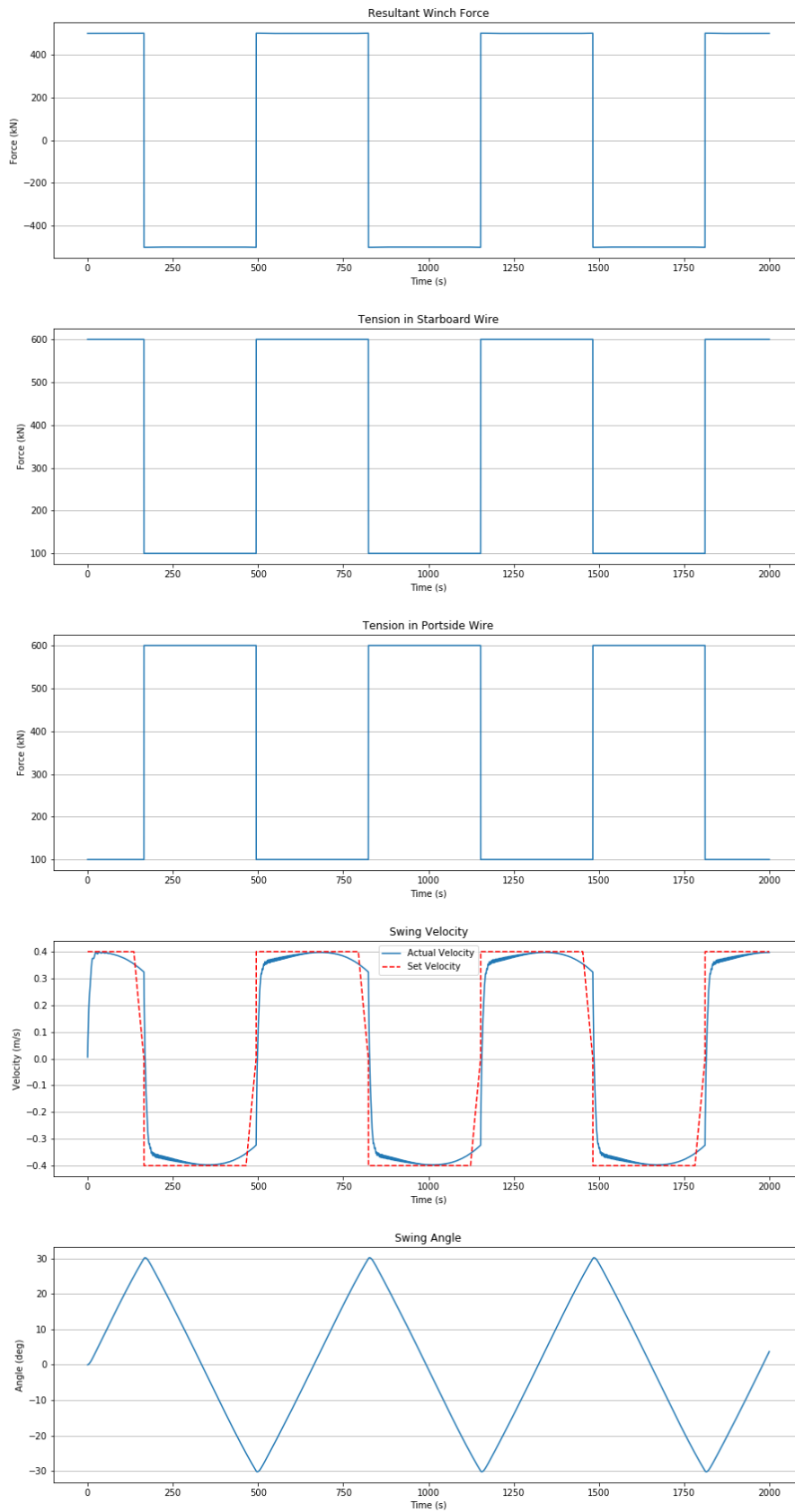


Figure 41 Winch forces over time with fixed force in pulling direction

The force diagram shows that at the end of the swing the change from 60 t to 10 t or vice versa is instantaneous, which is of course not realistic. This, however, does not lead to unexpected motions,

the swing velocity is quite continuous and the set velocity of 0.4 m/s is reached briefly during each swing. It is interesting to see that although there is no system is present to regulate the deceleration, other than the immediate switch of pulling and braking wire, that the swing velocity still reduces as the swing nears its completion. This is due to the fact that as the angle increases, the lateral component of the force in the hauling swing wire reduces and at the same time the lateral component of the braking wire increases, creating a natural velocity flow. The exact change in the lateral component, and the resulting force of the tension in both wires, depends on the placement of the side anchors and will also vary with the steps taken of the spud carriage as well as the maximum swing angle set.

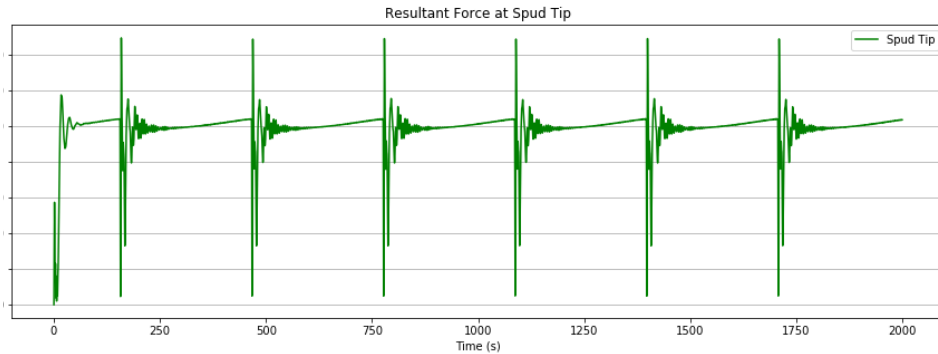


Figure 42 Resultant forces on spud due to fixed force in wires

Looking at the spud forces it can be seen that the sudden switch from hauling side to braking side per wire causes vibrations in the spud, with the resulting total force actually exceeding the applied hauling force. These vibrations are due to longitudinal motions in surge and pitch direction, as can be seen in the overview in Appendix G.

It can be concluded that for certain application this very basic approach is quite effective and certainly has potential to generate reliable results. The main advantage is the complete control of the tension in the wires and their directional vector, which changes as it should. The major drawback is the inability to adjust the tension during the process as some situations may warrant. For this research, a variable tension is more interesting, but for design purposes it may not always be required.

6.4 Fixed Wire Length

In this approach, the force in the wire depends directly on the length of the wire. As the wire is winded in by the winch, its length will decrease. However, due to the inertia of the vessel, the wire cannot shorten immediately, leading to strain in the wire which is the consequence of the difference between intended wire length and actual wire length. This strain can be used to define a stiffness, which can be used to find the winch force acting on the vessel. The downside of this approach is that if the vessel moves as intended no strain is seen in the model and therefore no force would be present in the wires. Adding a basic tension to both wires could solve this issue, and this is what occurs in reality as well since the wires are prevented from falling slack.

It should also be noted that this approach omits the fact that the wire, although always at least slightly tensioned, is actually not a straight line from the sheave on the ladder to the side anchor. Due to its own submerged weight and other factors such as an underwater current or drag, the wire will sag. This makes the application of strain a bit more complicated as it actually is a dynamic relation rather than a linear one. To include the wire dynamics would increase the complexity of the module to a degree that surpasses its purpose, therefore only the linear approach with fixed minimum tension is applied here.

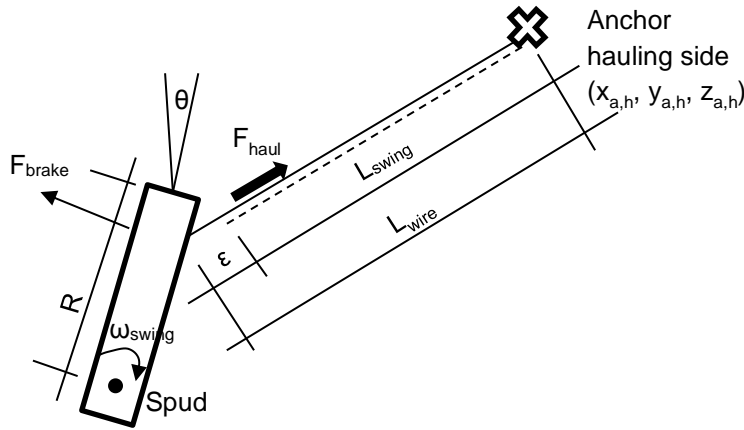


Figure 43 Schematic for fixed wire length

The net resultant force on the ladder is calculated the same way as in 6.3, however, the hauling force is now calculated according to

$$F_{\text{haul}} = F_{\text{brake}} + EA \cdot \epsilon \text{ with } \epsilon = (L_{\text{wire,h}} - L_{\text{swing,h}}) / L_{\text{swing,h}}$$

$$L_{\text{swing}} = \sqrt{x^2 + y^2} \text{ with } x = x_{a,h} - R \cdot \sin(\theta) \text{ and } y = y_{a,h} - R \cdot \cos(\theta)$$

$$\theta = d\theta * t \text{ with } d\theta = \frac{v_{\text{swing}} * dt}{R} = \omega_{\text{swing}} * dt$$

In this equation, the v_{swing} is the desired velocity. The length $L_{\text{swing,h}}$ is calculated each timestep by knowing the desired angle θ and finding the desired x,y,z coordinates of the cutterhead using the radius R from the spud pile to the cutterhead. This radius will change as the CSD is stepping forward.

Table 11 Parameters for fixed wire length controller

Variable	Value	Unit	Remark
F_{min}	100	kN	Minimum tension in wire
E	$2 \cdot 10^{11}$	N/m ²	Young's modulus for steel
A	0.0045	m ²	For wire with 76 mm diameter
EA	$9 \cdot 10^8$	N/m	Stiffness of wire
R	120-126	m	Radius between spud and cutterhead
v_s	0.4	m/s	Desired swing velocity

Just as in 6.3, the CSD will be set to start at the centerline and proceed to swing to starboard. Other than in the fixed force method, however, the starting tension is 100 kN, or 10 t, in both wires. Obviously, if the tension in both wires is equal and at equal relative angles to the ladder, there will be no resultant force to pull the ladder in the correct direction. The module will start to reduce the length of the portside wire, the reduction in length being the equivalent of the cutterhead swinging at the desired swing velocity of 0.4 m/s. The starboard wire now starts to become shorter than the actual distance between cutterhead and starboard anchor is. This causes strain in the wire and therefore the initial tension of 100 kN starts to increase. Due to this increase, the ladder is accelerated. If the acceleration exceeds the desired velocity, the strain in the wire will become negative and the wire will fall slack. Now only the braking wire has tension applied on the ladder, which means it will slow down again. At the end of the swing, when θ_{max} is reached, the starboard wire will be set at a fixed braking tension of 100 kN and the portside wire will be set to haul with the strain related tension.

From this description, it can become quite clear that this approach has the risk to become quite an intermittent process. In the figures below it can be seen how stable the results turn out to be during the test of this approach.

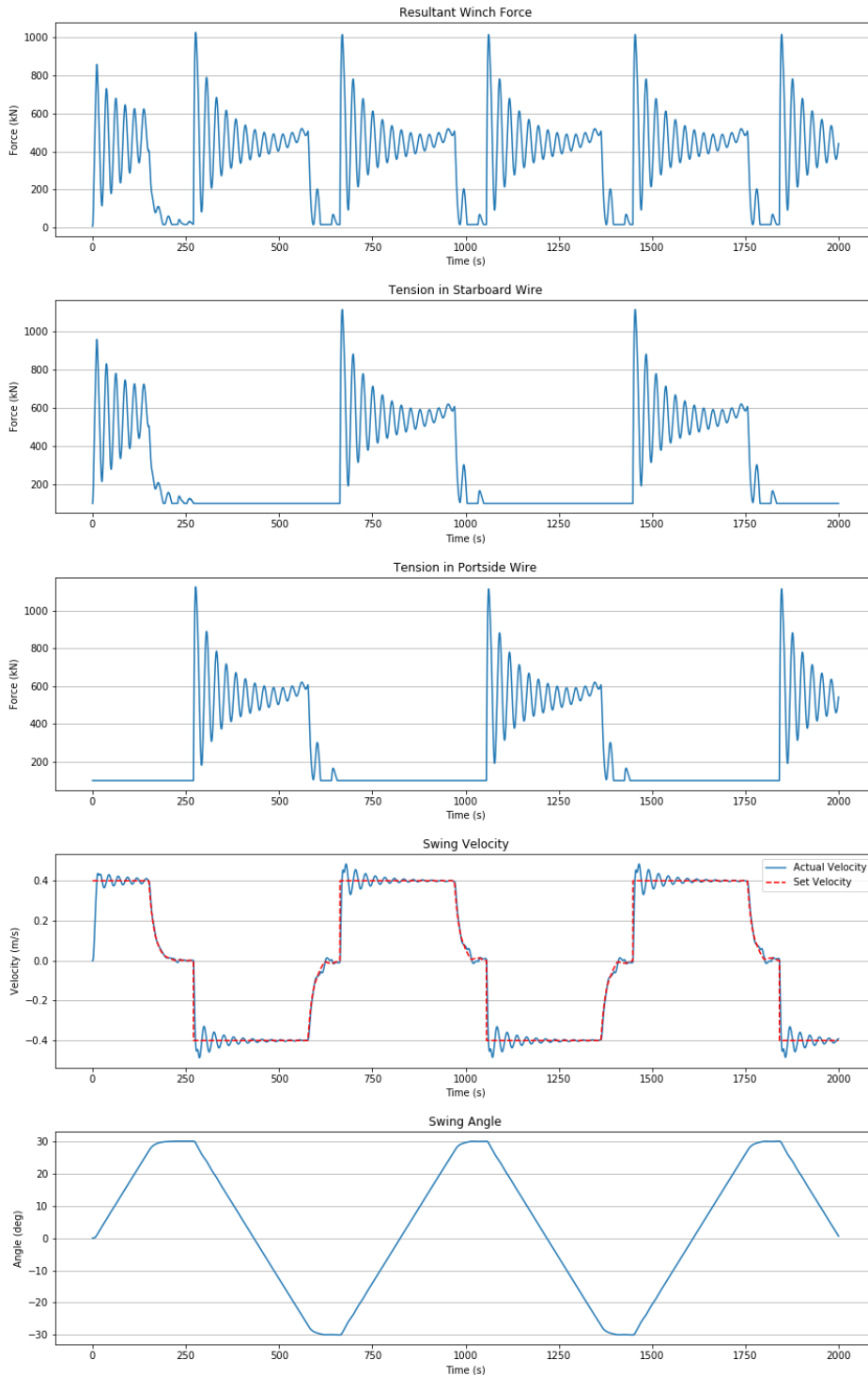


Figure 44 Forces over time due to wire strain

From the graphs, it is immediately clear that this method produces large peaks in both the velocity and force diagrams. This is due to the fact that as the reference position of the cutterhead advances, the position where it should be, the real position, where it actually is, will not have advanced due to the inertia of the whole system. Therefore a very large tension occurs to create the correct motion, which results in a too high velocity that ‘catches up’ with the reference velocity. After they have reached the same position a stable velocity and force profile is visible until the swing ends and the peak to swing in the opposite direction occurs. During the stable part of the swing, the force required to reach the swing velocity of 0.4 m/s can be seen to be around 600 kN or 60 tonnes. It can also be seen to slightly increase at the end of the swing, exhibiting the same behavior as the fixed force

approach, where the lateral component of the tension in the wire decreases as the swing angle increases.



Figure 45 Resultant spud force from wire strain

The resultant spud force diagram shows exactly the same pattern as the wire force diagrams. This is in contrast with the fixed force approach, where the spud force diagram showed peaks occurring every time the swing direction was reversed. The reason that the spud and wire diagrams are similar in this approach is that the tension builds up gradually during each timestep, whereas with the fixed force approach it happened instantaneously. Overall this approach has the potential to be expanded to be more accurate with the addition of a few control mechanisms, creating a better feedback between actual position and desired position could lower the peaks considerably.

6.5 PID Controller

Since the controlling system on the actual ship is a PID controller regulating the forces required to achieve a set swing velocity, it makes sense to approach the winch module in this thesis as a PID controller as well. PID stands for Proportional, Integral and Derivative gain. It uses the variable error e , which is the difference between a set value and the actual value. For a detailed explanation on how PID controllers function, see Appendix C.

The equation for the resultant net winch force is defined as

$$F_{PID} = K_p * e + K_i * \sum e_t * dt + K_d * \frac{dv}{dt}$$

F_{PID} = Resultant winch force, always directed tangential to the ladder

e = error, $e = v_{set} - v_{actual}$

K_p = Proportional gain factor, directly multiplied with the error

K_i = Integral gain factor, multiplied with the sum of the error during all the previous timesteps

K_d = Derivative gain factor, multiplied by the difference between v_{actual} of the current and last timestep

$v = v_{actual}$ = tangential velocity of cutterhead, or swing velocity at cutterhead in the current timestep.

In this equation, the error e is the difference between the actual swing velocity, the tangential velocity at the cutterhead, and the desired, or set, velocity. The factors K_p , K_i , K_d are constants, which change the error variables into the required force F_{PID} . The process of tuning of these K-factors can be found in Appendix C.

It is important to note that the resulting force F_{PID} is always directed in tangential direction relative to the ladder. This has as advantage that the maximum angle and velocity can be set regardless of other parameters such as anchor locations or wire stiffness. Therefore, it is possible to create a swing pattern which follows the user's instruction perfectly. Only the gain factors and the set velocity have to be known. This also allows the user to instruct a certain part of the trajectory which is slower or faster than the rest. An example is the slowing down of the cutter at the end of the swing in order to avoid tension peaks in the wires when the swing direction is reversed.

The main disadvantage is directly related to the advantage, as the physically limiting parameters are not taken into account directly, the system can behave more ideal than in reality would be possible. Knowing the tension in the individual wires can give an insight whether the calculated force is realistic.

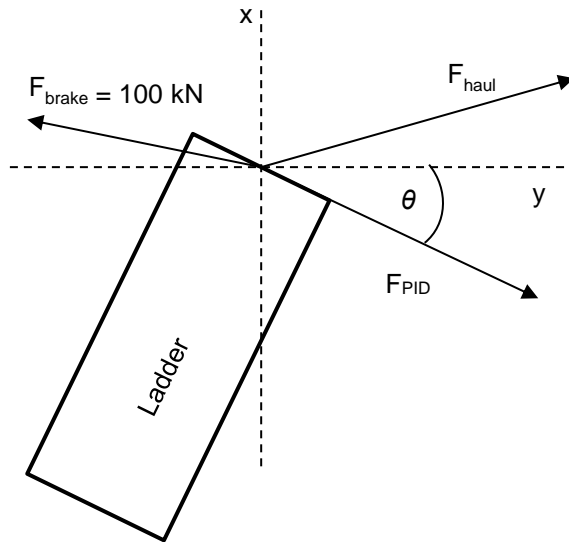


Figure 46 Vector diagram PID controller, $F_{haul} = F_{PID} - F_{brake}$.

The tension in the individual wires can be calculated from the net force on the ladder. However, this can only be done by setting the braking tension to a fixed value, such as also was done in 6.4. To find the tension in the side wires the following formula can be used.

$$F_{haul} = \sqrt{\left(F_{PID} * \sin \theta - F_{brake} * \frac{x_{a,b} - x_c}{L_b}\right)^2 + \left(F_{PID} * \cos \theta - F_{brake} * \frac{y_{a,b} - y_c}{L_b}\right)^2}$$

This will only give a solution if one of the two wires is assigned a value. Setting the braking wire at 100 kN allows finding the tension acting in the hauling wire. Contrary to previous methods, the assignment of which wire is the braking wire does not directly depend on the swing direction but depends on whether F_{PID} is positive or negative.

The set swing velocity will change sign when θ_{max} is reached, this effectively will tell the controller to start hauling in the opposite direction. The sudden change in set velocity can cause peaks in the force and velocity diagrams, called overshoot. Reducing the proportional gain K_p and increasing the integral gain K_i can reduce overshoots at the cost of a slower reacting system. Since in reality the system cannot react instantaneously, this setting might actually create a more realistic system. Therefore both settings will be tested and the results are presented below. The system in both cases is instructed to slow down when it nears the maximum angle and passes θ_{slow} .

Table 12 Gain values used

Variable	Value P-dominated	Value I-dominated	Unit
K_p	$1 * 10^5$	$1.5 * 10^3$	-
K_i	$1 * 10^4$	$1 * 10^3$	-
K_d	0.0	0.0	-
v_s	0.4	0.4	m/s
θ_{slow}	5	5	degrees
θ_{max}	30	30	degrees

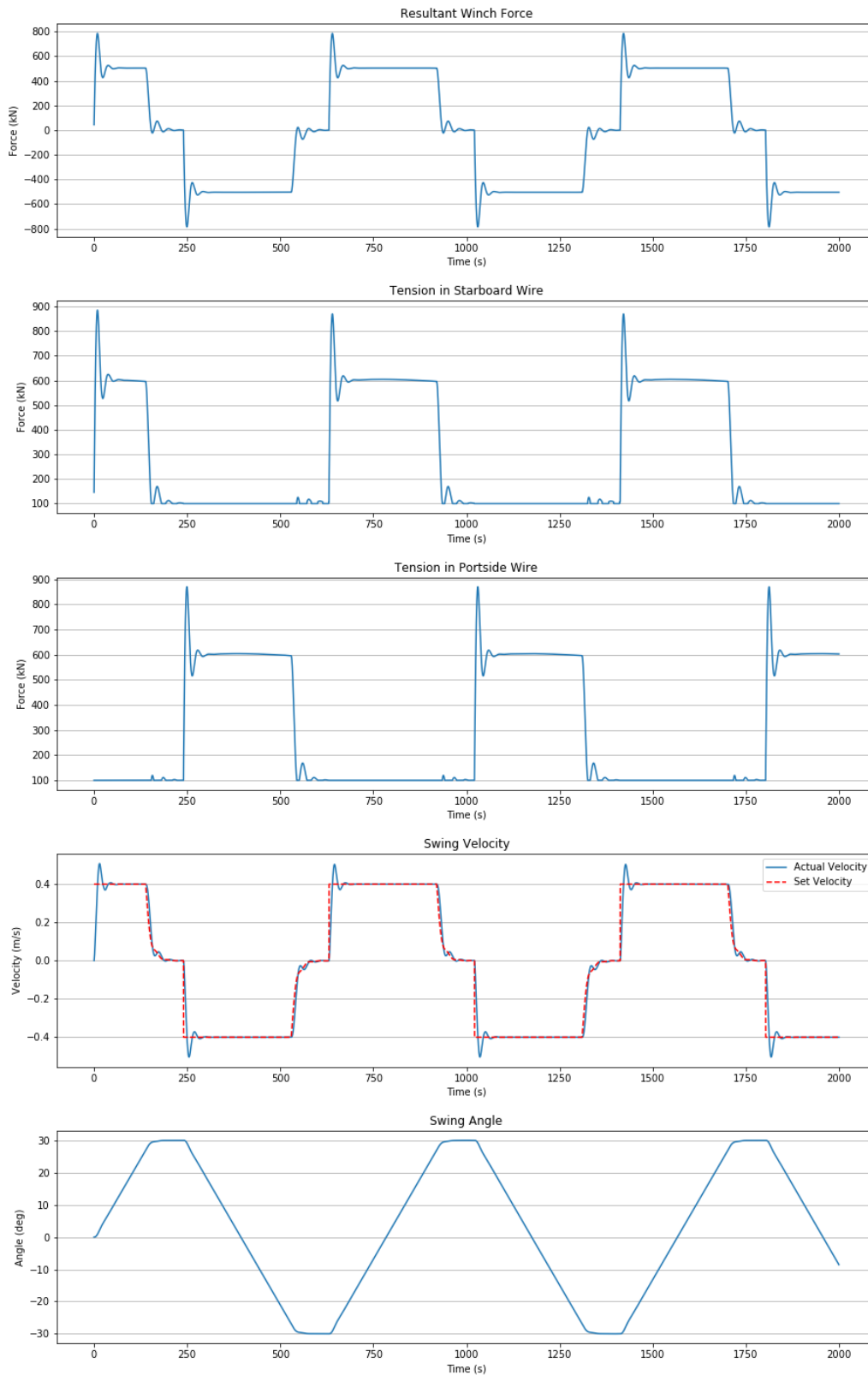


Figure 47 Forces over time when using a P-dominated controller

In Figure 47 it is noticeable that the velocity profile is followed almost perfectly, however, every time that the swing direction changes there are large peaks visible in the winch forces due to the error from one timestep to the next suddenly becoming very large. These short momentary peaks are unrealistic

because the winch drums in reality will not be able to rotate fast enough to provide the increase in tension this fast. The peaks are also visible in the forces on the spud pile, which is undesirable when looking at a CSD in operation including soil forces and wave forces.

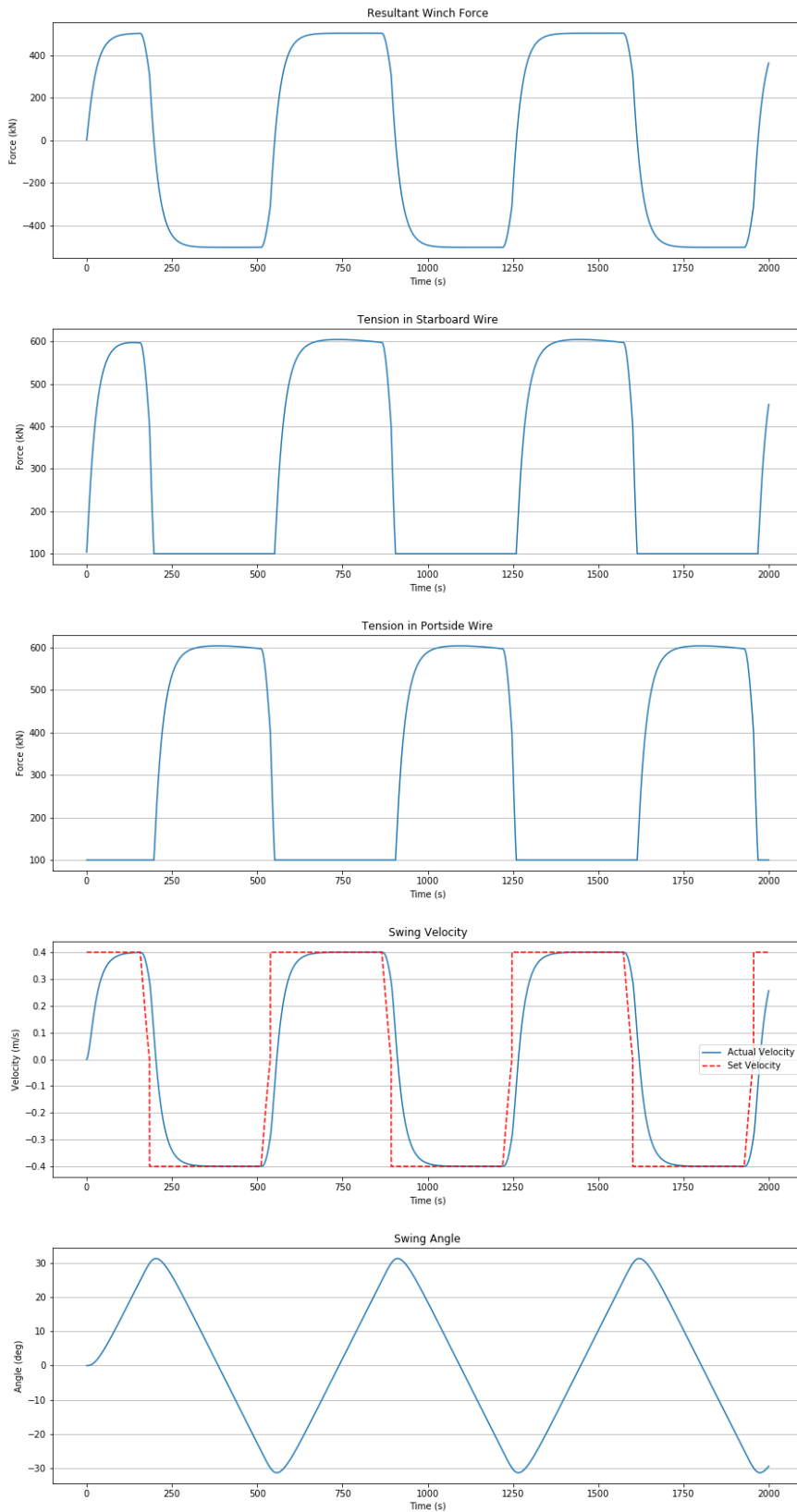


Figure 48 Forces over time with I-controller

The I-dominated controller shows good stability in the force output. The force diagrams are without peaks and the buildup is gradual. The force required to reach the desired velocity is 600 kN, which is similar to the other approaches. In contrast to the other approaches, the swing angle does not seem to have a clear influence on the needed hauling force, as no increase at extreme angles is visible. It can be seen that the angle precision is sacrificed since the set angle is passed with a minor amount. Although this exceedance is negligible and there are no real situations where a few degrees more would matter.



Figure 49 Resultant spud force for P-dominated controller



Figure 50 Resultant spud forces for I-dominated controller

Looking at Figure 49 and Figure 50, the advantage of using a gradually building up wire tension becomes visible. When taking into consideration that the goal of this research is to discover the dynamic forces which affect the CSD while it is in operation, it is clear that unnecessary peak forces on the spud are undesirable. The momentary peak forces in the wires greatly influence the forces on the spud. Since there is no cutting action yet, this is logical in order to maintain the equilibrium of forces on the system.

6.6 Conclusion

The PID controller, which actually is tuned here mostly as I-controller, can be concluded to give the best results. The main reasoning behind this conclusion is that the forces are built up gradually, which resembles the physical limitations of the winch system. However, as a side note, it should be clear that this approximation is artificial and in essence completely arbitrary. The most important argument is that in order to judge to what extent the cutting forces act on the spud, it is very convenient if the effect of the other forces, such as this force in the side wires, is as constant as possible.

Depending on the goal to which the simulation is run, the choice for the winch model can differ. For the purpose of this research, to find the behavior due to soil and waves, the I-controller is preferred.

6.7 Possible improvements

As noted in the paragraphs above, the module for the side wires can be improved in several ways. The main aspect has been the lack of physical phenomena which are always present in the real world. Each component related to the winch force acting on the wire can be modeled on its own to improve the accuracy or to be studied individually. A few examples are

- Drum characteristics; winch drums are dynamically complex components. The rotation is responsible for tensioning the wires, but due to the wire winding in or paying out, the diameter of the drum will vary. Furthermore, the actual drive of the drum might be a whole controller on its own, therefore it will suffice to state that a lot more time can be dedicated to obtain accurate insights in the behavior of the winch drums and how to incorporate it into the Python script.
- Realistic wire dynamics; the wires in the approach above are assumed to be linear with a fixed pretension of 100 kN. In reality, their shape is not a straight line but a slightly sagging line and near the anchors the wire could be pulled through the soil. These aspects can be taken into account, but depending on the approach used their added value might not always be clear since the driving force on the ladder might have much larger inaccuracies which could cloud the effects of neglecting the wire dynamics.
- Friction; as the wires move through the sheaves, and are wound in or out on the drums, they undergo friction. The friction present on the wires might lead to additional strain due to a larger resistance against their motion. It will depend on the approach taken whether this is a real issue.
- Anchor forces; the side anchors are responsible for the tension in the wires. As the winch winds in the wire, the anchor will have to maintain its location in order to obtain tension in the wire, and once sufficient tension has been reached, the fixation of the anchor will be responsible for the wire hauling the vessel to one side. Therefore the interaction between anchor and soil can be interesting to investigate. Similar to how the spud tip and the soil interact. Also the connection between anchor and wire can be of interest to discover its forces.

7 Cutting Soil

7.1 Cutterhead

The cutterhead is a cutting tool which is crown shaped. The crown is shaped by 5 or 6 arms which each hold a line of teeth or pick points. The teeth are responsible for cutting the soil. The layer of soil being cut by the cutterhead is called the breach. In reality, each tooth which comes into contact with the soil will undergo an individual cutting process. These processes are described extensively in cutting theories such as Miedema (2009). These theories explain how the angle between pick point and soil and the force and velocity involved are responsible for the amount of volume cut.

Looking at the bigger picture, the cutterhead in total is often portrayed as a circle in 2D diagrams, such as in Miedema (1987). Therefore when looking at 3 dimensions it is logical to model the cutterhead as a sphere, although in reality, it is half a sphere with a slightly flattened front. The main question to answer is then how the surface of that sphere rotates. In 2 dimensions the circumference of the sphere is obviously rotating around its center, but in 3 dimensions the area of the sphere rotates around its center axis. This axis can be defined by a vector which starts at the mount of the cutterhead and ends at the front. The direction of rotation of any point on the surface can then be defined by taking the in-product of the rotation axis and the normal of the surface, which is a vector which runs from the center of the sphere to the point of interest, as can be seen in Figure 52.



Figure 51 Cutterhead

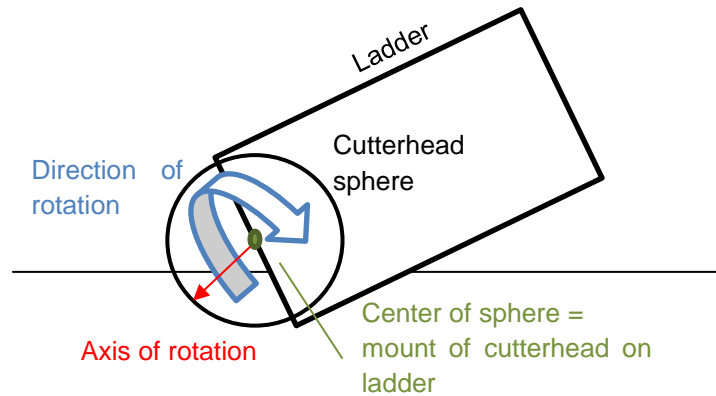


Figure 52 Schematic of vector representing the rotation axis

Table 13 Typical energy values per soil type

Type of soil	Specific Energy	Remarks
Sand	low-medium	Depends on water depth
Clay	low-medium	
Rock	medium-high	Upper limit is extremely hard

7.2 Reality

The cutting of soil is a complex process. Many different factors have to be taken into account at the same time. The exact description of the process requires the input of many parameters, or characteristics of the soil as well as the operational parameters. On top of that, different parameters need to be known for different types of soil or combinations of types of soil. For sand, the internal friction angle is important, while for clay the cohesion has great importance, and for rock, the breaking mechanism needs to be taken into account. For the tools used to cut the soil, it is important to know

the angle between blade, the tool which is cutting, and the soil, as well as the direction of its velocity. For each of these parameters mentioned a list of side notes can be added and different equations and approaches might be necessary.

In the dredging industry, the soil is often characterized by the Specific Energy (E_{sp}) value. It represents the amount of energy required to cut one cubic meter of soil, a general range per soil type is available in Table 13. Soft, sand-like soils will have a low specific energy as cutting them is quite easy, while hard rock-like soils will require a lot more force to cut and thus have a high specific energy. The main advantage of this method is that the failure mode of the soil, which occurs when it is cut, is irrelevant as only the volume cut is required. This is also the main disadvantage since the failure mode of the soil can cause a dynamically different behavior. The failure of rock is, for example, a more intermittent process than the failure of sand.

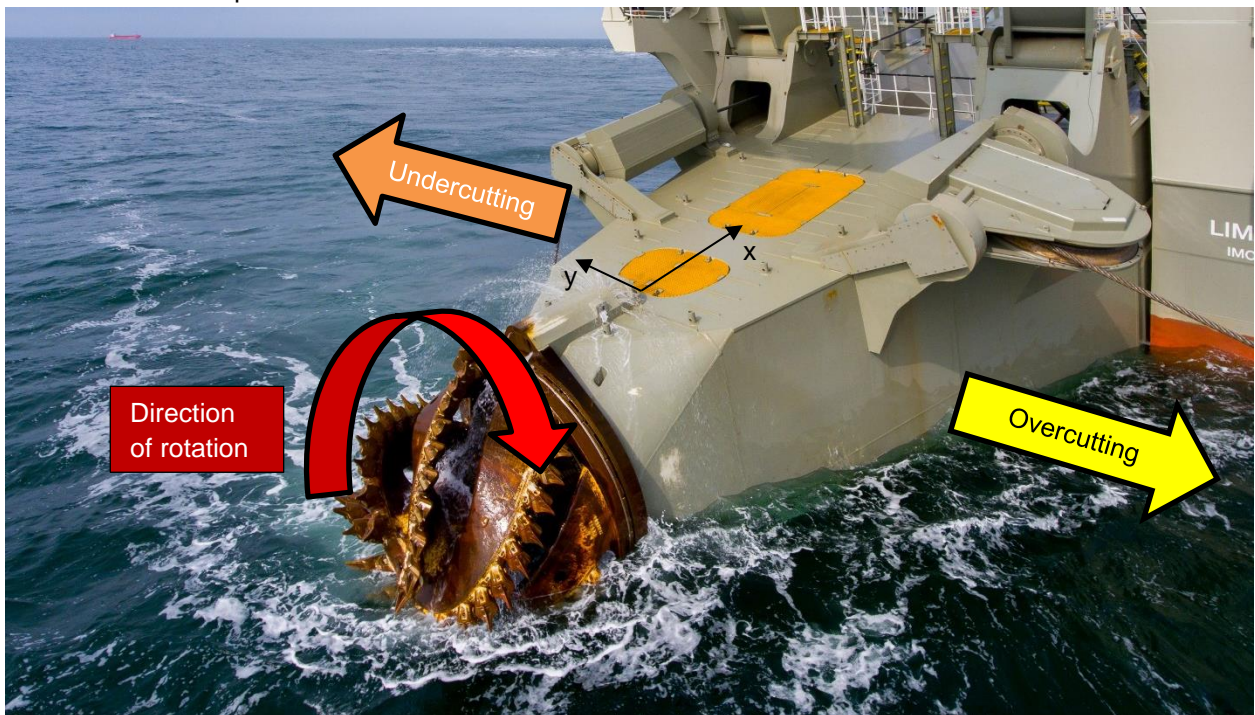


Figure 53 Difference between overcutting and undercutting

The resultant force can be calculated using the specific energy and the volume cut of a soil, but to know the direction of this force more information is needed. The direction of rotation and the swing direction are important to know as well. Most CSD's can rotate the cutterhead in only one direction, most common is clockwise when seen from the ship's axes system. The influence that the rotation of the cutterhead has on the resultant cutting forces changes however with the direction of the swing. There are two combinations possible of swing direction and cutterhead rotation. The first is called undercutting, which occurs when the cutter swings from starboard to portside with the cutterhead rotating clockwise, seen from the ship's axes. The teeth on the cutterhead will approach the breach at the bottom of the layer being cut. This will lead to the cutterhead having a tendency to want to dig deeper, pulling the ladder a bit down, it will also increase the needed hauling force in the swing wires.

If the swing is done in the opposite direction, from portside to starboard, while still rotating clockwise it is called overcutting. During overcutting, the teeth will approach the breach from the top. This will cause the cutterhead to try to climb onto the breach with a reduction in vertical forces as result. The climbing motion also is a forward motion, with cutterhead rolling itself into the direction it is swinging which could result in a reduction of the needed hauling force. In theory, the cutterhead could even accelerate itself to exceed the desired swing velocity while overcutting, which can be compensated by increasing the tension in the braking side wire. If the cutterhead rotates in counterclockwise direction

instead of clockwise, the terms overcutting and undercutting will have to be applied in their opposite direction.

7.3 Soil module

The requirements for a good soil cutting model are that the magnitude and direction of the forces on the ladder can be determined while also being able to keep track of where the soil has been cut and where the soil is untouched. There are several ways to incorporate the accounting of the cutting history in combination with the determination of the cutting forces. The most basic approach is to define a 2-dimensional grid representing the soil, with each point defined by a discretized x, y coordinate pair and assigned an initial height. The precision of this approach will depend on the distance between grid points. The ideal distance is a compromise between accuracy and calculation time. Through trial and error, a distance between points of 10 cm was found to give a good tradeoff between calculation time and accuracy of cutting forces.

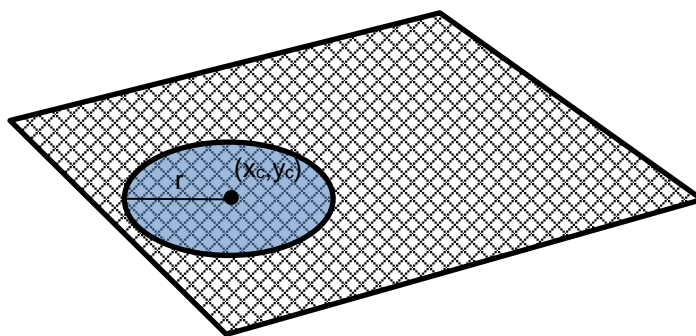


Figure 54 Collection of the grid points within radius r of cutterhead center

Assuming a spherical cutterhead then allows a simple search for all points within a radius of the center of the sphere. In this thesis, this step is done by creating a near-neighbor tree at the beginning of the run and comparing the cutterhead point to the points inside the radius of the tree using a KD-tree algorithm from the SciPy² package.

The position of the center of the sphere is the location on the ladder given by AQWA during each timestep. From this point, all the grid points within the radius of the sphere are collected, regardless of their height. Comparing the assigned height of these grid points with the height of the sphere's surface will then lead to the calculation of the amount of volume cut. If all the grid points have a height lower than that of the cutterhead, no soil will be cut as negative volumes cannot exist and it means the entire cutterhead is above the local breach. If soil at a point is cut, the assigned height will be adjusted accordingly in order to prevent that the same soil is cut twice.

Once the volume is known, the torque required to cut such a volume can be calculated using the specific energy value of the soil and the distance of the grid point to the rotation axis. The torque then is multiplied with the directional vectors of the sphere's surface in order to obtain the direction of the cutting force. The corresponding normal force can then be found by applying the fixed C/N ratio, which usually is kept at $C/N = 2$. This means that the normal forces are half the cutting forces. A summation of all the forces on all the points will give the total force and direction acting on the ladder.

The forces on the ladder are thus only related to the applied torque on the soil, which depends on the specific energy and volume cut per grid point. As a consequence, the swing direction and velocity are taken into account only indirectly through the amount of new volume cut and on which side of the cutterhead this volume is situated.

² <https://docs.scipy.org/>

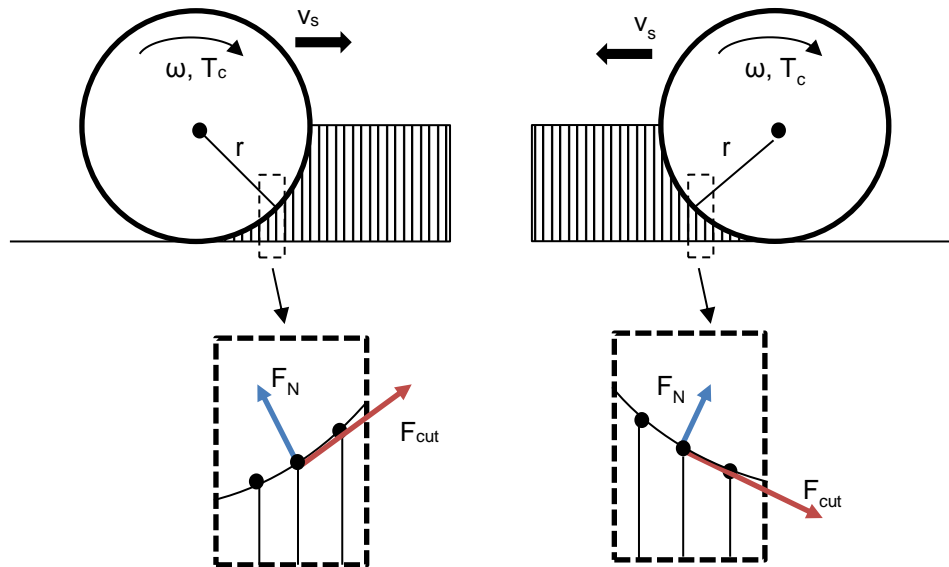


Figure 55 Schematic of forces on cutterhead per grid point for overcutting (left) and undercutting (right)

The sequence which is run to obtain the cutting forces is as follows:

1. Obtain coordinates of the center of cutterhead, x_c, y_c, z_c , from AQWA
2. Find all points on the seabed grid within the radius of the sphere using $(x_s - x_c)^2 + (y_s - y_c)^2 = r_c^2$
3. Per grid point (x_s, y_s) compare z_s with z_c . The latter can be found using $z_c = \sqrt{r^2 - (x_s - x_c)^2 - (y_s - y_c)^2}$ which leads to the difference in height between grid point and cutterhead surface: $dz = z_s - z_c$
4. From the grid definition, the area per grid point is known as the area of each grid point is the same, depending on the resolution chosen. Therefore the volume of the cut soil per grid point is known to be $V_{cut} = A_s \cdot dz$ then set $z_s = z_c$ for the next timestep to take into account that soil has been cut.
5. The required torque to cut the amount of soil per grid point can be calculated by $T_c = (V_{cut} \cdot E_{sp}) / (2 \cdot \pi \cdot (RPM/60) \cdot dt)$
6. Calculate the angle between rotation axis and normal vector by taking the dot-product between the two directions as $\theta = \arccos(\mathbf{n}_{rotation} \cdot \mathbf{n}_{normal})$
7. Orthogonal to the normal vector is the vector of the cutting force, therefore the cutting arm between rotation axis and cutterhead surface is $R_c = \sin(\theta)$, and the cutting force is obtained through $F_{cut} = T_c / R_c$
8. Divide F_{cut} vector in x, y, z components $F_{x,c}, F_{y,c}, F_{z,c}$ using the cross-product of the rotation axis and the normal vector
9. Obtain the normal forces corresponding to the found component cutting forces by dividing by the C/N ratio, $F_{x,n} = F_{x,c} / (C/N)$.
10. Sum all the forces and volumes from the grid points being cut
11. Send the sum of the total forces, translated into each component of the global axes directions F_x, F_y, F_z to AQWA

Inhomogeneous soil can be created by applying a random variable on top of the E_{sp} per coordinate pair. The shape of the cutterhead can also be adjusted by creating a function which outlines the shape and then by verifying that the found grid points are indeed within this shape, which means they comply with the function entered.

7.3.1 Static test of soil model

In the static test, the soil model will be tested without interaction with AQWA. This is necessary in order to be able to isolate the soil forces and to verify them in relation to the cutterhead's path. The path can be any desired direction or a collection of unconnected points. The latter will lead to the maximum amount of soil cut for the used z-coordinate of the cutterhead. The goal is to verify whether the direction and magnitude of the volume and the forces found from the soil model are computed correctly.

Table 14 Variables for soil module

Variable	Value	Unit	Remark
E_{sp}	medium	J/m ³	Specific Energy
r	1.5	m	Cutterhead radius
x_s, y_s	0.1	m	distance between grid points
(x_a, y_a, z_a)	(-1.0, 0.0, -1.0)	m	Rotation axis orientation

Without motion, the soil model only depends on the depth of the cutterhead compared to the seabed level. This means that if the cutterhead is without motion located halfway into the soil ($z_{center} = z_{seabed}$), half the sphere volume will be cut and nothing else. For a sphere with a radius of 1.5 meters, the total volume is $(4/3) \cdot \pi \cdot r^3 = 14 \text{ m}^3$, half of this should be about 7 m^3 . Which is visible for the first time step in Figure 56, note that during the rest of the time series the volume is not 0 m^3 but $V/(2 \cdot r) \cdot v_s \cdot dt = 7/(2 \cdot 1.5) \cdot 0.4 \cdot 0.1 = 0.09 \text{ m}^3$.

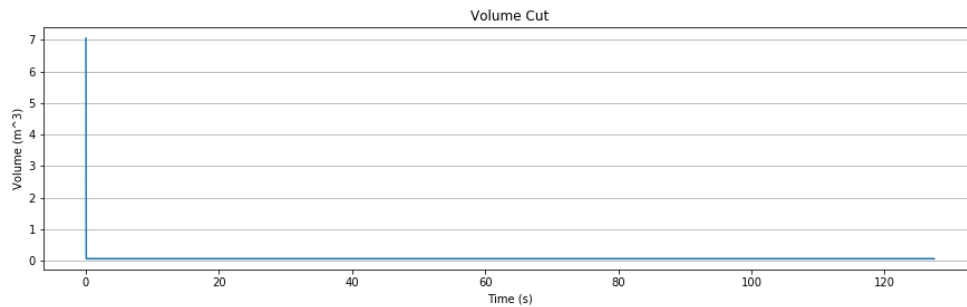


Figure 56 Volume cut in static test

If the cutterhead is then moved horizontally in y-direction, the total volume cut will have the shape of half a cylinder with spherical ends. The ends together should make the 7 m^3 again and the half of the cylinder shape should be $\frac{1}{2} \cdot L \cdot \pi \cdot r^2 = 0.5 \cdot 50 \cdot \pi \cdot 1.5^2 = 176.7 \text{ m}^3$, which when summed together should be 183.7 m^3 for $L = 50 \text{ m}$. The found total volume cut for a trajectory of 50 meters is 182.9 m^3 which corresponds fairly well to the expected value of 183.7 m^3 . The direction of the forces also matches the outcome of this first model.

Now that has been verified that the correct amount of volume is cut during a swing, it is time to verify whether the direction and magnitude of the cutting forces are correct. It is very important to realize that there are two main components for the magnitude and especially the direction of the cutting forces. First the direction of the rotation axis of the cutterhead has a lot of influence, and second, the location on the cutterhead where volume is being cut is of big importance. The location of the volume on the cutterhead is related to the swing direction. It is logical that a swing to starboard will lead to the starboard side of the cutterhead cutting soil while the port side is cutting none while assuming that the cutterhead doesn't move vertically. In Table 15 the directions for the standard cases are displayed, as mentioned above, certain combinations may result in a change of direction.

Table 15 Directions of the force components

	Overcutting positive direction	in y-	Undercutting negative direction	in y-	Undercutting positive direction	in y-	Overcutting negative direction	in y-
$F_{normal,x}$	+		+		+		+	
$F_{normal,y}$	-		+		-		+	
$F_{normal,z}$	+		+		+		+	
$F_{cut,x}$	-		+		+		-	
$F_{cut,y}$	+		+		-		-	
$F_{cut,z}$	+		-		-		+	

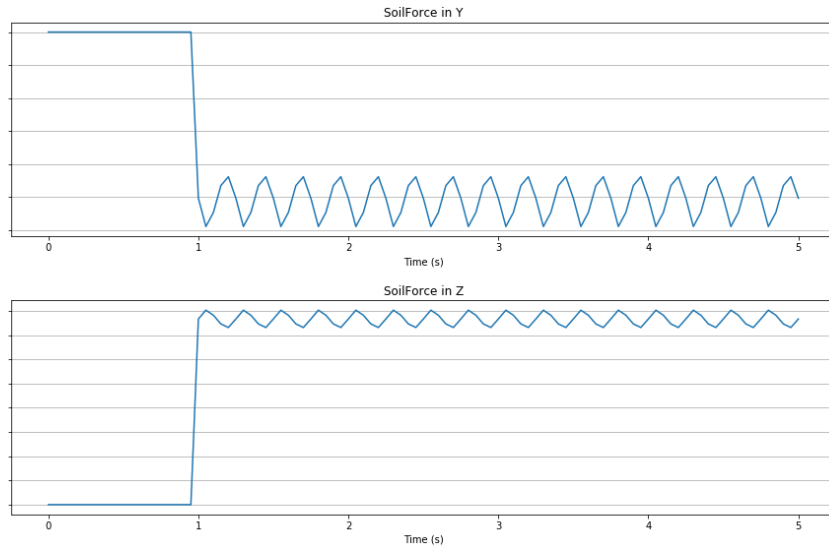


Figure 57 Resulting forces in static test

In Figure 57 it is visible that the resulting forces, the sum of cutting and normal forces, are already quite intermittent. Since there are no oscillations of the cutterhead, it must be caused by the discretization of the soil. The full results of the static test are presented in Appendix H.

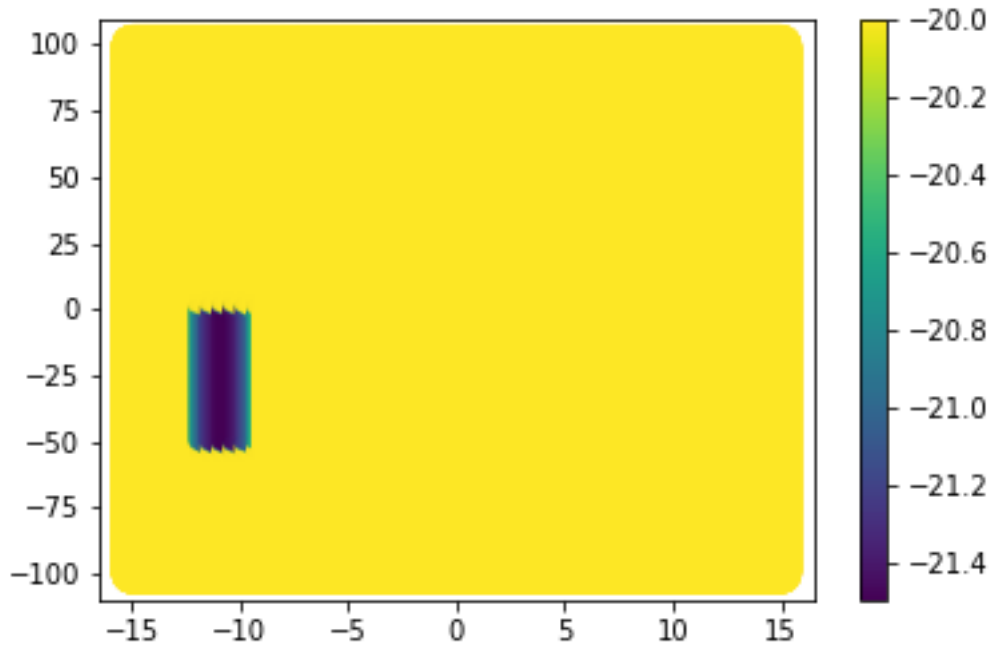


Figure 58 Contour plot of the static trajectory

When cutting in an arc, like a swing around the spud pile, the result is a bend half-cylinder, adjusting for the arc length by using $L_{arc} = R \cdot \theta$, with θ the swing angle in radians, then using L_{arc} for L in the volume equation above gives the total volume cut. In the global axes system the components of the cutting force will now vary, while in the local ladder axes system the forces should remain as above.

7.3.2 1 DOF test of ladder

The next step to verify the functioning of the soil model is to add a degree of freedom. Since the ladder is connected to the vessel through a hinge, restricting all relative motions except for relative pitch, the degree of freedom chosen for the model is the pitch angle of the ladder. In this approach, the hinge where the ladder is located will be the point which will determine the location of the cutterhead. If the hinge is moved laterally then the cutterhead will do so as well. The cutterhead is now allowed to experience variations in the vertical height, which should lead to a less smooth cutting process and a slightly different volume cut. The hoisting wires attached to the ladder are modeled as a spring between the A-frame on the vessel and the ladder. The actual situation has been explained already in 2.2.2.

Table 16 Parameters used in the 1 DOF test

Parameter	Value	Unit	Remarks
m	$1.5 \cdot 10^6$	kg	Mass of the ladder
k_{hoist}	$1 \cdot 10^7$	N/m	Stiffness of hoisting wire
c	$5 \cdot 10^6$	Ns/m	Total damping in system
ϕ_0	30	degrees	Initial angle
J	$2.0 \cdot 10^{10}$	kg.m ²	Mass moment of inertia

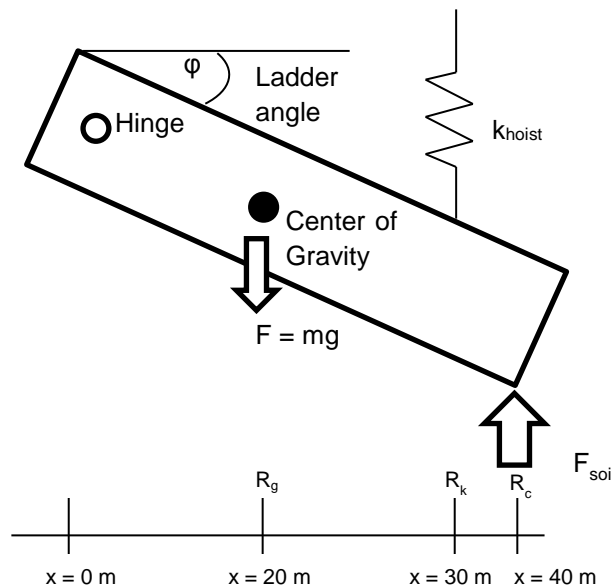


Figure 59 1 DOF model

Since the degree of freedom is the pitch of the ladder and the mass of the ladder, m , is modeled as a distributed load, the mass moment of inertia has to be calculated using $(m/12) \cdot R_c^2 \cdot H^2 + m \cdot R_g^2$ for a rectangular volume, which comes down to $J = (1.5 \cdot 10^6 / 12) \cdot 40^2 \cdot 10^2 + 1.5 \cdot 10^6 \cdot 20^2 = 2.0 \cdot 10^{10} \text{ kg.m}^2$.

Assuming small motions the equation of motion can be put in linear form as:

$$J\ddot{\varphi} + c\dot{\varphi} + k_{hoist} * R_k * \varphi = F_{soil} * R_c - m * g * R_g$$

In this equation the damping c is taken at the hinge and given a value of $5 \cdot 10^6$ Ns/m to simulate all the aspects which in reality would reduce the excitation of the system, such as friction in the hinge and sheaves, drag due to motions through water and damping due to the cutting of the soil.

The strain in the wire due to the static weight of the ladder has to be taken into account when determining the unstretched wire length of the hoisting wires. In the equation of motion $k = (l_1 - l_0) / l_0 * EA$ in which $l_1 = R_k * \varphi$ has been used and the most stable value for l_0 was found to be $l_0 = 9.0$ m. To simulate the viscous damping of the water, as well as friction in the hinge and other sources of damping a general damping value has been applied at the hinge.

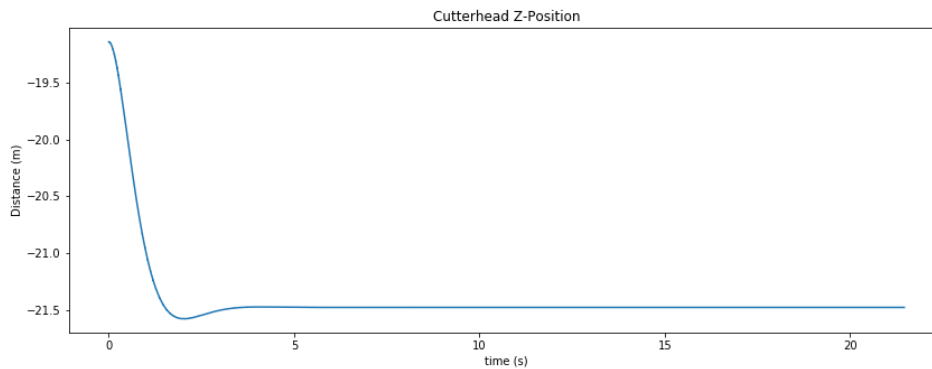


Figure 60 Single degree of freedom model motions, excluding cutting forces

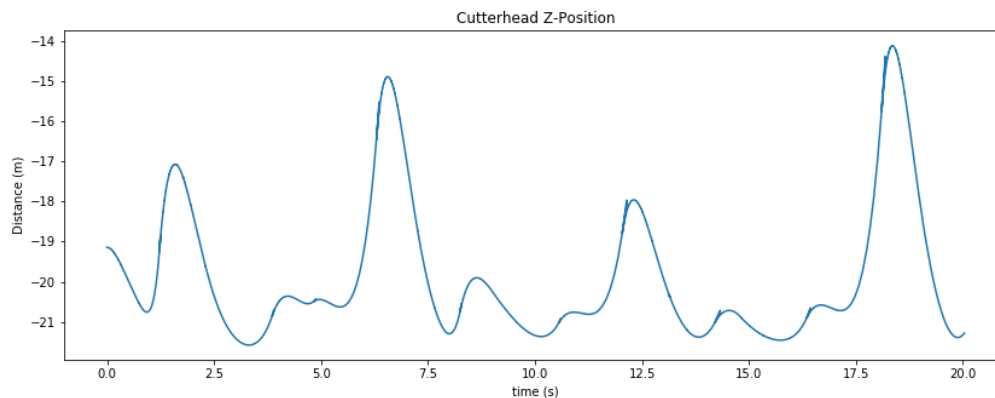


Figure 61 Single Degree of Freedom model motions, including cutting forces

The resulting motion of the ladder in the 1 degree of freedom system is in Figure 61. It reacts quite heavily as it struggles to find the delicate equilibrium between the large cutting forces and stiffness of the system. The resulting soil forces, shown in Figure 62, are of course also quite erratic, but the general trend seems to be in the same order of magnitude as the static model, with the exception of a few peaks corresponding to vertical motions below the -21 m in Figure 61. Note that the x- and y-values are a bit unreliable as the system is imposed a motion in these directions, resulting in perhaps unrealistic volumes of soil cut, such as visible at $t = 0.5$ s.

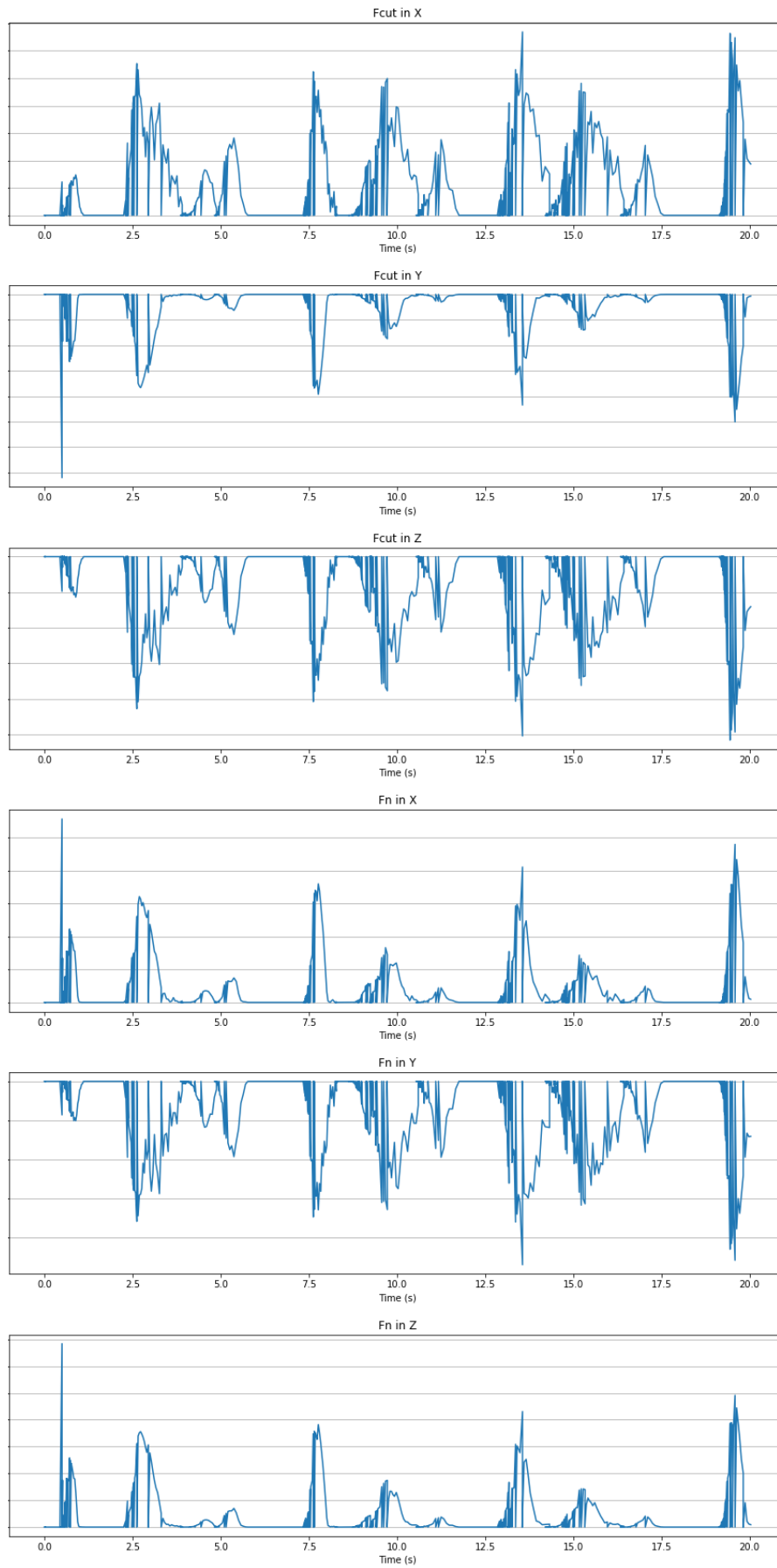


Figure 62 Cut and normal forces due to the 1DOF motion

7.3.3 Single swing

With confidence in the soil model obtained through the tests above, it is time to add the interaction with AQWA. Using the coordinates given by AQWA for the defined center of the cutterhead the soil reactions on the vessel can now be found. The rotation axis is now defined by the difference in the moving coordinates for the center of the cutterhead and the moving coordinates for the flat front of the cutterhead, which have been defined in the input for the script. This ensures that the rotation axis is always pointing in the correct direction in the local cutter axes system. A first run with a single swing from the centerline to starboard and back will indicate whether the interaction with AQWA is successful. There should be no cutting forces when the swing returns because no step forward has been made, as it should have cut all the soil on the first trajectory, with the exception of small oscillations due to slight bouncing of the cutterhead on the first half of the swing.

In Figure 63 the results of the swing are shown. The process is far more stable and has lost most of its intermittent character of the previous models. This is probably due to added mass and the inertia of the CSD, in combination with potential and viscous damping. The cutting force components are in the correct direction, and the order of magnitude is in line with the expectations. It is interesting to see that on the return part of the swing there is still some soil being cut. Looking at the height of the cutterhead it could be explained that the first cut the cutterhead is lifted by the presence of the soil, about 0.2 m upwards. On the return trip it falls in its equilibrium position and now encounters those 20 cm of soil for the duration of the swing back to the centerline.

Also note that near $t = 400$ s, the cutterhead crosses the centerline in the opposite direction, leading to a full layer of soil that needs to be cut. This causes large peaks in the forces, as would be expected with such a sudden transition.

For more graphs, see Appendix H.

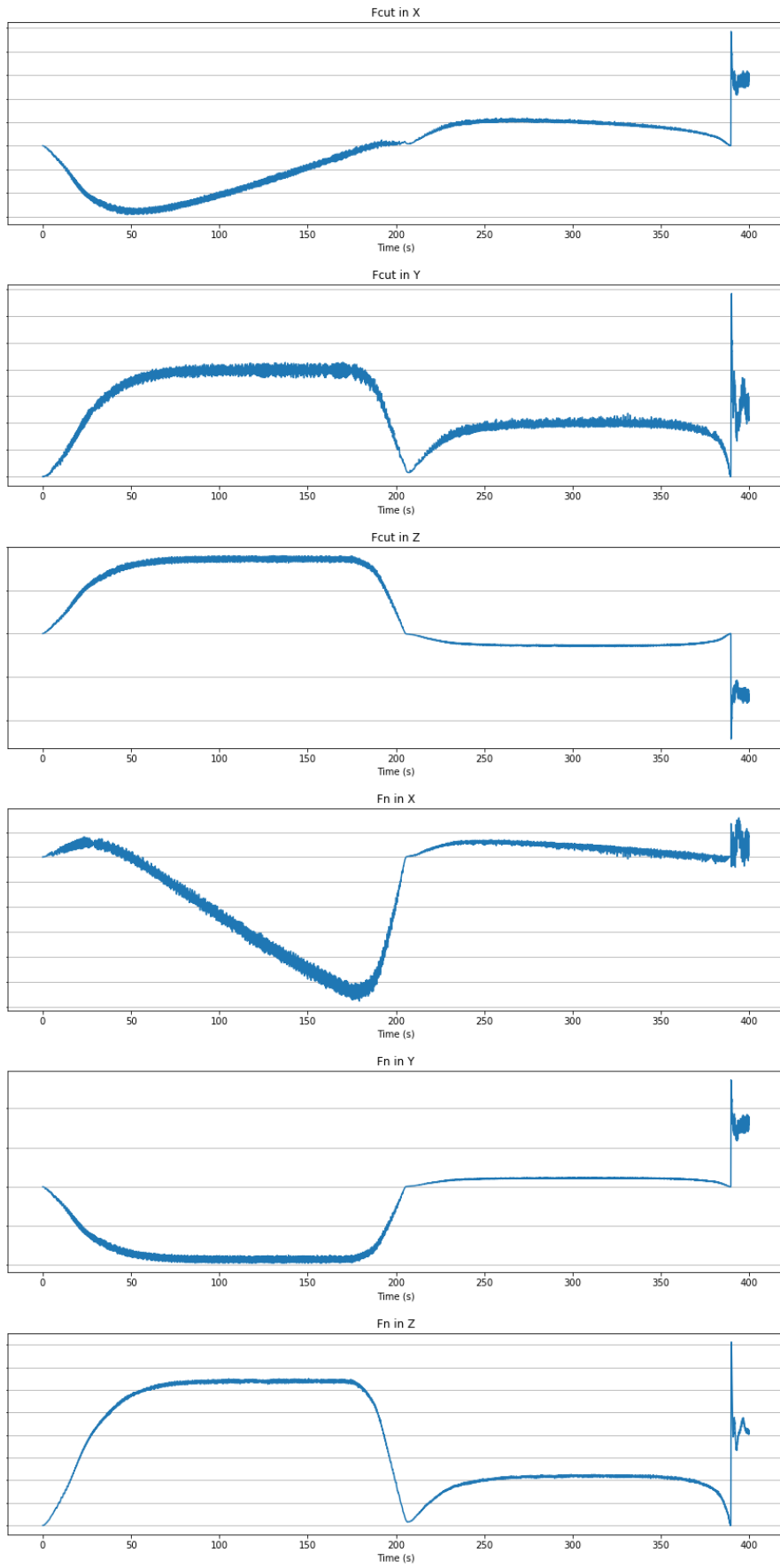


Figure 63 Cutting forces for a single swing

7.3.4 Full process

Incorporating the whole process with the soil model will show whether the system is stable. Stepping forward at the end of each swing ensures that fresh soil is cut continuously. It is expected that the results of the first half of the swing of the test at 7.3.3 will be continued throughout the swings and steps. Any irregularities in the forces should occur in combination with irregular motions of the CoG.

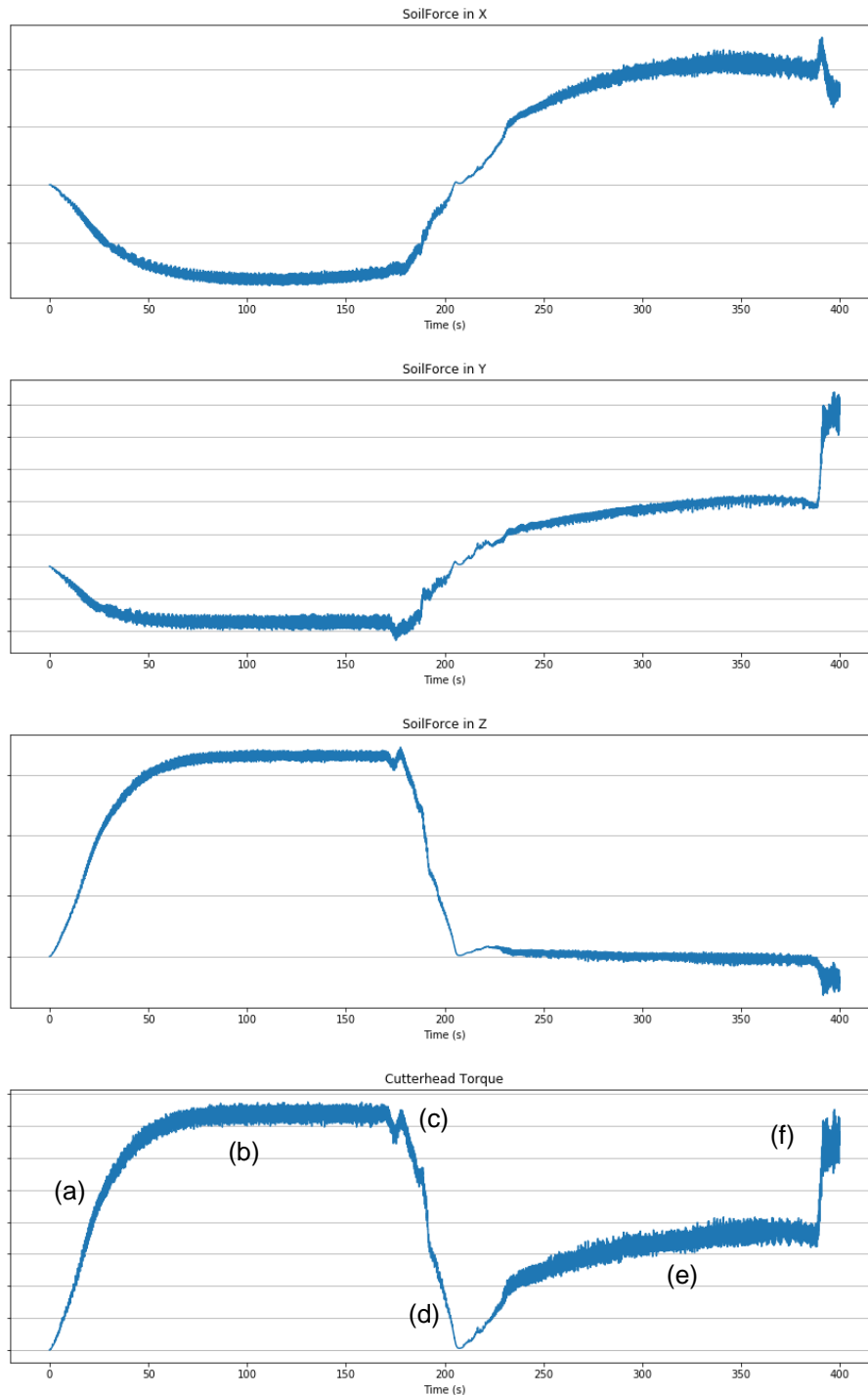


Figure 64 Volume cut and corresponding cutterhead torque

In Figure 64 the resulting forces in x, y, and z-direction and displayed with the rotational torque applied by the cutterhead. Several stages of the cutting process can be seen from the graphs.

- Is the startup stage, the swing velocity is gradually increasing and as a result, more volume per timestep is cut, which of course leads to an increase in torque and forces. The swing is

made towards portside and a counterclockwise rotation from the perspective of the ship's axes system.

- b. The swing velocity is now maintained constant and as a result, a continuous process is visible. There are small varieties present, due to the discretization of the grid. The vertical cutting reaction force is a combination of a positive normal force plus a positive cutting force since the cutterhead is overcutting.
- c. The swing angle is now near the maximum swing angle, the step forward is made while at the same time the swing velocity is reduced to start swinging to the other side. The effect of the step is slightly visible in the vertical cutting reaction forces and the torque diagram.
- d. The point where the cutter starts swinging in the other direction has a swing velocity of zero, therefore no new soil is being cut and the forces are zero as well. The swing will now start in starboard direction, having stepped forward almost 1 m.
- e. The swing towards starboard has less volume cut because of the even soil level created during the portside swing. For all the future swings following this arc, the volume cut, and therefore the reaction forces encountered, should be roughly the same. The resultant forces are of different proportion due to a different combination of cutting and normal forces.
- f. The cutterhead crosses the centerline and encounters a larger volume of soil, which has not previously been cut by the swing to portside. As a result, a large peak is visible in the forces.

It is interesting to note that although the cutting forces are relatively small, at the same order of magnitude as the side wire forces, there is a very small effect noticeable in the increase in winch force, this perhaps also is related to the use of a PID controller versus the use of individual wire forces. The effect is especially visible when the cutterhead approaches a higher volume of soil towards the end of the time series.

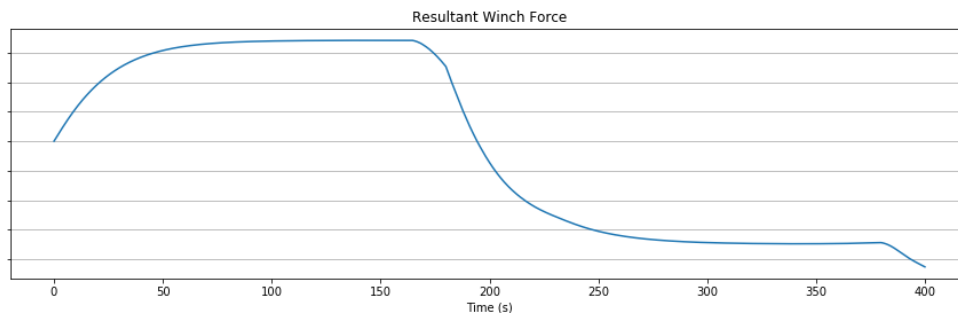


Figure 65 Resultant winch force when cutting soil



Figure 66 Spud force at full operation

The spud forces are barely affected by the cutting of the soil. The step force is the main peak in the diagram, due to the inertia of the vessel always causing a discrepancy between the step the model thinks it has taken and the actual step which was made. Over time it is visible that this effect balances itself out again. The little dip in the diagram at the end is the moment that more soil is encountered. Since overcutting occurs at this moment the cutting force is in the same direction of the winch force on the ladder, since the resultant force on the spud actually reduces.

7.4 Different soil types

With the model fully functioning a study of the effects of different soil types can be made. It is expected that hard soils will generate larger loads on the cutterhead, which then are transferred onto the spud pile. The specific energy of the soil will be the only parameter which will be adjusted, the rest will be kept constant. This also means that the swing velocity might be unrealistically high since in reality, for very hard soils it is set at a lower value.

Table 17 Values used for comparison of soil types

Soil Type	Specific Energy	Swing Velocity	Winch Model	Spud Model
Clay	Low	0.4 m/s	PID, I-dominated	Pinned, linear
Sand	Medium	0.4 m/s	PID, I-dominated	Pinned, linear
Rock	High	0.4 m/s	PID, I-dominated	Pinned, linear

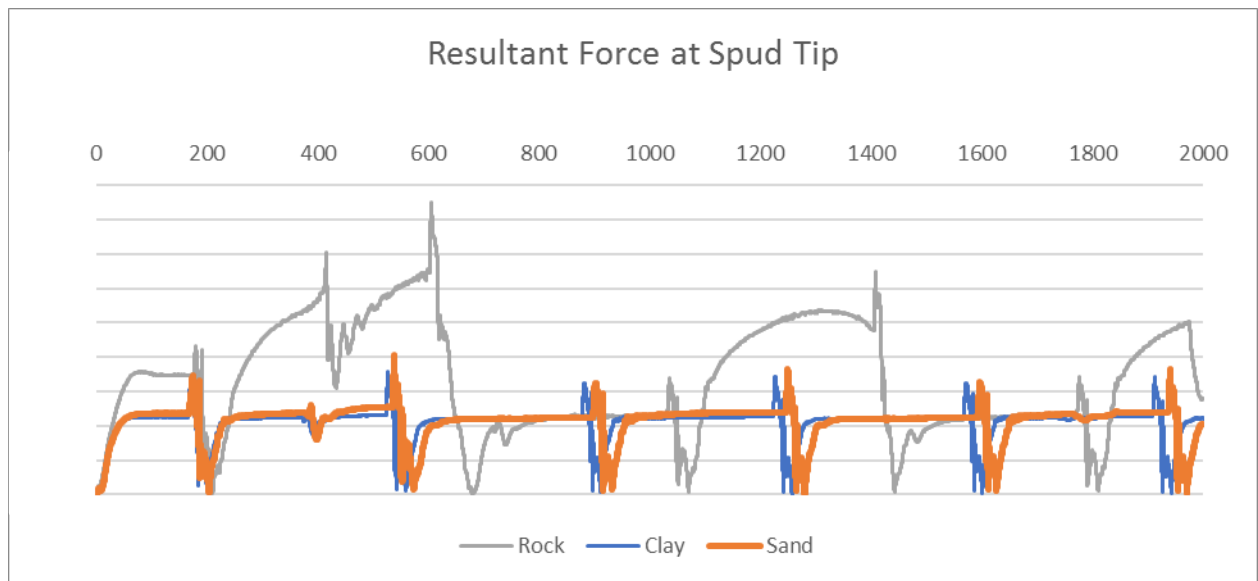


Figure 67 Resultant force at spud tip for 3 different soil types

The complete overview of all the results can be found in Appendix H. It is clear that indeed with hard soil types, such as rock, larger forces occur on the spud pile. A few interesting points which can be seen in the graphs are:

- The time when the step forward is made is later for rock, indicating that the average swing velocity is lower than the set swing velocity.
- The effect of overcutting and undercutting becomes clearly visible on the spud pile for rock, whereas for sand and clay it is difficult to spot.

7.5 Conclusion

A general overview of the results generated by the soil module shows that the module indeed functions as intended. The module consists of a discretized soil grid which uses specific energy as its input. Through the directional vectors acting on the grid points the energy is translated into force components. The comparison between different soil types shows that the effect of cutting soft soils has little influence on the spud and winch forces. While for rock there is a clear increase visible. This is a good indication that indeed the combination of all the modules is successful.

7.6 Possible Improvements

The cutting module could be expanded in the future. These aspects have not been taken into account in this study as the focus was on the determination of the forces. This model could also be applied for different goals and therefore the following points could be studied or incorporated.

- Inhomogeneous soil; as discussed before the effects of inhomogeneous soil can be simulated by either applying a random generator on the specific energy value per grid point being calculated or by applying a conditional statement for specific grid points which when found true will use a different specific energy value, thereby simulating obstacles. A third method is adjusting the height at specific grid points, which can also simulate a different specific energy value.
- Faster soil model; the current approach can lower the calculation speed considerably. The accounting of the soil height per grid point, and its comparison to the cutterhead's height, is what takes up most of this additional processing power. Therefore, an alternative model could be created which does not account the actual soil but solely works with deviations from the ideal path. The main advantage of CSD's is their high precision, this characteristic can be used in the numerical modeling as well to reduce the processor load.
- Modeling of teeth; an approach where each tooth is modeled and its forces are translated to the cutting axle is possible. Here the individual blade angle per tooth will determine the direction of the cutting forces. This approach might give more accurate results, also due to a better fit with the real shape of a cutterhead, but will be resource intensive since large cutterheads can have about 50 teeth installed, which all need to be translated and rotated each timestep in order to obtain the correct angle. When modeling the individual teeth, the wear per tooth can also be included.
- Stall effects; if the cutterhead encounters too much or too hard soil, the possibility exists that it can no longer make the rotation and stall. The effects of a stalling cutterhead on the soil and the forces this creates on the ladder could be quite interesting.
- Lowering of the head into the breach; the current model assumes the ladder is always on -20 m, or a ladder angle of 30°. Using the 2 body approach the model can also be applied to simulate the lowering of the ladder from horizontal position to the contact with the breach. The hoisting wire then needs to be modeled in the Python script, and no longer in the AQWA input. This additional force might be difficult to control, especially as the length of the wire will change, and if not done precisely this could cause undesirable dynamic effects.
- Production; by introducing spillage into the equation of the amount of soil cut, production of cubic meters of soil can be calculated. The question remains whether the environmental and operational parameters are sufficiently accurate in order for the production volume to be relevant. This can be a subject for future investigation.

8 Waves

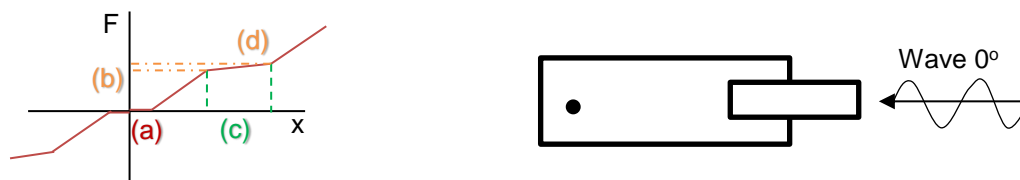
The testing of the modules in the previous chapters was done in a still water environment in order to be able to isolate the effects of each module. Large CSD's, such as the Helios, are built to operate at sea. This means that the vessels will be subjected to wave loads which should increase the forces acting on the spud. The study to the effects of wave loads in this chapter is limited to a single wave spectrum from one direction. This is due to the limited time that remained to hand in this thesis, several operational situations, such as the combination of the flexible spud carriage and the cutting of soil, have therefore not been included.

8.1 Flexible spud carriage

The main goal of a flexible spud carriage is to reduce the loads on the spud due to wave motions. To verify that this is also the case a comparison between the vessel modeled with a linear carriage and a flexible carriage will be made. The CSD is assumed to be moored just with the spud and without forces from the side wires or cutting soil present.

Table 18 Parameters used in comparison

Parameter	Value	Unit	Remarks
H_s	2.0	m	Significant wave height
T_p	7.5	s	Peak period
Wave Heading	0	degrees	See also 4.1
Buffer activation (b)	250	t	Load on spud pile
Cylinder stroke (c)	0.3	m	Includes effects of wire strain
Tension increase (d)	50	t	Throughout cylinder stroke
Clearance (a)	0.01	m	between pile and guide
Spud Model	Cantilever	Flexible	See also 5.4



Stiffness of flexible spud carriage

Figure 68 Overview of stiffness and wave direction

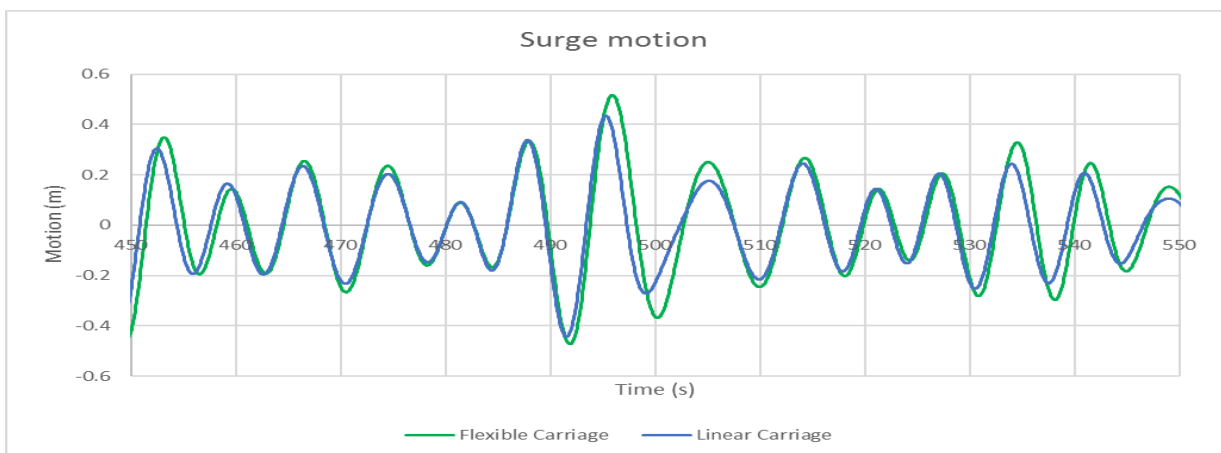


Figure 69 Surge motion with linear and flexible carriage

Since CSD's are often used for cutting soil with precision it is important that the flexible carriage does not compromise on the ability to maintain position. In Figure 69 is visible that the flexible spud carriage has slightly larger motions. The difference in the surge motion is always smaller than the maximum stroke of the cylinder. Therefore when looking at the resultant spud force, the peaks should always remain below the 300 t. It should be noted that the cantilever spud model used here, takes the flexibility of the carriage in the surge motion, whereas in reality the flexibility of the carriage is in the pitch motion of the vessel³.

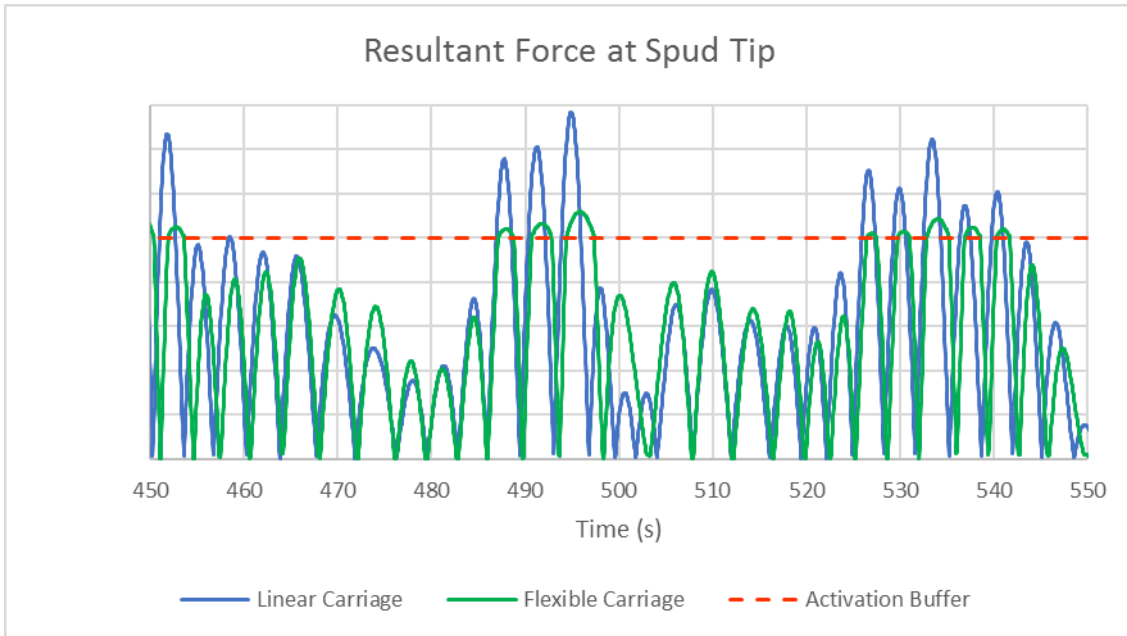


Figure 70 Spud forces due to waves with linear and flexible carriage

In Figure 70 is shown that once the spud load exceeds 250 t, the difference between the linear and flexible carriage becomes very clear, with significantly lower forces occurring on the spud pile. It is also visible that indeed the maximum spud force for the flexible carriage is below the 300 t, confirming the observation in Figure 69. It is remarkable, however, that the differences between the peaks in the surge motion and the differences between the peak in the spud force do not exactly coincide. The cause is that the oscillations of the spud forces are at a higher frequency than the oscillations of the surge motion, which indicates that there is a delay due to inertia between the two.

8.2 Combination of waves and cutting

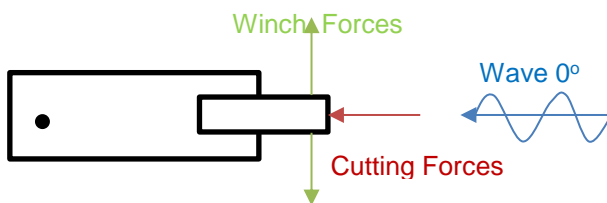


Figure 71 Overview of combination of waves and cutting soil

Adding waves to the cutting process is the final objective of this research. In 8.1 it was already visible that waves can introduce large forces into the system, while in 7.4 it shows that for hard soil types the cutting forces can become quite large as well. Therefore the combination of the two is interesting. In general, it is often assumed that the cutting of soil reduces the wave loads on the spud pile. This is

³ IHC Merwede. (2008, Spring). Dynamic simulation of a Cutter Dredger at sea. *Ports and Dredging*, pp. 6-13.

because the cutter can transfer some of the wave loads on the vessel onto the soil. However, the additional motion can lead to a more intermittent cutting process, where the volume cut per timestep can vary more, leading to higher peak forces on the cutterhead.

Table 19 Parameters used for cutting of 3 soil types in waves

Parameter	Value	Unit	Remarks
H_s	1.0	m	Significant Wave Height
T_p	7.5	s	Peak period
v_s	0.4	m/s	Swing Velocity
E_{sp} clay	Low	kJ/m^3	
E_{sp} sand	Medium	kJ/m^3	
E_{sp} rock	High	kJ/m^3	
Spud Model	Pinned	Linear	See also 5.2.2
Winch Model	PID	I-dominated	See also 6.5

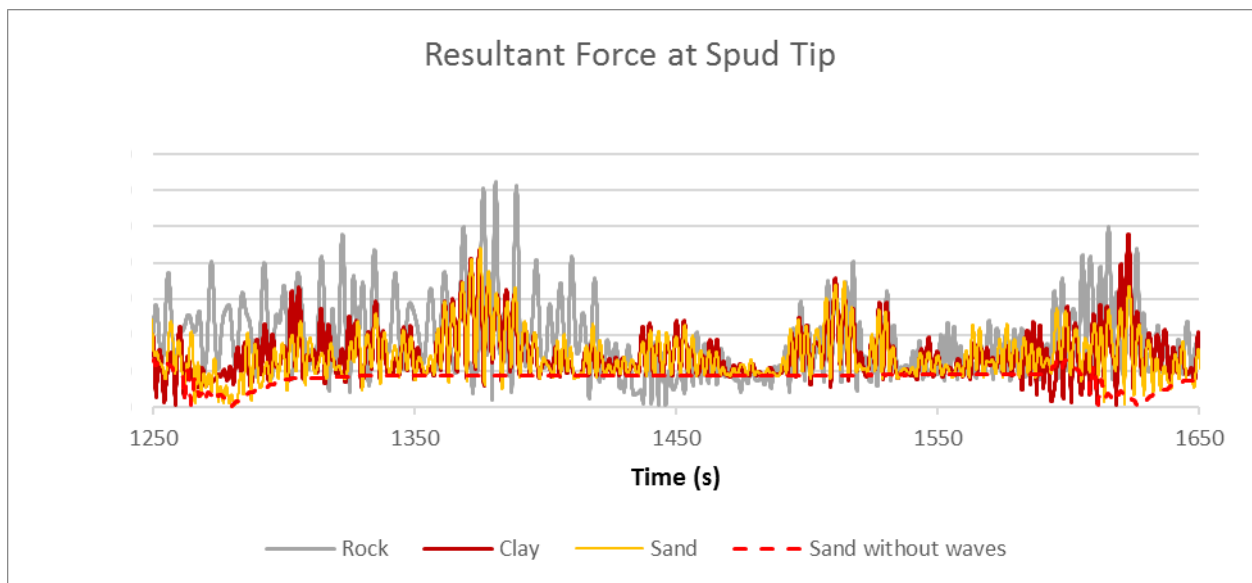


Figure 72 Resultant spud forces due to waves and cutting soil

In Figure 72 it can be seen that the process is now very intermittent. The dashed line from the settings without waves shows that a single swing has been made during the timespan displayed. It is also worth noting that even though the values for cutting rock are a lot higher, that the difference between the soil types has become slightly smaller. This makes a lot of sense considering that the wave loads alone cause higher loads than the cutting forces without waves.

8.3 1 Body vs 2 Body

In 3.3 two different approaches for the modeling of the geometry were explained. With all the features of the different modules incorporated into the model, it is time to look back and compare how the two geometries behave. The main difference is the mass and inertia that are modeled as rigidly connected to the cutterhead. For the 2 Body approach this is just the ladder because of the additional degree of freedom and for the 1 Body approach it is the entire vessel. This means for the 2 Body approach that the cutterhead can have larger motions because it is not directly constrained by the relatively large mass of the hull. How large this additional motion is when cutting soil and how this affects the forces acting on the vessel will be shown in the graph below.

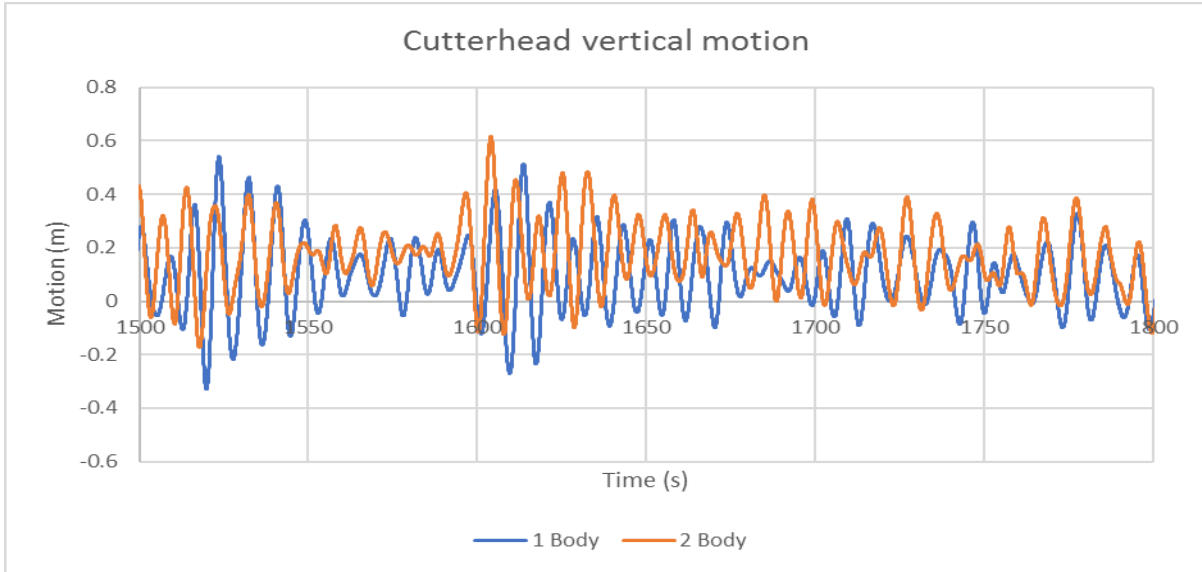


Figure 73 Cutterhead motions due to the cutting of soil in waves

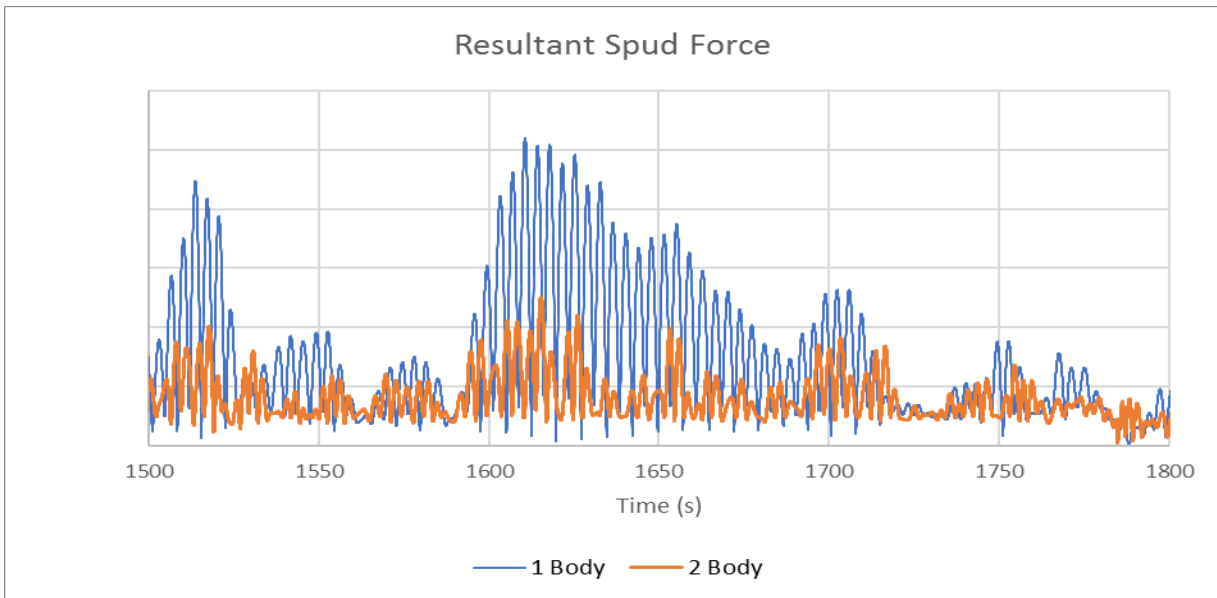


Figure 74 Difference between 1-body and 2-body approach

As can be seen, the vertical motion of the cutterhead is of the same order of magnitude. The resulting forces on the spud pile are, however, much larger in the single body approach. In Figure 75 the difference in pitch motion is visible, showing the effect of the additional degree of freedom in the 2 Body approach. It can be determined from the graph that the relative pitch motion of the ladder reduces the total pitch of the vessel, leading to lower forces on the spud. It should be noted that the calculation here is done with equal timesteps but that the single body can be run with a timestep twice as big; 0.1 s instead of 0.05 s. For long simulations, of more than 1 hour, this is a big advantage. The sacrifice then is the accuracy of the forces acting on the spud pile, which will be largely overestimated when using a single rigid body approach.

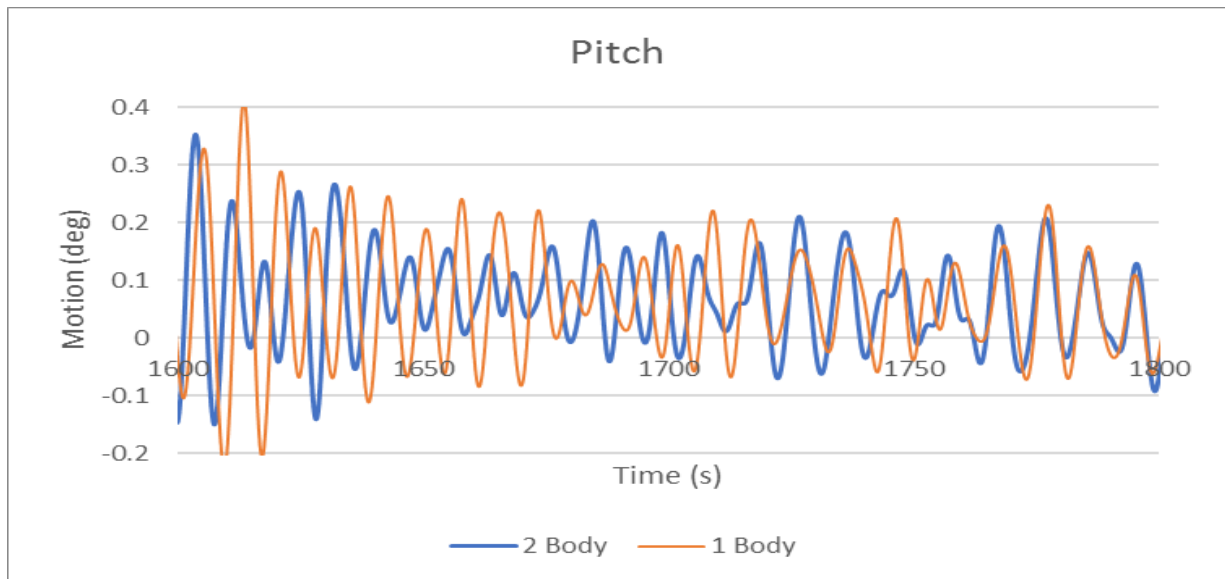


Figure 75 Pitch motions of 1-body and 2-body approach

8.4 Conclusion

The addition of waves to the model introduces large forces into the system. The installation of a flexible spud carriage definitely reduces these loads on the spud pile according to the results presented here. The effect of waves on the cutting of soil is also as expected, more intermittent and in general slightly larger than in still water but still a better situation than the wave loads without soil. The difference between using a single rigid body and a separate body for the ladder and hull, is remarkably small.

8.5 Recommendations

The flexible spud carriage has only been tested while being moored by just the spud. It would be interesting how the flexibility of the carriage effects the loads on the spud when combined with the full operation of cutting soil in waves. To reach to this stage it is recommended to first investigate the difference a flexible spud carriage makes for a swing without soil but including waves and for the cutting of soil without waves. The reduction in stiffness could lead to a less precise cutting process. It should be interesting to see whether the flexible carriage still leads to a reduction of the spud forces or whether the effects of the flexibility disappear amongst the combination of all the loads.

Furthermore, the combination of cutting soil and waves has only been investigated for one type of wave spectrum. The CSD does rotate around the spud pile, which means that a wave from 0° becomes a relative wave of 30° . This choice is due to the principal focus of interest on the surge and pitch motions of the vessel. However, it could be interesting to run the model for other wave directions, periods and significant wave heights. The results can be used for a workability study of the CSD.

The combination of different wave environments might also be necessary in order to do a validation study. At the time of writing limited data of actual operation was available. Using the environmental data of an actual project, including soil parameters, will allow validating the accuracy of the model created in this thesis.

9 Results

The objective of this thesis is to create a model of a cutter suction dredger in operation. In order to be able to include all the dynamics and nonlinearities of the forces acting on a CSD while it is cutting soil, the model was created in the time domain. This is a big advantage over frequency domain models of CSD's. In essence, the model can be split up into two main components.

1. The Ansys AQWA component:

This contains the 3D mesh and is responsible for the calculation of the hydrodynamic loads. A quick overview of the capabilities of this part of the model is:

- Choice between modeling the CSD as a single rigid body (1 Body) or with ladder and hull as two separate bodies (2 Body). The main advantage of the latter is that it is a closer resemblance to reality and it gives the tension in the hoisting wires during each timestep and lower forces on the spud pile. The main advantage of the single rigid body approach is that it can run with a larger timestep, thus performing faster.
- Linearized drag is included for the yaw motion around the spud pile since viscous effects are unaccounted for in AQWA.
- Irregular wave spectrum has been included to study the effect of waves on the vessel motions and spud forces.

2. The Python script; This script calculates all the external forces acting on the CSD as it is cutting soil. The script consists out of three main modules, which can be turned on, or off, depending on the objective of the analysis:

a) The spud module

The module consists of two different approaches to calculate the forces on the spud pile. The results of these approaches are:

- The cantilever spud approach calculates the spud force by taking the deflection at the spud tip.
- The pinned spud approach calculates the spud force by taking the relative deflection of the two spud guides. This approach has a lot of potential to be expanded to include some more advanced phenomena in future adaptations.
- Both approaches give virtually identical results, which is a good verification on its own. The pinned approach was chosen to perform most of the calculations in this thesis because it is visually closer to reality.
- The presence of a flexible spud carriage has been taken into account for both approaches. A clear and controlled reduction of the forces on the spud pile is visible during tests.
- Also the steps forward, which are taken at the end of each swing, are modeled in the spud module. A drawback of the implemented approach is the occurrence of peaks during stepping. Due to the relatively short time these peaks occur, it was decided that the current implementation is sufficient for the purpose of this thesis.

b) The winch module

This module contains three separate approaches to be able to obtain the swing forces. Previous implementations of CSD models usually consisted of a static tension model. Therefore the application of a dynamic tension model gives better insight in the actual behavior of CSD's. The different approaches are:

- Fixed force approach, where a hauling and a braking tension are defined in the wires and maintained constant throughout the swing. At the end of the swing the wires switch of tension. The resulting tension on the ladder will vary due to the changing angle of wires relative to the ladder. This approach gave smooth

motions but large peaks on the spud pile when changing of swing direction, it is also not capable to respond to varying requirements while cutting soil.

- Fixed wire length approach, in this model the tension in the hauling wire will vary and the tension of the braking wire is set at a constant value. The hauling tension is calculated by taking the minimum tension plus the strain in the hauling wire due to the reduction of length while the ship moves slower due to its inertia. This approach can respond well to varying requirements in hauling tension due to the cutting of the soil. However, even while swinging without soil interaction, large peaks occur in both the swing velocity and the spud forces.
- PID controller approach, which has been tuned for two different settings. The powerful setting, or P-dominated setting, gave a very accurate velocity profile. However, this came at the cost of large peaks on the spud pile. In contrast, the softer setting, or I-dominated setting, gave very smooth spud forces, with a gradual increase or decrease in velocity, resulting in a less accurate velocity profile.
- The I-dominated PID controller approach was preferred and used throughout this thesis. The main argument is that it resembles the reality better because instantaneous increases in tension are not possible due to the delay of winch rotations and other aspects. Also, in order to obtain a clear view on the peak forces due to the cutting of soil or waves, it is undesirable to have peak forces present on the spuds created by the winch module.

c) The soil module

The capabilities of the applied soil module are:

- The module is capable of accounting the cutting history. It keeps track of the soil which has been cut by creating a two-dimensional grid, where each grid point is assigned a certain height. This height is adjusted if the cutterhead has cut soil at that point.
- The cutterhead is simplified as a sphere, with an axis of rotation defined as a 3D vector. Using the specific energy of volume cut and its distance to the rotation axis, the individual force components are determined per grid point.
- The soil is simplified by defining it with the specific energy value. This means that it is only necessary to know the volume being cut during each timestep.
- The module was verified to function as intended, however, the discretization of the grid does cause some intermittent behavior. This was not considered a problem since the magnitude of these variations is quite small compared to the actual forces.

The final result is a fully functional model in the time domain of a cutter suction dredger in operation. The model takes the principal forces acting on the CSD and determines the resulting motions and reaction forces. The different components in the modules, and the related advantages and disadvantages, have been discussed individually and as a combination to obtain insight into the complete operation of a CSD. One of the main advantages of the way the Python script has been written, which is not very obvious from the points described above, is the adaptability. Modules can be altered, added or removed without influencing the other modules.

10 Recommendations

As stated at the end of each module, there are several expansions possible for this model. Many components could be included to investigate how they are loaded when the cutter is in operation. Depending on the goal to which the simulation is run different aspects can be incorporated. It is not recommended to include everything at once, as this will slow down the calculation excessively. Some of the main points of expansion or further research mentioned throughout the thesis are:

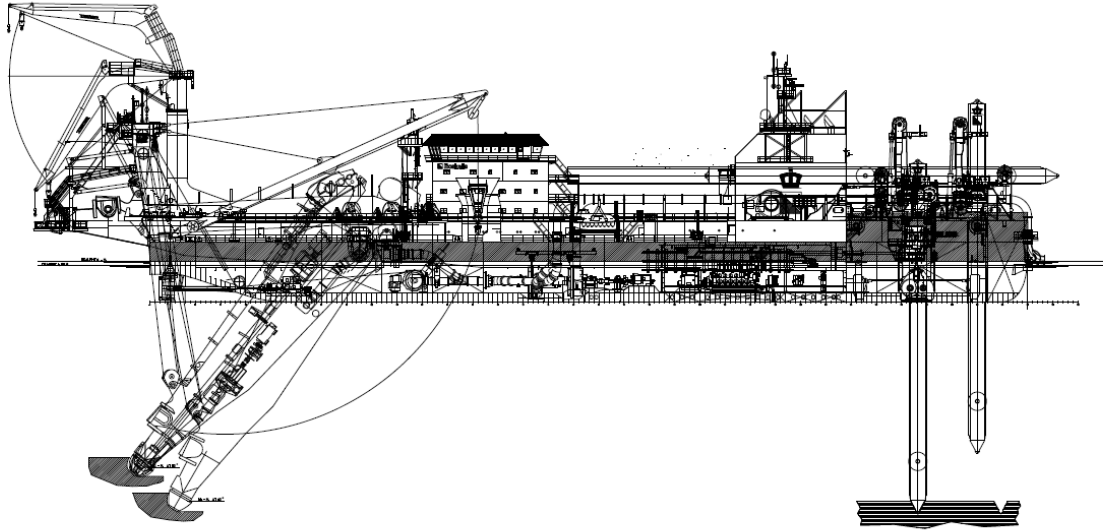
- A study to alternative numerical soil models. A more detailed model on tooth level, or a faster approach on global level using an ideal path, are two examples that come to mind. Each can be useful for different situations or perhaps an ideal model for all situations could be created, which can incorporate things like production, inhomogeneous soil and cutter teeth wear.
- A study to improve the model of the spud pile. Things like spud tip penetration, cylinder stroke, and wire strain are now incorporated indirectly. By expanding the model to include these aspects, a study to the effect they have on the system as a whole can be performed.
- A study to validate the results still has to be done, this is of course, crucial to determine the accuracy of the model created during this research and finding topics of improvement in order to increase accuracy.
- Further testing with the effects of wave loads still needs to be done. In this thesis a single wave spectrum with head waves has been used in simulations. The effect of beam waves as well as the effects a flexible spud carriage with wave loads has on the cutting of soil, are two examples for further investigation.

One of the main advantages of the current setup is the adaptability for different components or objectives. Therefore it should be possible to apply the model to other CSD's without much effort. It could thus be interesting to do a study on the differences between various CSD's and investigate the effects of different design choices. It is just a simple example of the variety of applications for which this developed numerical model can be used.

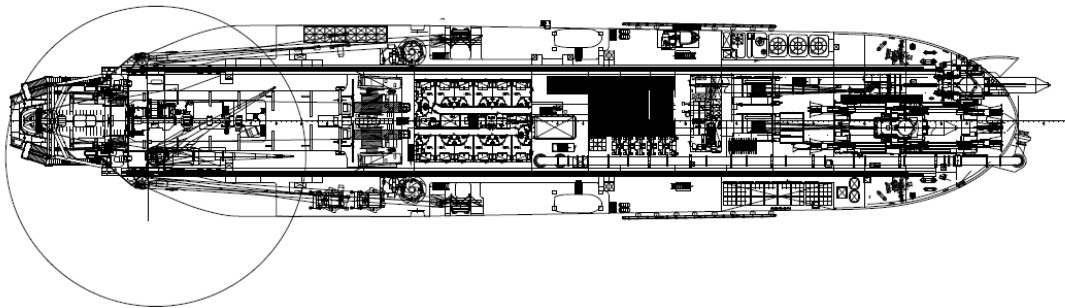
Bibliography

- Haan, J. d. (2016). Lecture Slides OE4652 Floating Structures. *TU Delft*. Delft, The Netherlands.
- Hannot, S. D., Los, J. G., L, d. K., Kruijswijk, A. B., & W, v. S. (2013). *A validated tool for evaluating the design and predicting the workability of dredgers*. Kinderdijk: IHC.
- IHC Merwede. (2008, Spring). Dynamic simulation of a Cutter Dredger at sea. *Ports and Dredging*, pp. 6-13.
- Journée, J. (1993). *Hydromechanic Coefficients for Calculating Time Domain Motions of Cutter Suction Dredges by Cummins Equations*. Delft, The Netherlands: TU Delft.
- Journée, J., & Massie, W. (2001). *Offshore Hydromechanics*. Delft, The Netherlands: TU Delft.
- Keuning, P., & Journée, J. (1983). Calculation Method for the Behaviour of a Cutter Suction Dredge Operating in Irregular Waves. *10th World Dredging Congress*. Singapore.
- MARIN. (2002). *DREDSIM 2000 User's guide*. Wageningen, The Netherlands.
- Miedema, S. (1987). *Calculation of the Cutting Forces for Cutting Saturated Sand*. Delft, The Netherlands: TU Delft (in Dutch).
- Miedema, S. (1989). On the Cutting Forces in Saturated Sand of a Seagoing Cutter Suction Dredge. *WODCON XII*. Orlando, Florida.
- Miedema, S. (2016). *OE4607 Introduction Dredging Engineering. 2nd Edition*. Delft, The Netherlands: TU Delft.
- Miedema, S. (2016). *The Delft Sand, Clay & Rock Cutting Model. 3rd Edition*. Delft, The Netherlands: Delft University Press.
- Miedema, S., Journée, J., & Schuurmans, S. (1992). On the Motions of a Seagoing Cutter Suction Dredge. *13th World Dredging Congress*. Bombay, India.
- Miedema, S.A., Koning, J. de, & Zwartbol, A. (1983). SOIL / CUTTERHEAD INTERACTION UNDER WAVE CONDITIONS. *WODCON X*. Singapore.
- Reus, R. d. (2016). *A Cutter Suction Dredger in Waves*. Delft, The Netherlands: TU Delft.
- Wichers, J. (1980). *On the Forces on a Cutter Suction Dredger in Waves*. Wagening, The Netherlands: N.S.M.B.
- Wichers, J. (1981). Hydrodynamic Behavior of Cutter Suction Dredger in Waves. *World Dredging and Marine Construction*.
- Young, D. (2009). *Forces on Laboratory Model Dredge Cutterhead*. Texas A&M University.

Appendix A. General Arrangement and data Helios



SIDE VIEW



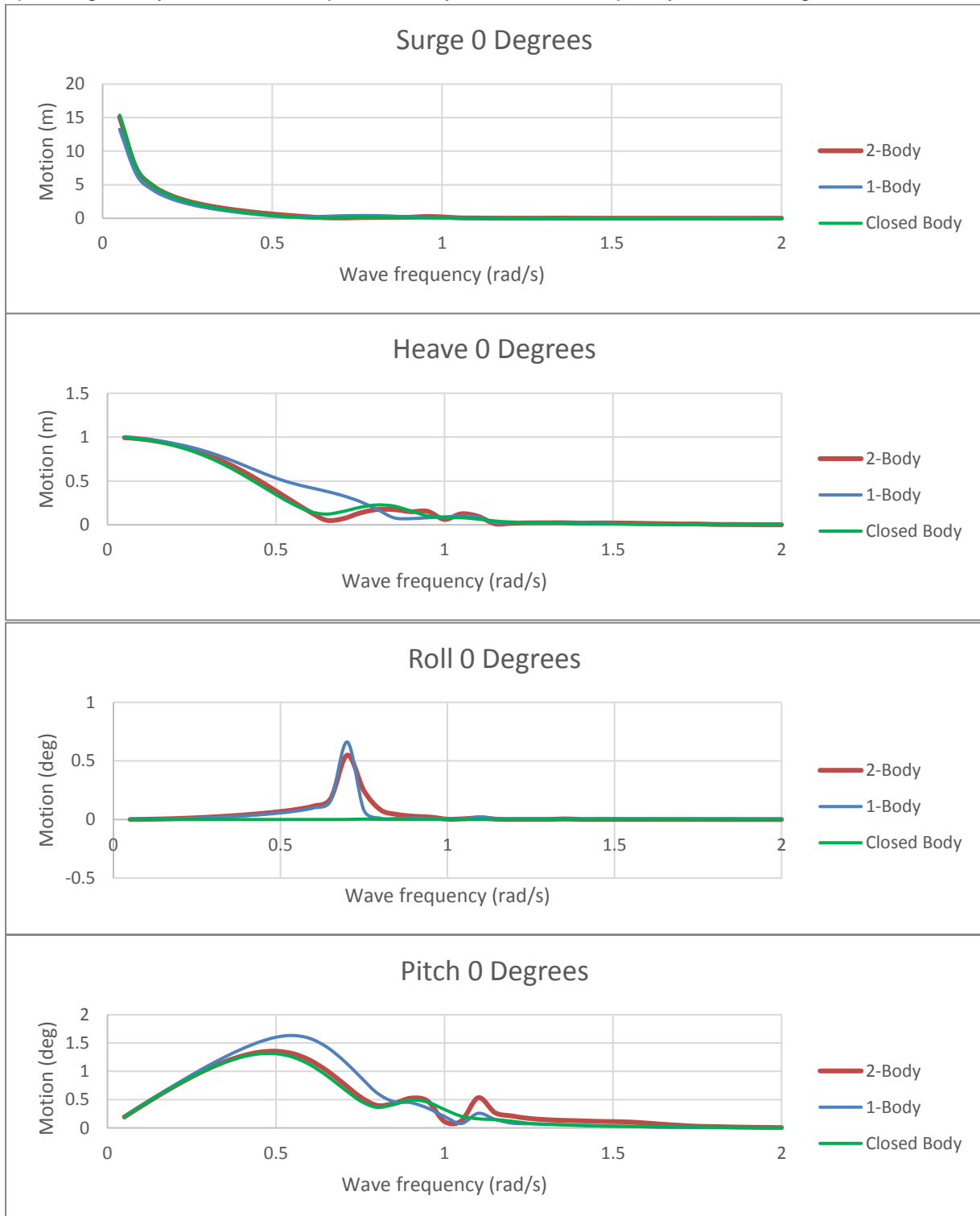
TOP VIEW DECK LEVEL

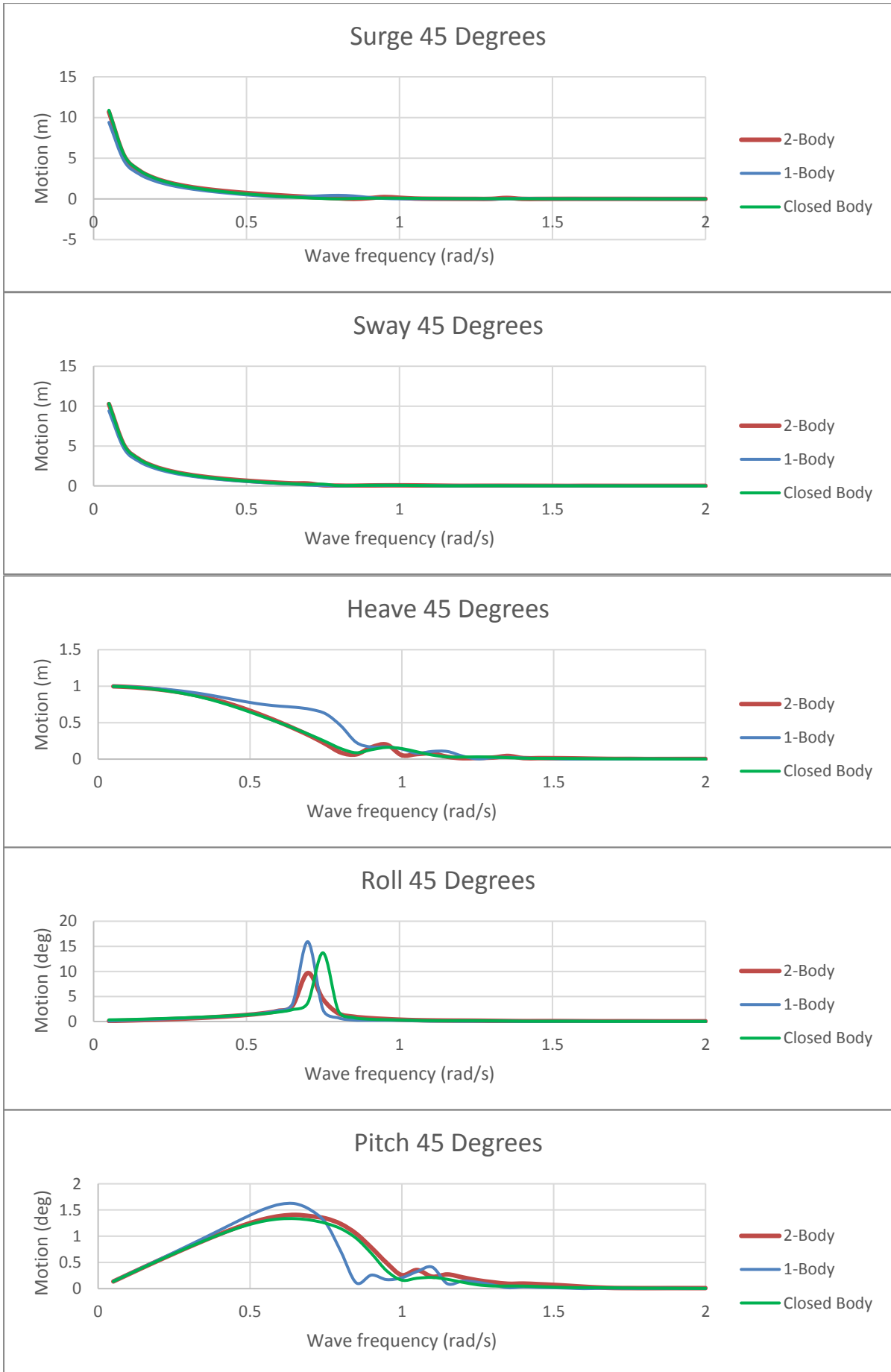
CONSTRUCTION/CLASSIFICATION		MAIN DATA	
Built by	IHC Holland B.V.	Sailing speed	± 11.5 kn
Year of delivery	2017	Length overall	152 m
Classification	Bureau Veritas	Length b.p.p.	127.5 m
Complete class notation	1 * HULL * MACH * AUT-UMS Dredger SP (45) Dredging within 15 miles from shore or within 20 miles from port; extended with dredging over 15 miles from shore with H.S. ≤ 2.5 m Green Passport, Clean ship 7+ (14 days)	Moulded Breadth	28 m
		Moulded depth	8.9 m
		Design draught	5.35 m
		Suction pipe diameter	1000 mm
		Max dredging depth	35 m
		Min dredging depth	6.35 m
		Positioning system	Spud carrier
		Total installed power	23,886 kW *)
		Cutter output maximum	7,000 kW
		Discharge pump output	15,600 kW
		Max. draught	6.00 m
		Gross Tonnage	8981 GT
		Net Tonnage	2694 NT
FEATURES			
A heavy duty, rock cutting, self-propelled dredger for Dredging within 15 miles from shore or within 20 miles from port			
Fully equipped for dredging trenches, navigation channels and harbors			
Fully automated dredging process centrally controlled			
Barge loading facility is optional			
Accommodation for 45 persons			

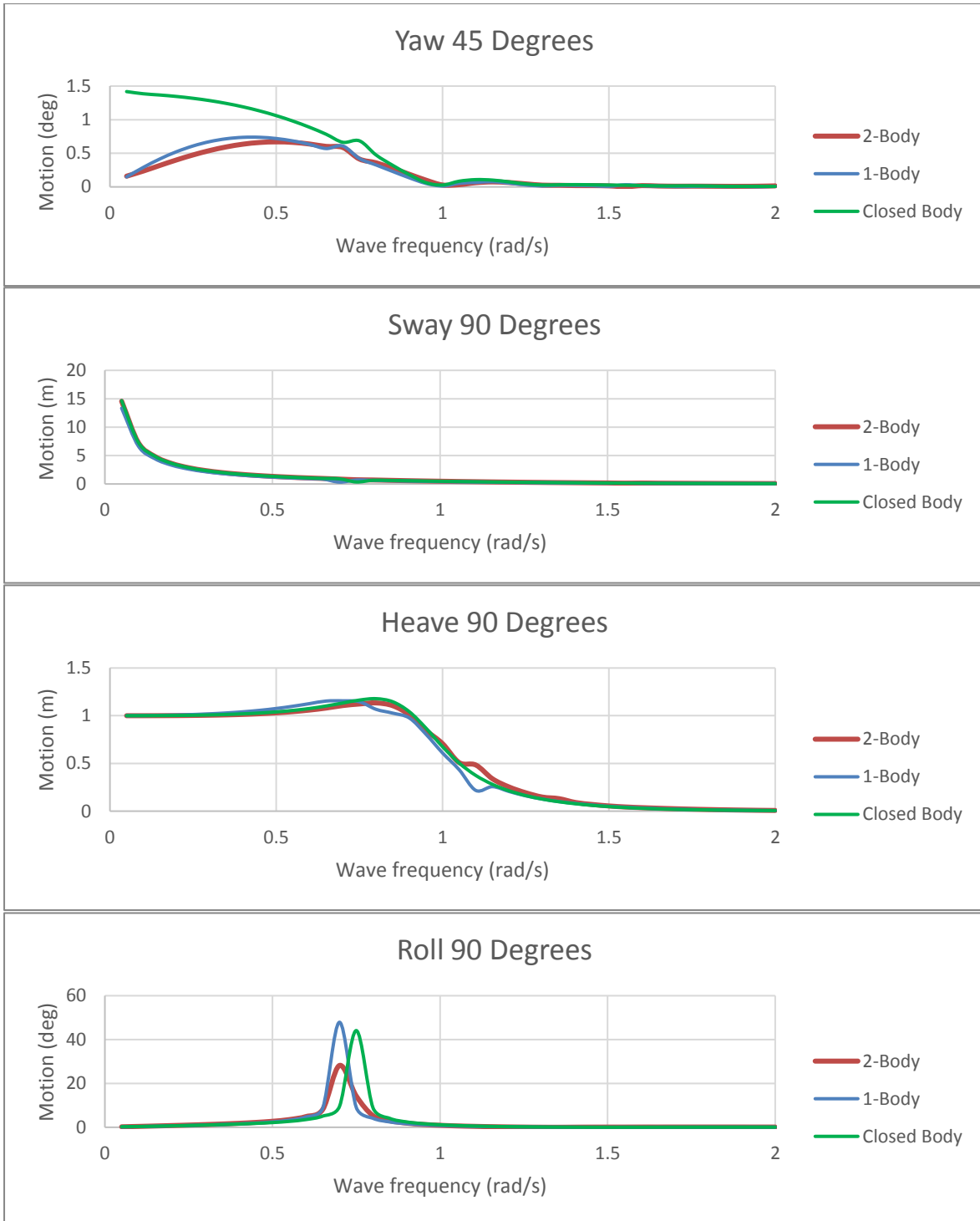
Appendix B. Initial time domain verifications

Comparison of the different geometric models used

The geometric model which was created specifically for compatibility with the requirements of Seaway has now been verified to function as expected. The rest of this research, however, will use a more realistic geometric model, with both recesses open. The differences in geometry between the models can be seen in 3.3. The closed model, used in the comparison with Seaway, will be compared to the open single body model and the open two body model in the frequency domain using AQWA.







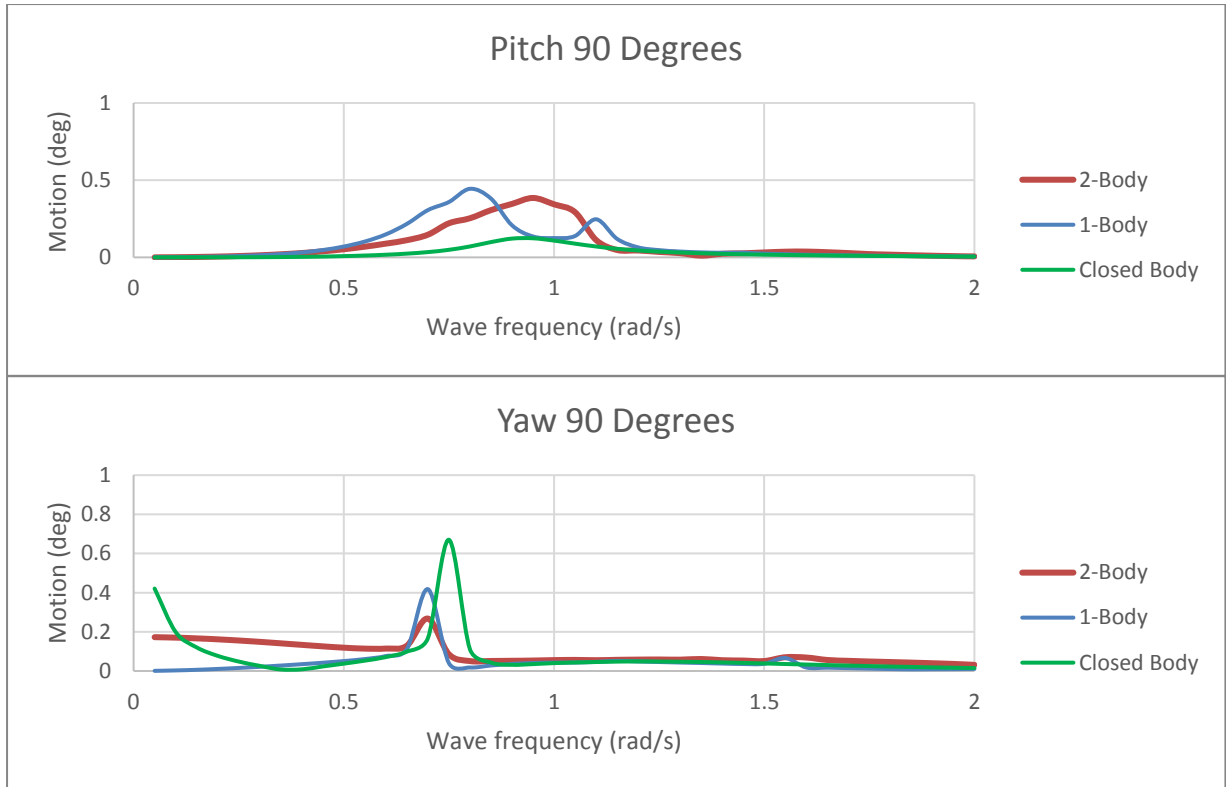


Figure 76 Comparison of the 3 geometric models in the frequency domain

From the graphs, it can be concluded that opening the spud recess and the ladder area leads to similar responses as the closed model. It has to be taken into consideration that the presented RAO's of the 2-body model are just the responses for the hull, as the interaction between bodies is not taken into account in the frequency domain. As a consequence, the potential loads, the displacement and location of the CoG is different from the single body approach in these graphs. A comparison between single body and 2-body in the time domain shows that when interaction is taken into account the results are indeed quite similar.

First time domain run of the free-floating body

Before adding any external forces it is important to see whether the floating body is in equilibrium. If it has excessive initial motions due to its search in balance it can cause unwanted behavior when adding external forces which incidentally might reinforce this initial motion. The results can be found in Figure 77.

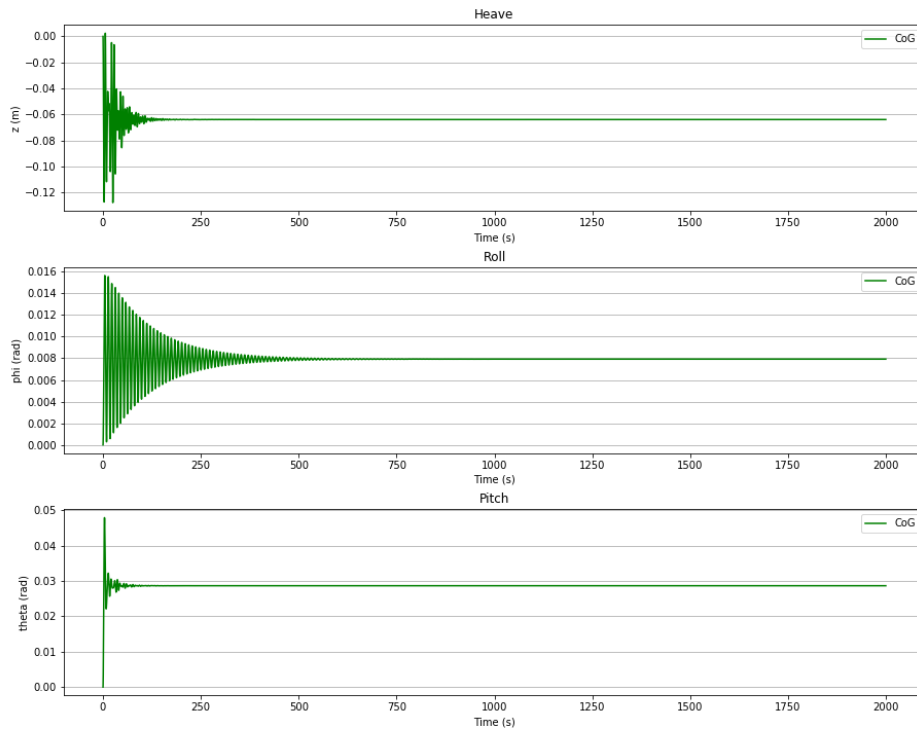


Figure 77 Initial balance for the free-floating vessel

It can be seen that the ship tends to be slightly out of balance in roll and pitch, which is attributed to the eccentric location of the spud recess. Looking back at the stability book, this is confirmed. In reality it will not have much influence, the angle is sufficiently small that when the spud is dropped, it will not cause bending stresses due to the initial angle. In the simulation, however, this small roll displacement can cause spud reactions before any motion has taken place, which is undesirable. Therefore to improve the overall behavior of the system, it has been chosen to adjust the CoG in AQWA to the equilibrium position above the center of buoyancy.

For the two body approach, this creates an additional challenge as the body representing the hull will have a different center of buoyancy than the system as a whole. The CoG, therefore, needs to be placed in the right place that when the hull ‘feels’ the ladder in the initial timestep, it will be in equilibrium. The combination of the defined location of the CoG and the correct initial coordinates at $t = 0$ s will ensure a stable starting point for the simulation.

The initial equilibrium for the 2-body approach does not only depend on the correct placement of the CoG, it also depends on the hoisting wire having the correct stiffness and corresponding unstretched length, as discussed in 2.2.2.

Table 20 New values for initial stability

Point	(x, y, z)	Unit	Remark
Original location CoG	(62.1, 0, 7.3)	m	See 2.2.1
Center of Buoyancy 1 Body	(56.7, 0.04, 2.7)	m	Calculated by AQWA-LINE
Corrected CoG for use in AQWA	(56.7, 0.04, 7.3)	m	Directly above Center of Buoyancy
2-Body CoG of Hull	(62.5, 0.03, 9.0)	m	See 2.2.2
2-Body CoG of Ladder	(13.5, 0.0, 0.0)	m	See 2.2.2
Center of Buoyancy Ladder	(-1.0, 0.0, -7.0)	m	Calculated by AQWA-LINE
Center of Buoyancy Hull	(60.9, 0.05, 3.4)	m	Calculated by AQWA-LINE
Corrected CoG of Hull	(65.3, 0.05, 9.0)	m	To improve initial stability

Appendix C. PID Tuning

PID Explanation

One of the most well-known applications of PID controllers is cruise control in cars. The user sets the desired velocity and the PID controller will control the amount of gasoline fed to the engine in order to stay at this speed as constant as possible.

In this example, the error is the difference between the desired speed of the driver and the actual speed of the car. The proportional term K_p then is a factor which relates the difference in speed to the amount of gasoline needed. It is clear that with just a proportional term the process will not be very stable, if the car accelerates and reaches the speed it will not stop accelerating instantly and therefore will go faster than the desired velocity. As a result, the controller will then stop the flow of gasoline to the engine and the car will decelerate to a speed below the set velocity, after which it will need to accelerate again. This process can continue for quite a few cycles. If the value of K_p has been defined correctly, the velocity will stabilize, however in other cases it will continue to fluctuate.

To improve this behavior and help the controller to stop accelerating at the right time, Integral control is added with the factor K_i . Integral control is based on the history of the controller. It looks how the error has developed over time, it is the sum of the error over the number of timesteps taken. If the error is decreasing, the integral gain will decrease as well, thus narrowing in on the right velocity.

Since proportional gain reacts to the current circumstances, integral gain reacts to the past circumstances, it would be convenient to also look at what the situation in the near future will be. For that reason, the Derivative control is part of the PID controller. It takes the derivative of the error, the difference between the current error and the error of the last timestep, and applies the factor K_d in order to anticipate the needs of the next timestep. It, therefore, is mostly used to reduce overshoot peaks and stabilize a PID controlled process faster.

Ziegler-Nichols method

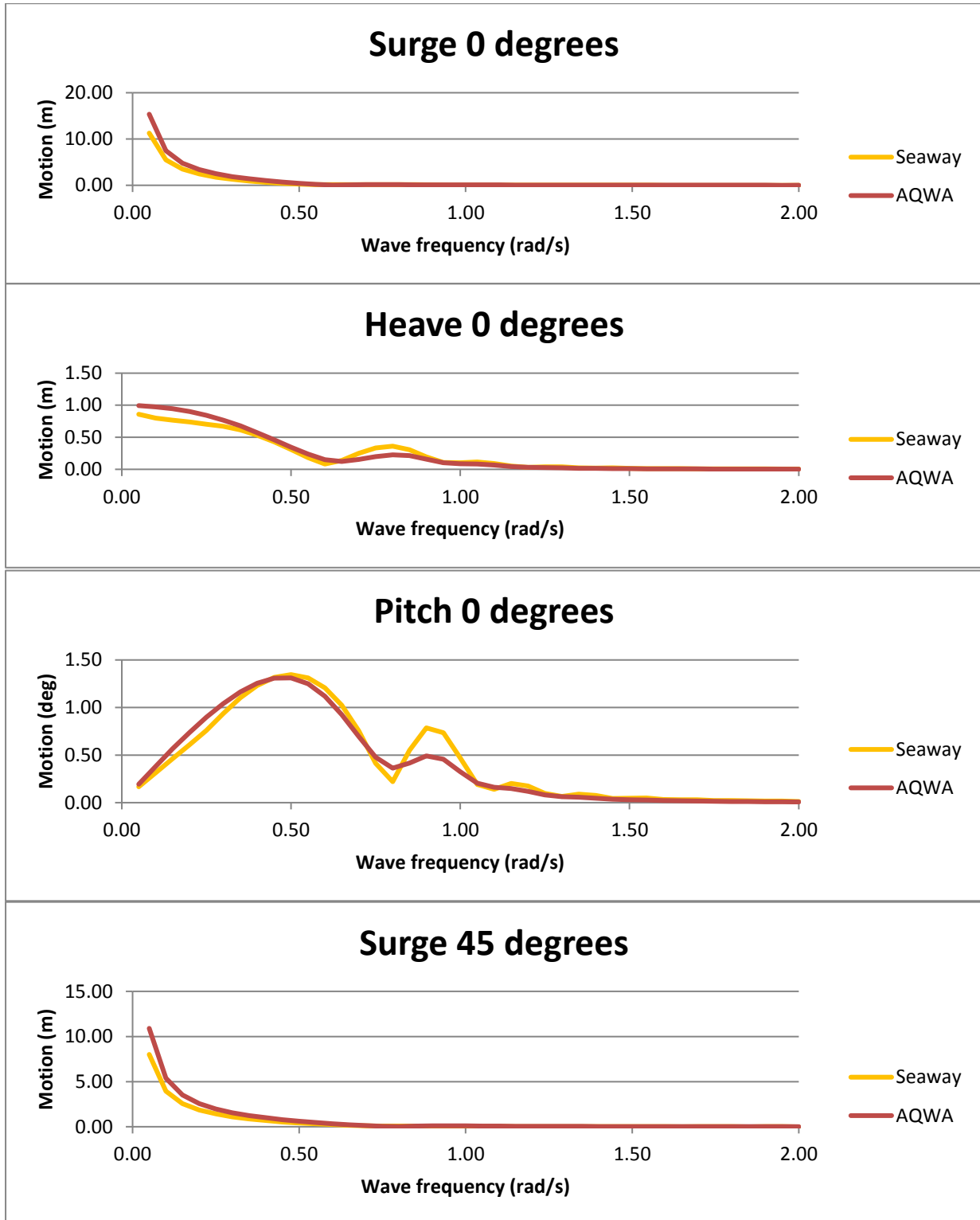
The values for K_p , K_i , and K_d can be found by calibrating the system according to the Ziegler-Nichols method, or a different known method within systems theory. The Ziegler-Nichols method specifies to run the process and introduce a sudden change, such as an increase in set velocity, with every run the gain parameters are increased until the system starts to oscillate. The reference parameter at which the system started to oscillate and the oscillation period are then used to calculate the actual gain factors.

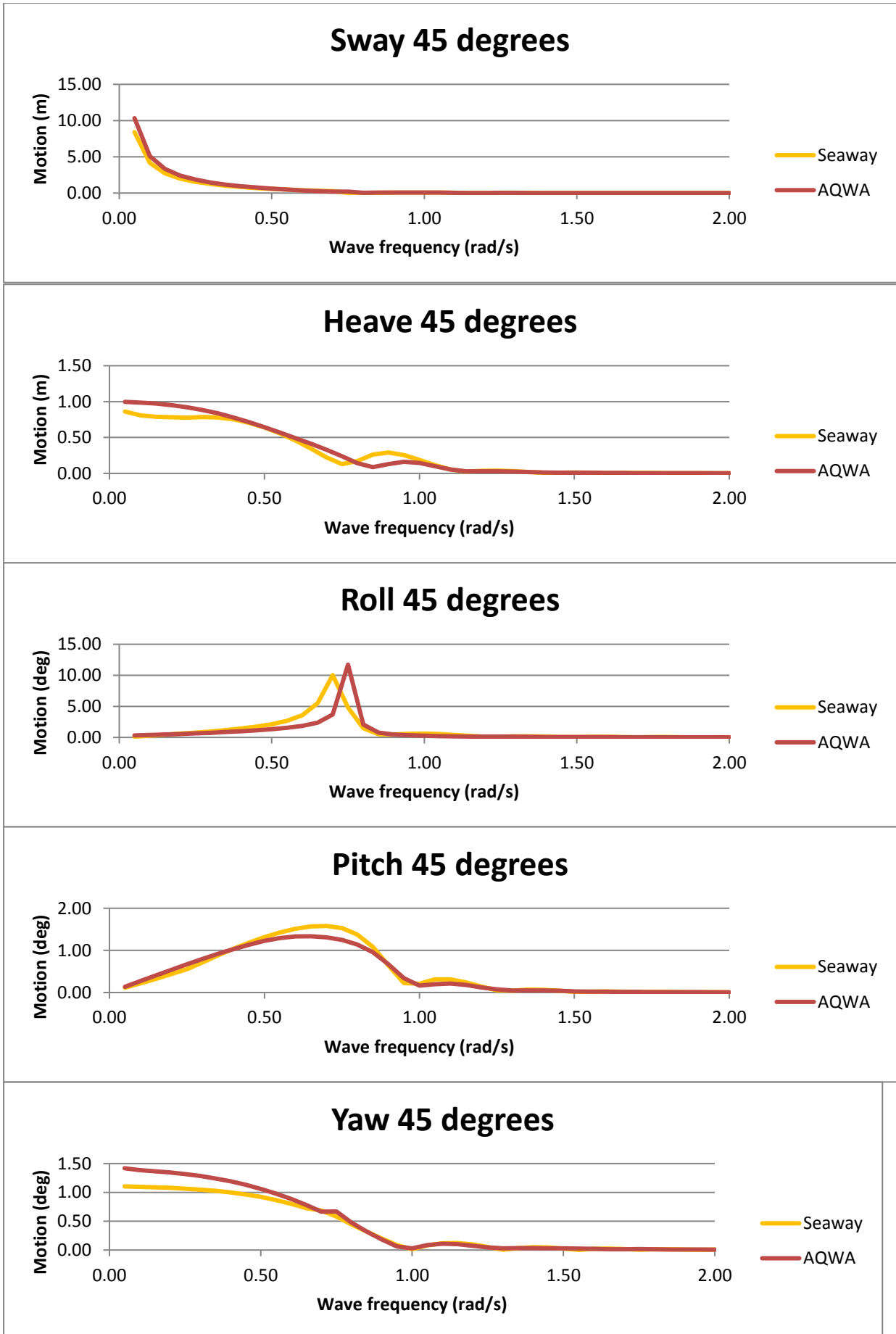
The first run will be done with a P-dominated system. The proportional gain has been obtained through the Ziegler-Nichols method described above and it has been applied. The corresponding K_i -value has been modified as the original value was $K_p/T_i = 1 \cdot 10^3$ which was too small to be noticed with the large K_p . The factor K_i was increased in a few steps until it added stability to the system.

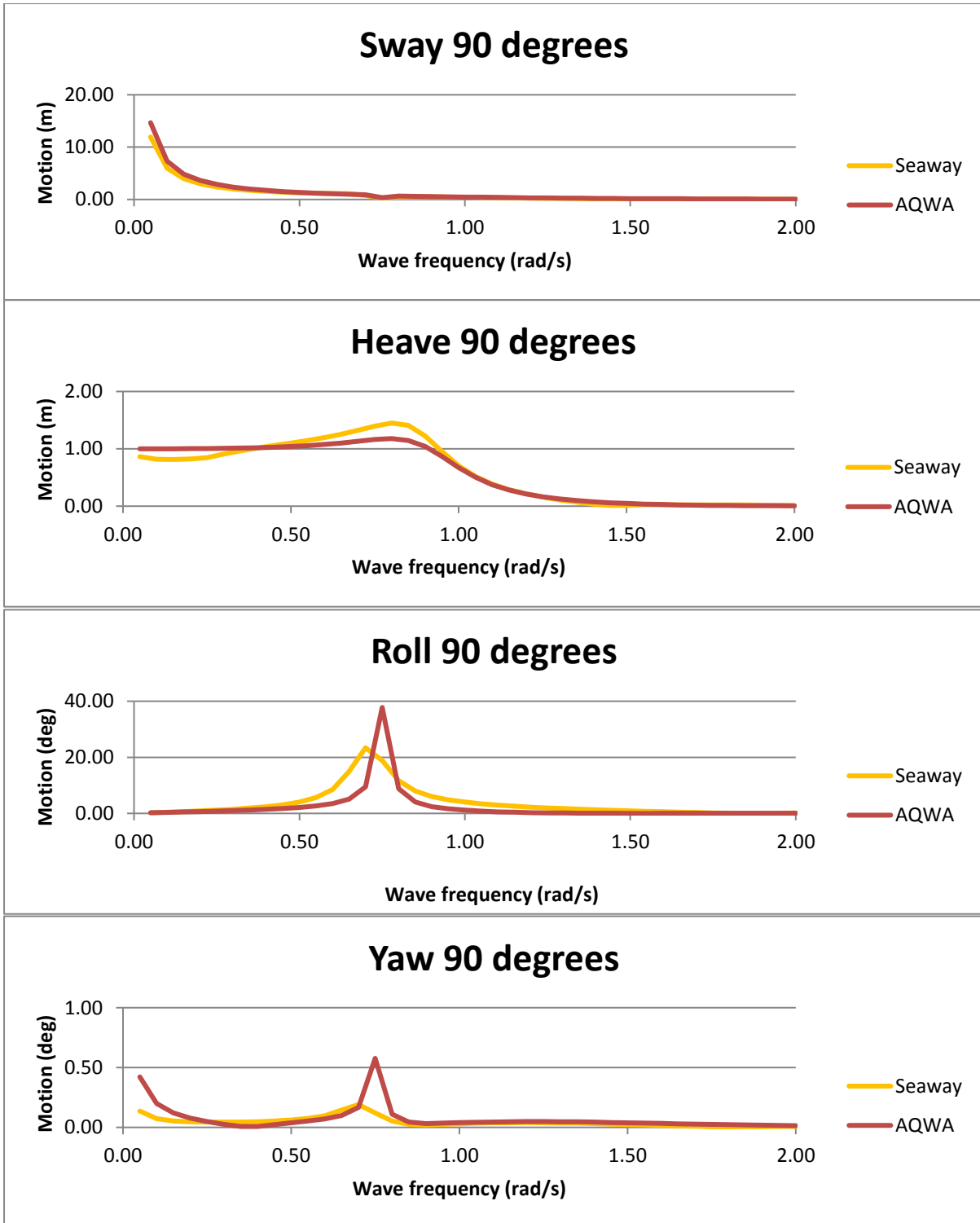
Using the original value of K_i a second run was made. This run showed completely different behavior and is assigned the term I-dominated system since the integral gain has the greatest influence. The K_p gain factor has been modified in steps, similar to the modification of K_i in the P-dominated system. The derivative gain was set at $K_d = 0$ for both runs because it was found that the gain was either not noticeable or destabilizing the system. The exact cause is unknown but given the lack of physical limits, it could be a purely numerical issue. Also, the results of the two runs do not seem to require input of the derivative gain, and therefore the issue is not further investigated here.

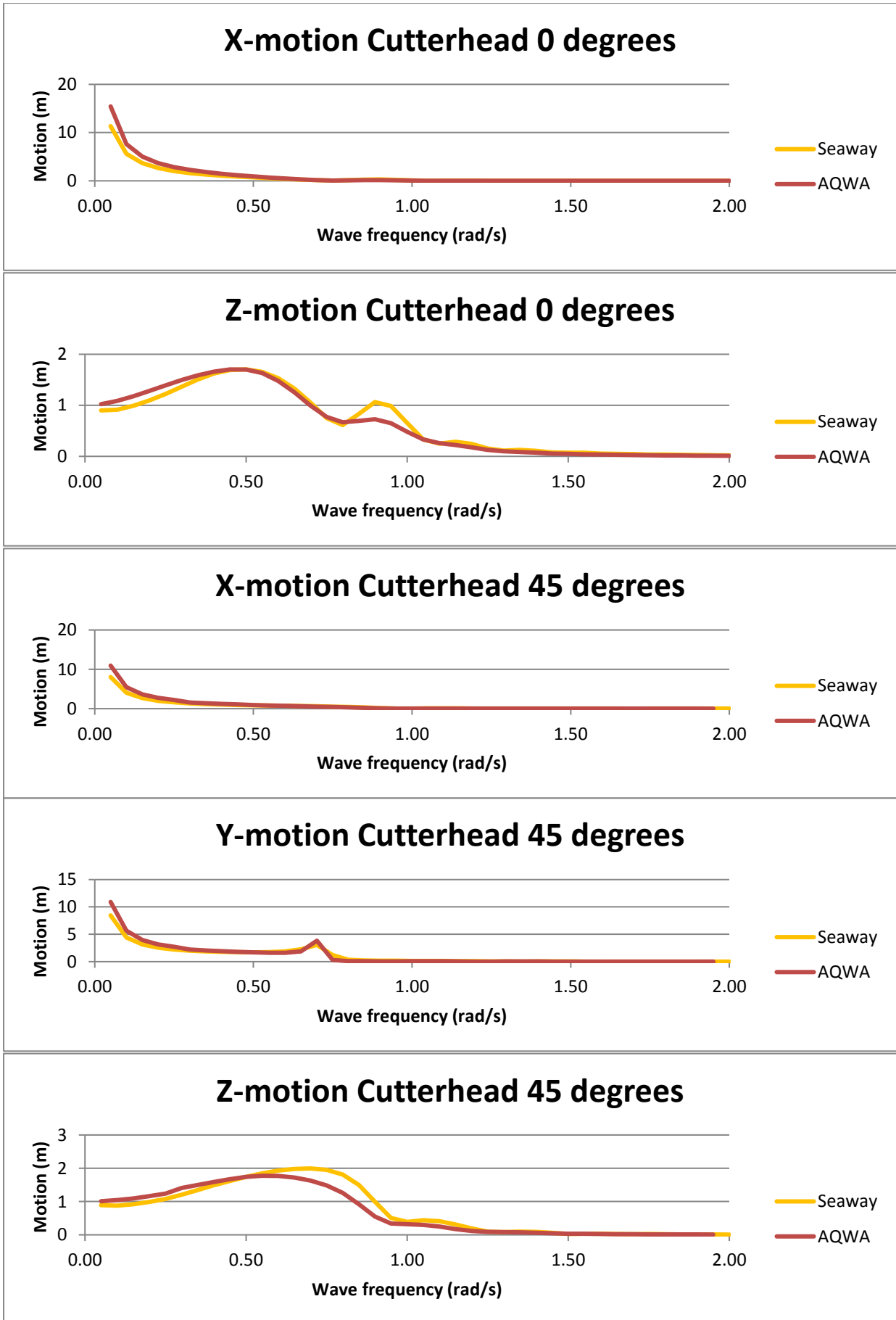
Appendix D. Results of the comparison between AQWA and Seaway

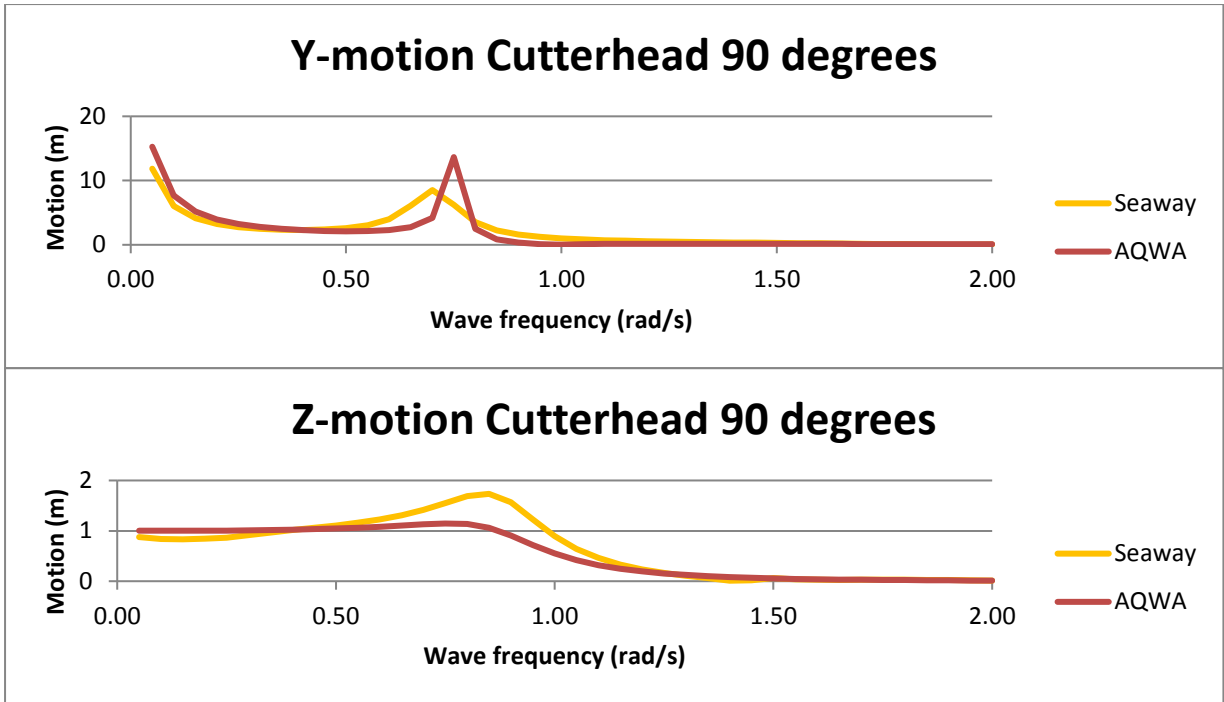
Freefloating



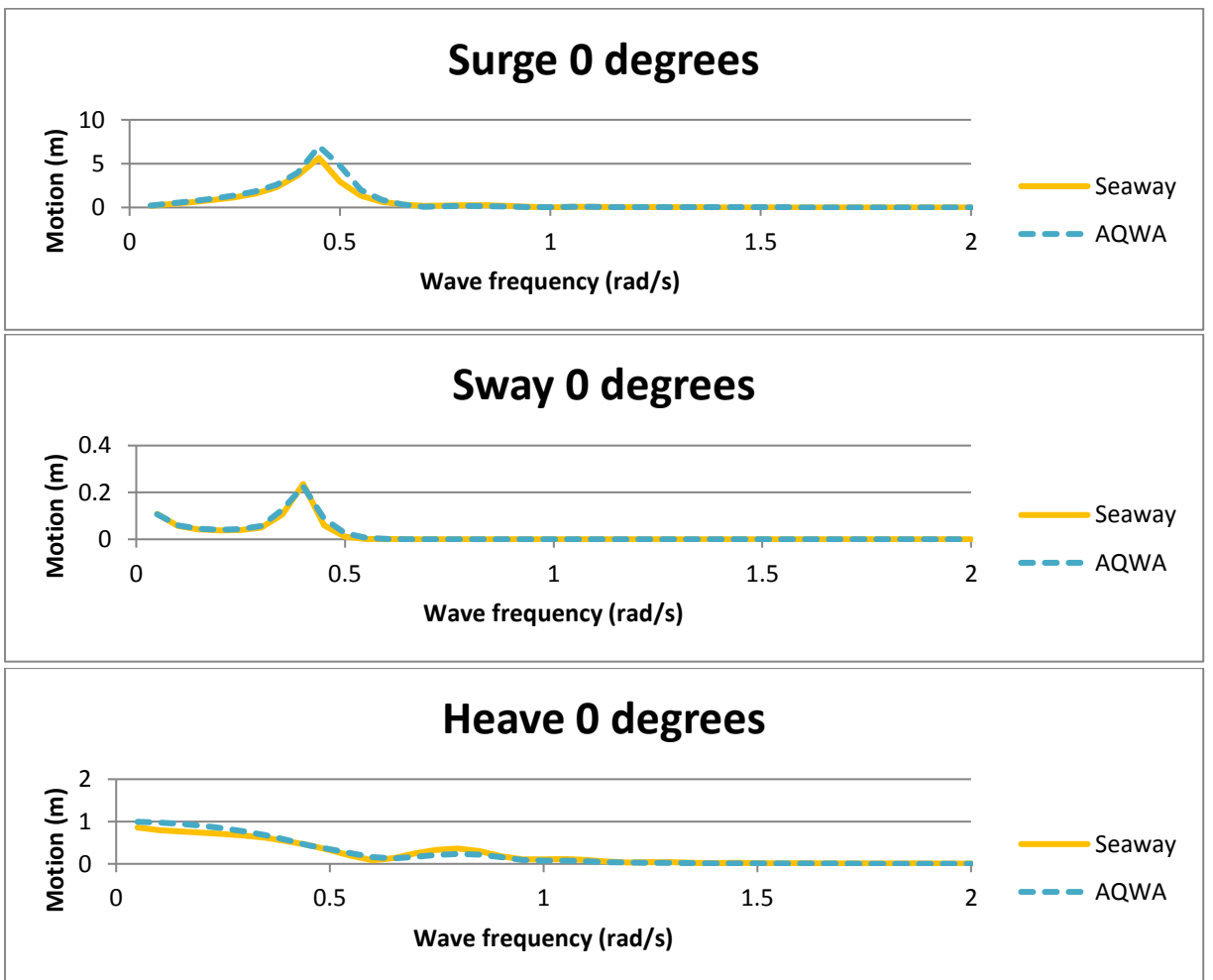


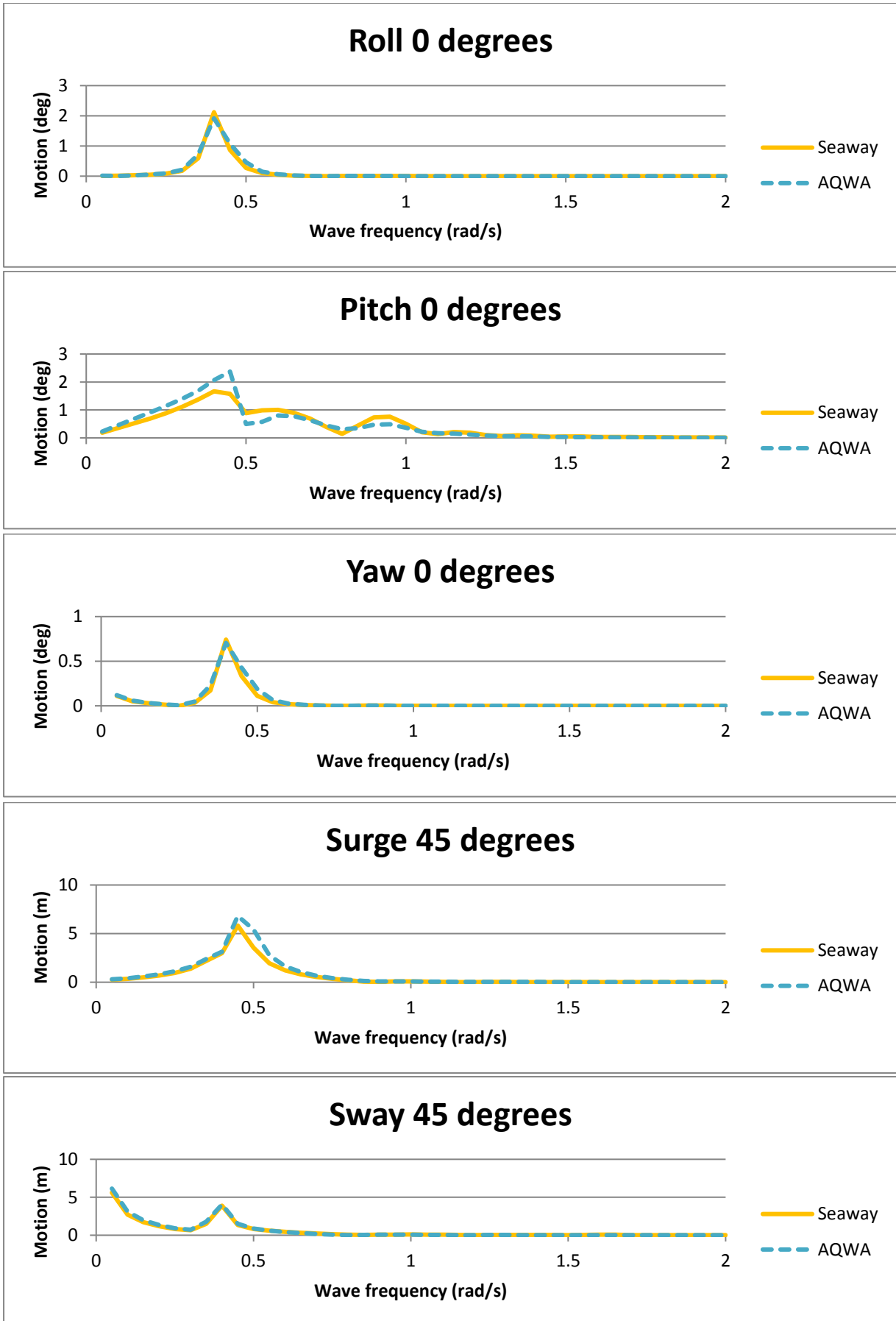


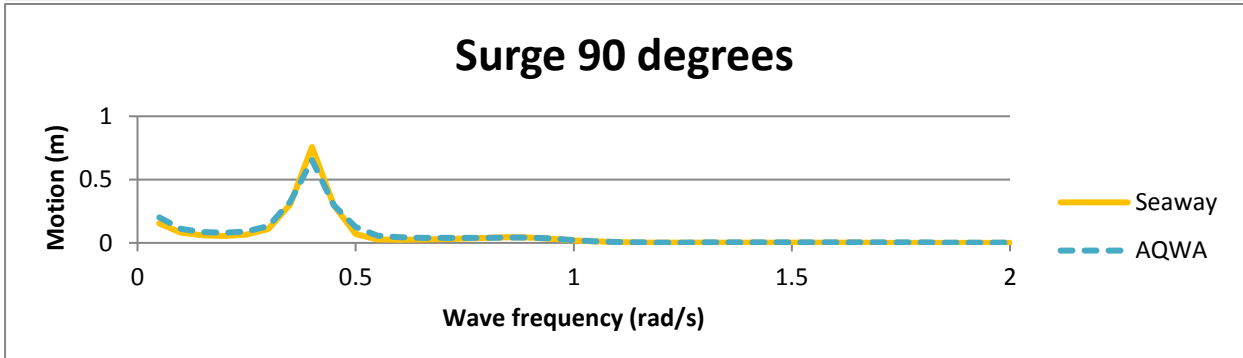
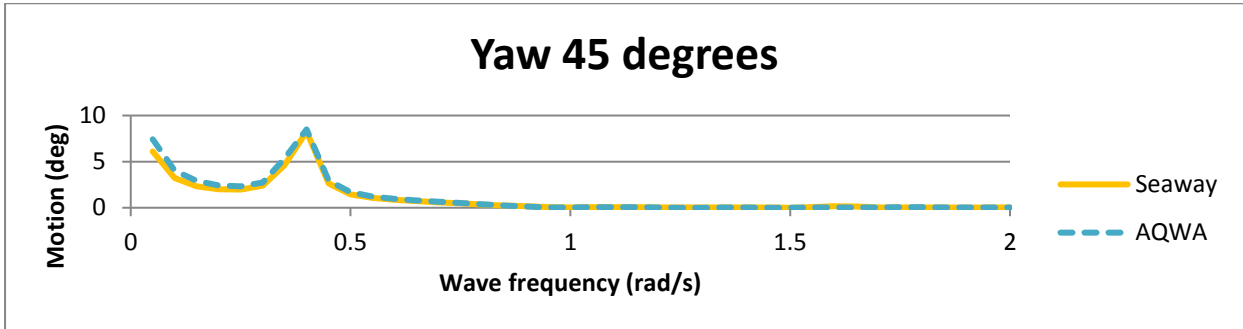
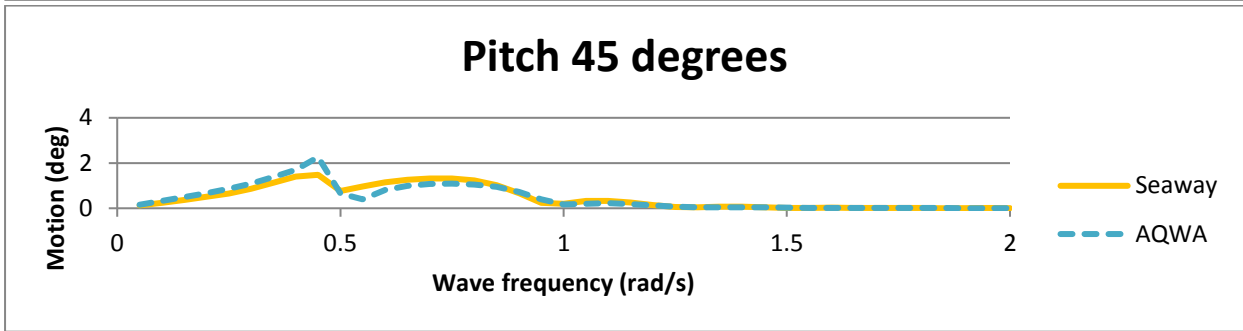
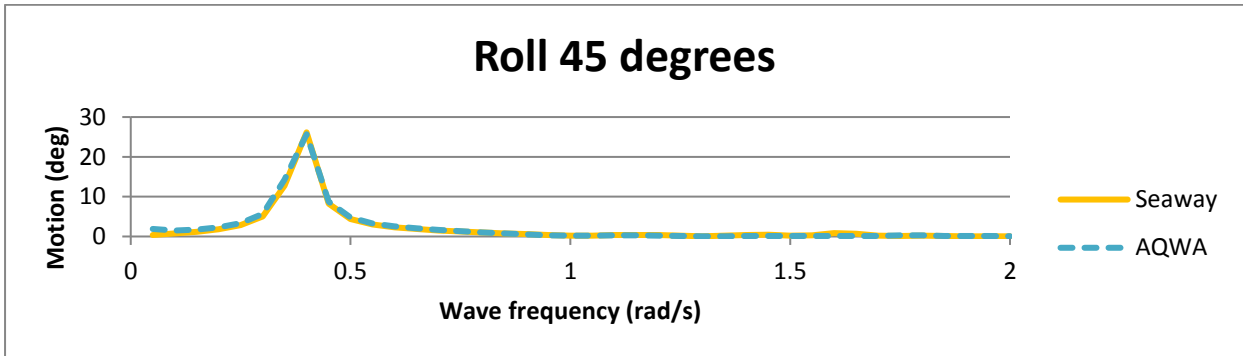
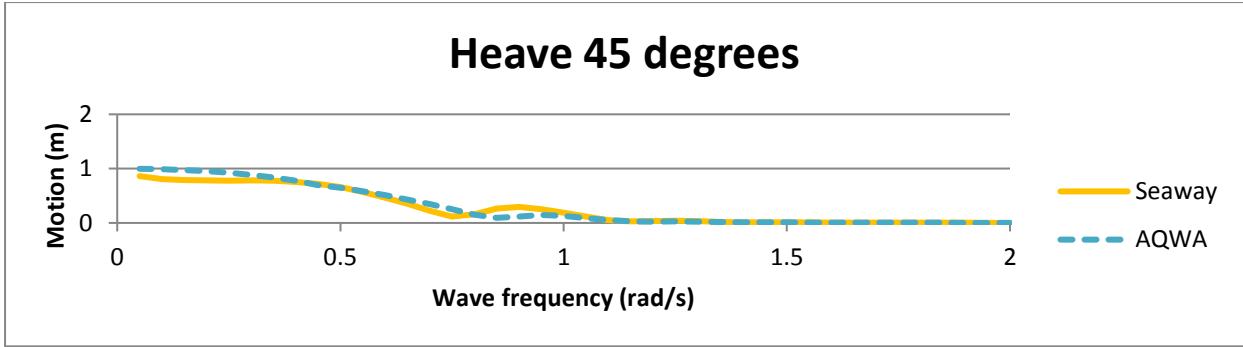


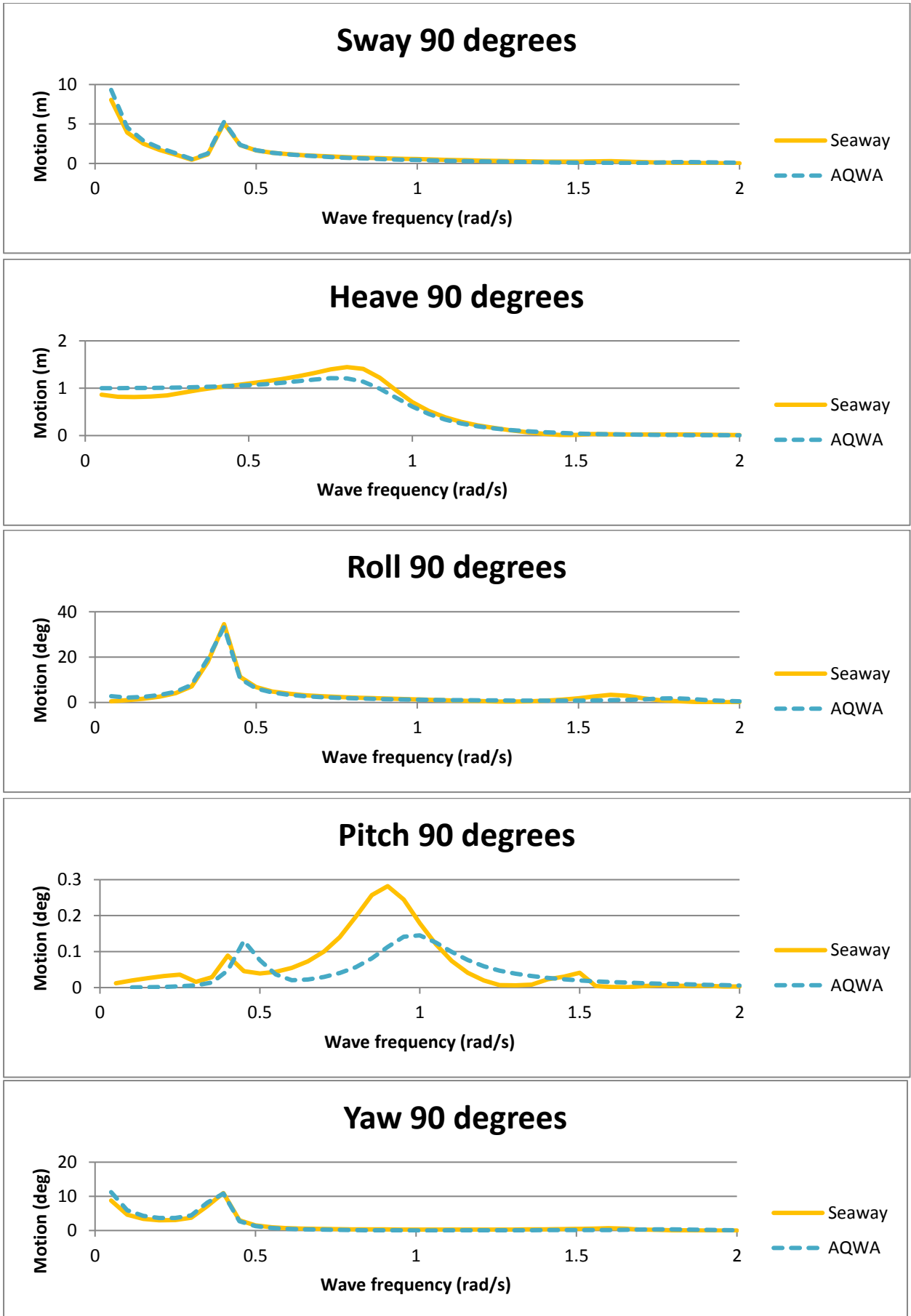


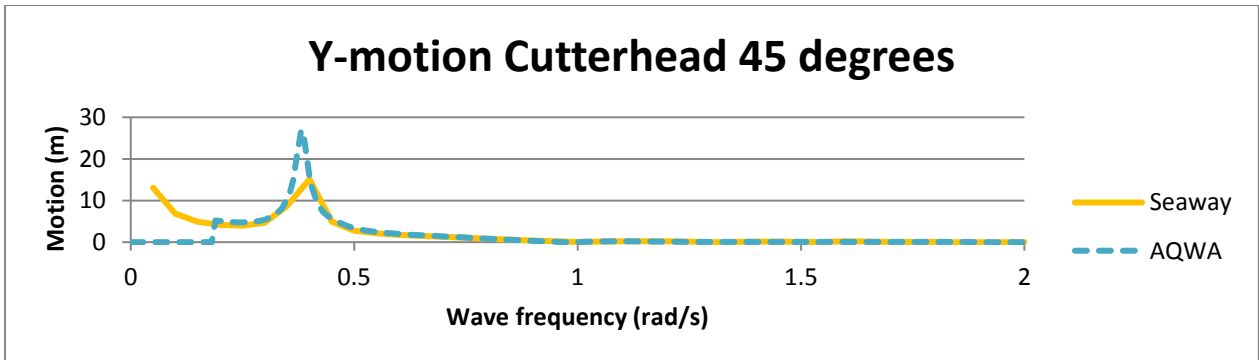
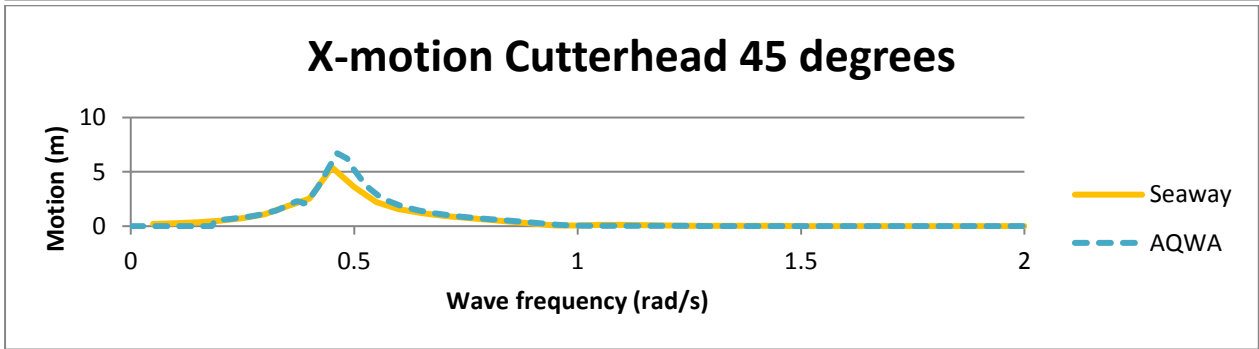
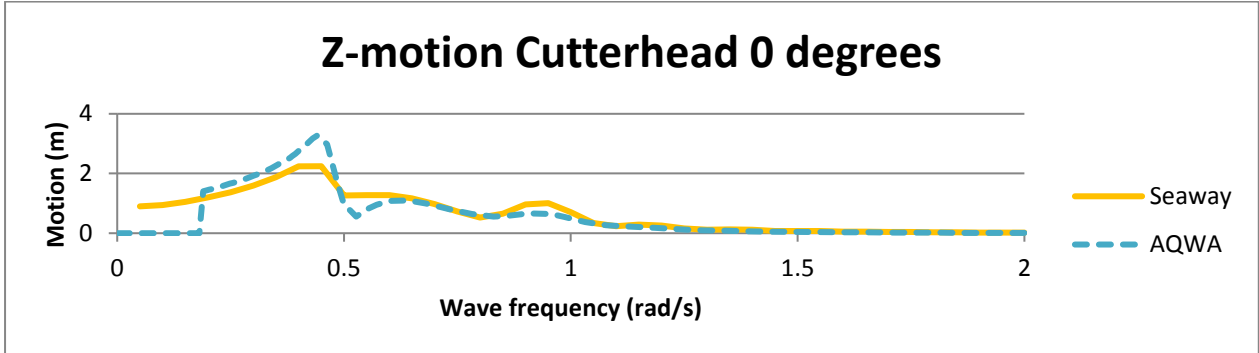
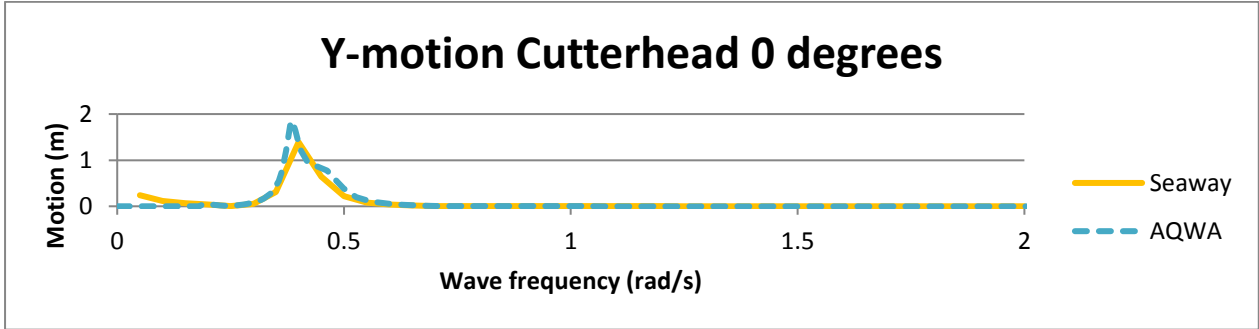
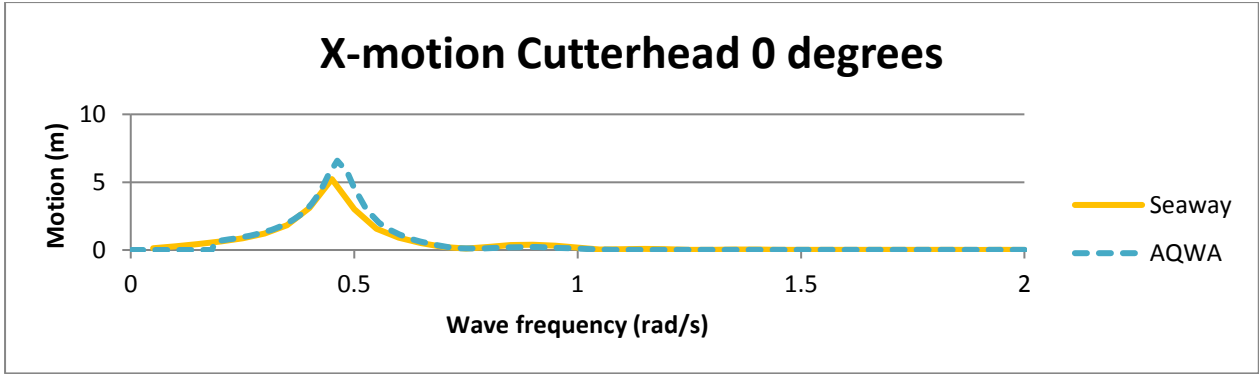
1 Spring

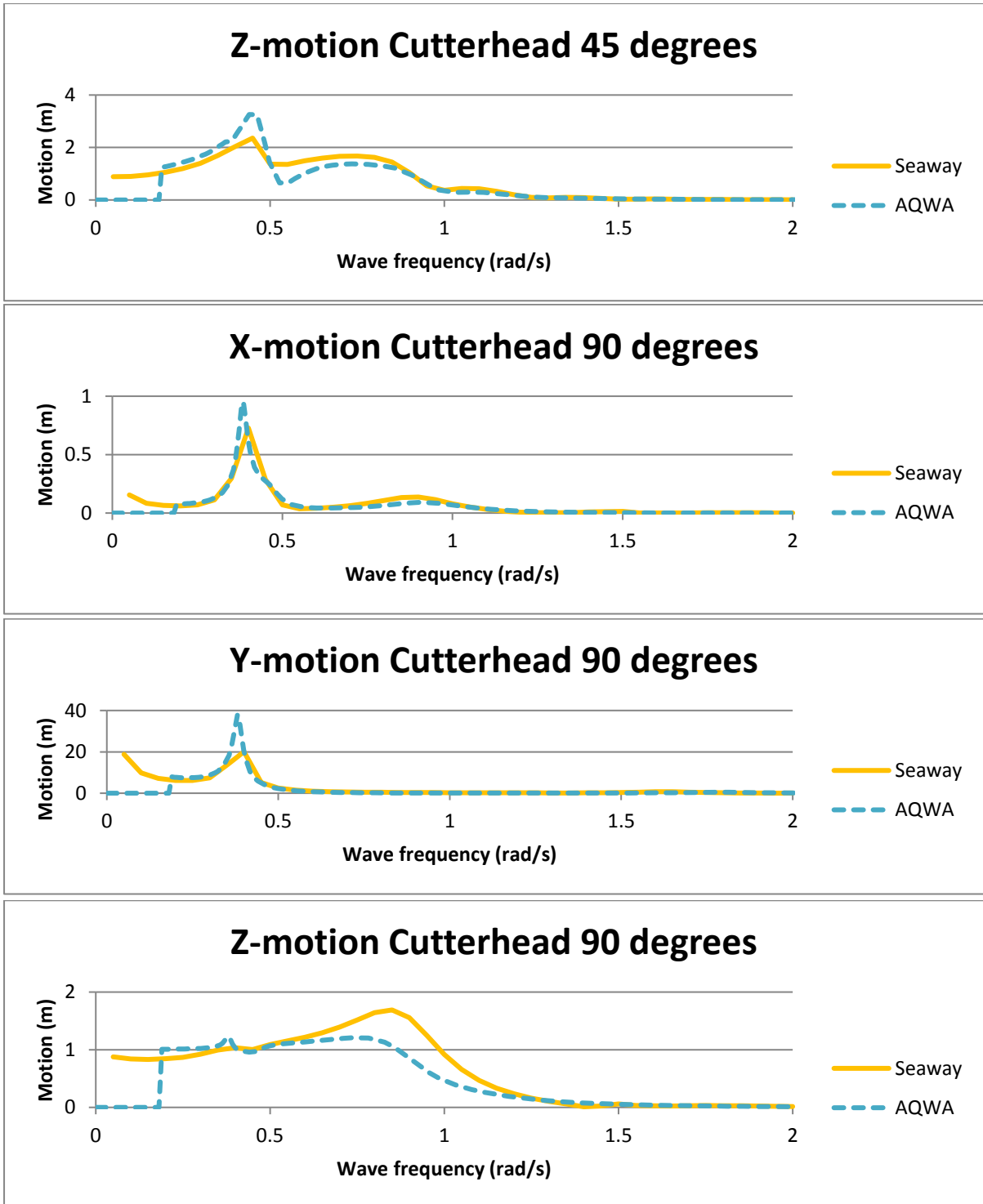




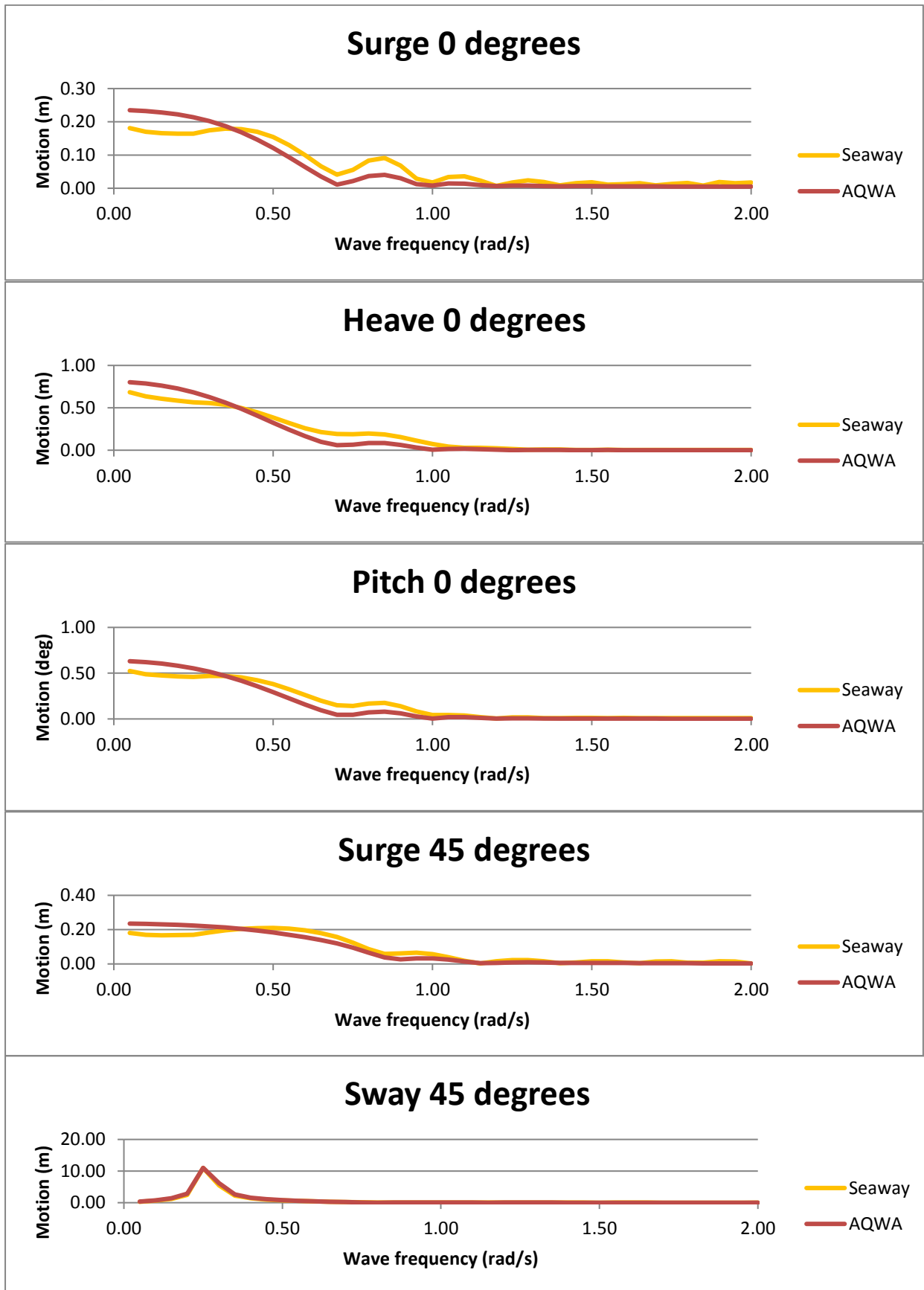


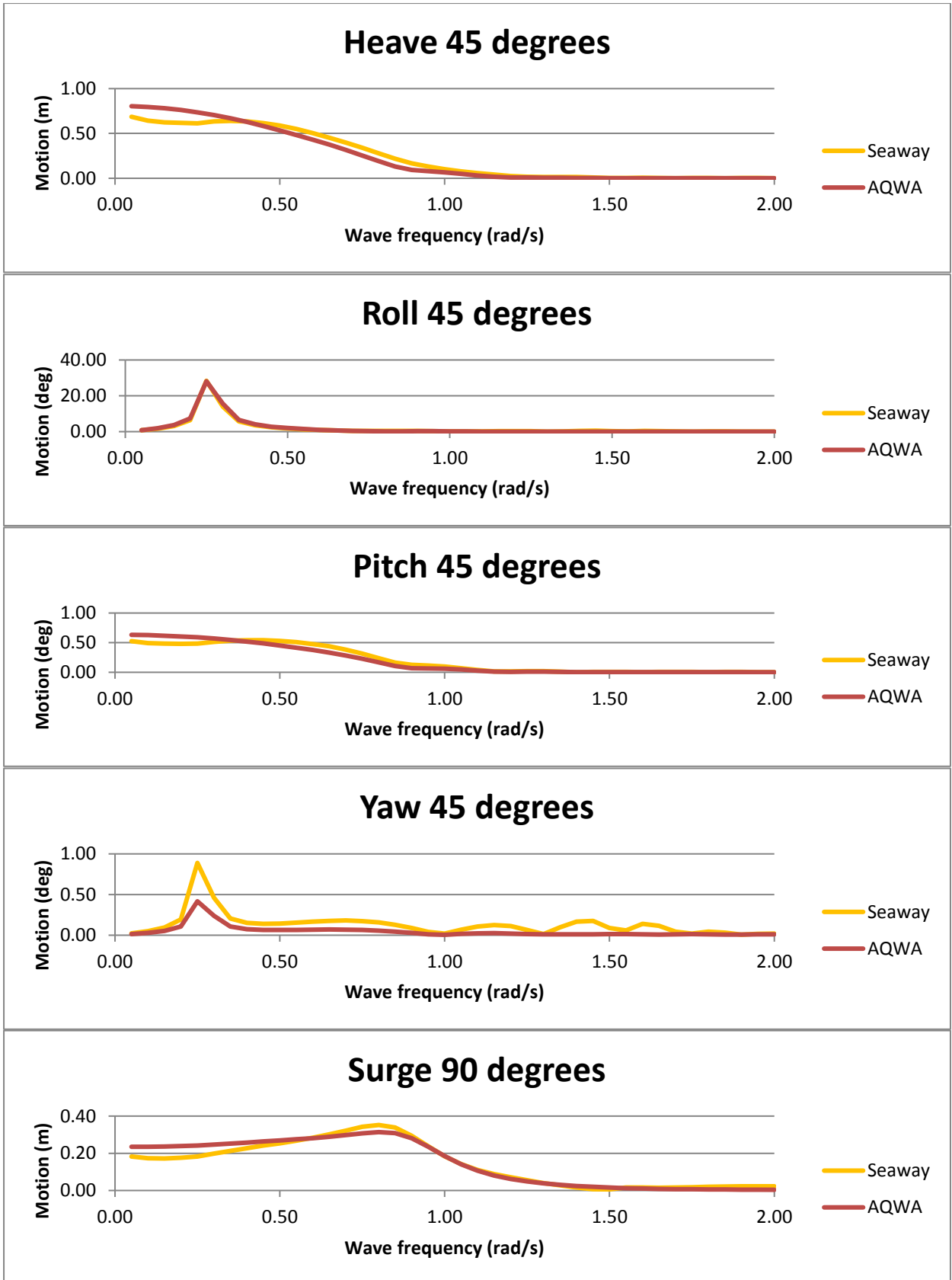


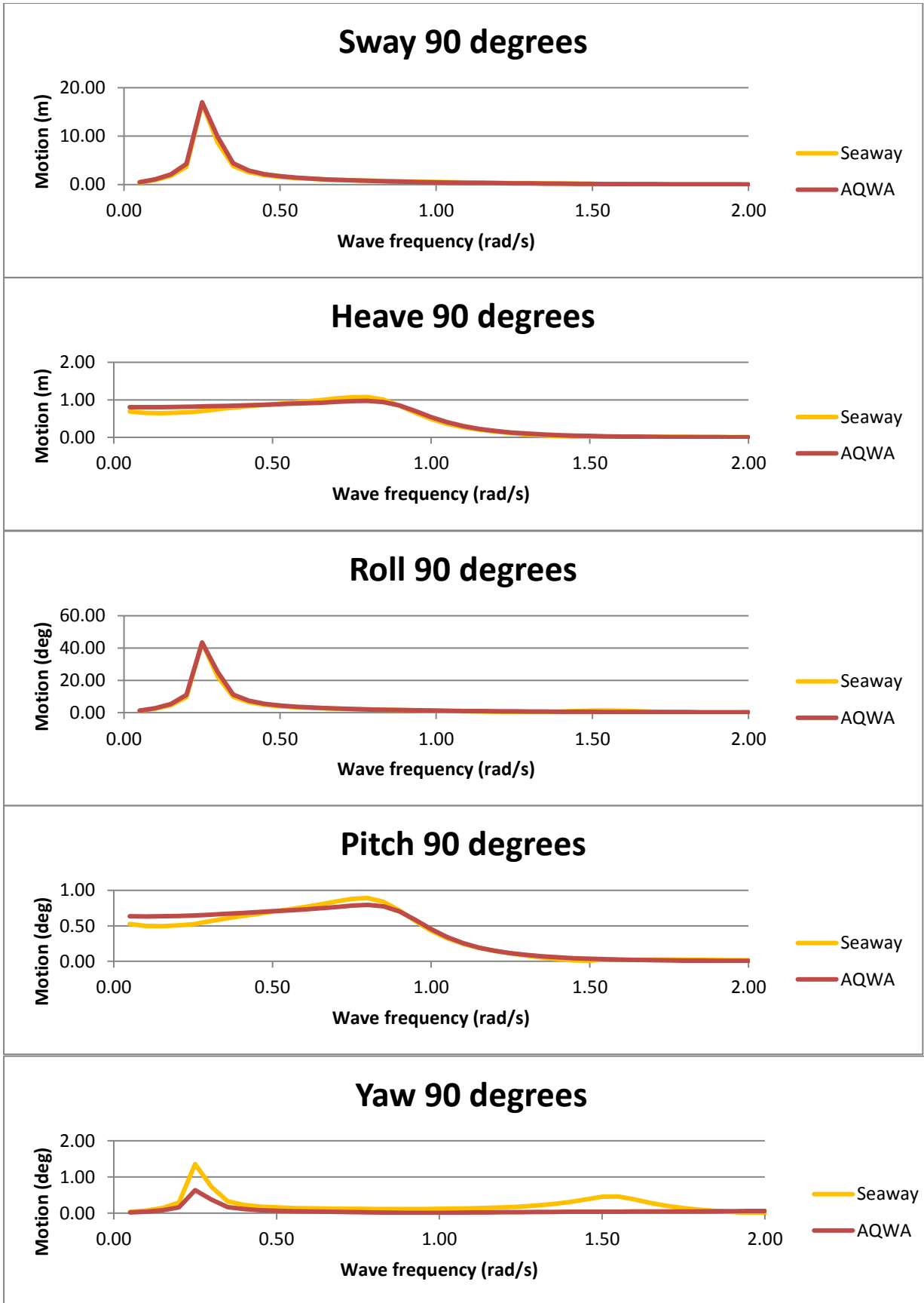


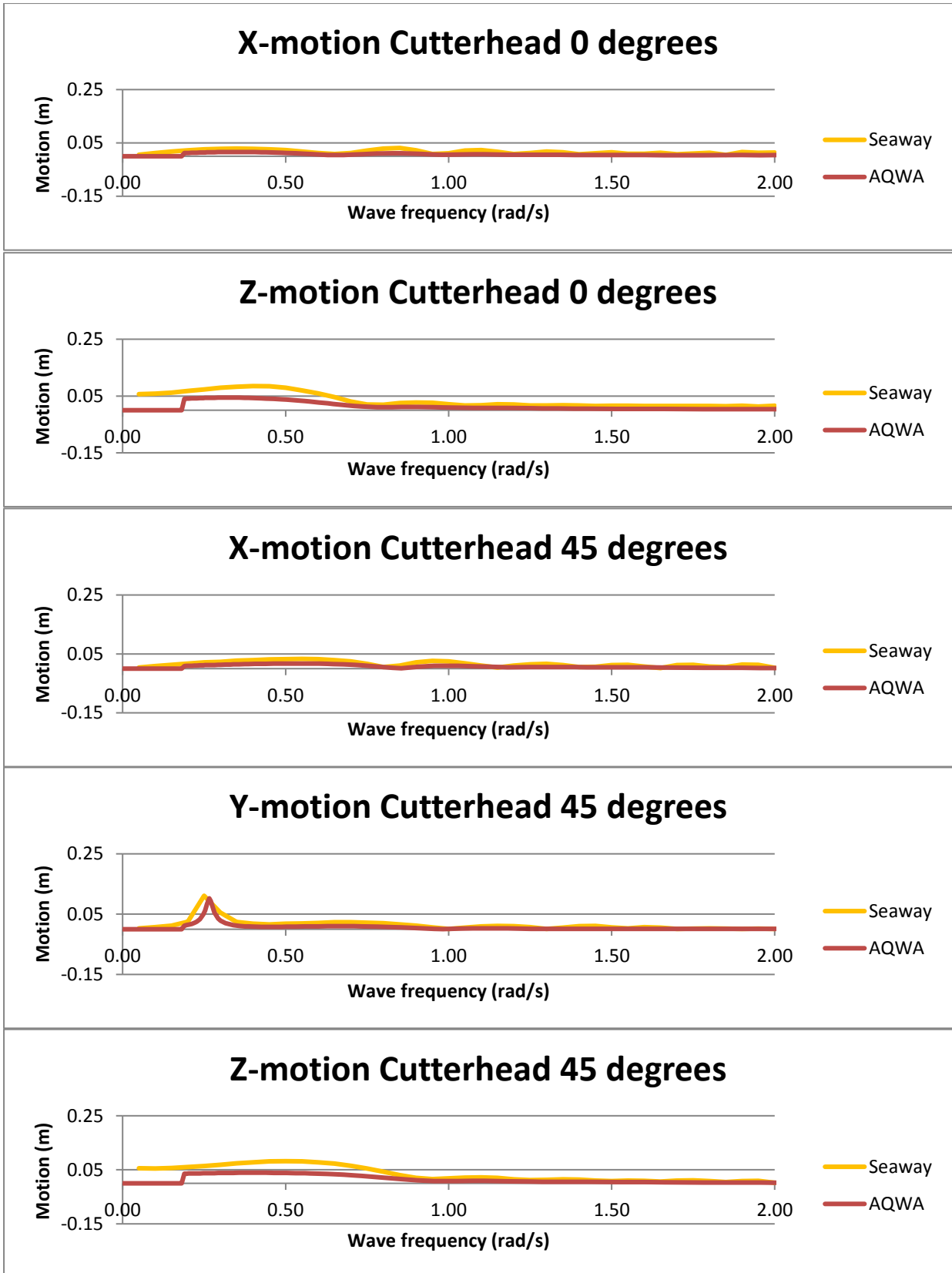


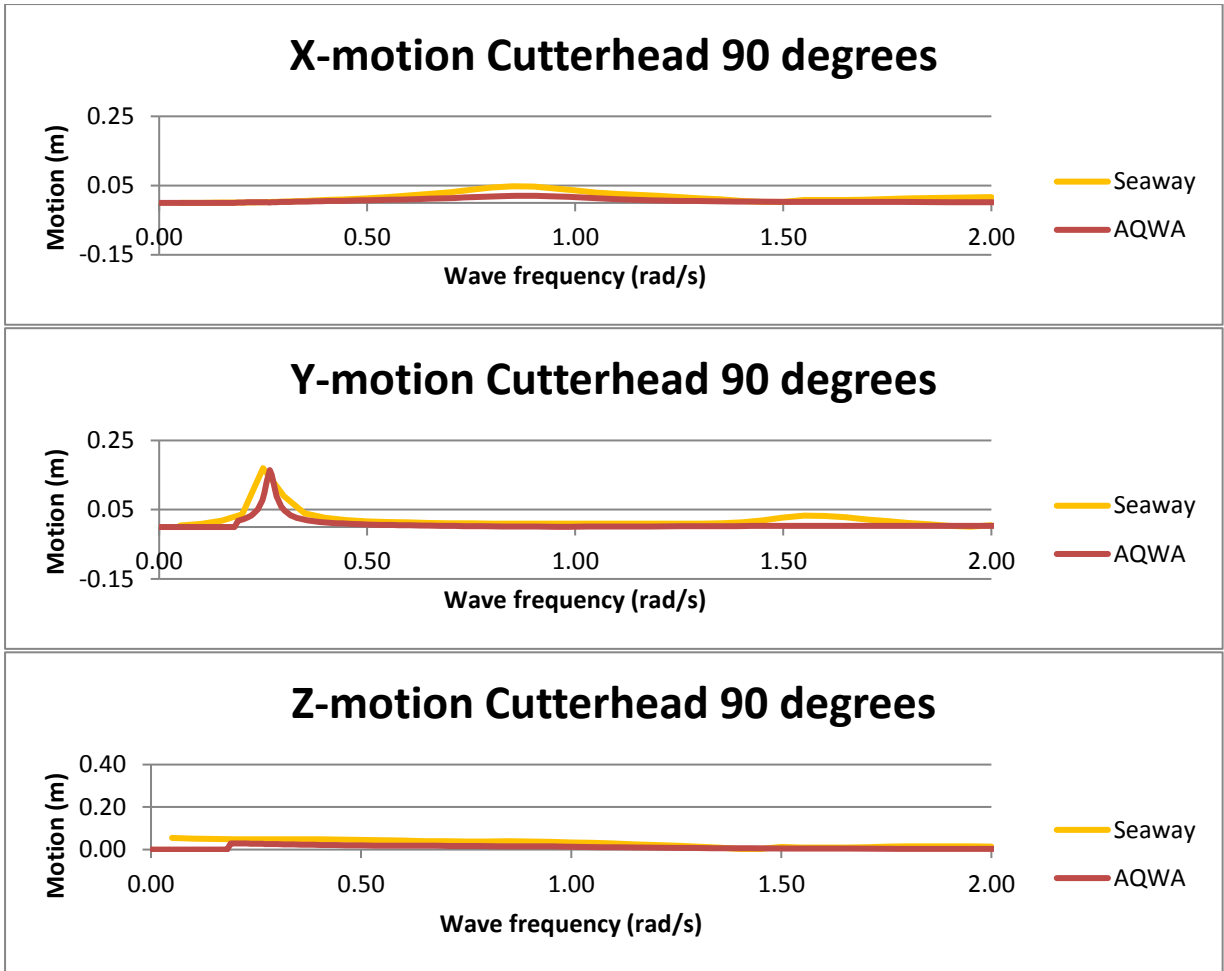
2 Springs





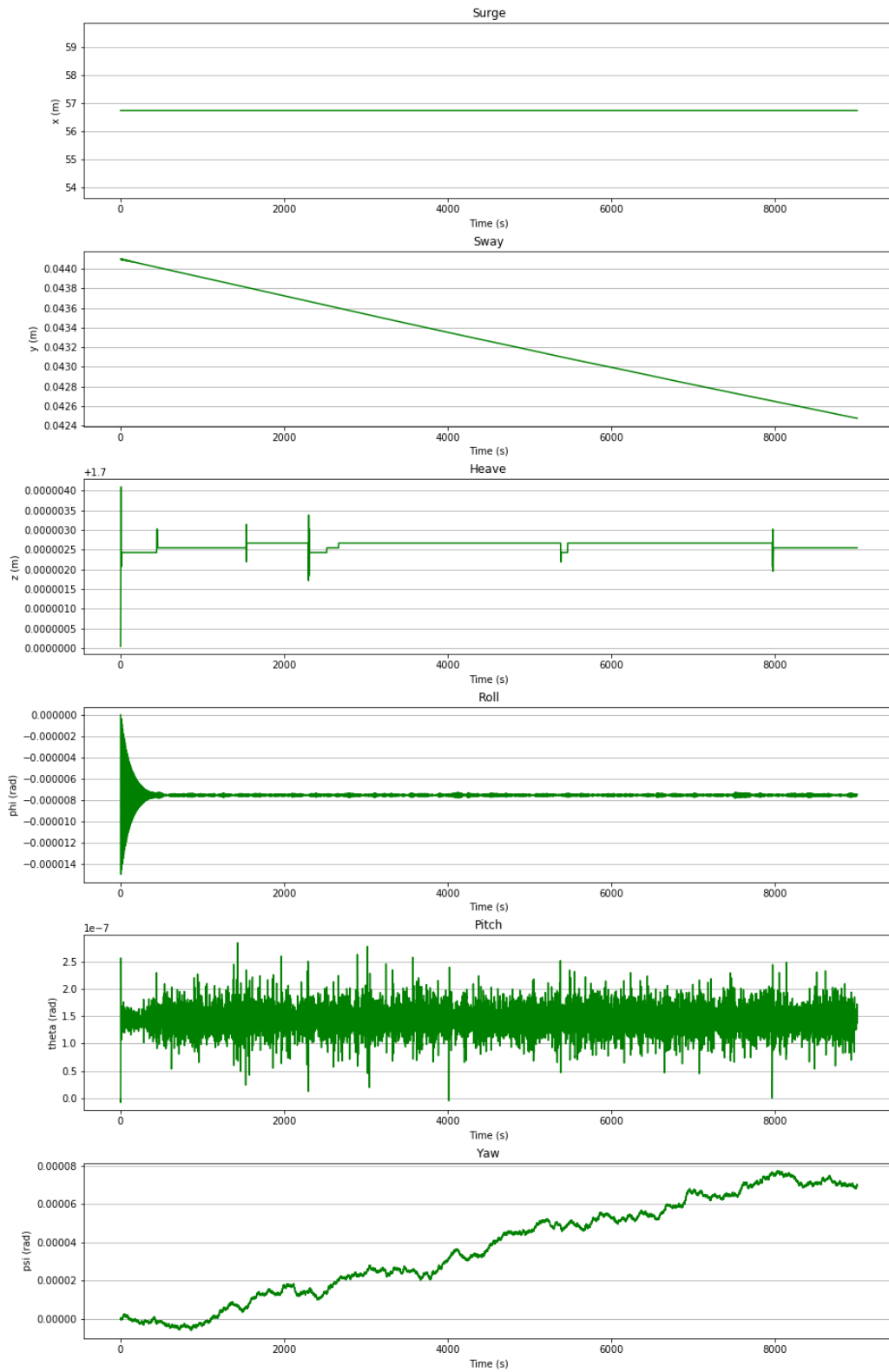




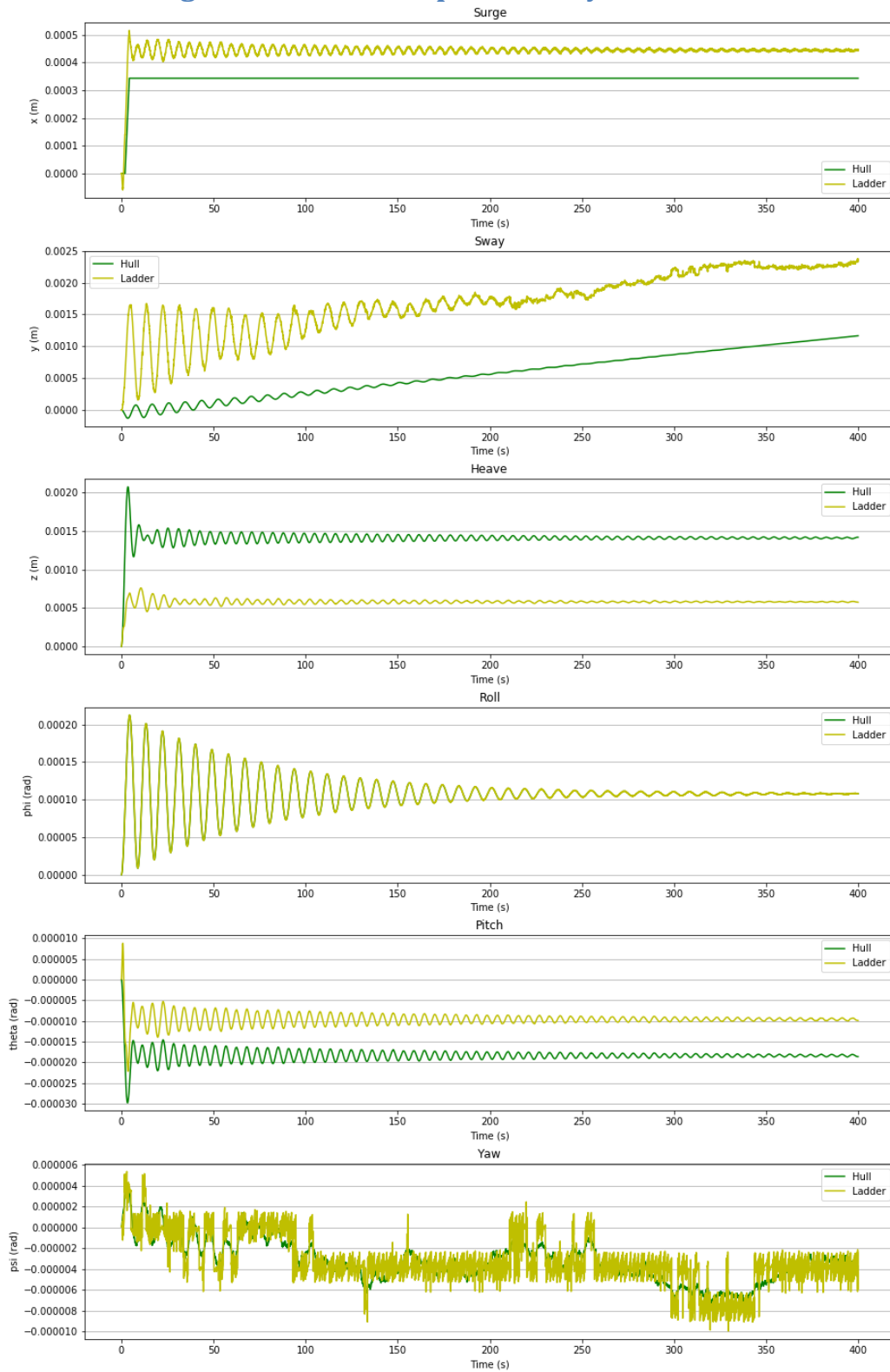


Appendix E. Free floating in time domain results

Free-floating single rigid body

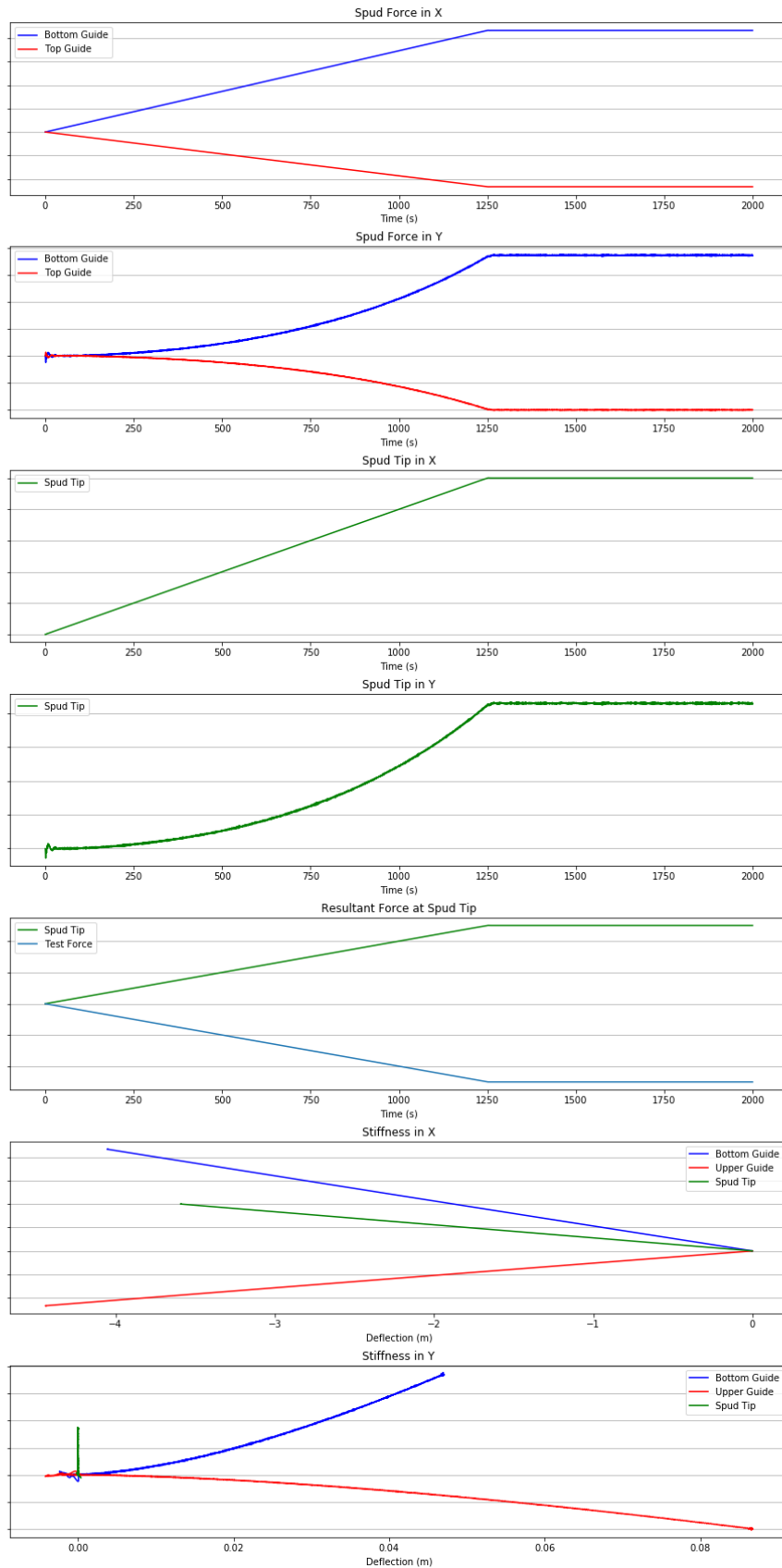


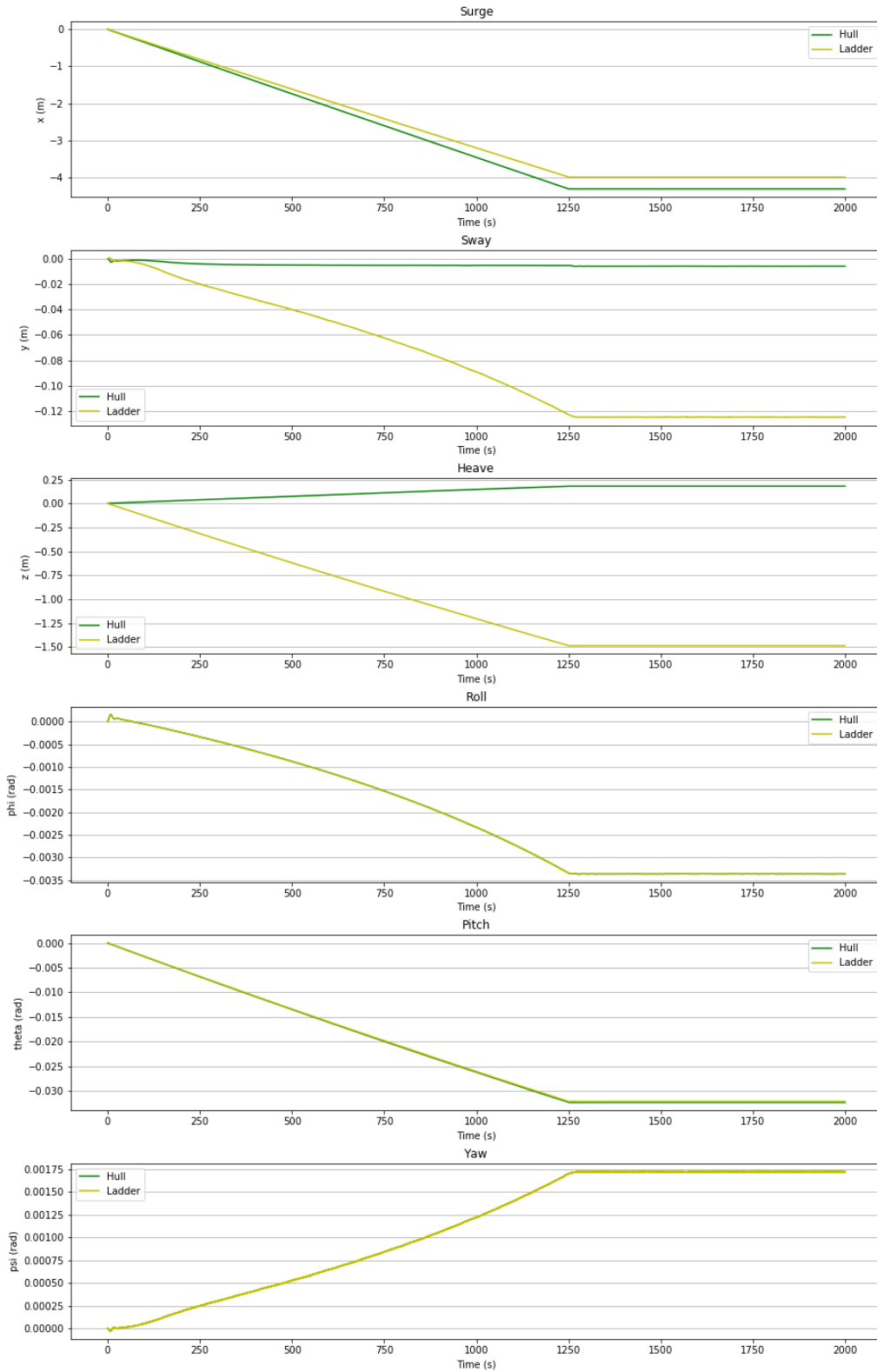
Free floating with ladder as separate body



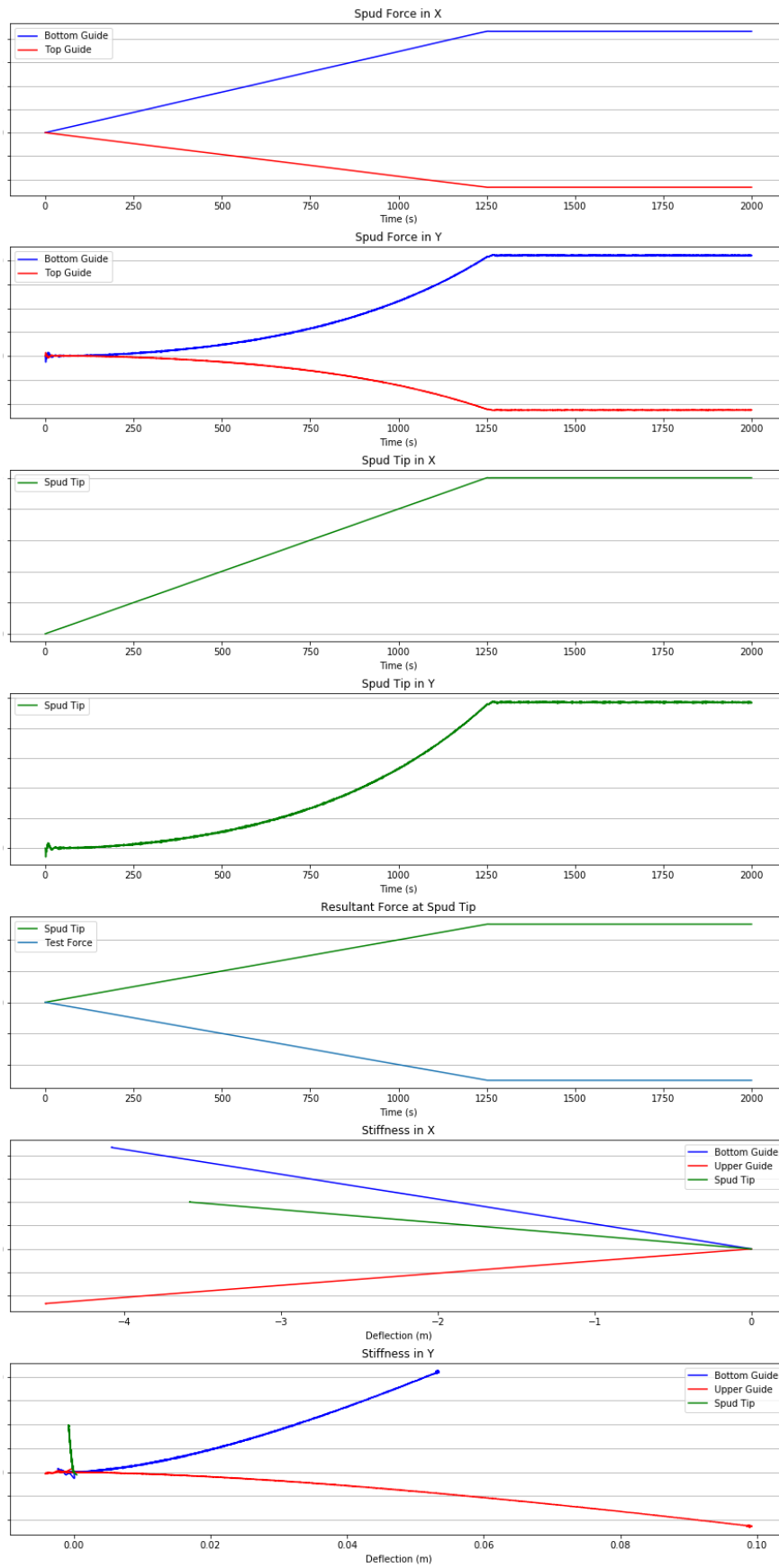
Appendix F. Results of Spud tests

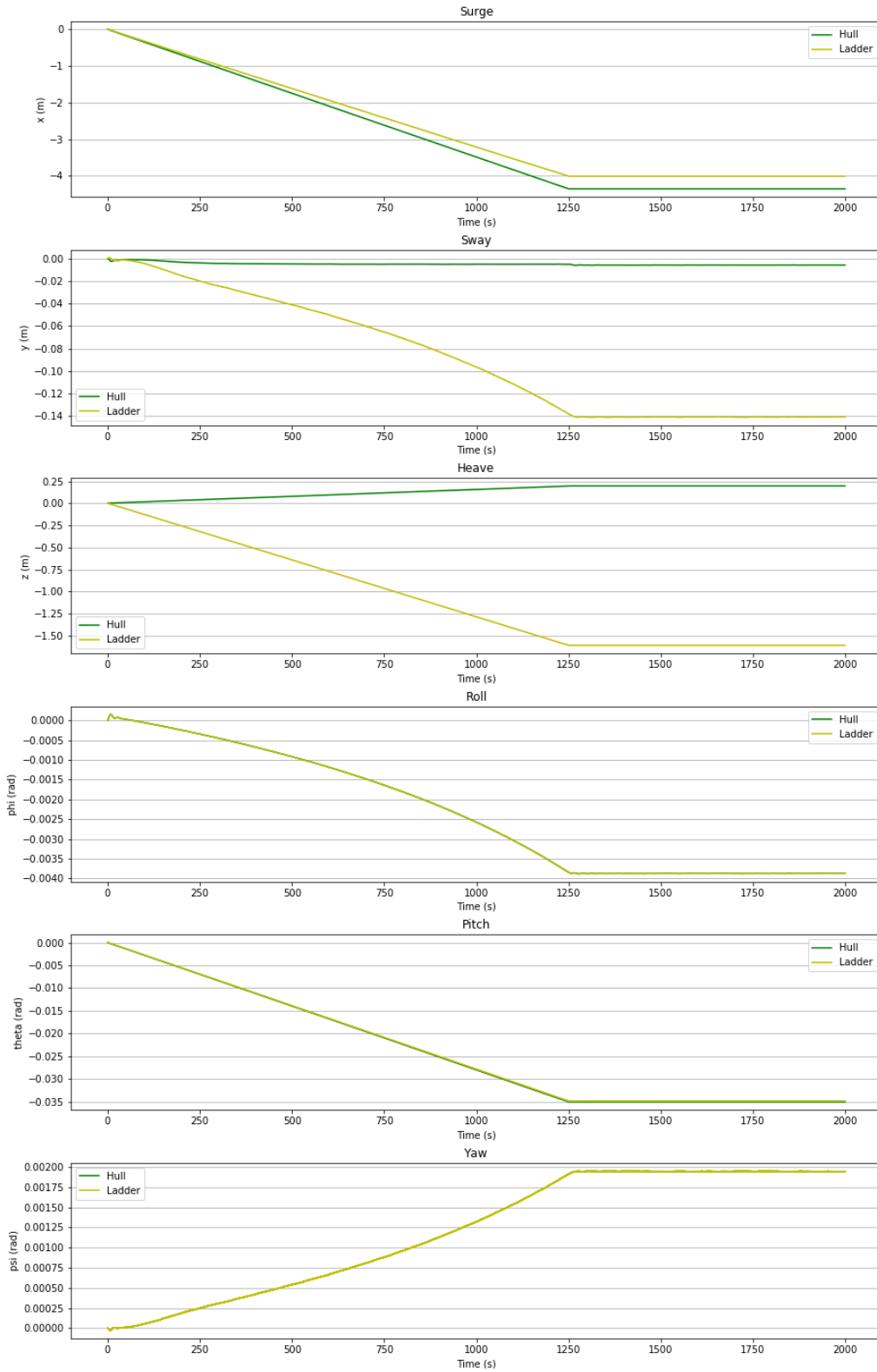
Cantilever Spud



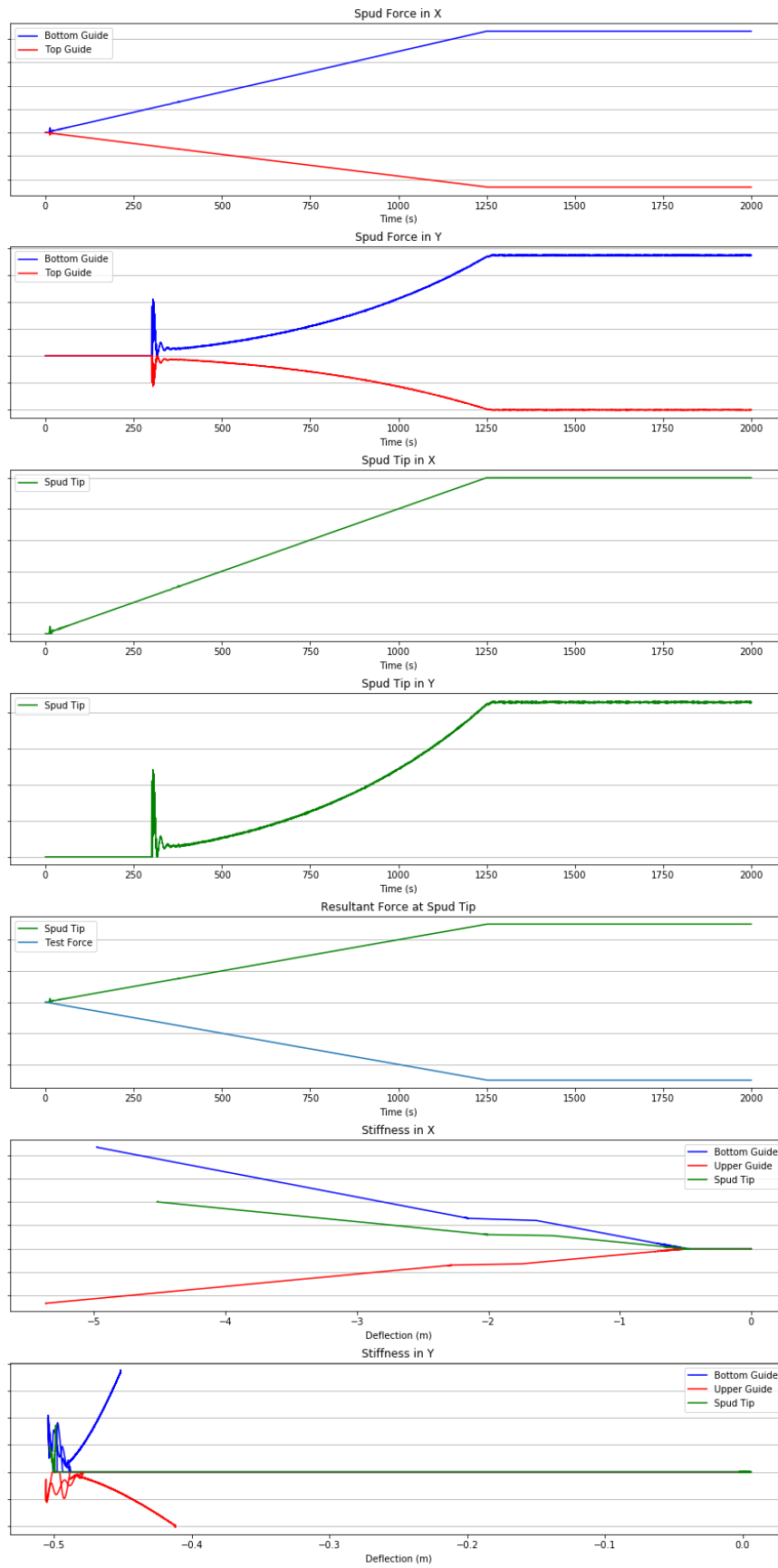


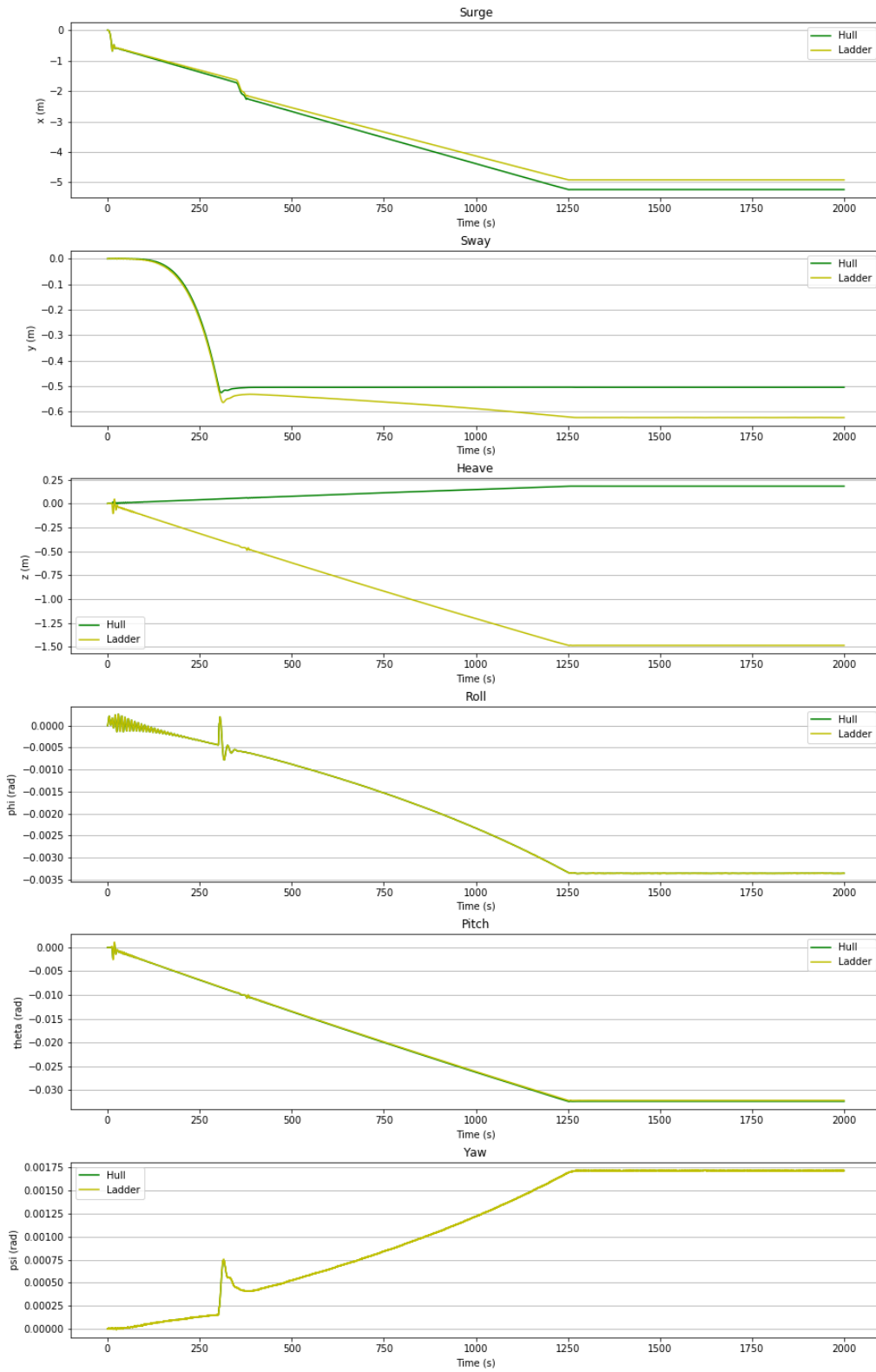
Pinned Spud





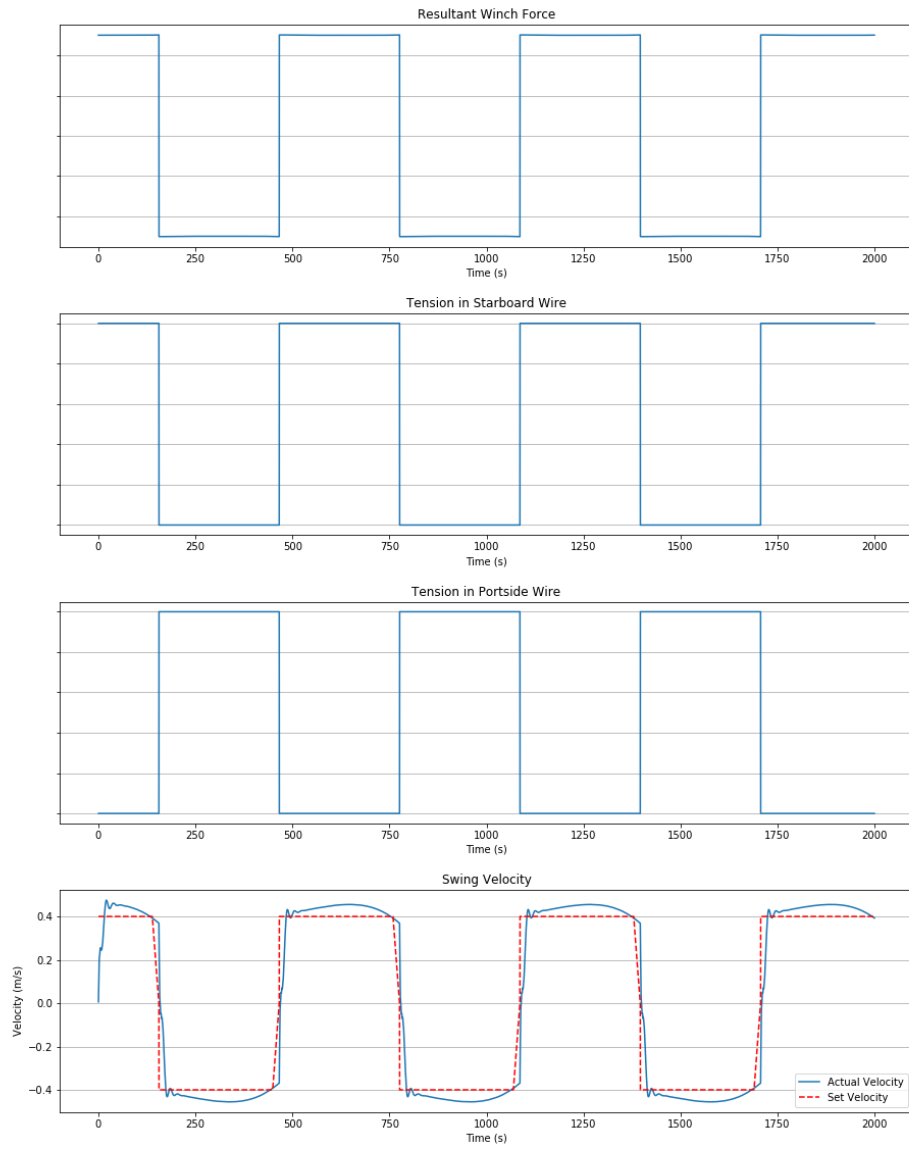
Flexible spud carriage

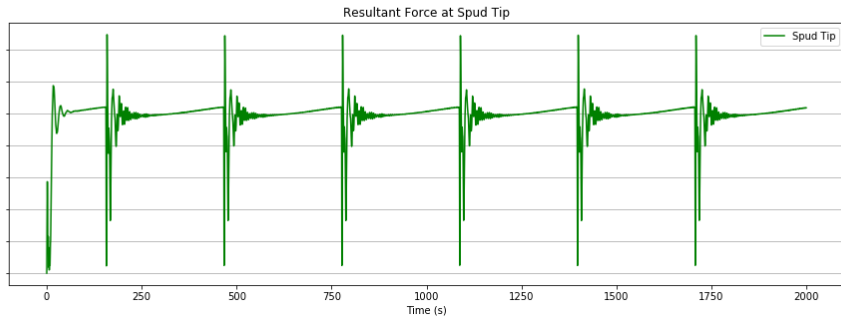
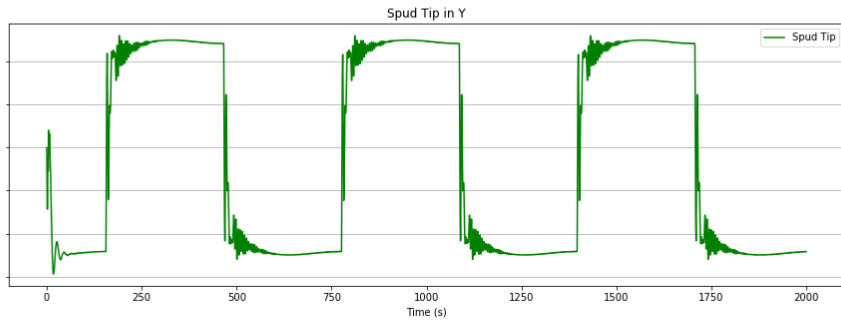
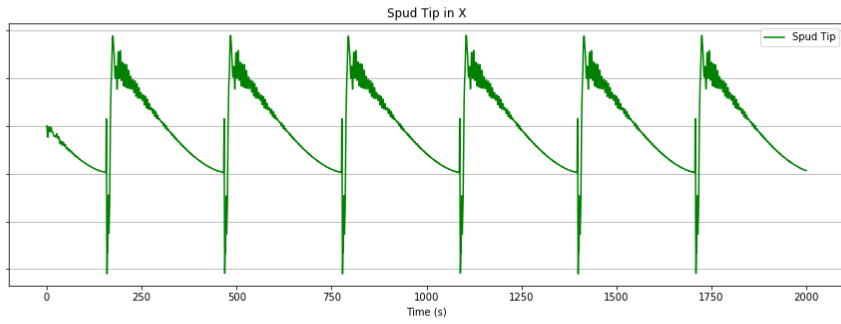
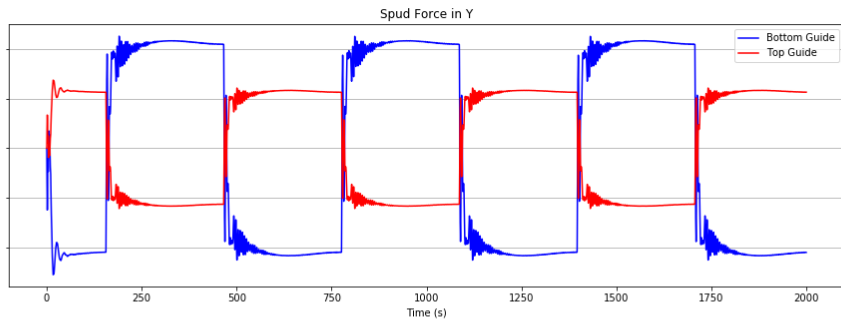
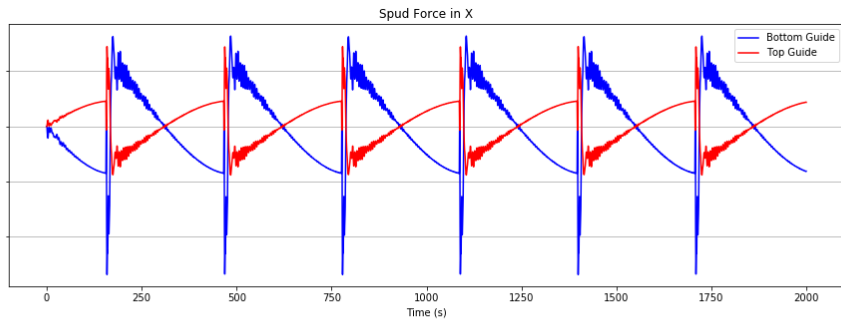


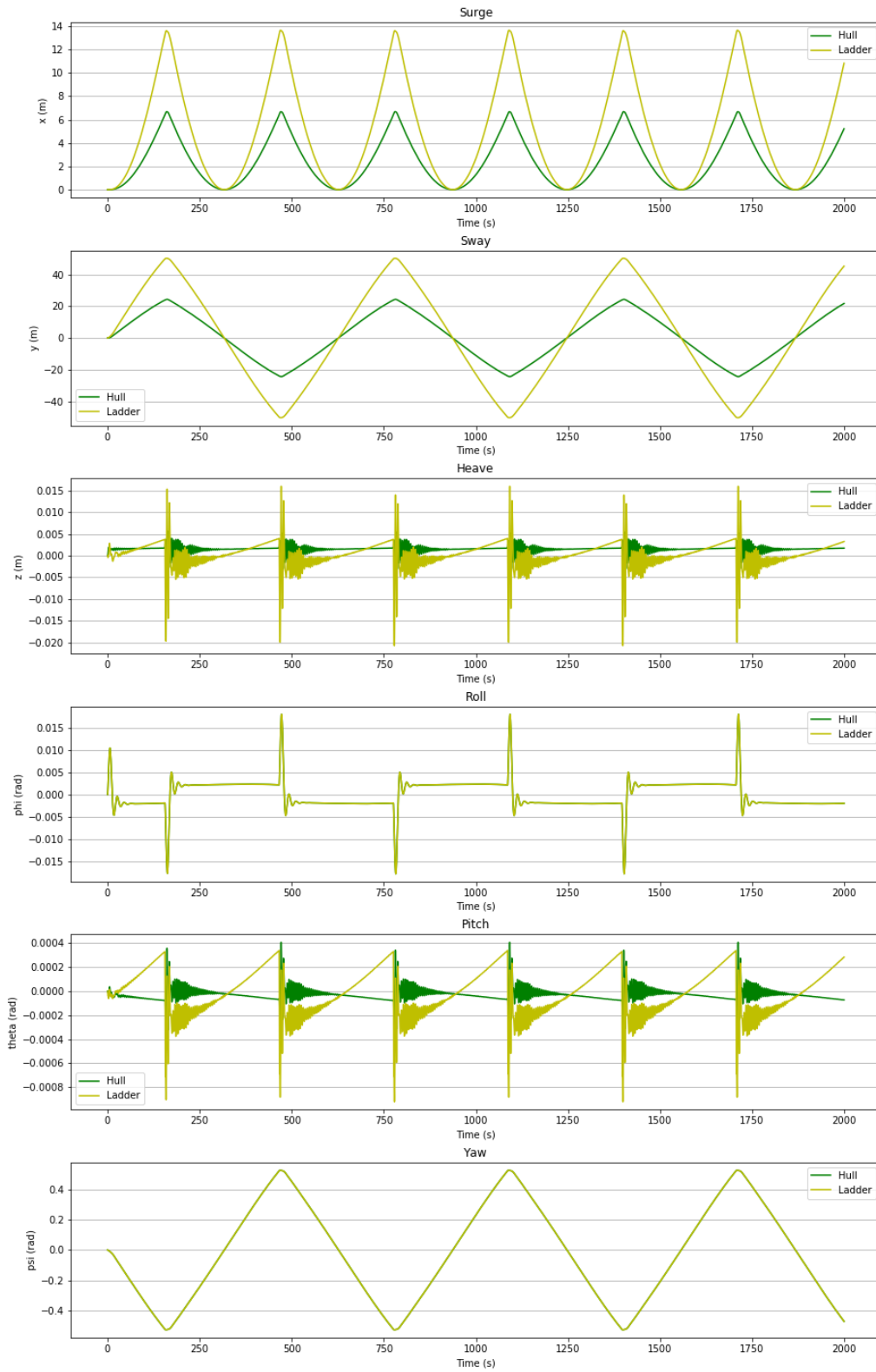


Appendix G. Results of Winch tests

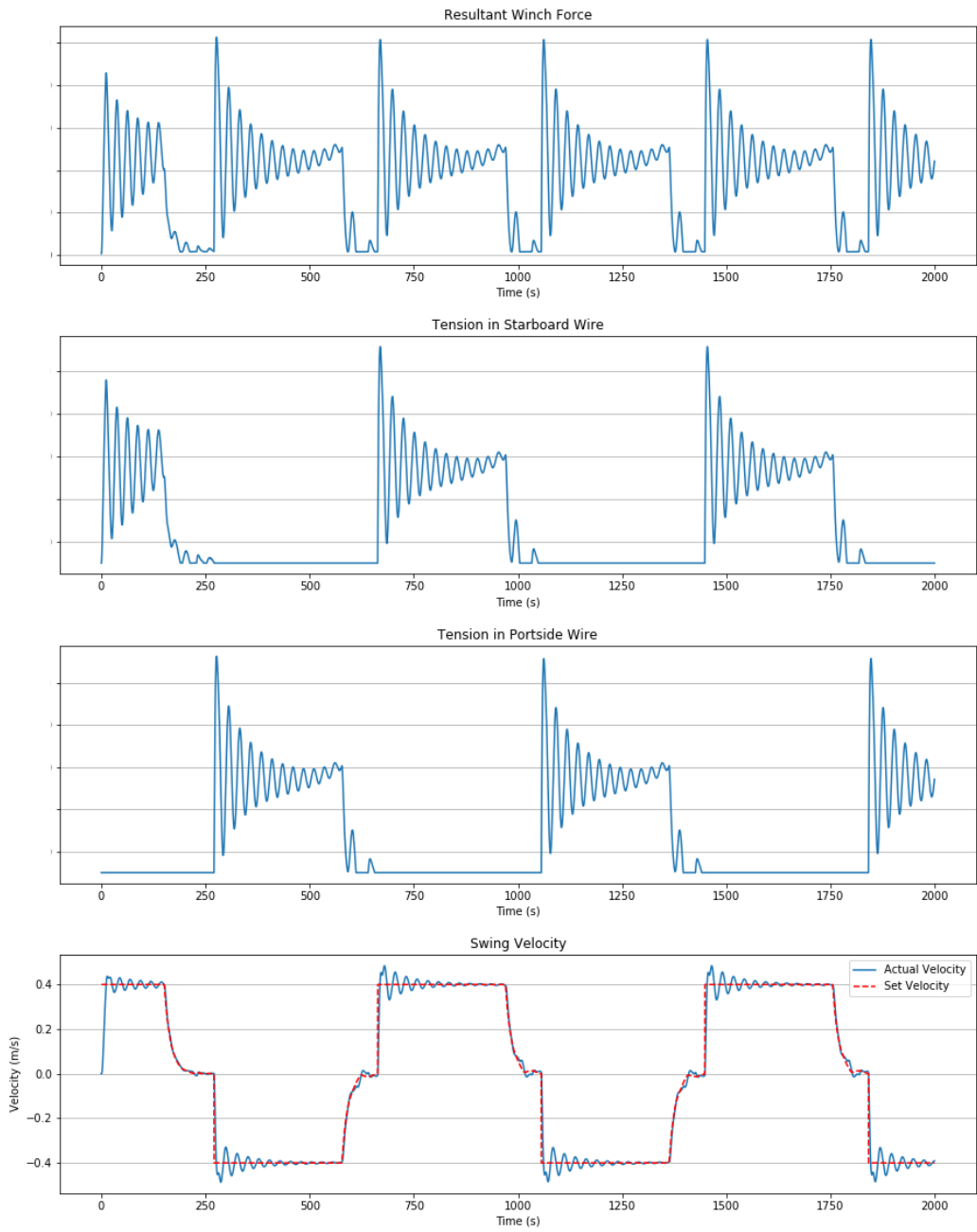
Fixed Force

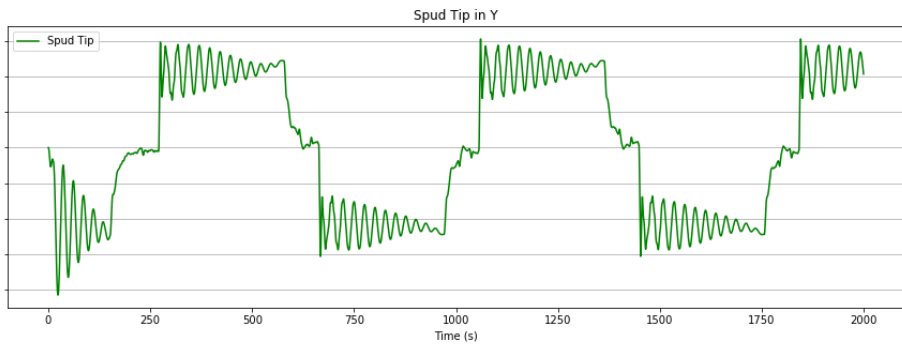
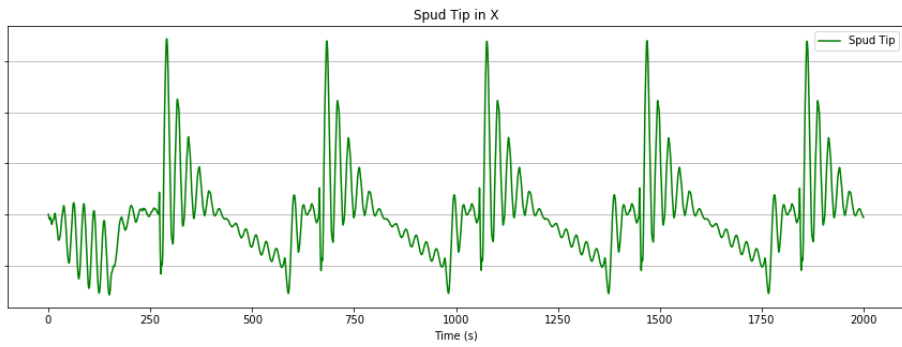
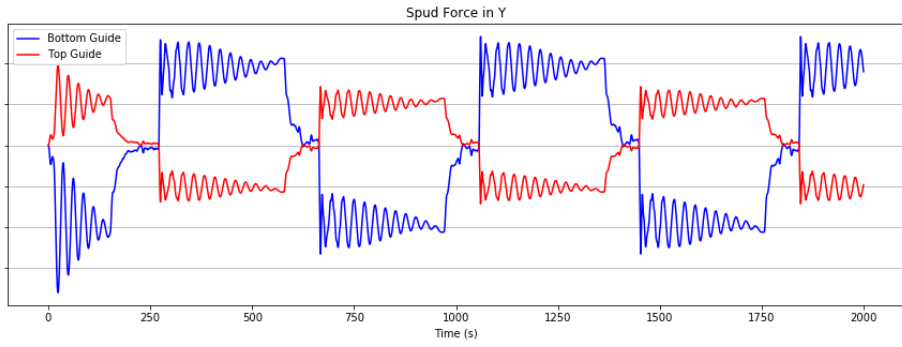
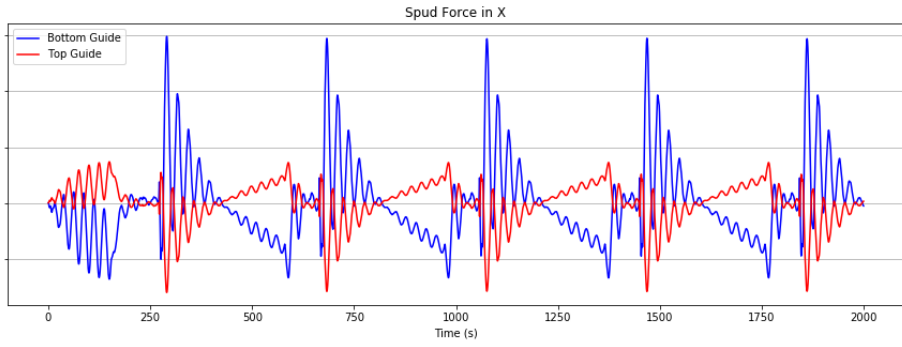


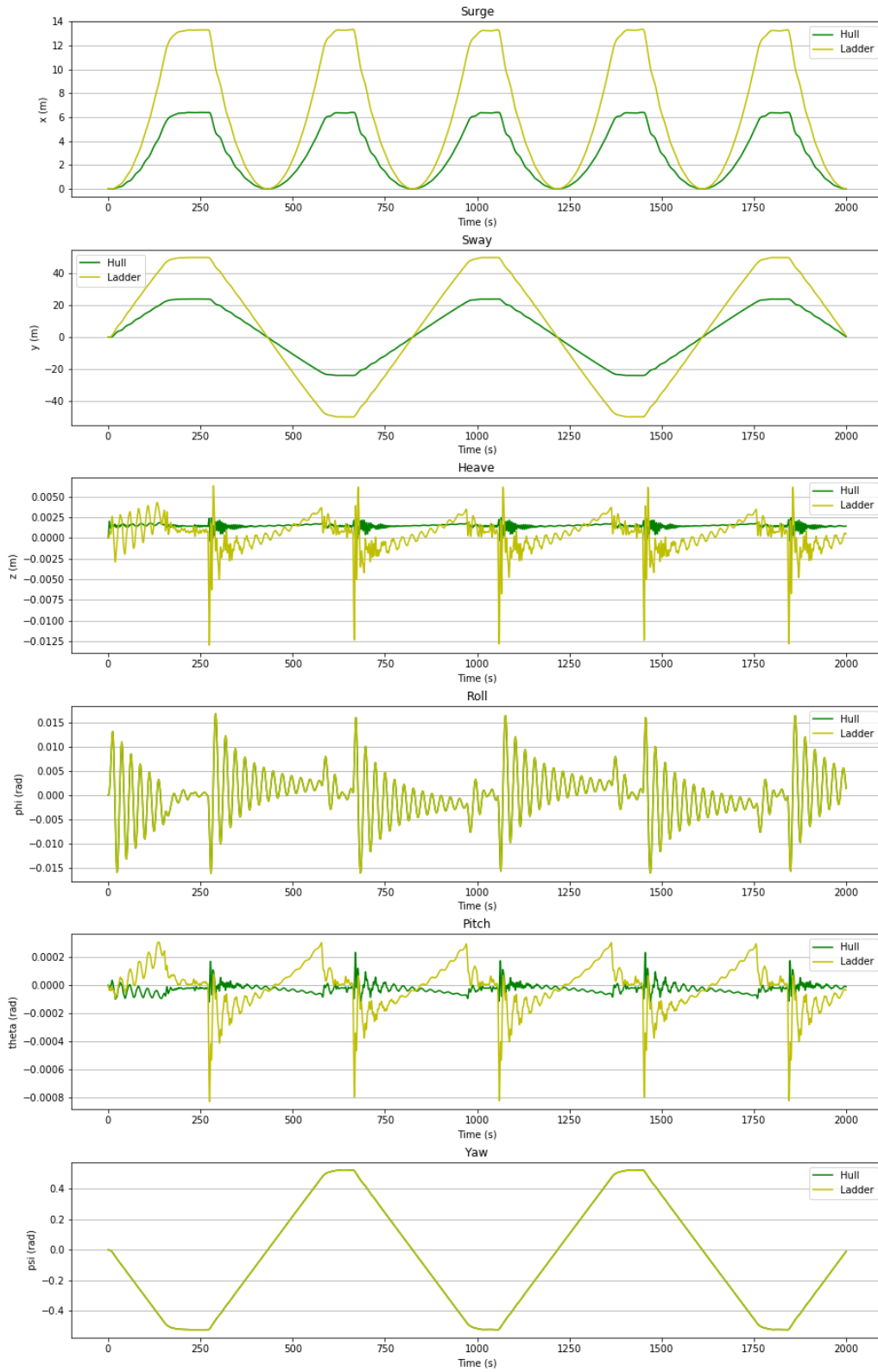




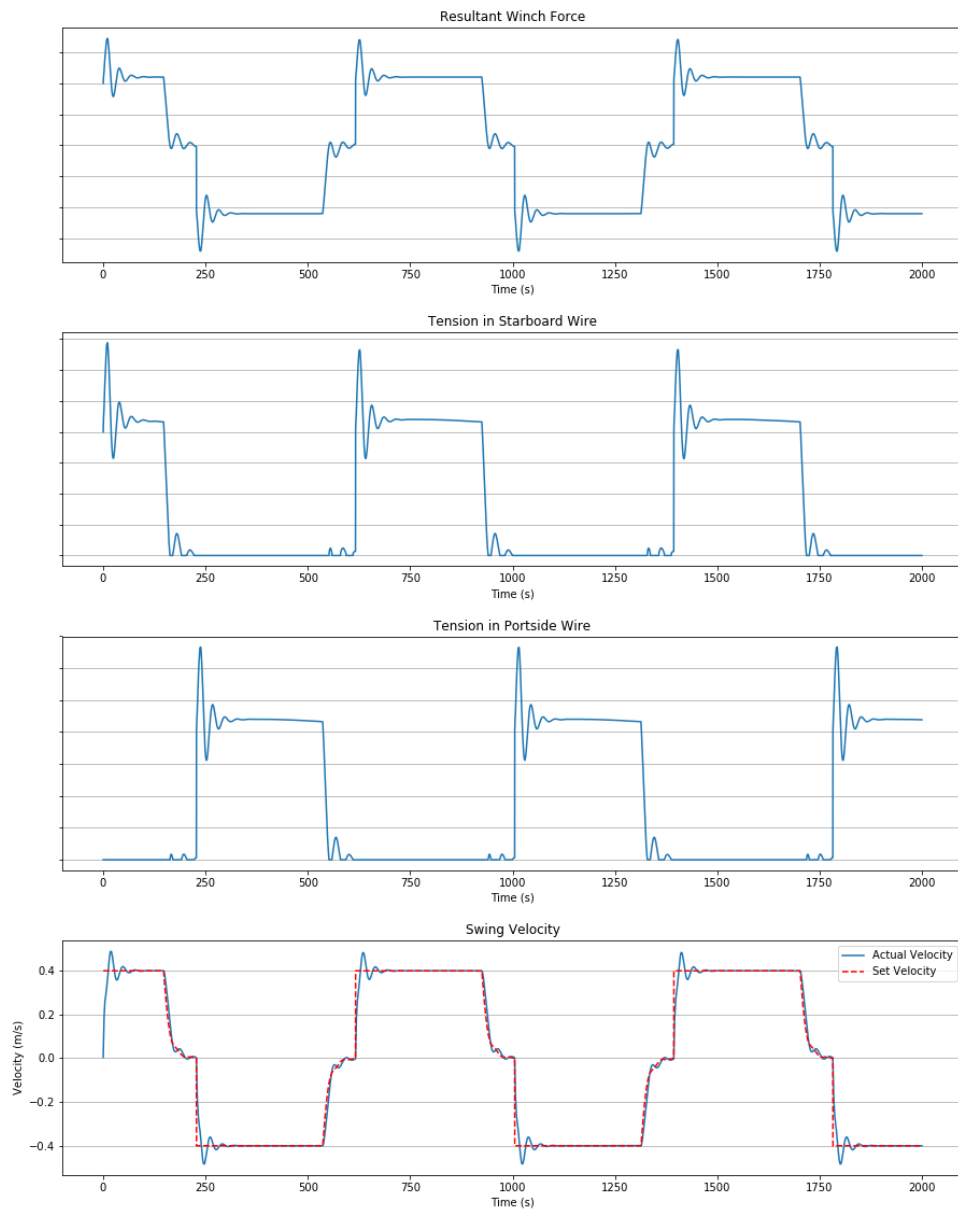
Fixed Length

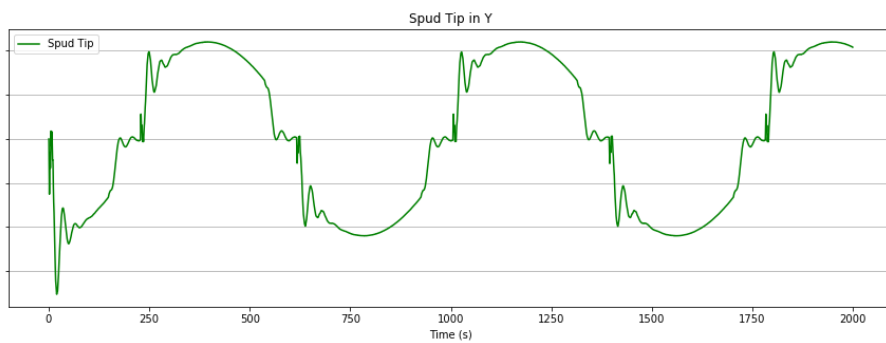
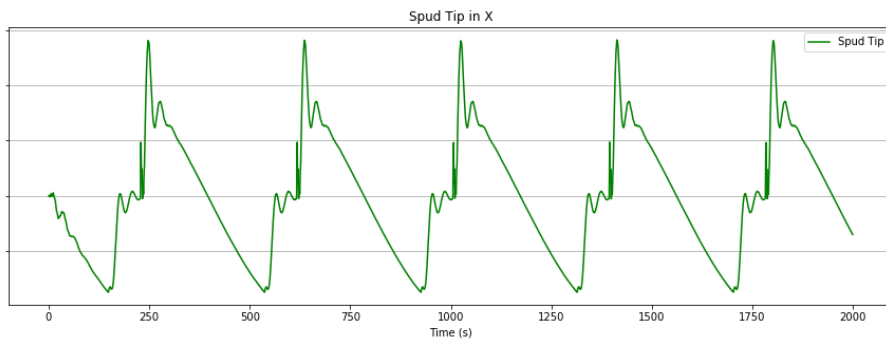
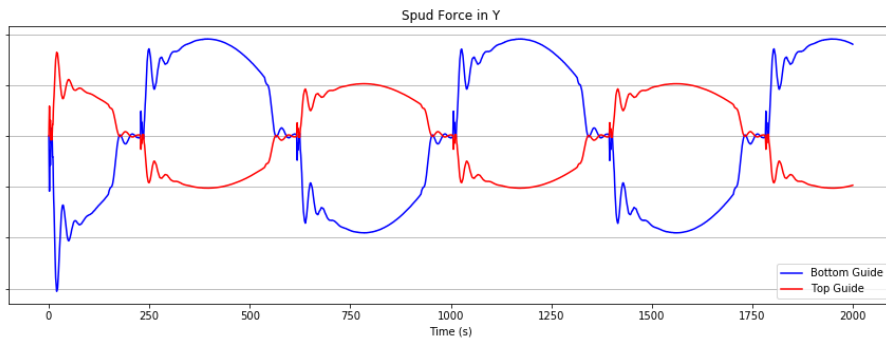
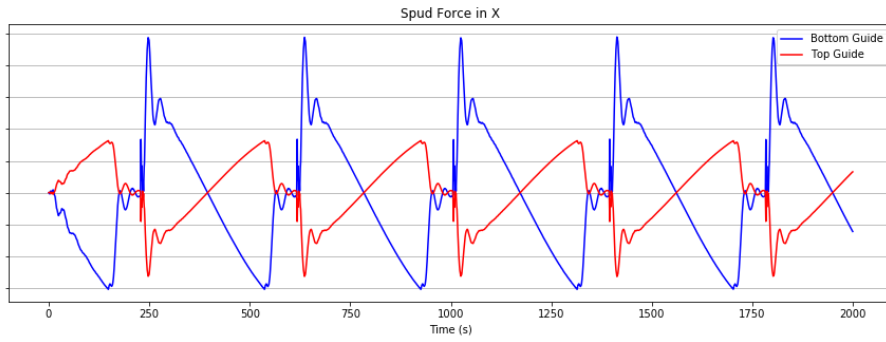


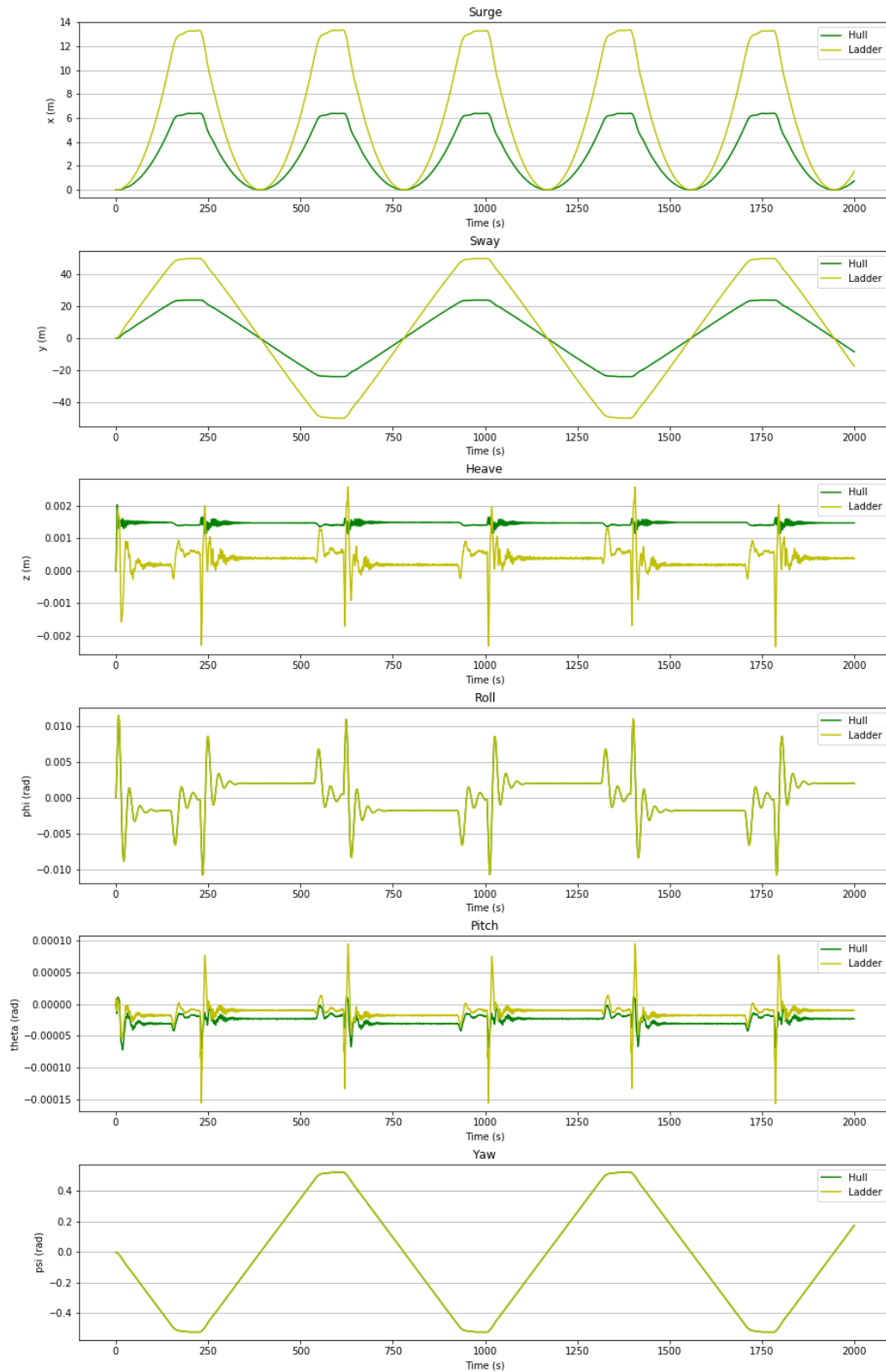




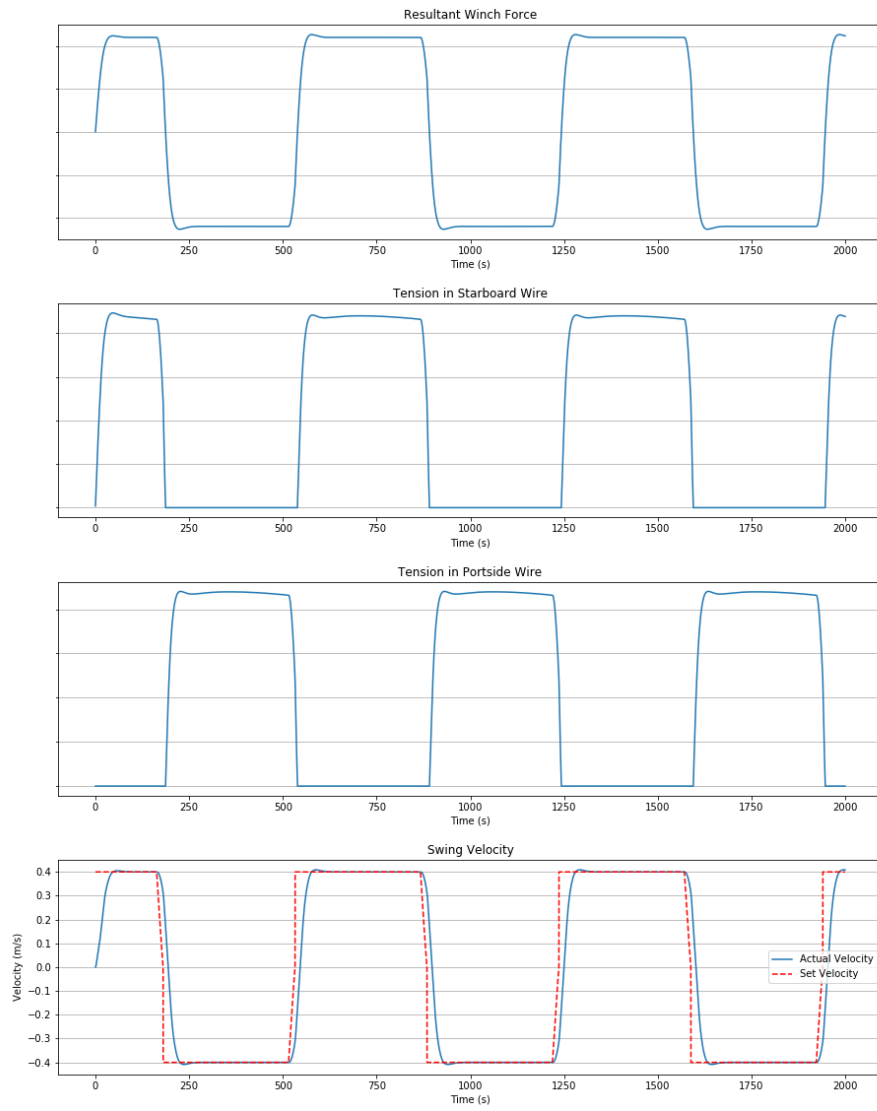
PID Controller, P-dominated

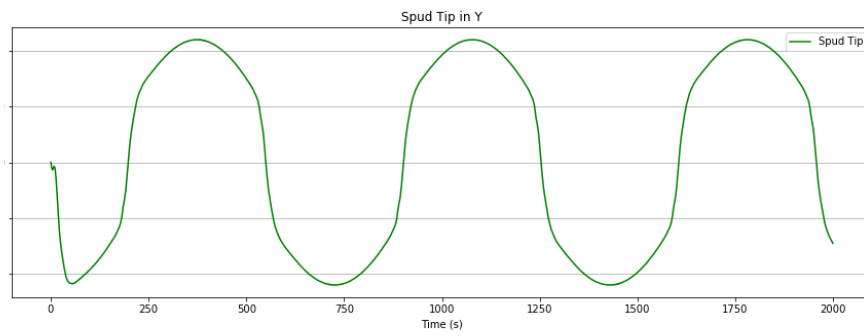
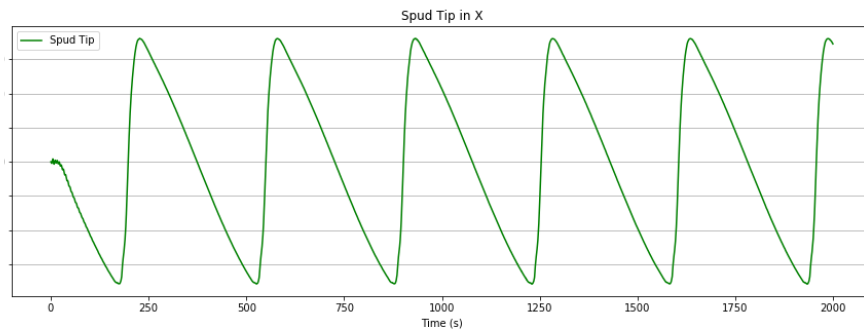
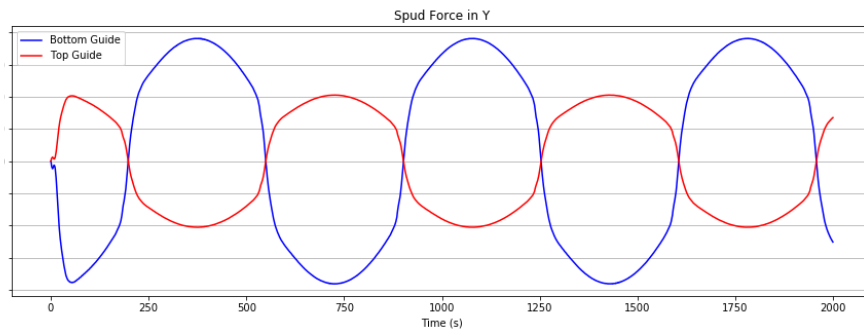
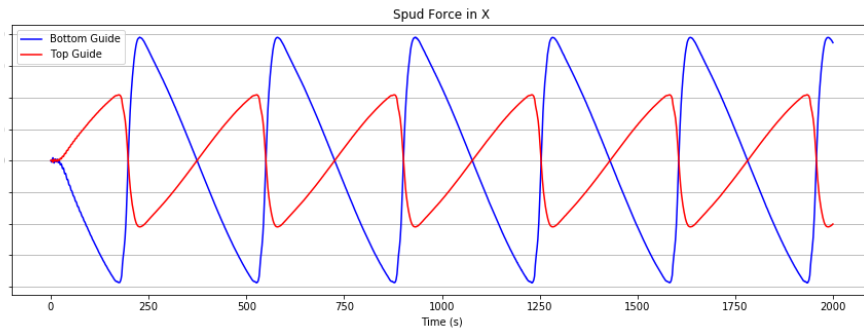


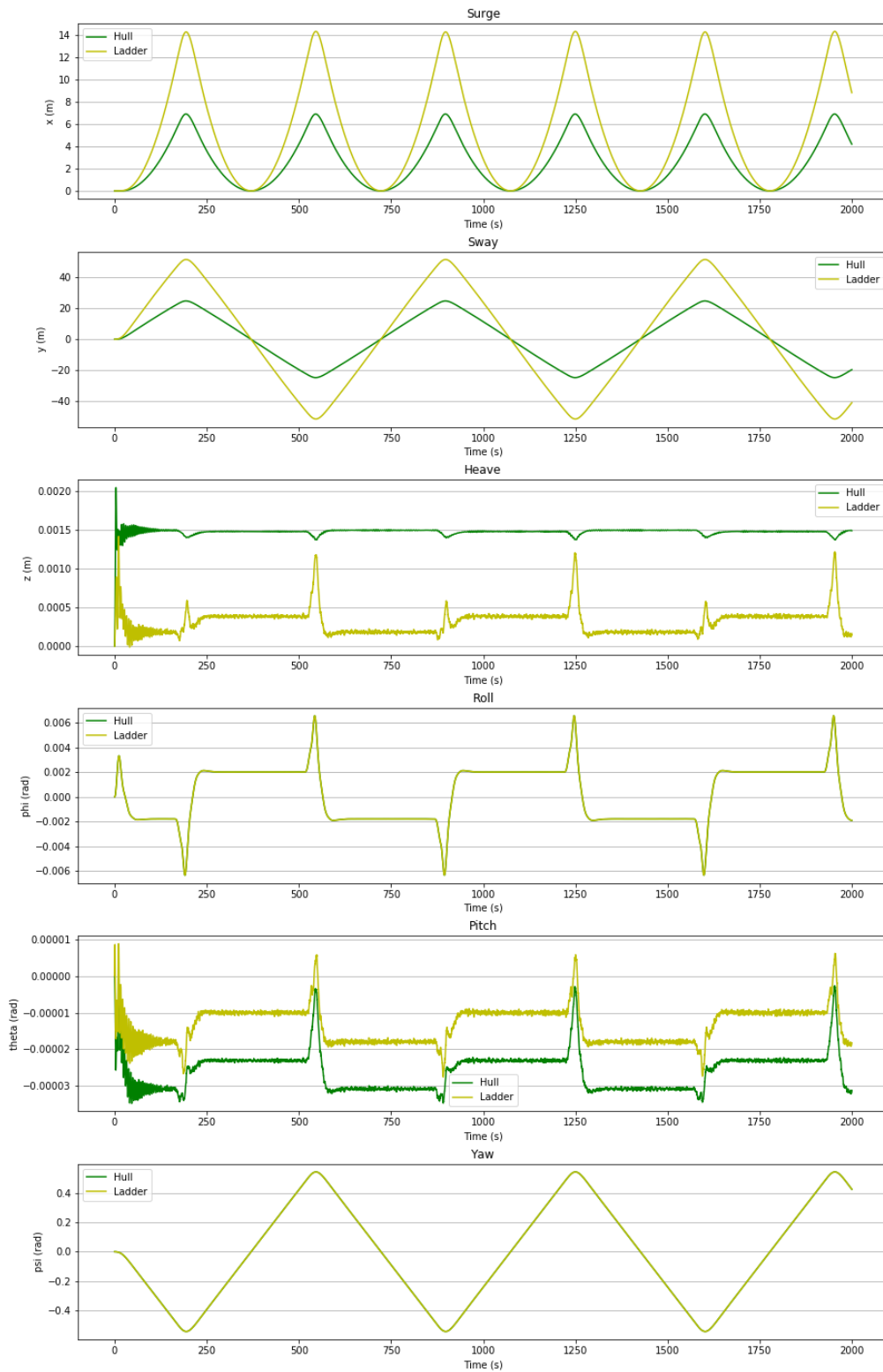




PID Controller, I-dominated

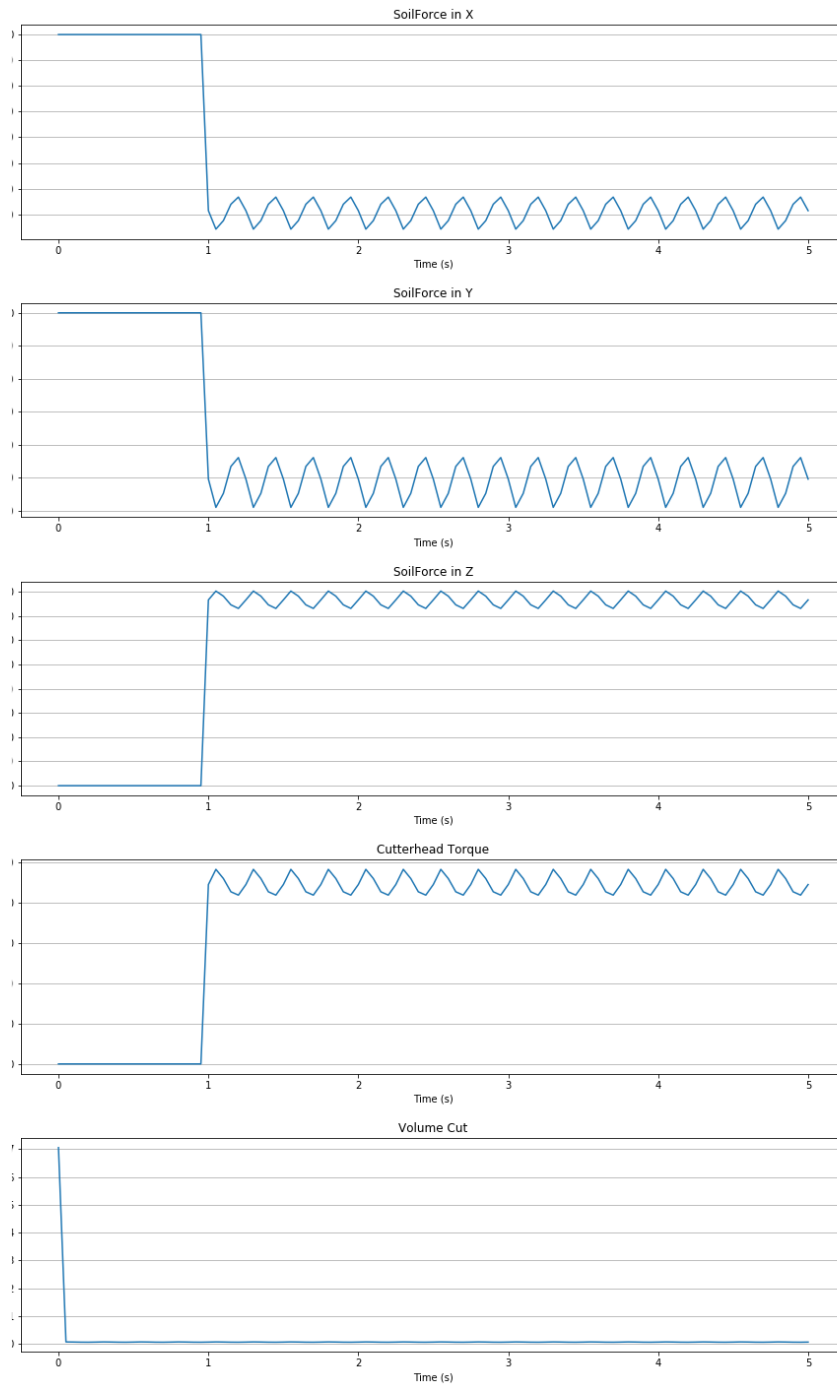




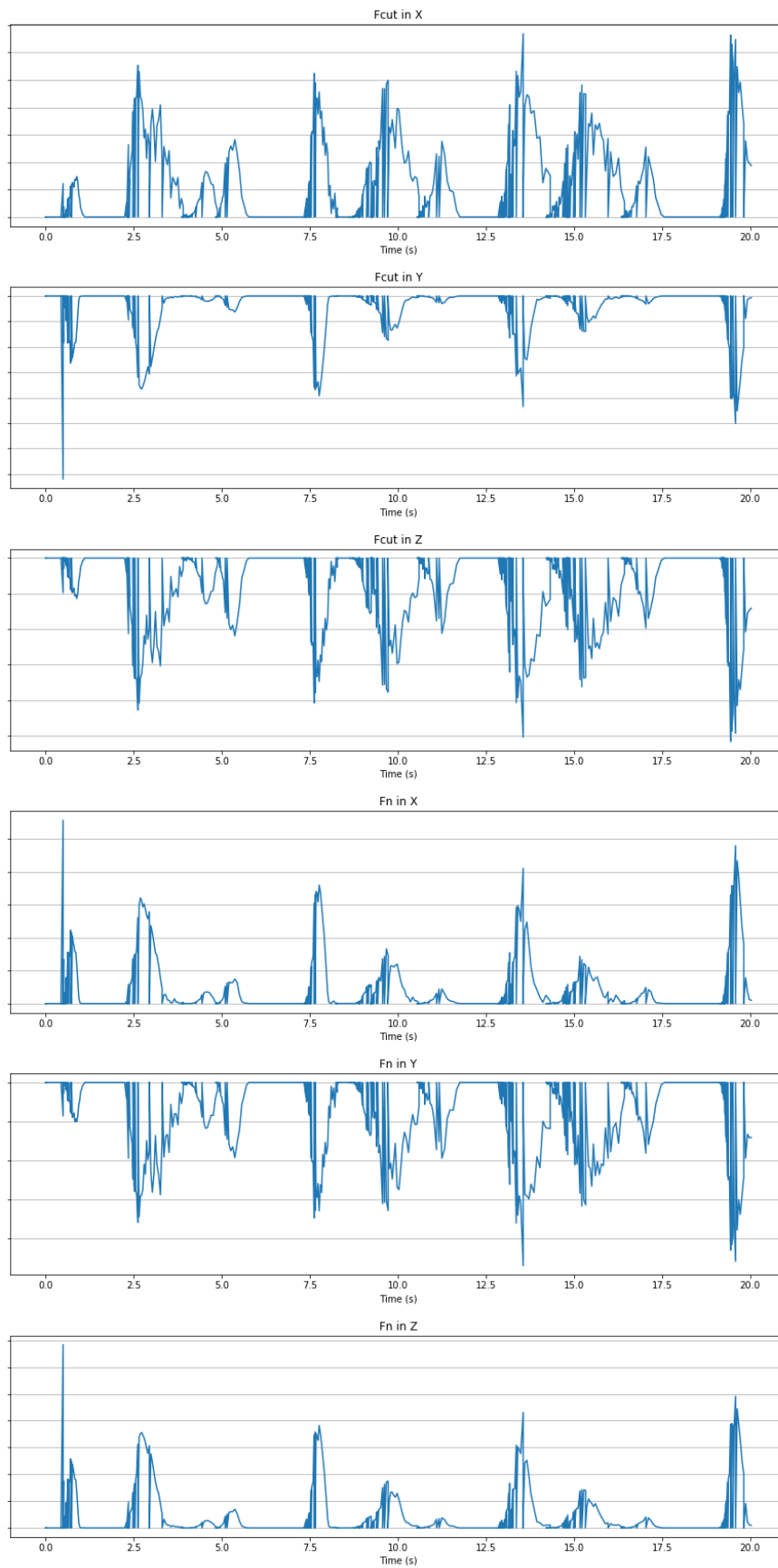


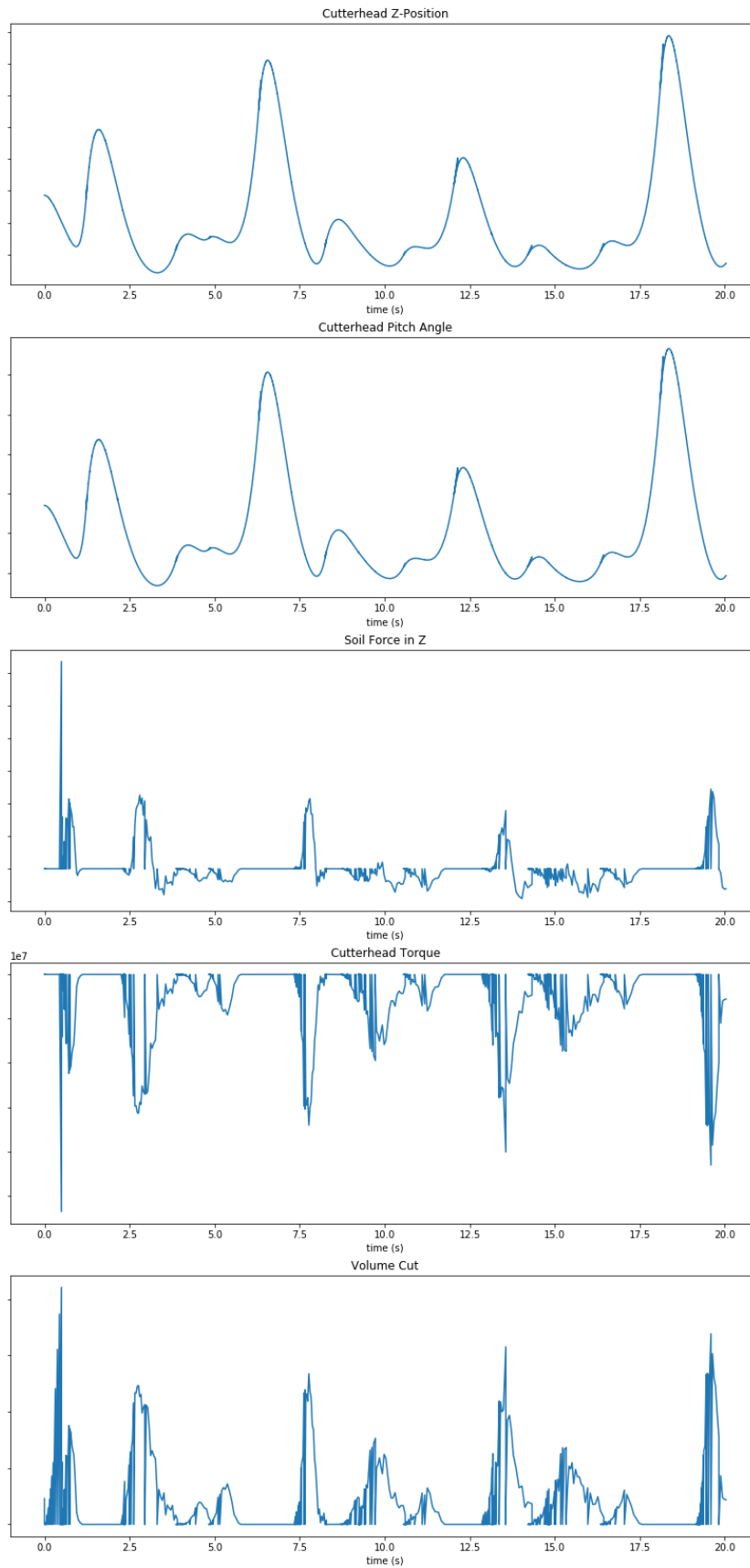
Appendix H. Soil tests

Static soil test

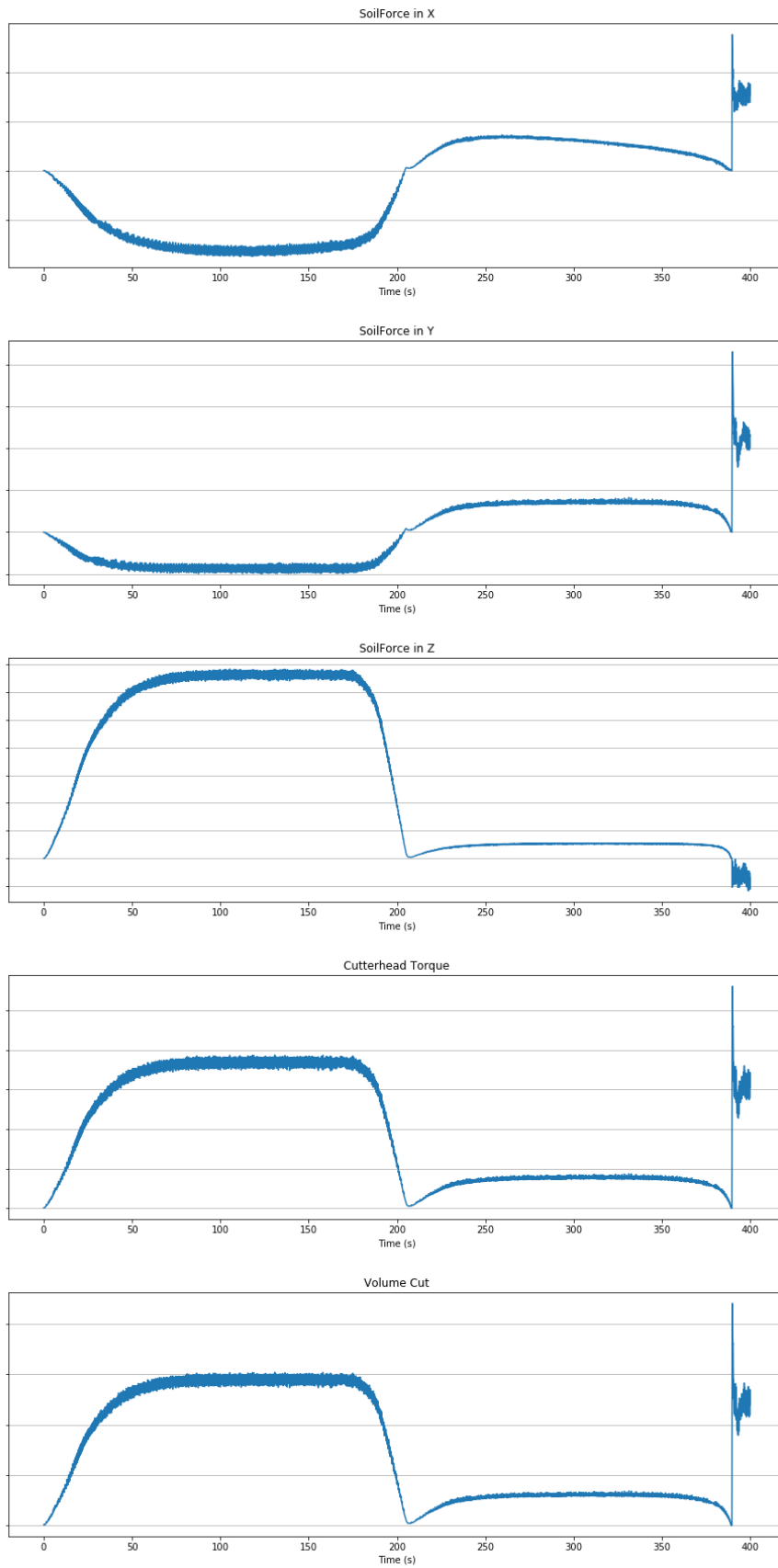


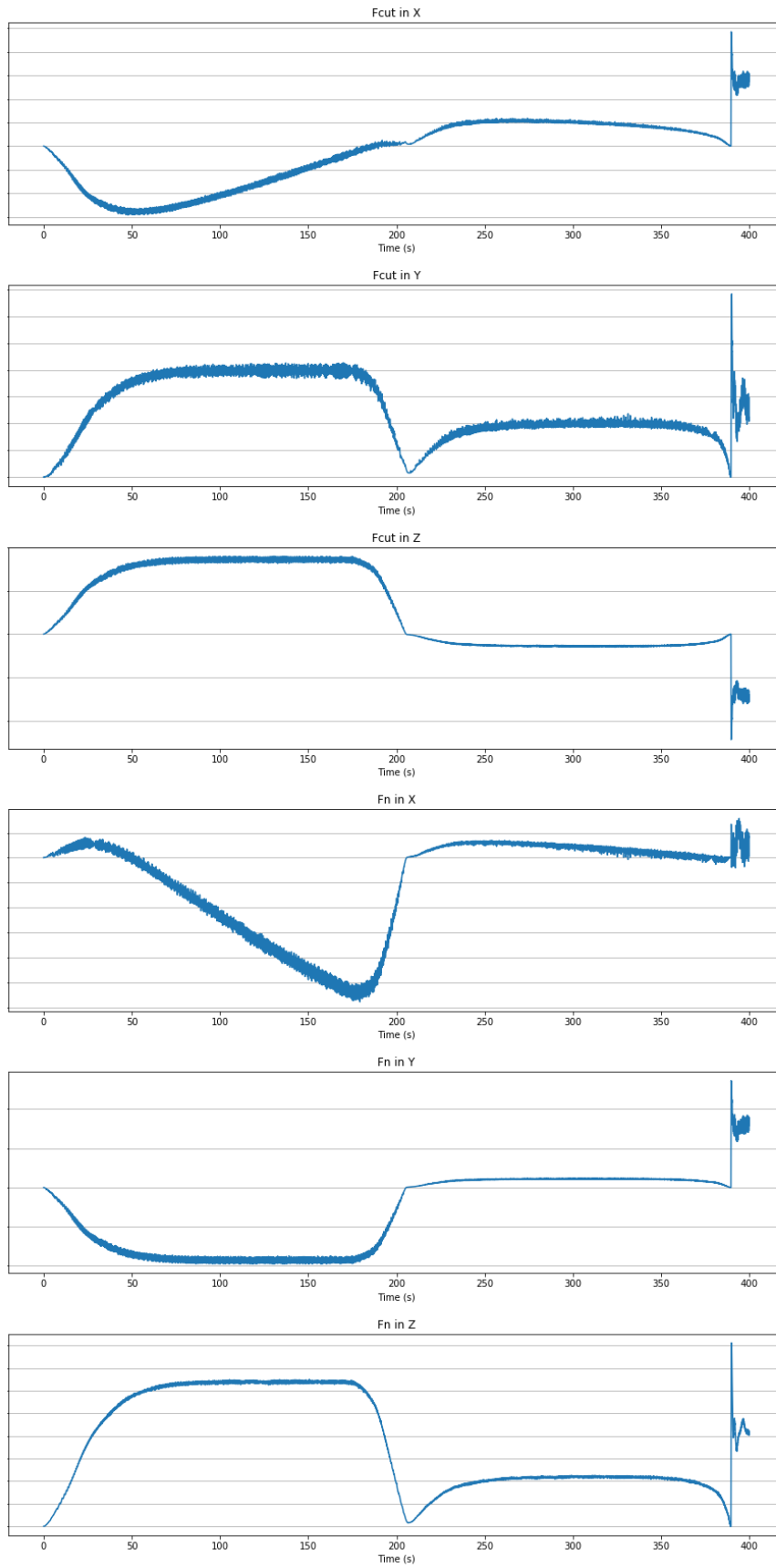
1 DOF test

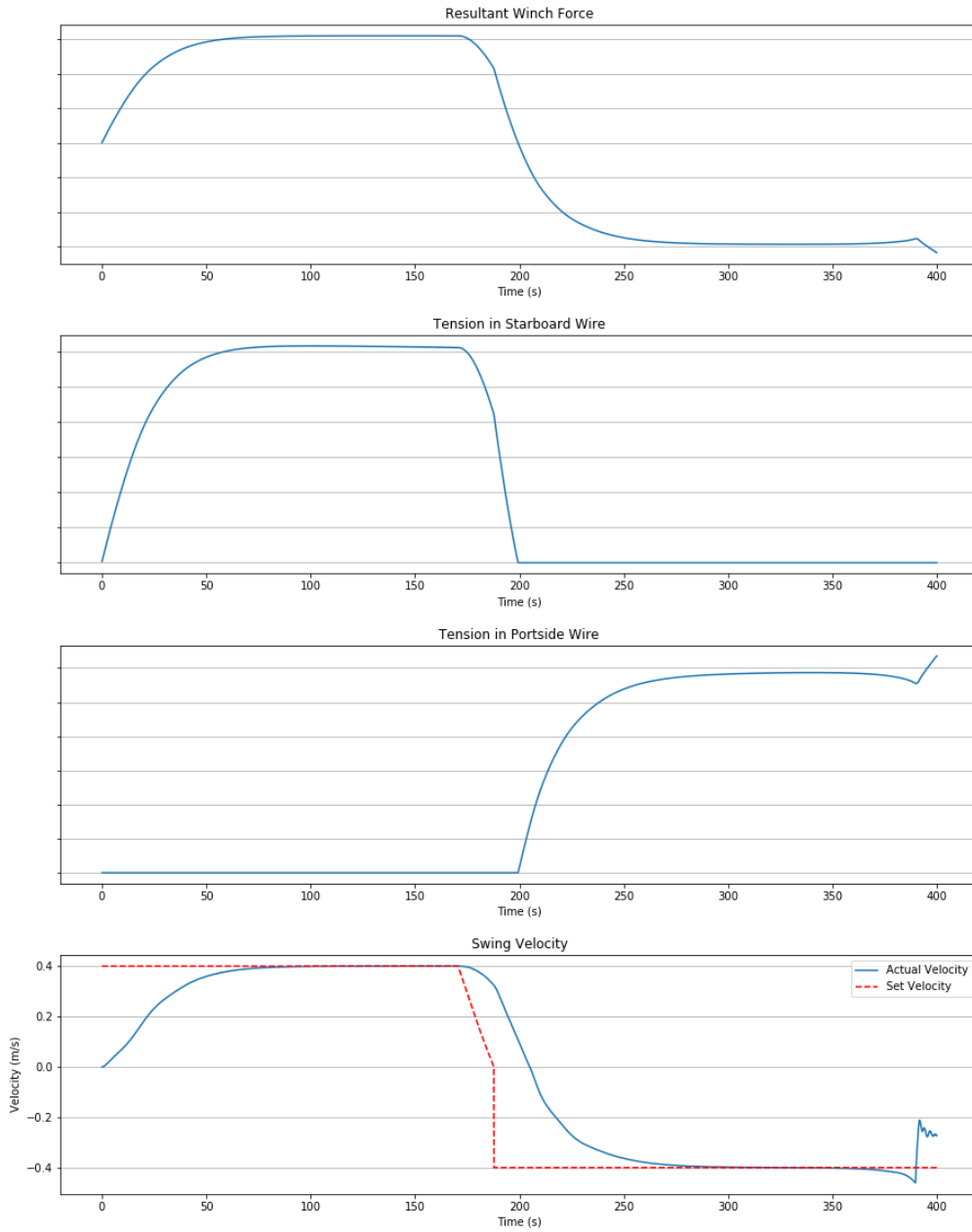


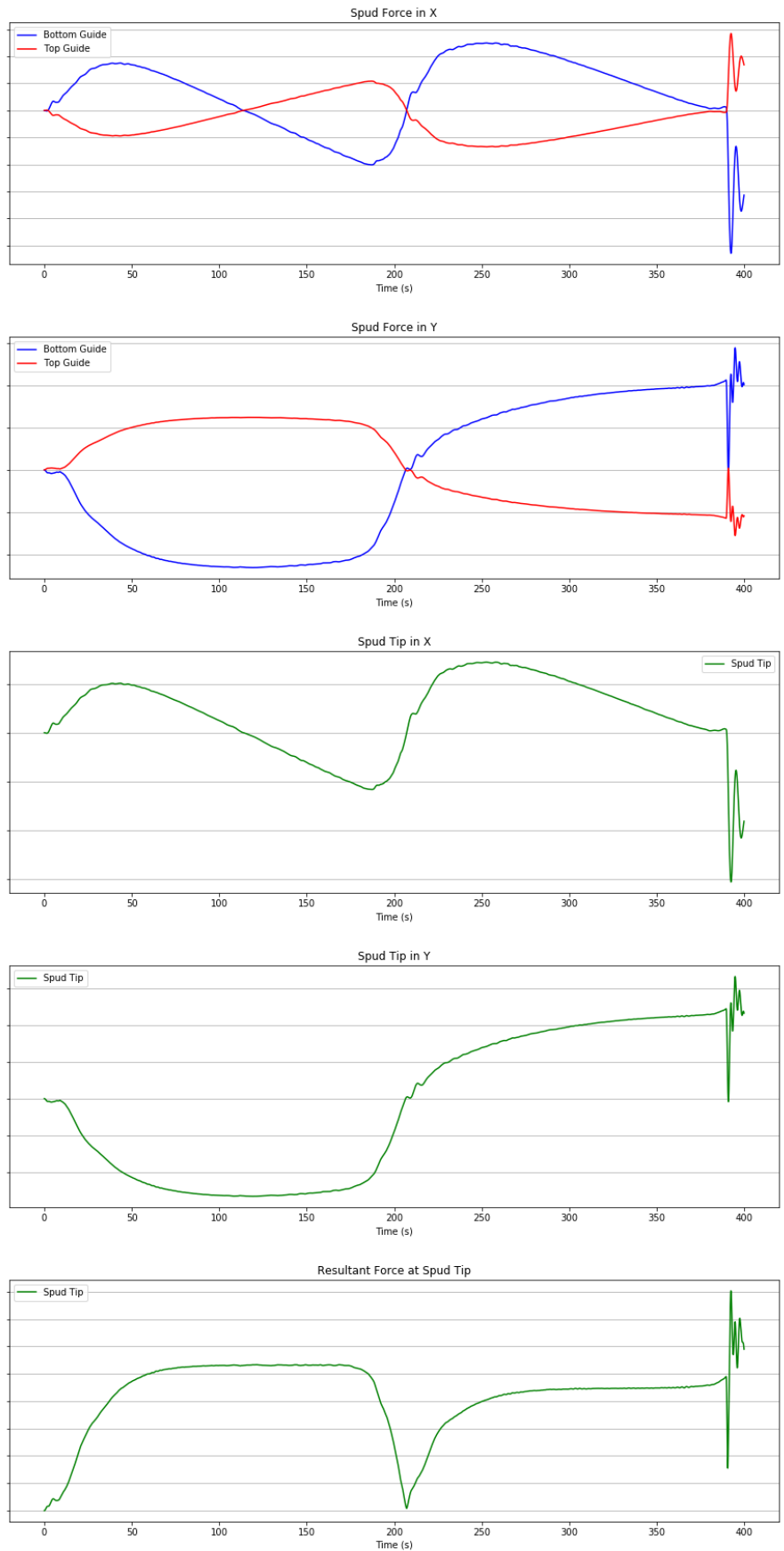


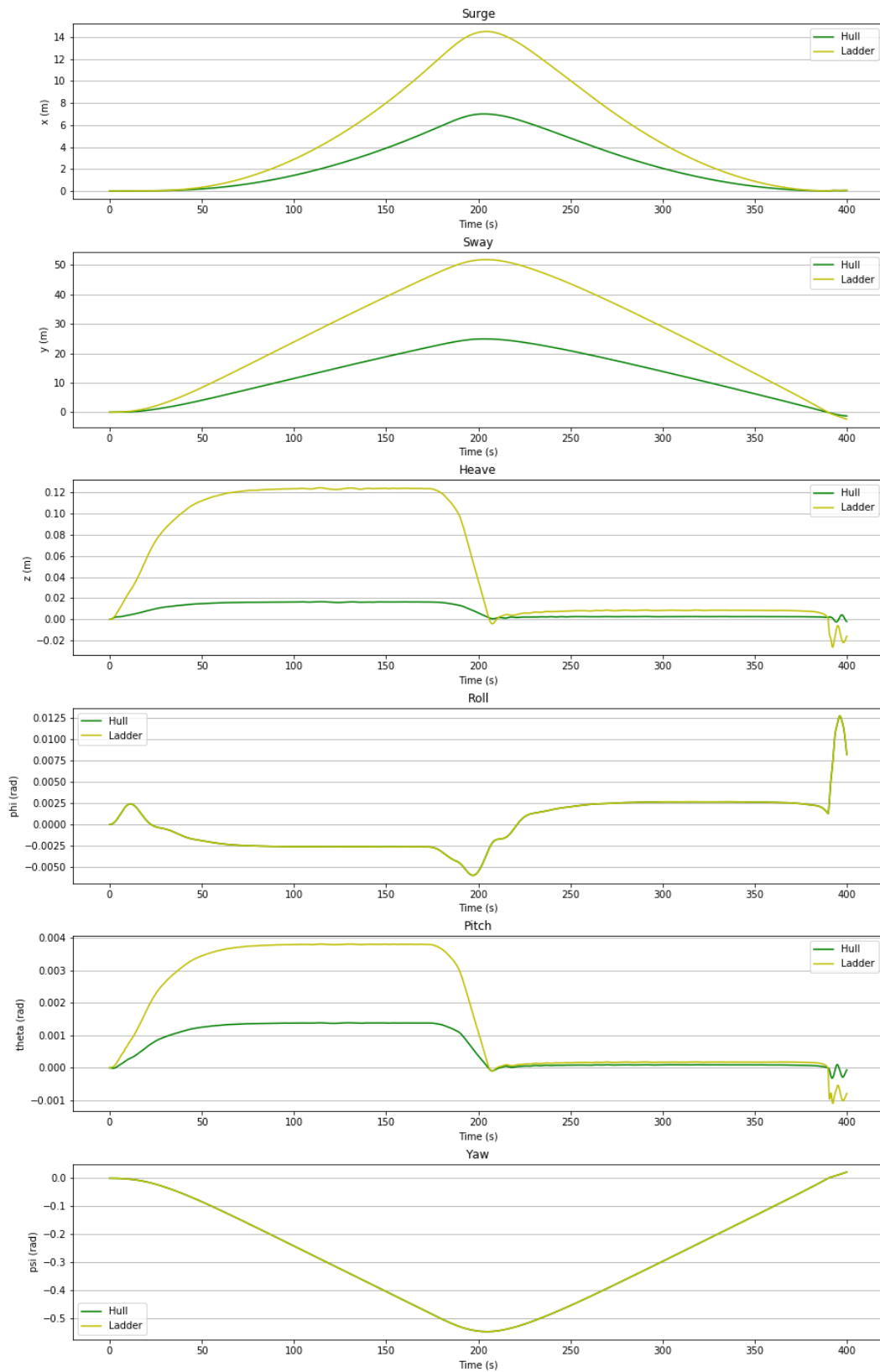
Single swing



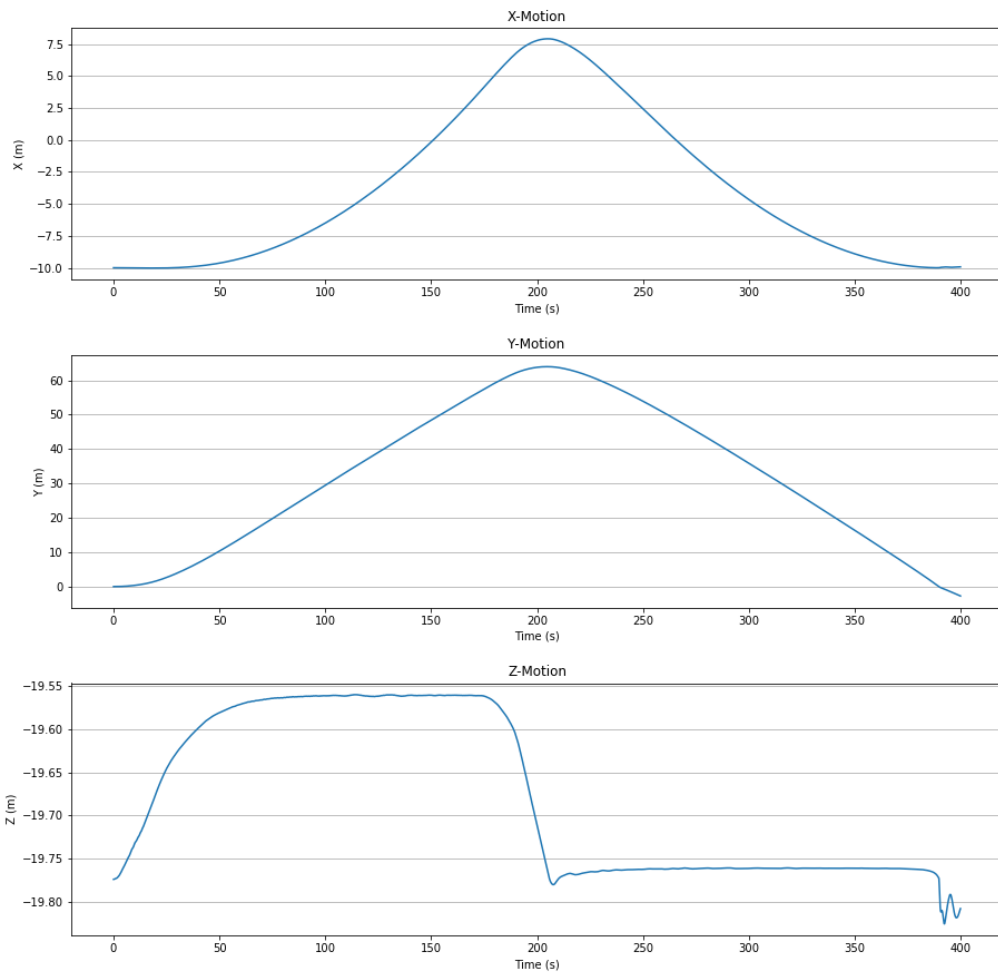




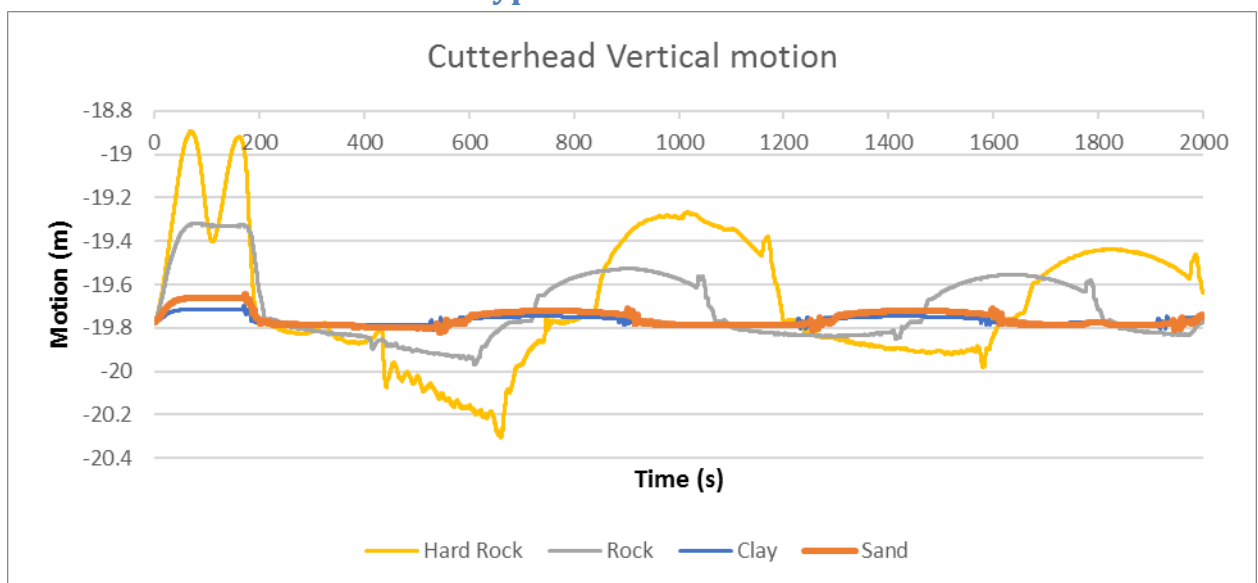


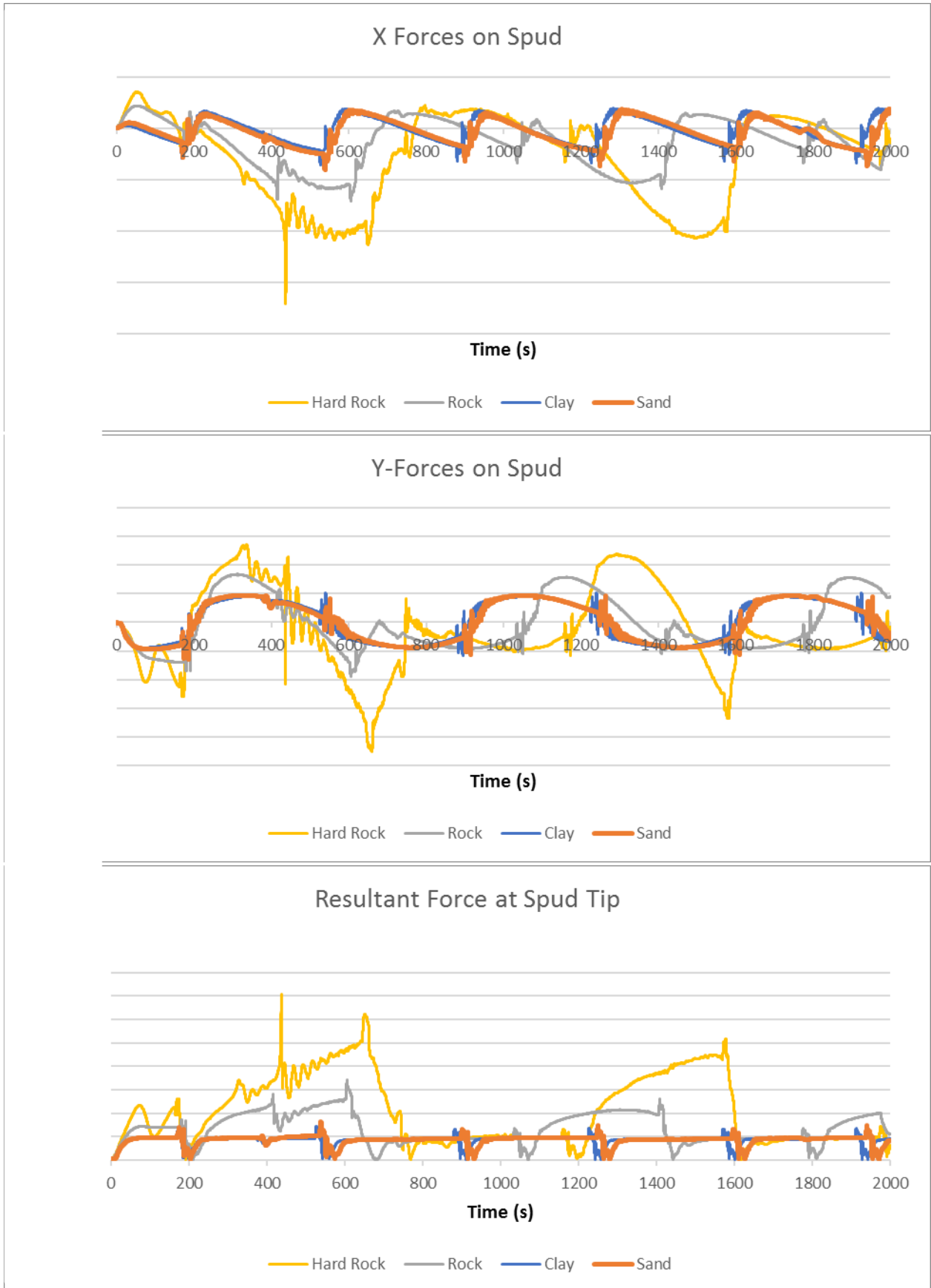


Cutterhead Motions



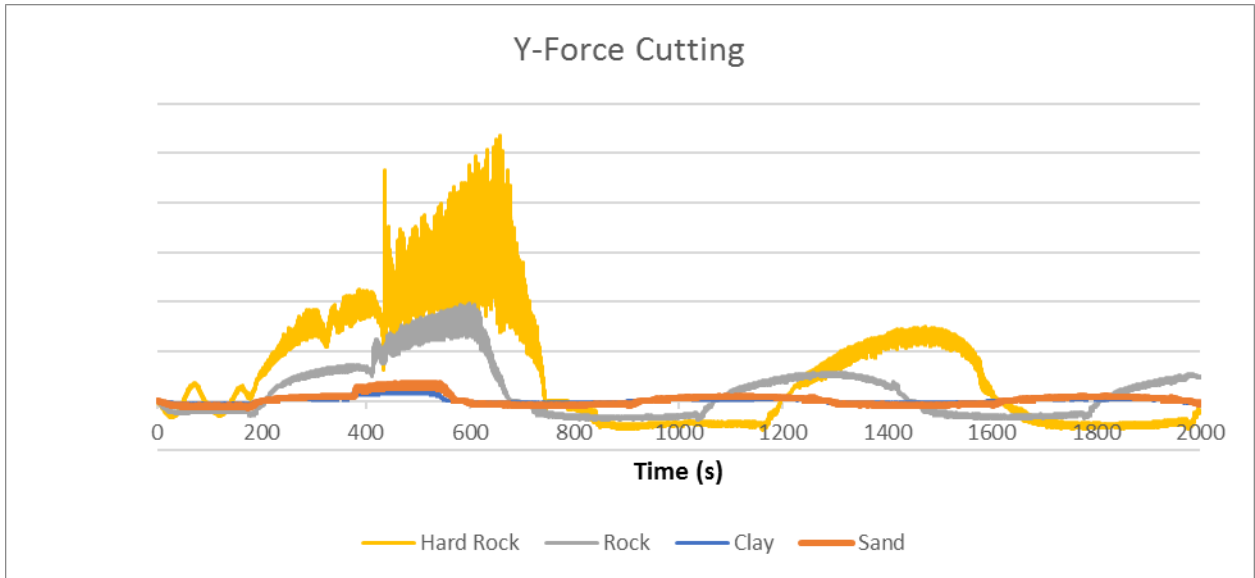
Full simulation for 3 soil types



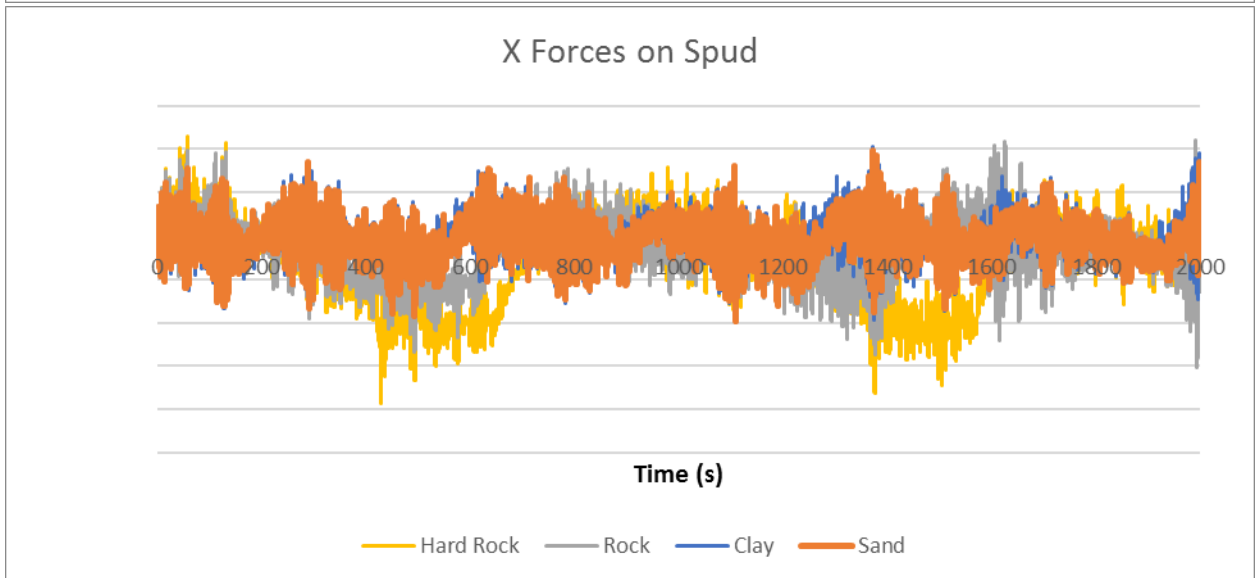
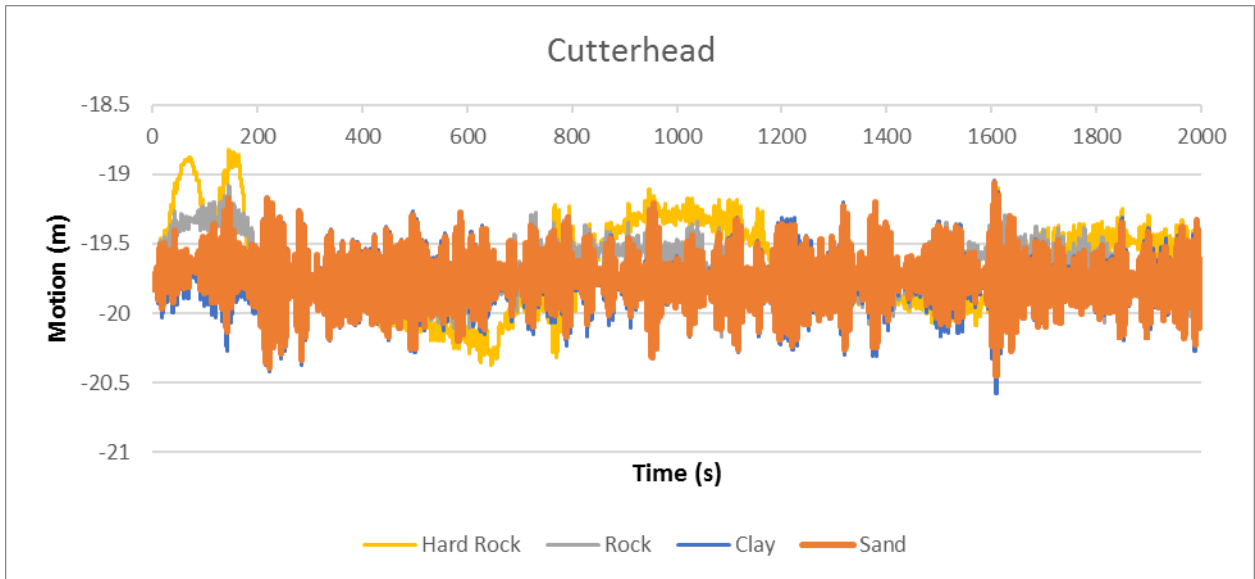




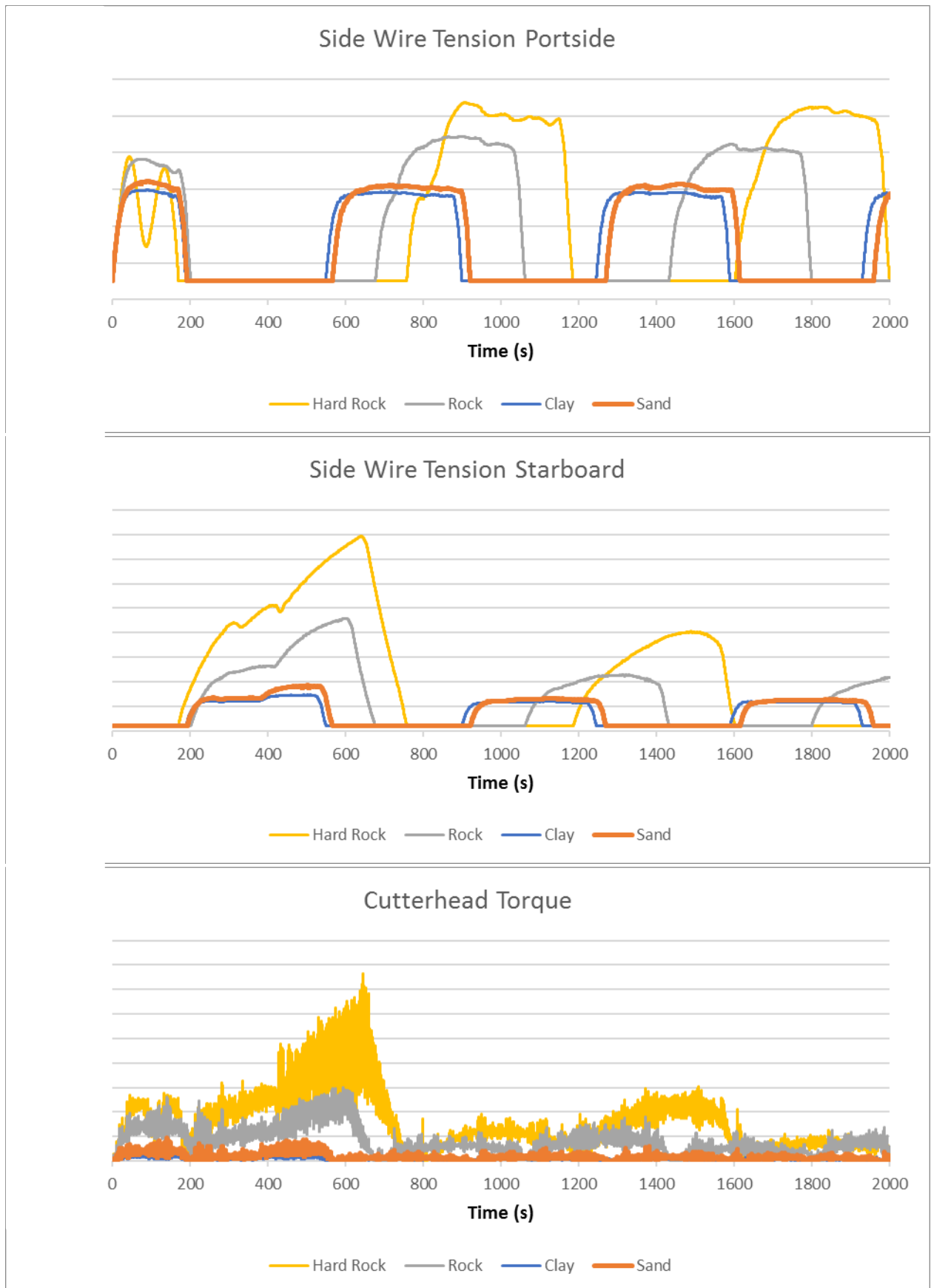


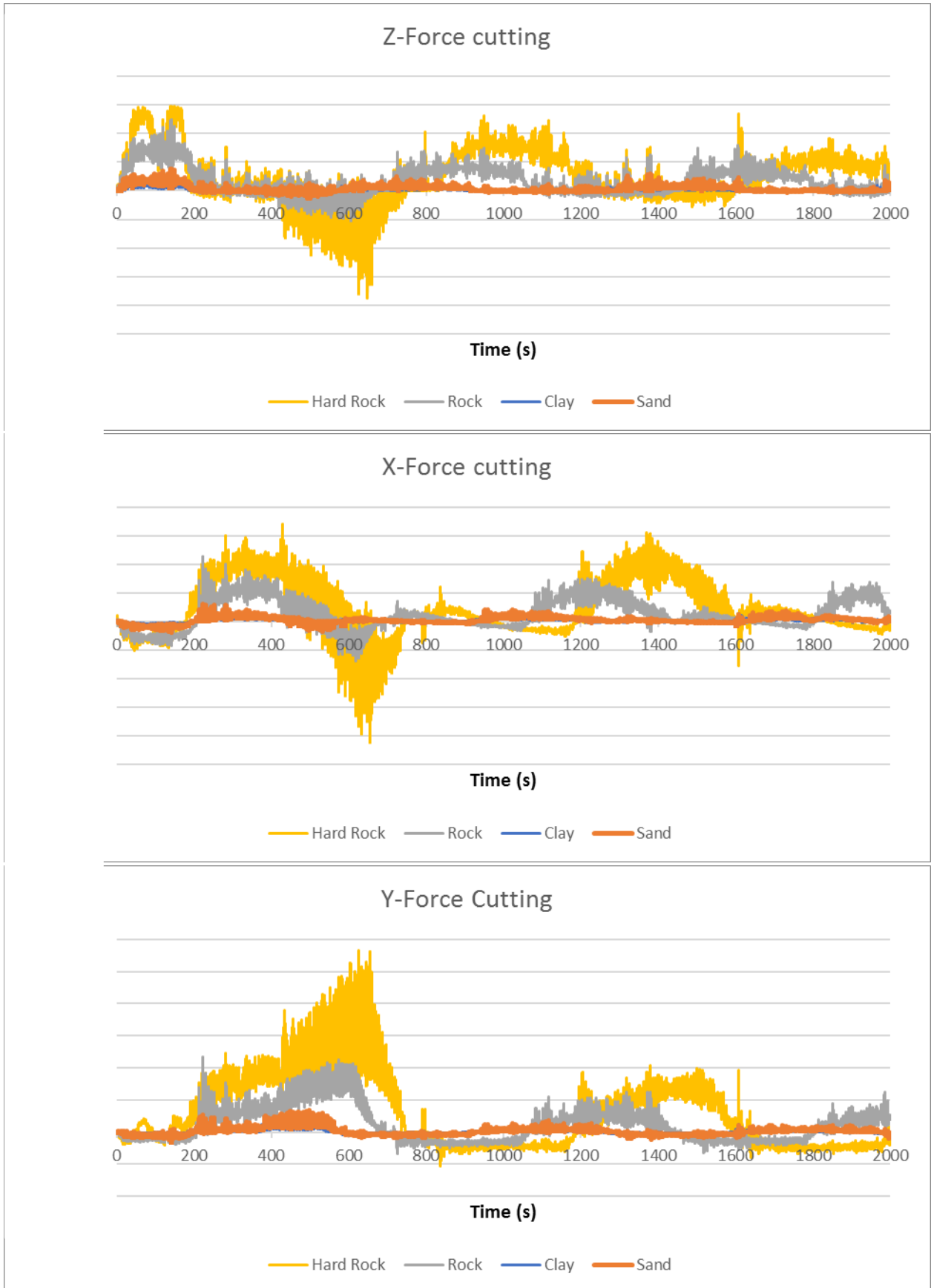


Full simulation for 3 soil types including waves









Comparison of single rigid body and 2 body approach

